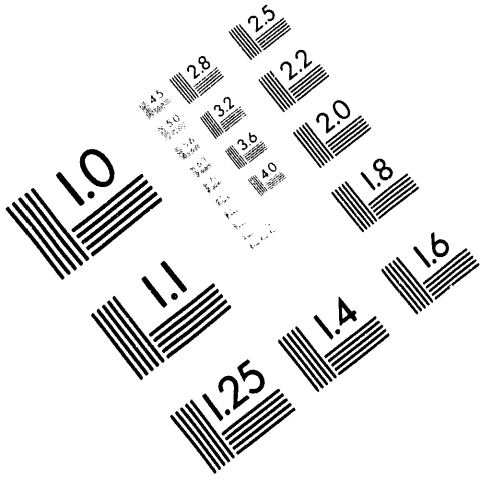

Association for Information and Image Management
1100 Wayne Avenue, Suite 1100
Silver Spring, Maryland 20910
301/587-8202

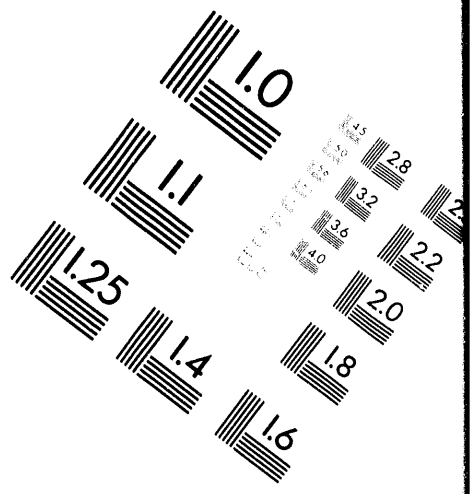

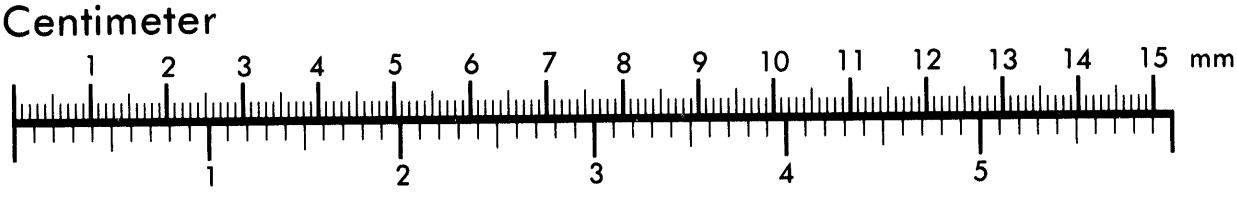

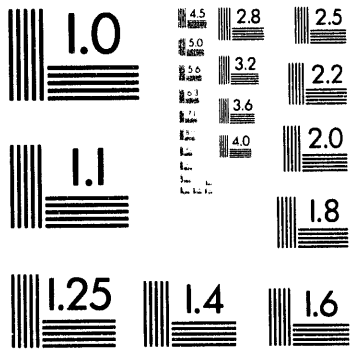

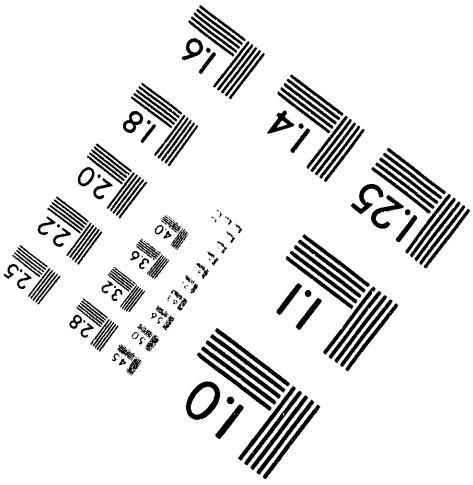

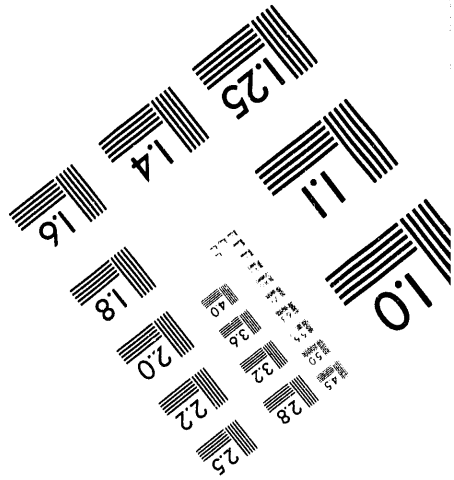

MANUFACTURED TO AIIM STANDARDS
BY APPLIED IMAGE, INC.

1 of 2

FOSSIL

DOE/MC/29267-3655
(DE94004075)

Anaylsis of Deep Seismic Reflection and Other Data from the Southern Washington Cascades

Final Report
September 15, 1992 - December 31, 1993

W. D. Stanley
S. Y. Johnson
V. F. Nuccio

December 1993

Work Performed Under Contract No.: DE-AT21-92MC29267

For
U.S. Department of Energy
Office of Fossil Energy
Morgantown Energy Technology Center
Morgantown, West Virginia

By
Interior Department of Geological Survey
Denver, Colorado

DISCLAIMER

DOE/MC/29267-3655
(DE94004075)
Distribution Category UC-132

Anaylsis of Deep Seismic Reflection and Other Data from the Southern Washington Cascades

Final Report
September 15, 1992 - December 31, 1993

W. D. Stanley
S. Y. Johnson
V. F. Nuccio

Work Performed Under Contract No.: DE-AT21-92MC29267

For
U.S. Department of Energy
Office of Fossil Energy
Morgantown Energy Technology Center
P.O. Box 880
Morgantown, West Virginia 26507-0880

By
Interior Department of Geological Survey
Box 25046
Denver, Colorado 80225

December 1993

Table of Contents

List of Illustrations

*-denotes page following text page

PREFACE

This report describes results of a synthesis of geological, geophysical and geochemical data from a largely volcanic rock covered region in southwestern Washington that has been identified as a underlain by thick marine sedimentary rocks. The work was funded by the Deep Source Gas projects at the Morgantown Energy Technology Center. The subproject which resulted in this report is centered in the Branch of Geophysics, U.S. Geological Survey in Denver. A lengthy period of cooperation between METC and the USGS has involved one task focused on the application of geophysical methods to the study of phenomena associated with fossil and active subduction zones and non-subduction suture zones that may have deeply emplaced sedimentary rocks. This report represents a summary synthesis of several geophysical and geological data sets.

EXECUTIVE SUMMARY

Limited possibilities exist for new hydrocarbon exploration regimes in the Pacific Northwest. Our goal in this presentation is to outline recent knowledge concerning a possible new exploration environment in the State of Washington. This frontier area occurs in southwestern Washington where extensive geophysical studies have been used to outline a proposed sedimentary basin hidden beneath volcanic rocks in the southern Cascades region (Stanley et. al, 1992). Electrical geophysical imaging using the magnetotelluric (MT) method first detected thick, electrically-conductive sequences believed to be associated with Eocene to Oligocene marine sedimentary rocks. The conductive section occurs at depths from about 1 km to 10 km in the southern Cascades region with thicknesses up to 10 km. Careful consideration of physical properties and the correspondence of the morphology of the units to known fold sets suggests that the high conductivities are related to lithologic/stratigraphic units rather than to variations in physical properties. Our preference for the lithology of the anomalous section, based upon a study of regional geology and structure, is one dominated by marine shales of Eocene and older in age. Other possible lithologies that have been evaluated for the conductive section include non-marine sedimentary units of Tertiary age, highly altered volcanic flows, and pre-Tertiary metasedimentary rocks with large percentages of graphite. We refer to this anomalously conductive region as the southern Washington Cascades conductor (SWCC, Fig. 1).

Based upon evidence from the MT surveys, a large scale seismic reflection program was implemented by the Department of Energy. The surveys utilized a 1000-channel sign-bit recording system with five Vibroseis source units as energy. Downsweeps of the vibrators was employed with recording out to 15 seconds, although there was generally very little useable information in the seismic data below

Figure 1-Location index for western Washington with seismic profile locations.

about four seconds two-way travel time. The data have been released on CD-ROM (Zilman, 1992) as USGS Open File Report 92-714. In addition, a high-resolution aeromagnetic survey of the suspected marine basin region has been completed and is available as USGS Open File Report No. 92-251 (Abrams, 1992). Although no new gravity data have been acquired, modeling of existing data has proved useful in examining certain aspects of the geology in the region.

The region in question has been examined using several types of data in addition to MT, seismic, magnetic, and gravity. Specific geological mapping tasks have been completed through funding by the Department of Energy and the USGS in the western part of the proposed basin near Morton, WA. Other regional geological studies using wells and outcrops done as part of the USGS Evolution of Sedimentary Basins programs have added information that constrain the possible nature of the SWCC rocks and their tectonic setting. Recently, evaluation of patterns of seismicity in the SWCC region has demonstrated the likelihood of several parallel and step-over strike-slip faults that may have produced the proposed basin or altered its geometry. In addition, the seismicity patterns trace the axis of key anticlinal structures and thrusts.

The nature of the SWCC is still largely a mystery in spite of our inferences regarding the rock types, as well as other factors that are important in evaluating the region for hydrocarbon potential. Tracing the conductive rocks to the surface in the area near Morton, WA and close to the surface just west of Mount Rainier suggests a correlation of the anomalous units with rocks like those of the Raging River, Carbonado, and McIntosh Formations, all of middle Eocene age.

The Morton antiform near Morton, WA, a main structure within the SWCC region, is cored with Eocene Puget Group sedimentary rocks of both marine and nonmarine origin interpreted from surface measurements, seismic reflection and MT data. These units were largely deposited in a series of interconnected basins east of the terrane boundary between the Coast Range province (underlain by Eocene marine basaltic basement) and the Cascades/Pre-Tertiary province (underlain by a diverse basement of pre-Tertiary rocks). Puget Group strata exposed in the core of the antiform are deltaic in origin and consist of alternating intervals of nonmarine and shallow marine rocks. Elsewhere in the region, the Puget Group rocks are underlain by fine-grained marine strata of the Raging River Formation (Johnson, 1992); similar and older marine rocks probably underlie the Morton area. Samples of the Raging River Formation contain significant amounts of organic matter, but are overmature and do not yield reliable petroleum source-rock data. Occurrence of numerous coals indicates some possibility for methane sourced from the coals.

Vitrinite reflectance data from an AMOCO stratigraphic test well in the Morton

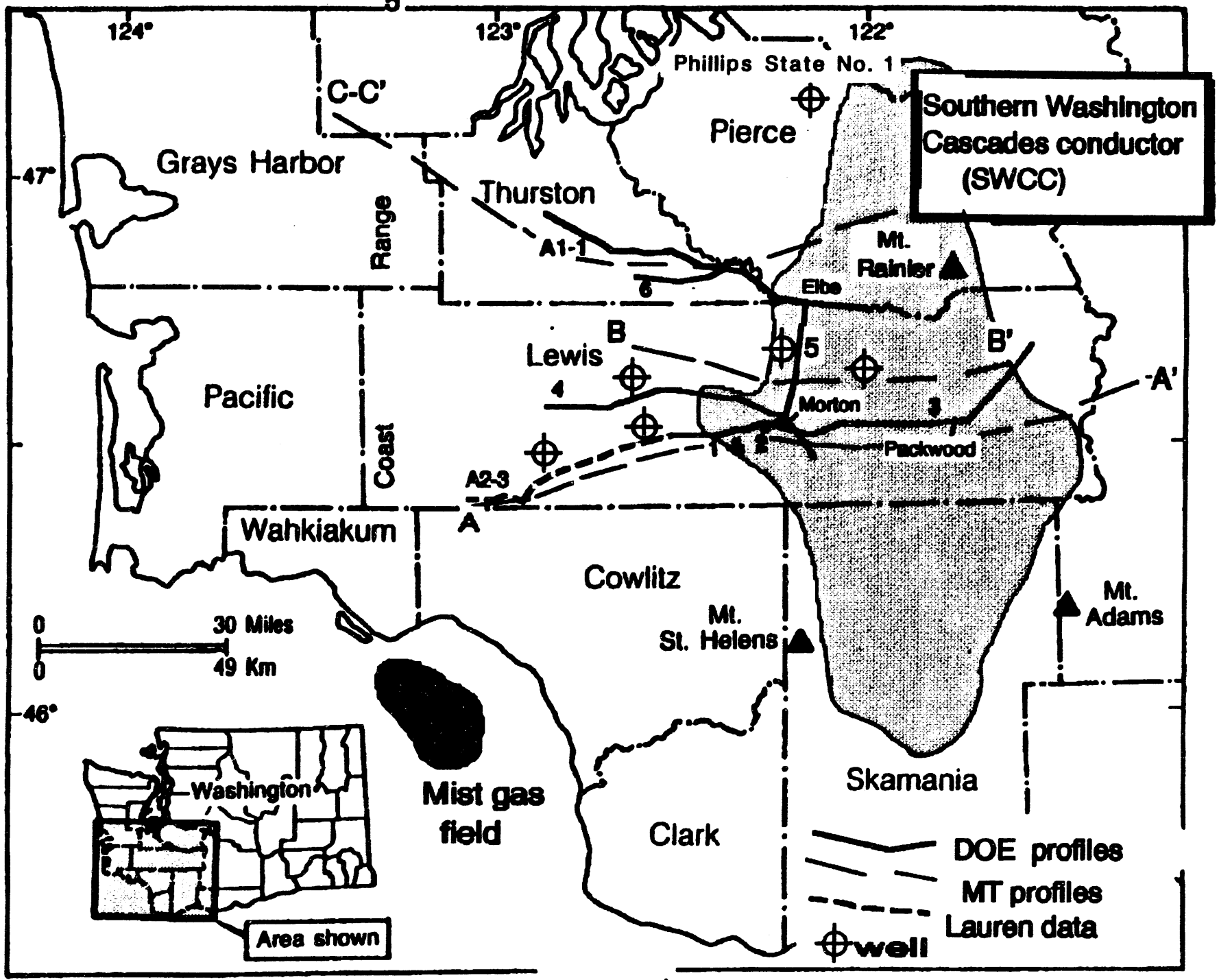
124°
123°
122°
Phillips State No. 1
C-C'
Pierce
Southern Washington Cascades conductor (SWCC)
Grays Harbor
47°
Thurston
Range
A1-1
Mt. Rainier
Elbe
B
B'
A'
Lewis
Pacific
Morton
Packwood
Coast
A2-3
A
Wahkiakum
Cowlitz
Mt. St. Helens
Mt. Adams
0 30 Miles
0 49 Km
46°
Washington
Area shown
Mist gas field
Clark
Skamania
DOE profiles
MT profiles
Lauren data
well

Figure 1

antiform range from $R_0 = 1.34$ to 0.96 percent (depths of 524 m and 171 m, respectively). Samples from two surface sections on the west flank of the antiform have R_0 values of 0.59 to 0.78 percent. Samples from a section in Coal Canyon on the east flank of the antiform have values ranging from 0.40 to 0.52 percent. Samples collected adjacent to small intrusions have elevated vitrinite reflectance values ranging up to 2.21 percent. Coal-rank data (Walsh and Phillips, 1982) show predictable increases in maturation eastward across the region as the Cascades magmatic arc is approached.

Preliminary petrographic analysis indicates that sandstones from the Morton antiform are largely plagioclase-rich, arkosic arenites, with variable porosity controlled by calcite cement and clay minerals. Unsubstantiated reports of secondary porosity in Puget Group units mapped in mines in the Morton area may be an indication of possible reservoir potential. However, extensive evidence for transpressive deformation, fracturing, and faulting of the Morton antiform must be considered negative factors for the occurrence of a suitable reservoir. Such considerations, along with the limited evidence for adequate source rocks, make the Morton antiform area a high risk exploration target, but possibly one of the few remaining to be tested in western Washington.

INTRODUCTION

The Deep Source Gas project is part of the Unconventional Gas Resources program in the Department of Energy. In 1982, deep gas research evolved as a natural outgrowth of research on geologically complex natural gas reservoirs (Gwilliam, 1990). Such natural gas resources require long-term, high-risk research and development. The level of risk is such that little or no private sector research is being done. Deeply sourced gas is defined as methane that is generated at depths greater than 10 km (30,480 feet). The Deep Source Gas project was the result of a workshop held in Morgantown, West Virginia in 1982, where it was recognized that the role of methane in the nation's energy budget was increasingly significant. This workshop reviewed deep methane sources from the perspective of three mechanisms for its development:

- Abiogenic gas-Gas of nonbiologic origin, emplaced primordially in the Earth's mantle.
- Subducted, organic carbon gas-Gas from hydrocarbon-generating marine sediments, deeply emplaced in the Earth's crust and mantle through plate tectonic movements in the Earth's crust.
- Deep Sedimentary Basin gas-Gas generated from known and unknown, deeply emplaced sedimentary rocks within basins.

Supportable estimates of a large component of carbon entering the mantle at subduction zones (Hilde, 1983) led to a more intense examination of key active and fossil subduction zones, especially to evaluate the processes active in such region as they impact methane generation. It was believed that there might be areas where

large sections of partially subducted or otherwise tectonically emplaced sedimentary rocks might occur at depths where active methane sourcing would occur. This deeply sourced methane might be trapped in overlying, possibly younger, structures. The complex environments which would be indicated for such regions make the application of normal seismic reflection methods difficult and expensive. Another geophysical technique, magnetotelluric (MT) sounding, was employed as a reconnaissance tool to investigate the occurrence of deeply emplaced sedimentary complexes, combined with gravity and magnetic methods, and followed by deep seismic reflection surveys in two instances.

The western borderland of the U.S., particularly in Washington, Oregon, northern California, and Alaska, was selected as the region to attempt to locate previously unidentified deep sedimentary systems that might serve as methane sources. Reconnaissance MT surveys and gravity/magnetic studies were carried out across the Klamath Mountains suture zone in northern California and southwestern Oregon, the Mist gas field area in northwestern Oregon, across Eocene suture zones in western Washington, and Cretaceous suture zones in the Methow Trough in northwestern Washington and the Alaska Range of Alaska (Stanley and others, 1990). Results from the Klamath Mountains region indicated a very low probability for deeply emplaced sedimentary rocks in the suture zone, and although the Methow Trough survey indicated deep, carbonaceous sedimentary rocks the thermal maturity data suggested that this region was not promising from a gas generation standpoint. The study in the Alaska Range found dramatic evidence for large-scale underthrusting of carbonaceous sedimentary rocks, but little is known about the thermal maturity (metamorphic state) of the hypothesized sedimentary rocks. In addition, because of the lack of commercial interest in frontier exploration for methane in Alaska, this study area was not deemed immediately appropriate for further research. The western Washington study, however, proved to be very interesting, with a possible thick marine sedimentary sequence found in the southern Washington Cascades. Many lines of evidence point to this sequence as being a possible good source for methane, as

Figure 2 (following page-Generalized geologic Index map of western Washington, with SWCC, Mist gas field, and location of MT and DOE seismic profiles.

detailed in the body of the report. The western Washington study area was also attractive because of nearby Mist gas field (Figure 2), northwest of Portland, Oregon, the lack of industry exploration in the area, and the existence of an established gas pipeline network nearby. Thus much of the effort in deep source gas exploration in the western U.S. using geophysical methods was focused upon this area and no further research was carried out in the other regions.

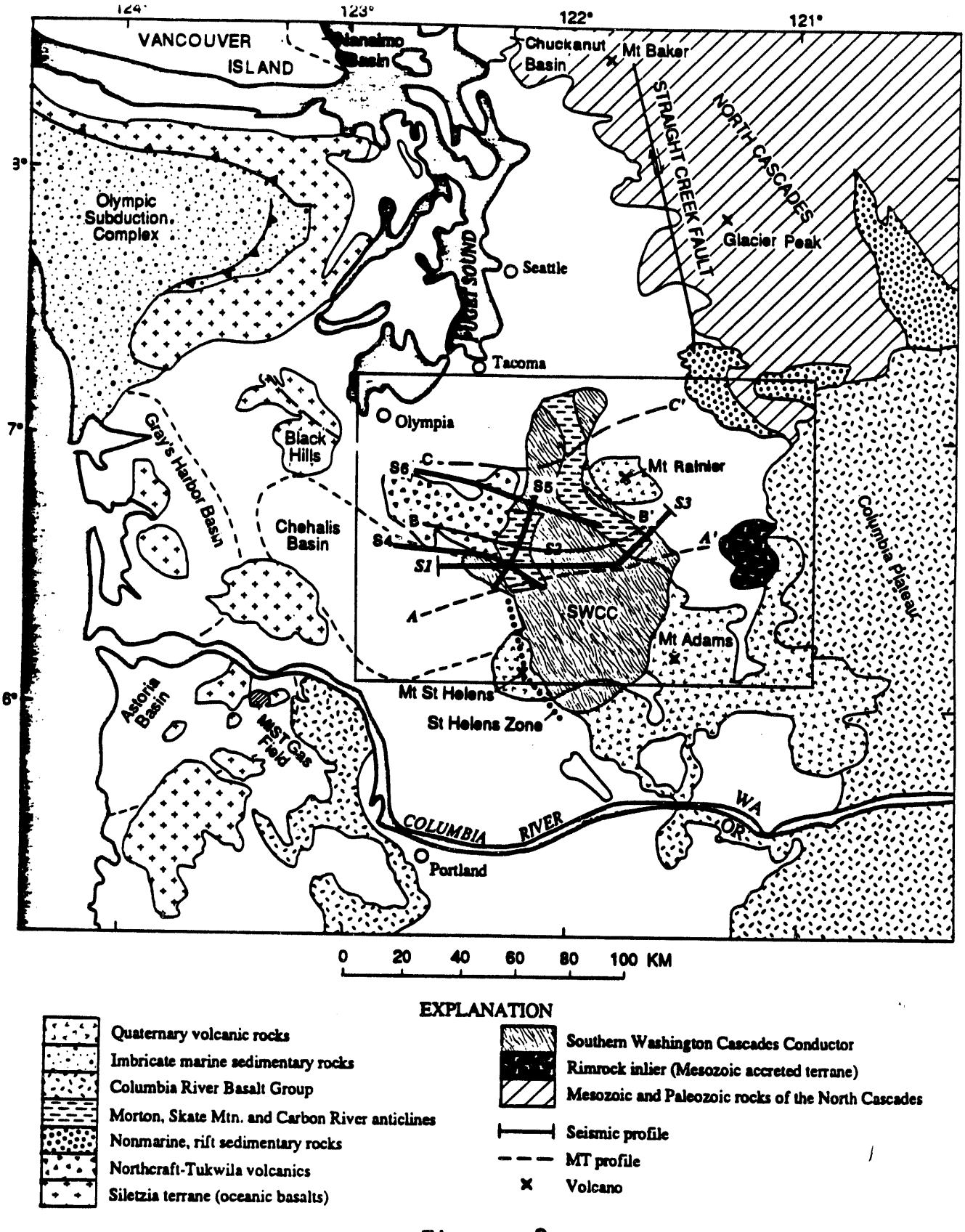
124°
123°
122°
121°
VANCOUVER ISLAND
Nanaimo Basin
Chuckanut Basin
Mt Baker
STRAIGHT CREEK FAULT
NORTH CASCADES
Glacier Peak
Olympic Subduction Complex
PUGET SOUND
Seattle
Tacoma
Olympia
Black Hills
Gray's Harbor Basin
Chehalis Basin
C'
C
S6
S5
S3
Mt Rainier
B
B'
S4
S2
A'
S1
A
SWCC
Mt Adams
Columbia Plateau
Mt St Helens
St Helens Zone
Astoria Basin
WEST Gas Field
COLUMBIA RIVER
WA
OR
Portland
3°
7°
6°
0 20 40 60 80 100 KM
EXPLANATION
Quaternary volcanic rocks
Imbricate marine sedimentary rocks
Columbia River Basalt Group
Morton, Skate Mtn. and Carbon River anticlines
Nonmarine, rift sedimentary rocks
Northcraft-Tukwila volcanics
Siletzia terrane (oceanic basalts)
Southern Washington Cascades Conductor
Rimrock inlier (Mesozoic accreted terrane)
Mesozoic and Paleozoic rocks of the North Cascades
Seismic profile
MT profile
Volcano

Figure 2

Overview of Hydrocarbon Exploration History in the Region

The Pacific Northwest states of Oregon and Washington encompass a region of complex geological settings in which petroleum exploration has been largely unsuccessful because of a variety of geological factors and the low quality of typical seismic data. The system of late Tertiary sedimentary basins west of the Cascades (Fig. 2) has been interpreted as containing largely immature source rocks, but with some good reservoir rocks (Armentrout and Suek, 1985). These basins formed on basement consisting of oceanic basalts of the Coast Range province, and are filled with 3-5 km of marine sandstones, shales, and minor volcanic rocks. The only producing field with ongoing development in the Pacific Northwest is the Mist gas field, west of Portland, Oregon (Fig. 2).

Eocene to Miocene sedimentary units in the Olympic Peninsula appear to contain good source rocks (Snavely, 1987) and some oil has been produced from the coastal zone of the Peninsula and in the Grays Harbor basin to the south (Braislin and others, 1971). Methane is venting from a fault zone on the north side of the Olympic Peninsula (Kvenvolden and others, 1987). Organic geochemical analyses by Kvenvolden and others (1987) suggest that the deep parts of the Olympic melange assemblage are mature for oil and gas, and Snavely (1987) suggests that the highest potential for oil and gas generation in the western Washington region occurs in the thick, accretionary melange-wedges of the Olympic Peninsula.

Drilling in the Puget Lowland of Washington (Fig. 2) has not resulted in production, but many wells have produced shows of oil and/or gas. Gas seeps in the Black Diamond, WA area (Mullineaux, 1970) and elsewhere in the Puget Lowland are believed to derive from coal bed methane at shallow depths. Testing of the Phillips State No. 1 well drilled east of Tacoma extracted a measurable quantity of high-paraffin oil at depths of 7060-7120 feet (Brown and Ruth Laboratories, 1982).

Extensive hydrocarbon exploration has been carried out in the Columbia River Plateau (Fig. 2), based upon initial, non-commercial, gas discoveries by Shell Oil Co. (Northwest Oil Report, 1983). This gas appears to have come from Tertiary nonmarine sediments in which flow is restricted by porosity-plugging authigenic minerals derived from volcanic clasts. Much speculation has developed concerning the possibility that the Plateau is underlain by Mesozoic sedimentary rocks similar to those that crop out in the Blue Mountains, Oregon (Kleinhaus and others, 1984; Miller, 1989).

GEOLOGICAL/TECTONIC SETTING

The SWCC occurs partially within the Cascade Range that extends from northern California to British Columbia; volcanos of the Cascades (Fig. 2) represent the magmatic arc associated with post 36 Ma subduction of the Juan de Fuca plate and its predecessors. The Cascades magmatic arc may have begun to develop about 44 Ma with andesitic dikes that intruded the Crescent Formation (Snavely, 1987) and certainly was well established by 36 Ma at the time of eruption of the thick Ohanapecosh Formation volcanic flows near Mt. Rainier (Fig. 2). Pre-Tertiary crust in the region is composed of Mesozoic and older accreted terranes, volcanic arcs, and underplated magmatic rocks. This older accreted crust is exposed in the North Cascades (Fig. 2) of Washington and in the Blue Mountains and Klamath Mountains of Oregon.

A key feature of the geology of the Pacific Northwest margin is a terrane of oceanic basalts (Fig. 2), called "Siletzia" by Irving (1979), that forms the basement in western Oregon and Washington. The oceanic basalt assemblage is represented by the Siletz River Volcanics in Oregon (Snavely, MacLeod, and Wagner, 1968), Crescent Formation in Washington (Cady, 1975), and Metchosin volcanics on southern Vancouver Island (Muller, 1977) and is estimated by Duncan (1982) to have a volume of 250,000 km^3. Gravity and magnetic data have been analyzed by Finn (1989) who, along with Stanley and others (1987 and 1989), interpret that the Siletzia units extend underneath the region between the Black Hills and Mount Rainier (Fig. 2).

Crescent Formation basalts and similar rocks in Oregon that form the basement rocks west of the Cascades are now widely believed to have formed in a continental-margin rift setting (Wells and others, 1984; Snavely, 1987; Babcock and others, 1992). Consistent with this interpretation, Johnson (1984, 1985) and Johnson and others (1994) suggested that the eastern margin of this rifted terrane was a dextral strike-slip fault, the Puget fault. Northward motion of the Coast Range block along the Puget fault. was accommodated to the north by south-directed thrusting on southern Vancouver Island (Clowes and others, 1987) and by folding and faulting within the Coast Range block in the Straits of Juan de Fuca and on the northern Olympic Peninsula (Snavely, 1987). Johnson (1984, 1985) suggested that most strike-slip motion on the crustal boundary occurred prior to the late Eocene, after which strike-slip motion diminished and was distributed on several fault zones in the southeastern Puget Lowland (Johnson and others, 1994).

Synchronous with Eocene rifting in the Coast Range province, the eastern pre-Tertiary basement province experienced significant transtensional deformation, characterized by dextral strike-slip faulting, formation of rapidly subsiding sedimentary basins, and uplift and(or) intrusion of crystalline rocks (Johnson, 1985). Eocene sedimentary rocks form units as thick as 6,000 m or more occur in these pull-apart structures and comprise some of thickest nonmarine sequences in North America (Johnson, 1985). Pull-apart basins are rifts or graben structures caused by the effects of differential movement on strike-slip faults. Other terms roughly synonymous with

pull-apart structures are "rhombochasm" (Carey, 1958) and wrench grabens (Belt, 1968); terminology and a review of tectonic aspects of this type of structure is given in Mann and others (1983). Subsidence in the Coast Range province following extrusion of the Crescent Formation was much slower and probably of thermal origin (Johnson and Yount, 1992).

Due to their different histories, there are significant contrasts in Eocene basin geology across the Cascades-Coast Range crustal boundary. In the Seattle area,

Figure 3-Detailed geologic map of central SWCC region and DOE seismic reflection profiles. The location of MT profile EE ' is also indicated. Geologic base was digitally scanned from Walsh and others (1987) and shotpoint maps for the reflection lines plotted from data on CD-ROM produced by Zilman (1993). The decade numbers on the seismic lines represent each tenth shotpoint. Actual shotpoint numbers are contained in Appendix C. Legend for selected units from Walsh and others (1987) is shown in the lower part of the figure.

Johnson and others (1994) describe major differences in thickness and facies of early and middle Eocene strata from west to east across the crustal boundary. In the southwest Washington area of the DOE seismic survey, there is also a major increase in thickness of Eocene strata from west to east across this zone. In the Chehalis basin (see discussion below) west of the zone, the thickness of the Eocene section from the Crescent basaltic basement to the base of the Northcraft Formation is about 2 km. In the Morton antiform east of the zone, there is as much as 4-8 km of Eocene strata below the base of the Northcraft Formation. This thickness contrast and other aspects of the regional geology of southwest Washington area are described later in this report in sections on the Chehalis basin and the Morton antiform.

Figure 4- Schematic geologic map of the Chehalis Basin and bounding uplifts. A-A', B-B', and C-C' show lines of cross section shown in Figures 6, 7, and 8. Abbreviations as follows: A5 = AMOCO WC-83-5 borehole; BC = Bear Canyon; BM = Bergen Mountain stratigraphic section; Ce = Centralia; Ch = Chehalis; K = Earl F. Siler and J.W. Tanner Kostick No. 1 borehole; M = Morton; MA = Morton antiform; MS = Mineral stratigraphic section; NL = Newaukum Lake eruptive center for Northcraft Formation of Hagen

In the area of the DOE seismic survey (Fig. 3), Stanley and others (1987, 1992) used diverse geophysical data sets to suggest this boundary occurs in the vicinity of Bear Canyon on the east flank of the Chehalis Basin (Fig. 4), and coincides

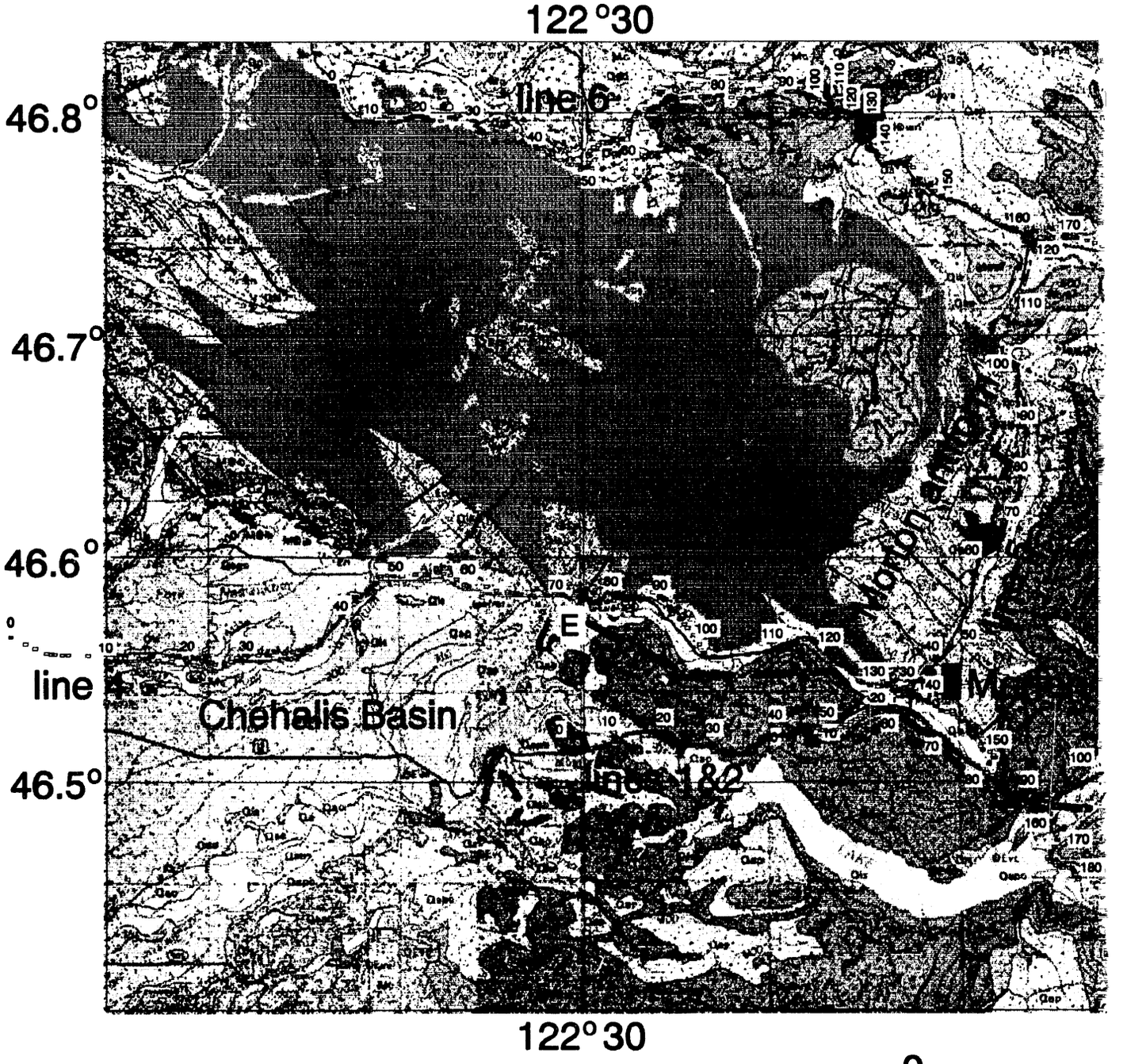
122°30
46.8°
46.7°
46.6°
46.5°
line 6
line 4
Chehalis Basin
E
M
122°30
0
MT profile
Quaternary alluvium
Oligocene Miocene volcanics
Eoce
volca

Figure 3

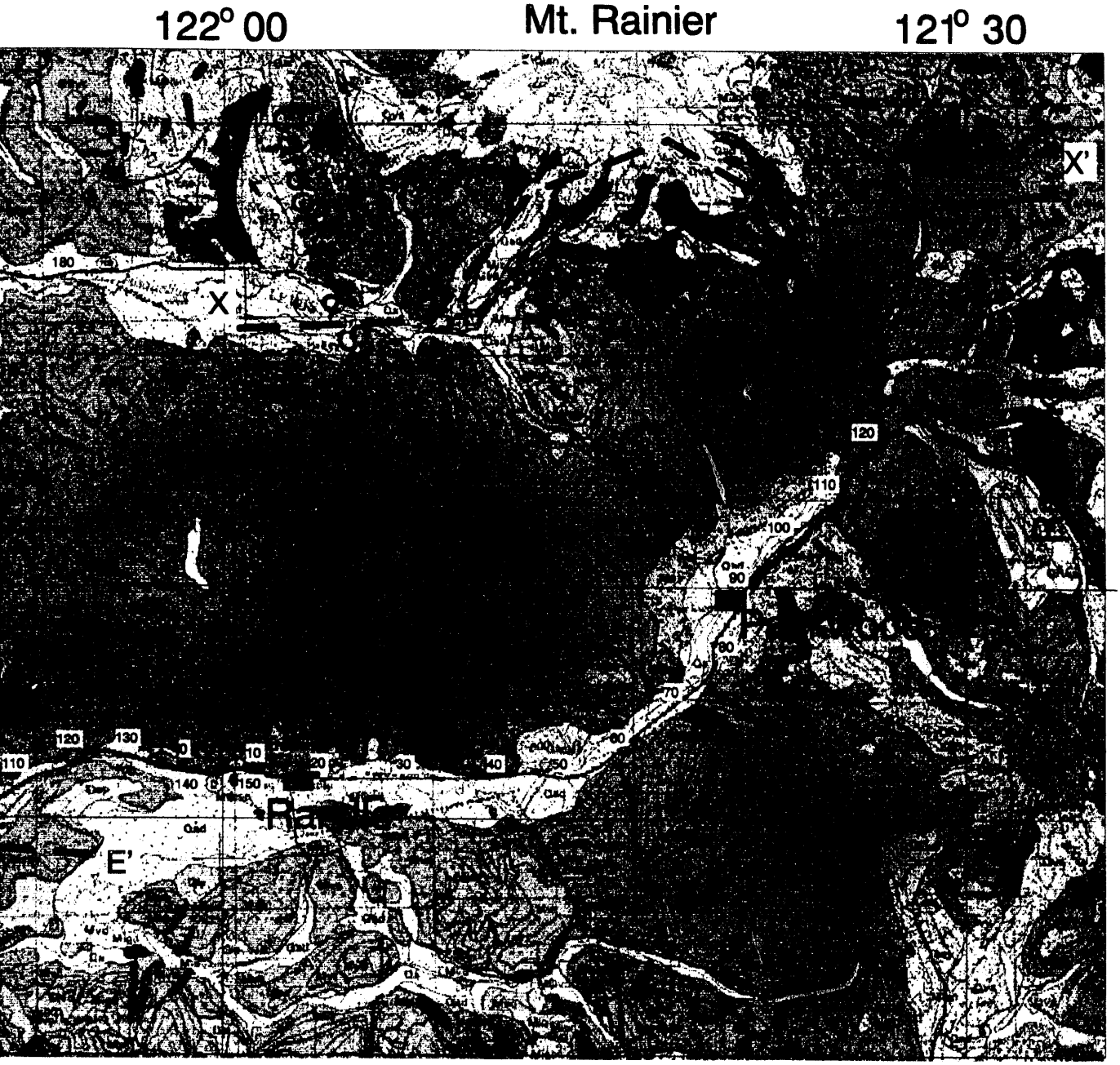
122° 00
Mt. Rainier
121° 30
X
X'
E'
122° 00
121° 30
50
KM
Eocene
sedimentary
rocks
Oligocene
Miocene
intrusives
Cretaceous
Jurassic
metamorphic rocks

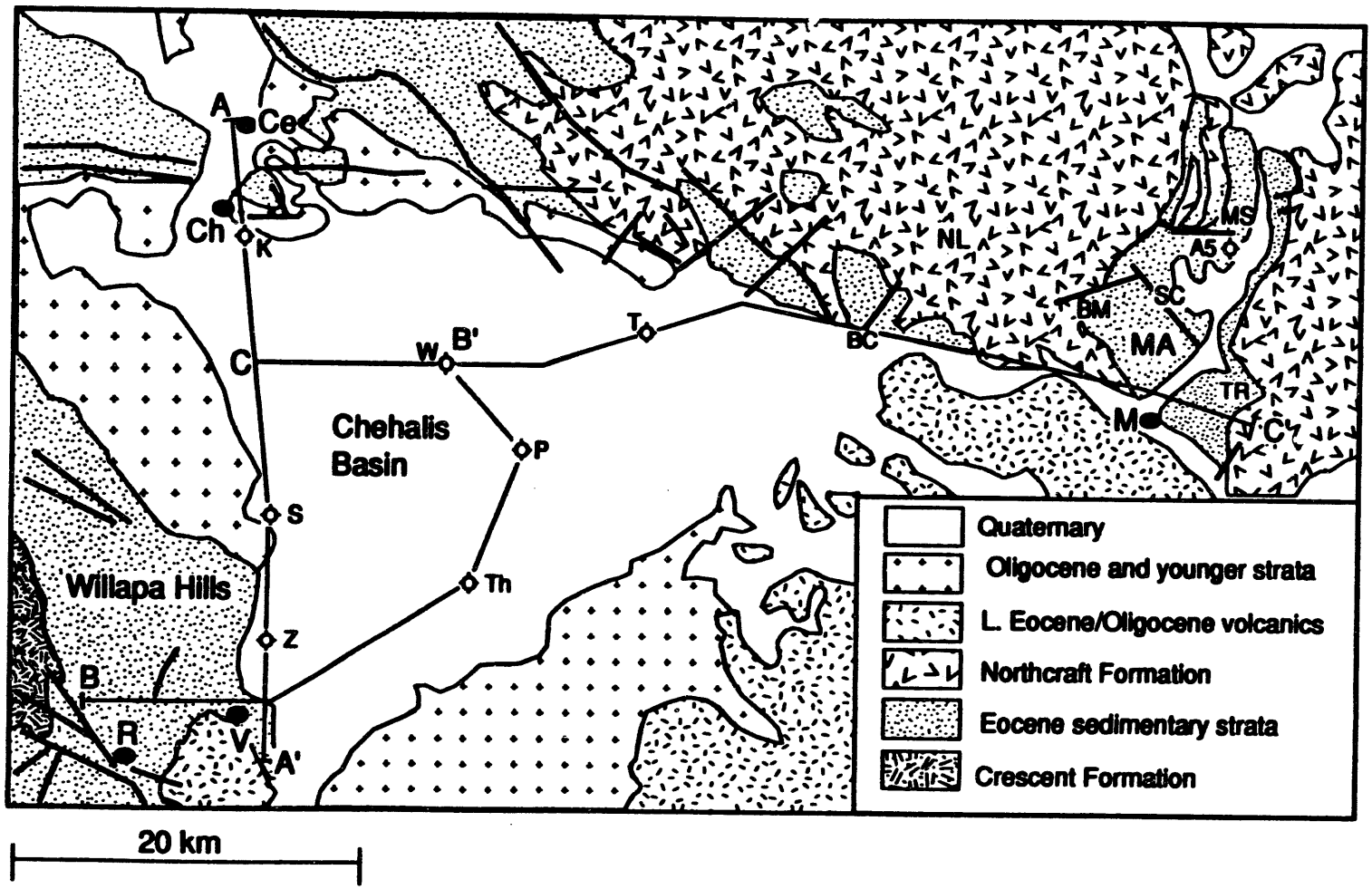
A
Ce
Ch
K
NL
MS
A5
SC
BM
MA
BC
T
W
B'
C
Chehalis
Basin
P
TR
M
C
S
Th
Willapa Hills
Z
B
R
V
A'
20 km
Quaternary
Oligocene and younger strata
L. Eocene/Oligocene volcanics
Northcraft Formation
Eocene sedimentary strata
Crescent Formation

Figure 4

approximately with the Saint Helens zone (SHZ) of Weaver and Smith (1983). The DOE network of seismic reflection lines in southwest Washington transects this major north-trending crustal boundary between basement rocks of the pre-Tertiary Cascade province to the east and the Eocene Coast Range province to the west, with the proposed sedimentary complex of the SWCC caught between. This contact is covered by late Eocene and younger rocks and can be located and characterized only on the basis of geophysical data.

Western Washington lies at the southern end of a belt of dextral slip related to oblique convergence of the Juan de Fuca plate and its predecessors, such as the Kula and Farallon plates. From several hundred to several thousands of km of strike slip have been postulated for the borderland terranes of British Columbia, the Yukon Territories, and Alaska in post-Cretaceous time (Irving, 1983; Irving and others, 1980; Jones and others, 1977). Misch (1977) and Davis and others (1978) postulated that the Straight Creek fault (Fig. 2) might have about 190 km of right-lateral displacement. Price and others (1985) suggest that the Fraser Fault (northern extension of Straight Creek fault) had about 70 km of offset since the mid-Cretaceous. Motion on the fault system must have ceased by time of intrusion of the Chilliwack batholith in Oligocene time (Price and others, 1981). Detailed study of the southern end of the Straight Creek fault by Tabor and others (1984), found a Tertiary history of dominantly vertical movement. However, they interpret that horst-and-graben structures and en-echelon fold axes in the Eocene Swauk Formation suggest early Eocene right-lateral shear along the Straight Creek fault.

Paleomagnetic data document significant block rotations of the Coast Range (Simpson and Cox, 1977; Globerman and Beck, 1979; Magill and others, 1981; Wells, 1989). There is agreement among these various authors that the Coast Range has undergone a relative clockwise rotation with respect to the North America craton of about 25° in the north and up to 75° in the south. There have been several models proposed by Simpson and Cox (1977) and Wells (1989) to explain this rotation. The most current analysis by Wells (1989) includes paleomagnetic data from the Black Hills (outcrops of Siletzia) near Olympia, Washington (Fig. 2); this information indicates that much of the overall rotation of the Coast Ranges was taken up in individual block rotations, probably associated with dextral shear.

In the middle Eocene, feldspathic-quartzose deltaic sediments (Armentrout and Suek, 1985) prograded across Oregon and Washington, filling the gaps between the seamounts. Isolated, but active volcanic centers developed within the prograding delta system, leading to eruption of the basalt to andesitic Tukwila and Northcraft Formations (Fig. 2). Marine shales and siltstones of units such as the McIntosh and Raging River Formations (Snavely and others, 1958) formed the basement for this deltaic system. The Cascades magmatic arc was the source of voluminous felsic lavas and ash flows of Oligocene age like the Ohanapecosh Formation that filled a continental depression in the area of the present Cascades and eastern Puget Lowland (Fig. 2). The Miocene Columbia River Basalt Group (Fig. 2) erupted from 17 to 6 m.y.b.p. (McKee, Swanson, and Wright, 1977), flooding the continental-sediment-filled, backarc basin east

Pre-Tertiary basement rocks of the Cascades include diverse metamorphic, igneous, and sedimentary rocks that comprise several distinct crustal terranes with allochthonous and(or) exotic origins. Final stages of accretion/assembly of these crustal terranes occurred by the Late Cretaceous, after which these rocks formed the "stable framework" of the Washington continental margin. The southernmost exposures of pre-Tertiary rocks in the Washington Cascades occur in the Rimrock Lake inlier (Miller, 1987; Miller and others, 1993), south-southeast of Mount Rainier and about 15 km east of the east end of DOE seismic line 3 (Fig. 3).

Deep Well Information

Several deep wells near the SWCC provide the best information about deeper parts of the Eocene stratigraphic section. The deepest well in the SWCC region is the Phillips State No. 1 (TD 12,920') that was completed east of Tacoma (Fig. 1). The well penetrated alternating sequences of sandstones, siltstones, shale, and coals of the Puget Group, interpreted in a report by Brown and Ruth Laboratories (1982) to be marginal marine facies. The upper 7120 feet of the section contains about 50% sandstone/siltstone and 50% shale. From 7120 to 7660 feet, greenish-gray, volcanic rocks of the Tukwila Formation were encountered. Below 7660 feet shales dominate, traces of coal start to appear, and zeolites fill most of the fractures. Greenish-gray volcanic rocks were also noted at 9320-9540 feet. Below 12,560 feet to TD, the well section consists of 100% shale. The induction electrical log for the Phillips well indicates resistivities for the upper 7200 feet of 40-60 ohm-m. Resistivities decrease rather steadily below this point to 15-20 ohm-m at the bottom of the well. This pattern is to be expected from the changes in the ratio of sandstones to shale; zeolites below 7660 feet also contribute to lowered resistivities.

An organic geochemical study of core and cuttings from the Phillips well (Brown and Ruth Laboratories, 1982) showed that the upper 7800 feet of the well had vitrinite reflectances of approximately 0.4% to 0.6%, whereas the section below this depth had reflectances more typically near 1%. The vitrinite reflectance values of the section below 7800 feet reflect maturity of the organic material compatible with oil generation (Tissot and Welte, 1980). This increase in thermal maturity of the organic material may be due to a thermal pulse connected with the Tukwila volcanic center. Measurable quantities of a high-paraffinic oil were extracted from the interval 7060-7120 and probably migrated in from below the measured section, because the zone in which they were found is thermally immature. The high vitrinite-reflectance values below 7200 feet in the well may increase with depth so that underlying pre- and lower Eocene marine units may be increasingly mature, but this scenario is dependent upon whether the maturation recorded in the Phillips well is indeed due to volcanism from the Tukwila magmatic center (Eocene) and later Cascades plutonism and not just to deep burial. Walsh and Phillips (1983) present evidence from coal rank data for increased thermal maturation associated with the Oligocene to Holocene Cascades magmatic arc. The Phillips State No. 1 well is within 30 km of Mount Rainier, the largest volcanic center in the Cascades, and the combined thermal effect of this

volcano, earlier Cascades vents, and the Tukwila volcanic center was just enough to put the rocks at depths greater than 7200' in the oil window. This observation suggests that the thermal maturation problem must be evaluated carefully.

Oil and gas shows have been documented in other drill holes in the area northwest of Mount Rainier. Mullineaux (1970) describes a large number of oil and gas shows from drilling on the Black Diamond anticline, a small structure sub-parallel to the Carbon River anticline (Figs. 2,3). Mullineaux states that wells in the area of the Black Diamond anticline produced oil and gas shows from all parts of the Puget Group. Although the documented evidence for Mullineaux's statements are not available, a gas well drilled at Flaming Geyser on the Black Diamond anticline produced salt water and continues to produce open flow of minor amounts of methane, although this gas has been thought to be produced largely from coal beds (pers. comm., T. J. Walsh, Washington Dept. of Natural Resources). In addition to hydrocarbon shows from wells in the region, a small oil seep has been noted in the Bear Canyon (Fig. 4) area (Hedges, 1949).

Snavely and others (1958) report on a drillhole of 6000' depth in the Tenino area that penetrated the complete section of Puget Group rocks and an extensive section of the McIntosh Formation. No information is available on hydrocarbon shows in the well, but it is safe to assume that there were no producible horizons. This well is important because of the stratigraphic information recorded on the McIntosh Formation, to be discussed in a subsequent section. A 10,820' TD well completed in the Chehalis Basin, the Shell Thompson No. 1 (Fig. 4) penetrated 7300 feet of coal-bearing, marginal marine clastic rocks of the Eocene Skookumchuck Formation (Fig. 5) and 3500' of Northcraft volcanic rocks.

A 8200' depth drillhole was completed in September, 1989 by Meridian Oil Company approximately 10 km NE of Morton, WA. Information from this hole is still proprietary, but it is likely that the drill was still in volcanic rocks, because the interpretation of MT profile BB' (Fig. 2) indicates resistivities of about 150 ohm-m to depths of 3-4 km in the vicinity of the drillhole. In addition, the geologic map of Walsh and others (Fig. 3) indicates that the well was drilled in a syncline where it would encounter thick Stevens Ridge or Ohanapecosh Formation volcanic rocks.

The focus of hydrocarbon exploration in western Washington has been largely upon Eocene to Oligocene marine sedimentary systems. The rocks in these basins are mostly too thermally immature to be hydrocarbon sources (Armentrout and Suek, 1985). The search for other sedimentary systems with mature source rocks has brought us to investigate the possibility that proposed sedimentary rocks in the southern Washington Cascades conductor (SWCC) constitute such viable source rocks. In order to evaluate the SWCC as a possible location for hydrocarbon source rocks, it is necessary to evaluate the available constraints upon lithology, thermal history and paleotectonics of the SWCC. We will attempt these tasks in the following sections, and discuss the details of recent seismic reflection data as they relate the SWCC anomaly. However, to understand essential stratigraphic controls that are needed to interpret the geophysical data, we will begin with a detailed discussion of the nearby Chehalis Basin.

CHEHALIS BASIN

The Chehalis basin is a ~500-600 km^2, three-sided depression of Quaternary sediments bounded to the north, west, and southeast by bedrock uplifts (Fig. 4). We discuss this basin in detail because it provides key stratigraphic information needed to understand the SWCC and details of the main hydrocarbon play identified in the

Figure 5- Stratigraphic correlation chart for Eocene and Oligocene rocks in four areas of southwest Washington. Based on Snavely and others (1958), Gard (1968), Vine (1969), Rau and others (1983), Wells and Rau (1983), and Johnson (1992, unpublished data).

Morton antiform (to be discussed in later stages of the report). The Chehalis basin is bounded to the north and separated from the Puget Lowland by an uplift of Paleogene rocks that extends eastward from the Centralia-Chehalis area to Bear Canyon. The

Figure 6- Schematic north-south cross section A-A' across the western Chehalis basin. Line of section is shown in Figure 4.

Willapa Hills, on the west flank of the Chehalis basin, are underlain by Paleogene and minor Neogene rocks. The southeast flank of the basin, underlain by Paleogene volcanic rocks and Neogene sedimentary strata, extends from Vader to the Bear Canyon area. Two large rivers, the Cowlitz and the Newaukum, flow west out of the Cascades and across the Chehalis basin. Geologic relationships in the Chehalis basin and on its northern, western, and eastern flanks are shown in the schematic cross sections of Figures 6, 7, and 8. These schematic cross sections are based largely on data from outcrop and borehole studies, seismic reflection profiles, and magnetotelluric surveys. We use the stratigraphic chart of Figure 5 as a guide to the interpretation.

Schematic Cross Section AA'

Schematic cross section A-A' (Fig. 6) extends south from Chehalis to Olequa, across the west flank of the Chehalis basin. The cross section roughly parallels Lauren seismic reflection profile A2-1. Geologic control is provided by outcrops near Centralia and Chehalis and in the eastern Willapa Hills, and by analysis of samples and logs from the Shell Sturdevant No. 1, Shell Zion No. 1, and Earl F. Siler and J.W. Tanner Kostick No. 1 boreholes (W.W. Rau, written commun. to Johnson, 1992, and S.Y. Johnson, this study).

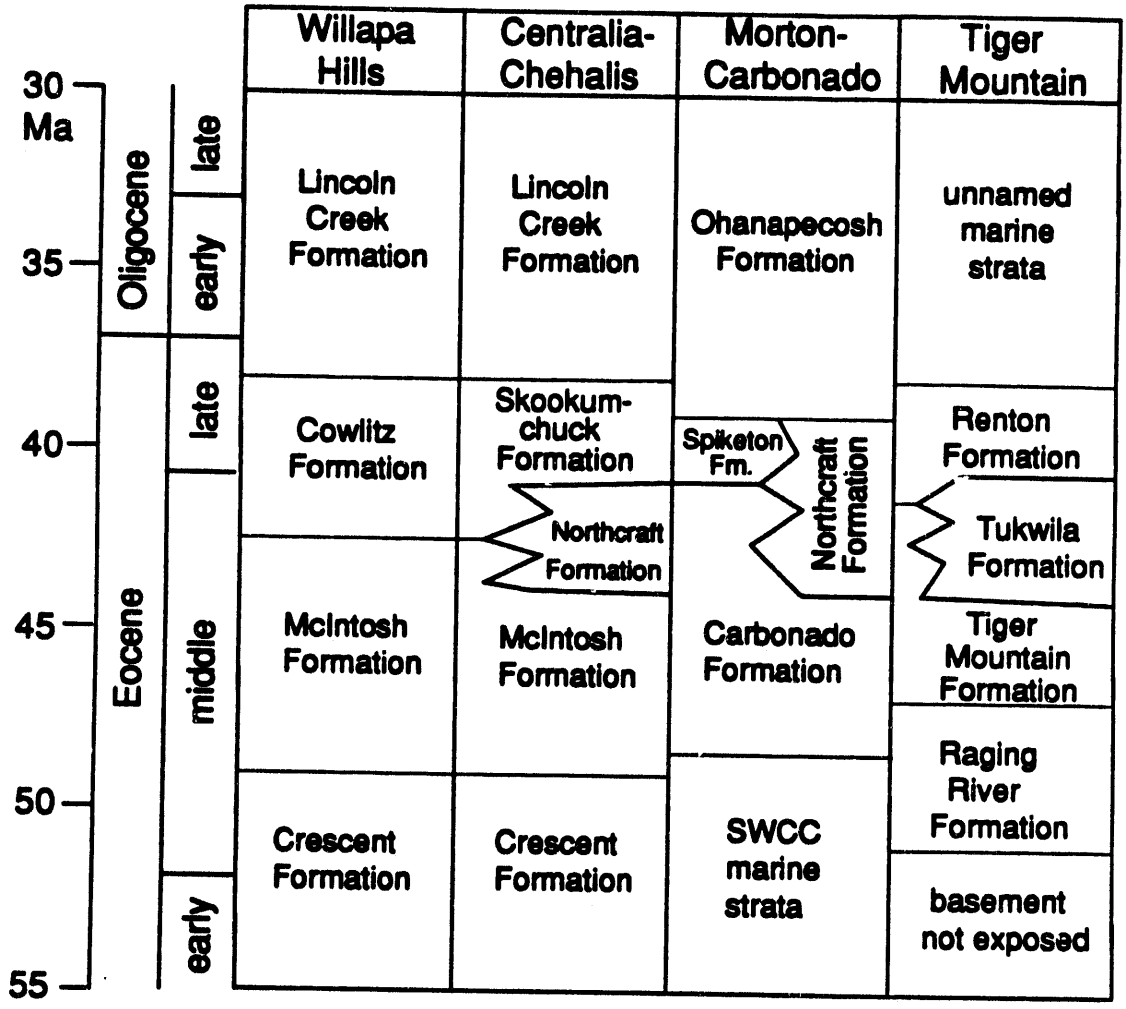
30
Ma
35
40
45
50
55
Oligocene
Eocene
late
early
late
middle
early
Willapa Hills
Centralia-Chehalis
Morton-Carbonado
Tiger Mountain
Lincoln Creek Formation
Lincoln Creek Formation
Ohanapecosh Formation
unnamed marine strata
Cowlitz Formation
Skookum-chuck Formation
Spiketon Fm.
Northcraft Formation
Renton Formation
Northcraft Formation
Tukwila Formation
McIntosh Formation
McIntosh Formation
Carbonado Formation
Tiger Mountain Formation
Raging River Formation
Crescent Formation
Crescent Formation
SWCC marine strata
basement not exposed

Figure 5

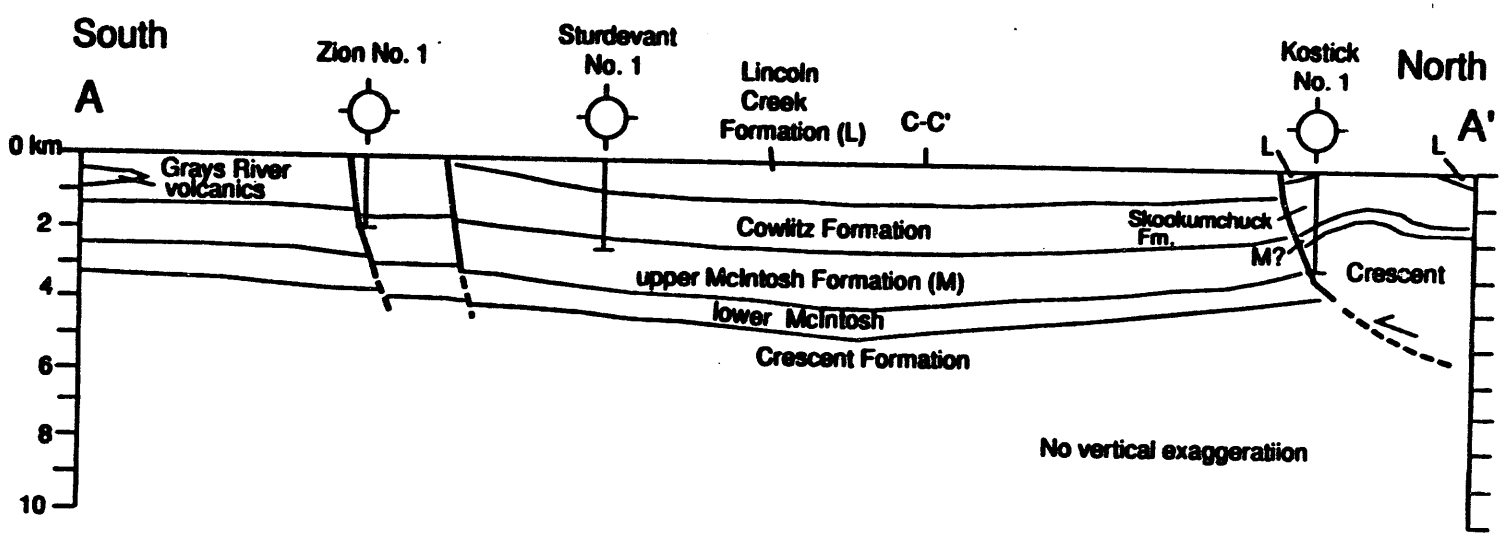
South
A
Zion No. 1
Sturdevant
No. 1
Lincoln
Creek
Formation (L)
C-C'
Kostick
No. 1
North
A'
0 km
2
4
6
8
10
Grays River
volcanics
Cowlitz Formation
Skookumchuck
Fm.
M?
upper McIntosh Formation (M)
lower McIntosh
Crescent Formation
Crescent
L
L
No vertical exaggeratiion

Figure 6

At its south end, the section above the Crescent Formation basaltic basement consists of the early Middle Eocene McIntosh Formation and the late Middle to Late Eocene Cowlitz Formation, which includes interbeds of the volcanic rocks of Grays River (Henriksen, 1956; Wells, 1981; Walsh and others, 1987). Using seismic reflection data, Ise (1985) designated part of what is here considered to be the lower McIntosh Formation as "unknown marine sediments". Krehbeil (1993b) adapted Ise's interpretation of the seismic data in a similar cross-section. In making this designation, Ise and Krehbiel correctly pointed out this almost certain marine section pinches out in the subsurface of the Chehalis Basin, is nowhere locally exposed, and has not been penetrated by boreholes. We prefer to designate these strata as a lower part of the McIntosh Formation, keeping with established stratigraphic nomenclature for rocks overlying the Crescent Formation elsewhere in southwest Washington (e.g., Wells and Rau, 1983; Rau and Armentrout, 1983; Rau and others, 1983).

To the north in the west-central part of the Chehalis basin, the Cowlitz Formation is overlain by a section as thick as about 500 m consisting of mainly Oligocene marine rocks of the Lincoln Creek Formation and lesser Quaternary strata. Basinal strata dip very gently into the center of the basin where Oligocene and younger strata reach their greatest thickness. Use of stratigraphic nomenclature for late Middle to Late Eocene sedimentary rocks changes at the northern basin margin; Cowlitz Formation-equivalent rocks are assigned to the Skookumchuck Formation in the Centralia-Chehalis area (Fig. 5) following Snavely and others (1958) and Rau and others (1983).

The northern end of schematic cross section A-A' shows a thrust fault along the northern basin margin. This fault is a continuation of a structural zone that forms the south flank of the Doty Hills to the west and is here referred to as the Doty fault. Based on interpretation of seismic reflection data, the block north of the Doty fault is characterized by a decreased depth to Crescent Formation basement and a much thinner Eocene section than in the Chehalis basin. This relationship suggests that the block north of the Doty fault was part of an Eocene basement high. We infer that this high was part of a basaltic seamount centered in the Black Hills to the north, where the Crescent is overlain by the Oligocene Lincoln Creek Formation and Eocene sedimentary rocks are absent. Eocene sedimentary rocks may have originally thinned over this uplift in the same way that they thin and pinch out over the Willapa Hills volcanic high of Crescent Formation on the southwest margin of the basin (see schematic cross section B-B'; Boswell and others, 1988; Ise, 1985). The amount of vertical displacement on the Doty fault (about 1700 m) shown on the cross section thus probably reflects a combination of faulting and original basement topography. Faulting is Eocene and younger in age.

Schematic cross section B-B'

Schematic cross section B-B' (Fig. 7) extends east through the eastern Willapa Hills from the Ryderwood area to Vader; then northeast along the Cowlitz River into the southern part of the Chehalis basin; then north into the central part of the basin. The western three-quarters of the cross section roughly parallels the western part of

Figure 7- Schematic southwest-northeast cross section B-B' through part of the Chehalis basin. Line of section is shown in Figure 4.

Lauren seismic reflection profile A2-3. Geologic control is provided by outcrops in the eastern Willapa Hills, and by analysis of samples and logs from the Shell Thompson No. 1, Humble Oil and Refining Company Roscoe B. Perry No. 1, and the Selburn-Washington Oil Corporation Wulz No. 1 boreholes (W.W. Rau, written commun. to Johnson, 1992, and S.Y. Johnson, this study). Boswell and others (1988) have described seismic facies on the western portion of the Lauren seismic line, which parallels this section. Krehbiel (1993b) used all of Lauren A2-3 line in a regional schematic cross section that extends from the Willapa Hills into the central Cascade Mountains.

As in line A-A', the stratigraphy above Crescent basement in the eastern Willapa Hills and southern Chehalis basin consists of the lower McIntosh Formation (unknown marine sediments of Kreihbiel, 1993), the upper McIntosh Formation, the Cowlitz Formation, the Lincoln Creek Formation, and a thin layer of Miocene to Quaternary sediment. Both McIntosh units onlap the Crescent basement in the Willapa Hills, indicating this area formed an Eocene basement high attributed to seamount topography at the top of the Crescent Formation. From the Willapa Hills, Crescent basement dips gently northeast into the central part of the Chehalis basin.

Use of stratigraphic nomenclature in this section changes from southwest to northeast across the line based on the appearance of the volcanic Northcraft Formation at the stratigraphic level of the upper McIntosh Formation (Fig. 5). Following Snavely and others (1958) and Rau and others (1983), strata above the Northcraft at approximately the same stratigraphic level as the Cowlitz Formation are referred to as the Skookumchuck Formation. By stratigraphic convention (Snavely and others, 1958; Rau and others, 1983), strata below the Northcraft are assigned to the McIntosh Formation. The cross section compiled by Krehbiel (1993b) along the same transect violates this convention by designating considerable strata below the Northcraft as part of the Skookumchuck Formation. The proportion of volcanic rocks of the Northcraft Formation increase to the north and northeast, reflecting proximity to Northcraft volcanic centers (Hagen, 1987). In addition, Krehbiel (1993b) interpreted Lower Oligocene volcanic rocks of the Goble Formation to occur above the Skookumchuck Formation in the central part of the Chehalis Basin. This occurrence is unlikely, since the vents for the Goble Formation are considerably further to the south, near the Columbia River.

Schematic cross section C-C'

Schematic cross section C-C' (Fig. 8) is a regional line that extends east across

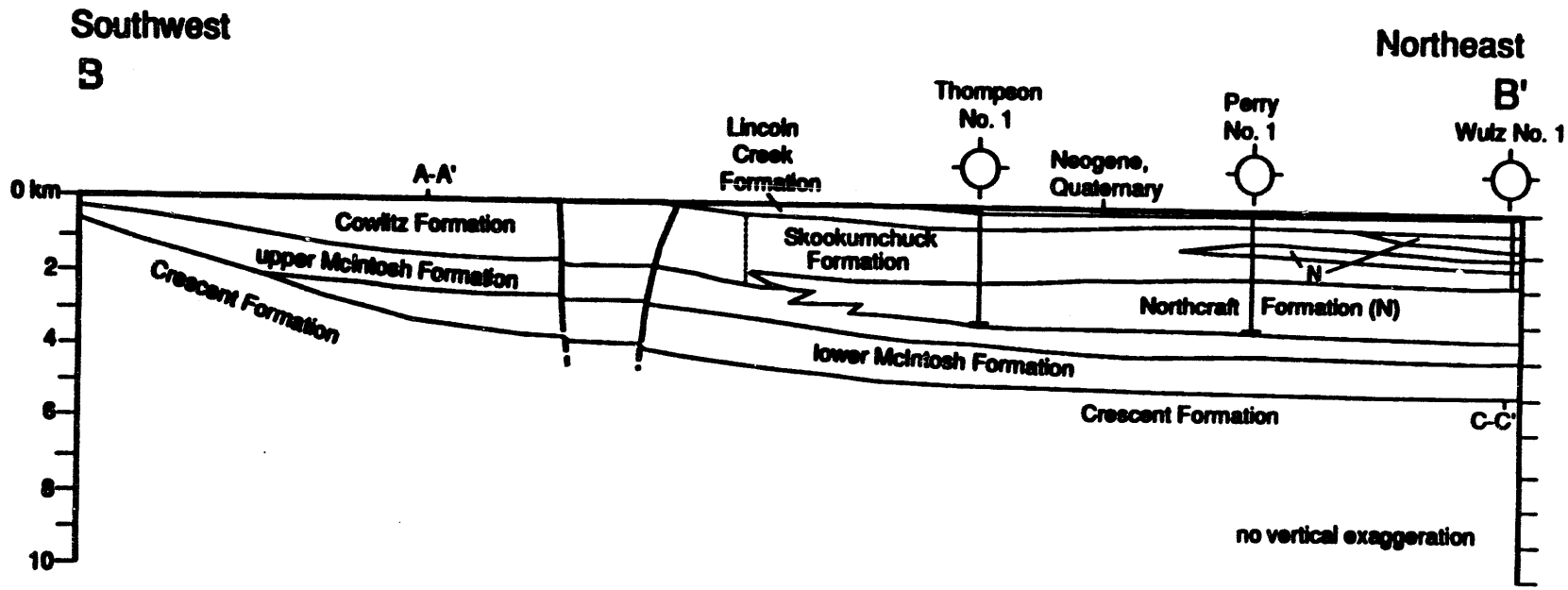
Southwest
B
Northeast
B'
Thompson No. 1
Perry No. 1
Wutz No. 1
Lincoln Creek Formation
Neogene, Quaternary
A-A'
0 km
2
4
6
8
10
Cowlitz Formation
upper McIntosh Formation
Crescent Formation
Skookumchuck Formation
N
Northcraft Formation (N)
lower McIntosh Formation
Crescent Formation
C-C'
no vertical exaggeration

Figure 7

the entire Chehalis basin to the Morton antiform. The cross section roughly parallels the eastern part of Lauren seismic reflection profile A2-4, and DOE line 4 (Figs. 2, 3)

Figure 8- Schematic west-east cross section C-C′ across the Chehalis basin and into the Cascade foothills to Morton. Line of section is shown in Figure 4.

Geologic control is provided by outcrops on the northern margin of the Chehalis basin, along the Tilton River, and in the Morton antiform, and by analysis of samples and logs from the Everett Trust and Savings Bank Trustee No. 1 and the Selburn-Washington Oil Corporation Wulz No. 1 boreholes (W.W. Rau, written comm. to Johnson, 1992, and S.Y. Johnson, this study). Ise (1985) constructed a cross section of the Chehalis Basin slightly to the south using the Lauren A2-3 data and Krehbiel (1993b) adapted Ise's interpretation combined with interpretations of DOE 1 and 2 seismic lines. We think that geologic and geophysical controls are far better along our line C-C′, particularly in the area corresponding to the eastern part of Lauren A2-3, because data quality on the eastern end of the Lauren profile was very poor. The western part of this line intersects schematic cross sections A-A′ and B-B′ (Figs. 7,8).

The geology of the Chehalis basin on the western end of line C-C′ is similar to that described on lines A-A′ and B-B′. Strata are relatively horizontal and cut by a few smaller faults, and a change in stratigraphic nomenclature is shown based on the presence of the volcanic Northcraft Formation. In the eastern part of the Chehalis basin, basinal strata are cut by a series of high-angle faults. These faults appear to line up with both northwest- and northeast-trending structures mapped by Schasse (1987) and Walsh and others (1987) at and west of Bear Canyon. Cumulative east-side-up displacement on these structures is inferred to be about 2,000 to 2,500 m, based on offset of the presumed base of the Northcraft Formation. Faults clearly imaged on DOE line 4 occur at about CDP's (common-depth-point) 12510, 12200, 11940, and 11300. The gray-scale amplitude plot of the complete profile is shown in

Figure 9-Gray scale amplitude plot of seismic data from DOE line 4.

Figure 9 and details of the data at the CDP's where faults were interpreted are shown in Figure 10. A discussion of processing and display procedures for the seismic data appears in a later section, but we introduce line 4 at this point because of its importance to the stratigraphic interpretation. Between the noted structures on the seismic line, there is a combination of noise interspersed with panels of coherent reflectors. The inferred uplift of Crescent basement within this zone corresponds

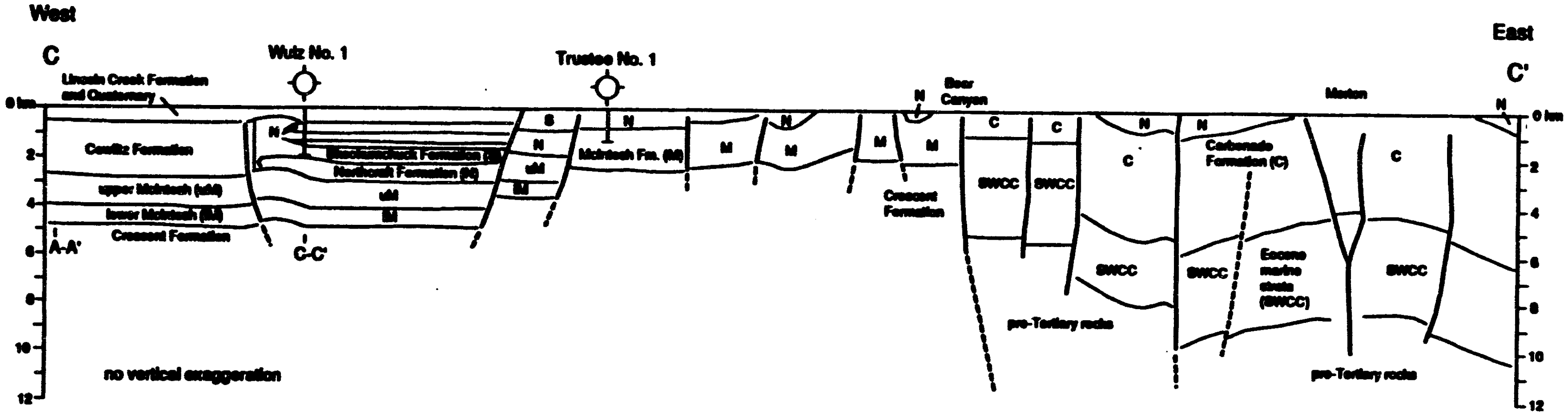
West
C
Wulz No. 1
Trustee No. 1
East
C'
Crescent Formation
A-A'
C-C'
no vertical exaggeration
Bear Canyon
Crescent Formation
Carbonado Formation (C)
Eocene marine strata (SWCC)
SWCC
pre-Tertiary rocks
0 km

Figure 8

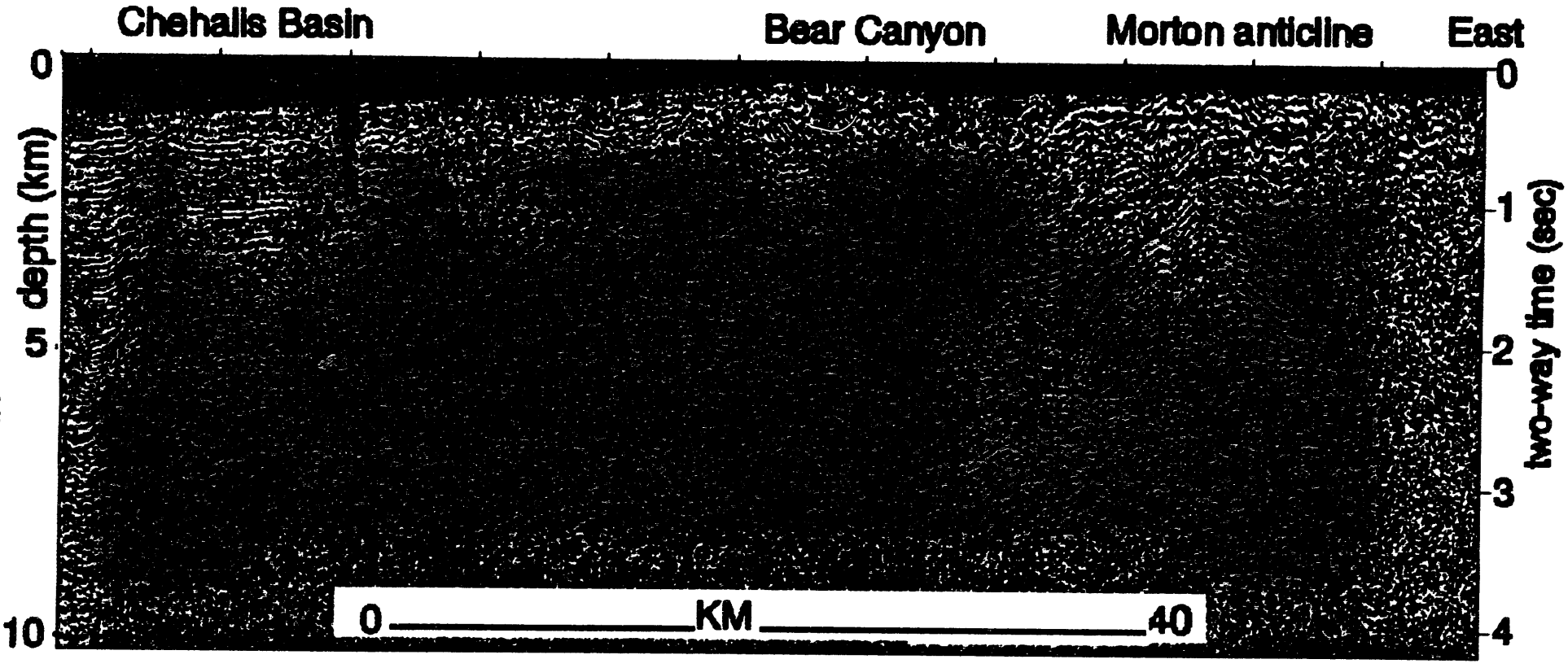
Chehalis Basin
Bear Canyon
Morton anticline
East
0
5
10
depth (km)
0
1
2
3
4
two-way time (sec)
0
KM
40

16b

Figure 9

roughly to the horst-like uplifts of Crescent basement shown by Stanley and others (1992) on their lines A-A' (MT sounding 22) and E-E' (MT sounding 13) based on magnetotelluric
data.

East of this network of faults, DOE line 4 images the crustal boundary between uplifted basement of the Chehalis Basin (Crescent Formation) and unknown basement of the main part of the SWCC to the east. This boundary occurs in the Bear Canyon area. From aeromagnetic and gravity interpretation, the Crescent basement is inferred to extend some distance beneath the Morton antiform in the SWCC, but the actual basement beneath most of the SWCC is unknown. A deep, west dipping set of reflections may image the base of this basement slice, suggestive of a thrust wedge bounding the Morton antiform on the west side. In a later section, we will point out that this thrust is apparently seismically active and may interact in a complex manner with other regional faults.

East of this uplifted margin of the Chehalis Basin, the upper 3-4 km of strata

Figure 10a,b,c-Details of seismic data at CDP's on line 4 referenced in text.

beneath the Northcraft Formation are nonmarine and deltaic in origin (see section on the Morton antiform) and more similar to the Carbonado Formation to the north in the Carbon River antiform (Figs. 2, 3; Gard, 1968) than to the McIntosh Formation to the west. Strata beneath the Carbonado Formation and above pre-Tertiary basement are inferred marine strata based on magnetotelluric data (Stanley and others, 1992) and are probably contemporaneous with the Crescent Formation (see discussion of the Morton antiform below). These rocks are referred to on the schematic cross section as part of the SWCC.

The net displacement across the transition zone from the Chehalis Basin to the Morton antiform is east-side down, however much if not all of the displacement occurred before deposition of the Northcraft Formation. There are no markers to quantify displacement. Offset of the basement cannot be used because much of the SWCC part of the basin fill on section CC' is probably contemporaneous with the Crescent Formation basement of the western crustal block (Fig. 8). There are numerous faults within the eastern crustal block, some of which have clear reverse or thrust displacement (for example, in the Morton antiform). These faults, which originated as normal faults during Eocene transtensional deformation and basin subsidence, have no doubt been reactivated throughout the Cenozoic.

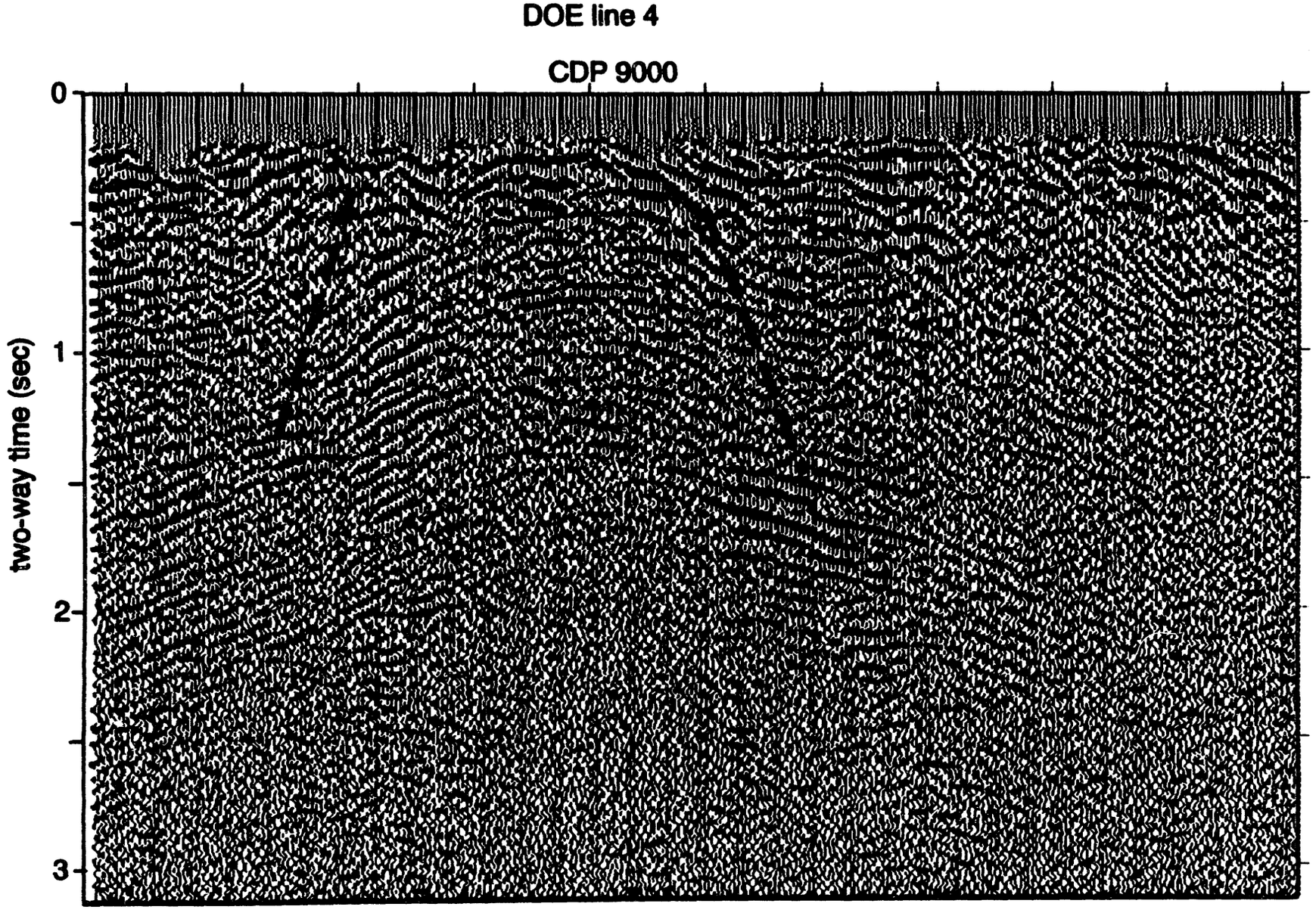

Figure 10a

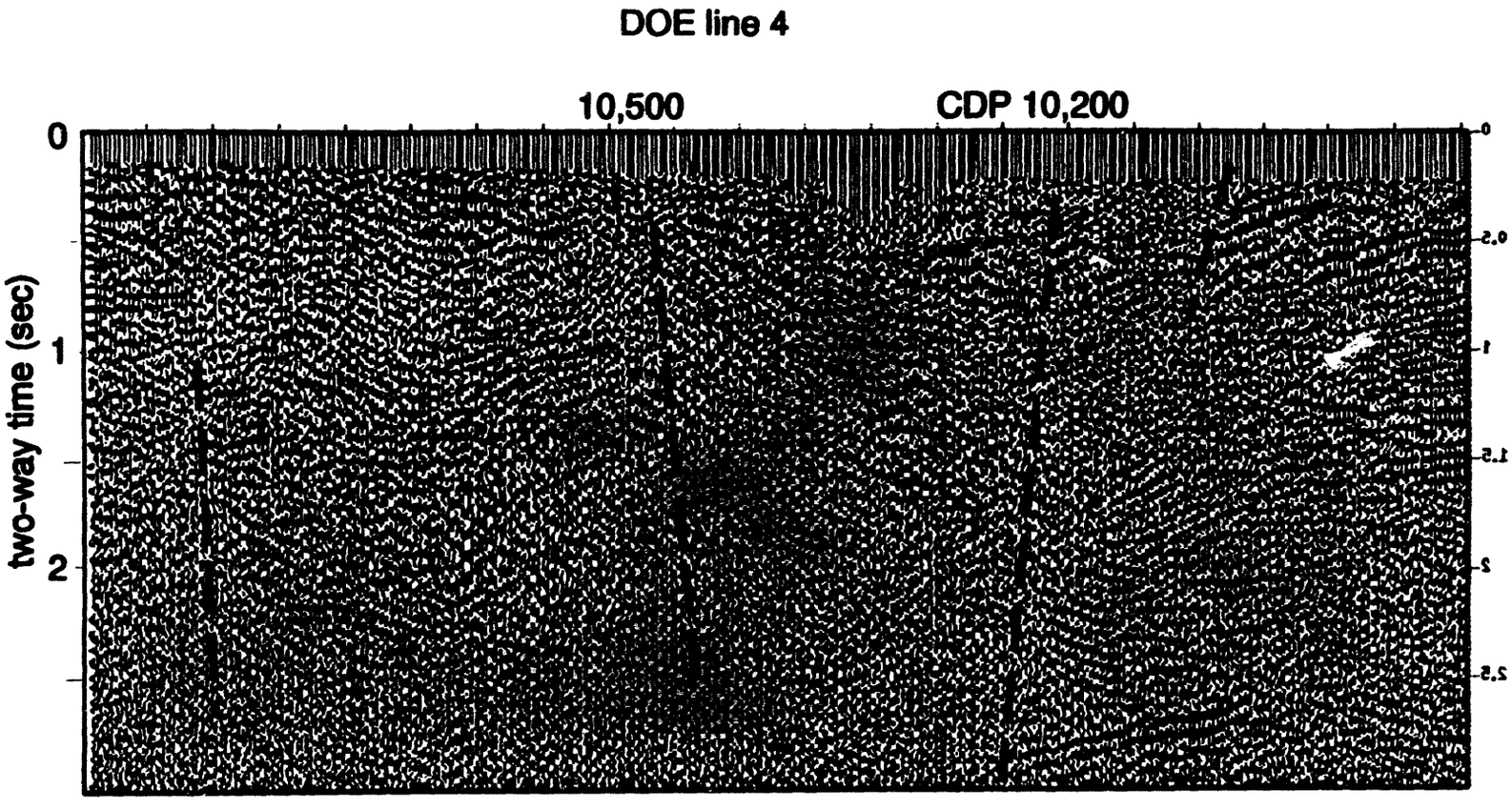

Figure 10b

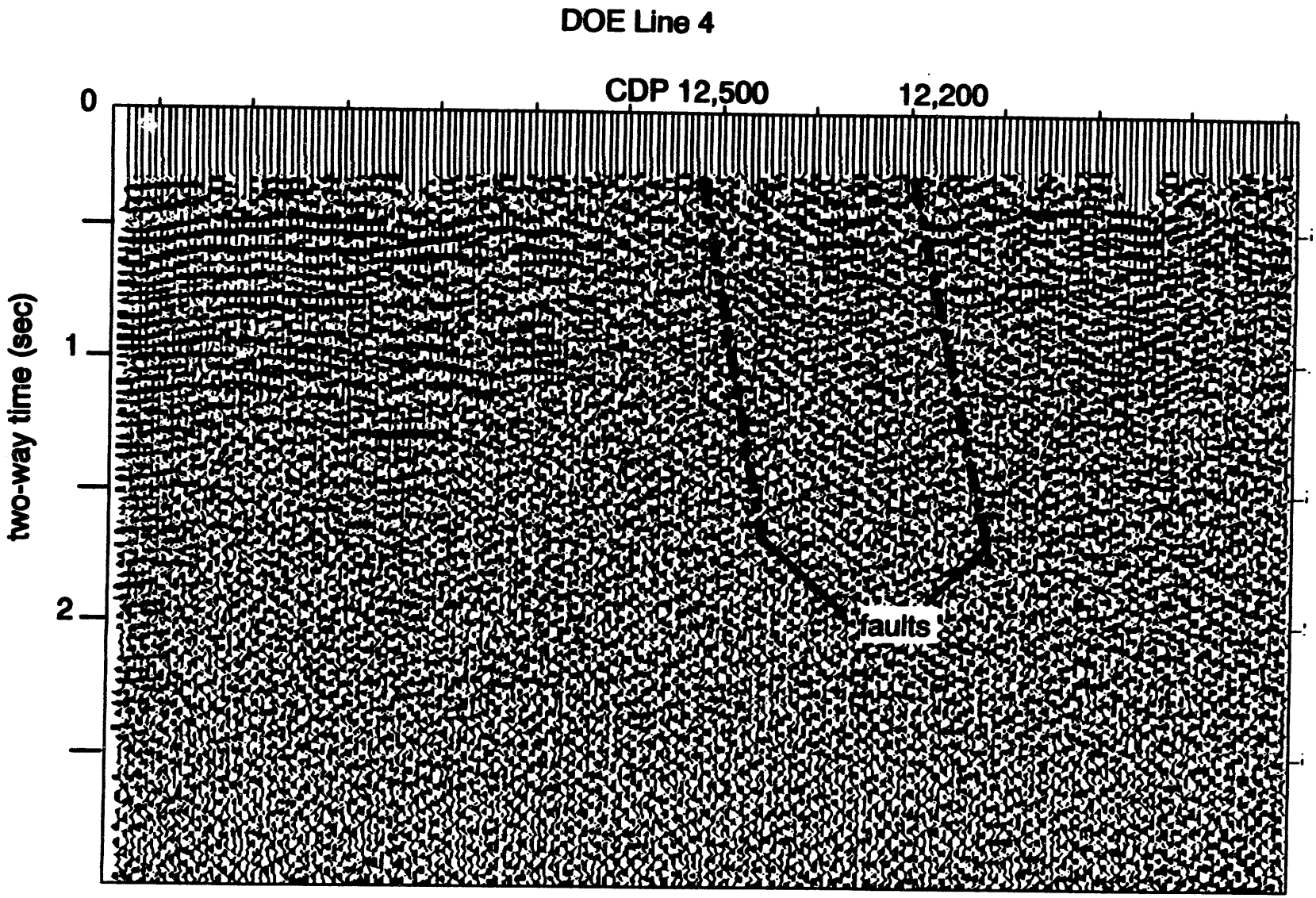

Figure 10c

MAGNETOTELLURIC RESULTS

Three regional MT model cross-sections are shown in Figure 11 and a detailed model of the Morton area in Fig. 12 (locations of profiles in Fig. 2). These profiles represent one-dimensional (layered) interpretations of MT soundings done in the region of the SWCC, but two-dimensional interpretations of profiles AA' and CC' have also been completed, as described in Stanley and others (1987). The two-dimensional models provide more accurate constraints on deeper structures, such as the base of the conductive SWCC units (2-5 ohm-m resistivities) on profiles CC' and AA', but the upper surface configuration of the SWCC is more accurately determined on the one-dimensional models. In two-dimensional modeling using finite-element algorithms, it is impractical to model all aspects of the geology in the upper few kilometers because of the requirement for a very large model-grid; thus, most of our discussion will center around details of the one-dimensional models as they relate to structure on the upper surface of the SWCC.

Units of 30-500 ohm-m from the surface to depths of 5 km on the model for

Figure 11-MT model sections based upon one-dimensional modeling for profile AA'(a), BB'(b), and CC'(c) (locations in Fig. 3). Interpreted resistivities for the various model layers are indicated by the patterns in the explanation. OLP=Olympic Peninsula, CR=Carbon River anticline, NC=North Cascades, PB=Puget Lowland Basin, MA=Morton anticline, SM=Skate Mountain anticline, CB=Chehalis Basin, GR=Goat Rocks pluton, CRP=Columbia River Plateau. Numbered, inverted triangles are MT sounding locations. Vertical exaggeration is 1:1.

profiles AA' and BB' (Fig. 11) largely correspond to volcanic rocks of the Eocene Northcraft Formation the Oligocene Ohanapecosh Formation and the Miocene Stevens Ridge Formation (Vance and others, 1987). Very thick units with resistivities of 100-500 ohm-m, averaging about 150 ohm-m on the west ends of profiles AA' and CC' correspond to gravity and magnetic highs and were interpreted by Stanley and others (1987) to be made up of Siletzia seamounts or other oceanic basalts. Wannamaker and others (1989) interpreted that equivalent oceanic basalts in the Oregon Coast Range had resistivities of about 100 ohm-m or slightly less. Rocks with resistivities of 500-5000 ohm-m that reach within 2 km of the surface on the east end of profiles AA', BB', and CC' correspond to Tertiary plutons and North Cascades crystalline

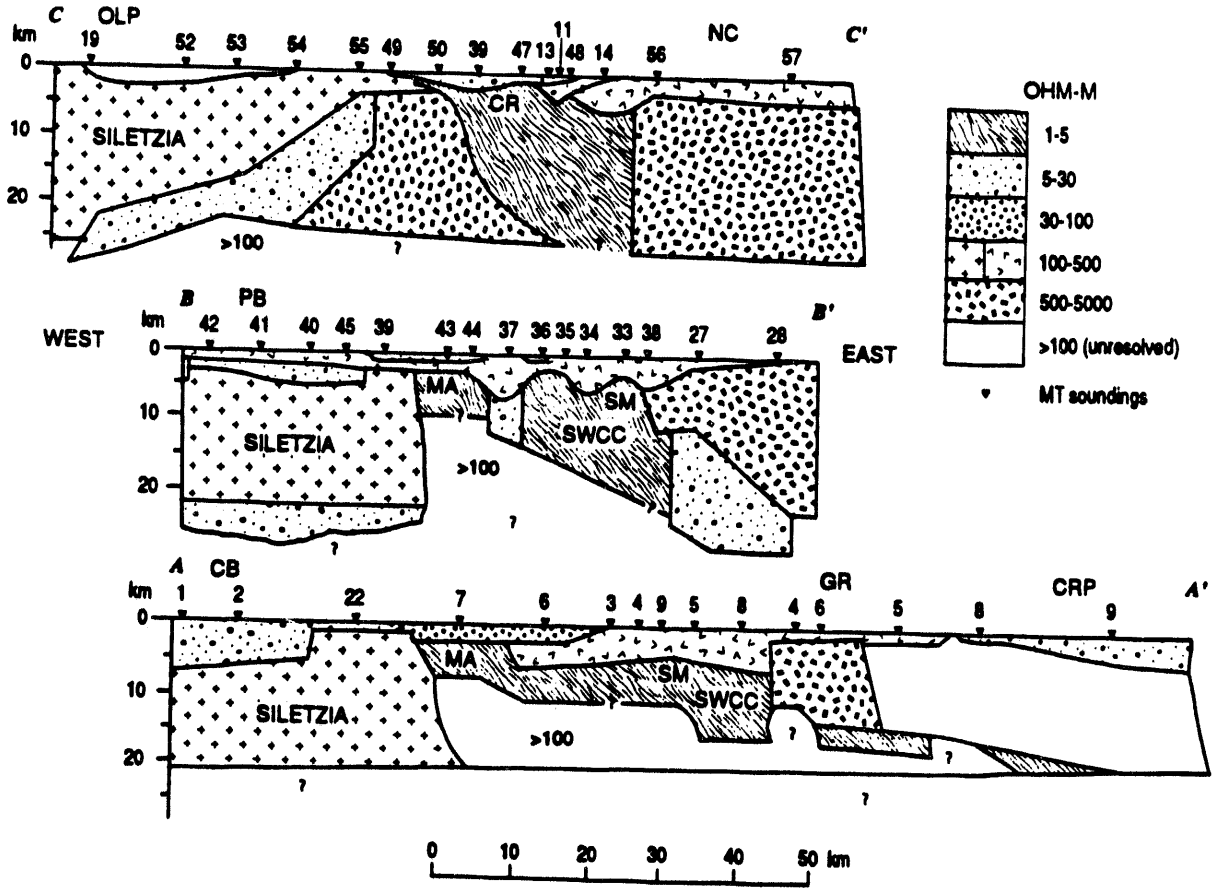

Figure 11. MT model sections based upon one-dimensional modeling for profile AA'(a), BB'(b), and CC'(c) (locations in Fig. 3). Interpreted resistivities for the various model layers are indicated by the patterns in the explanation. OLP=Olympic Peninsula, CR=Carbon River anticline, NC=North Cascades, PB=Puget Lowland Basin, MA=Morton anticline, SM=Skate Mountain anticline, CB=Chehalis Basin, GR=Goat Rocks pluton, CRP=Columbia River Plateau. Numbered, inverted triangles are MT sounding locations. Vertical exaggeration is 1:1.

rocks. It is not clear what high resistivity units beneath soundings B55 to B39 on profile CC' signify; they may represent intrusions connected with Siletzia or younger intrusions, probably of Oligocene or Miocene age. The most significant feature of the three MT profiles is the thick, conductive section with resistivities of 1-5 (averaging about 3) ohm-m. The top surface of this conductive package (SWCC) occurs at depths of only 1-3 km near the axis of the Carbon River (profile CC', station 47), Skate Mountain (profile BB') and Morton (profile AA', stations 3 and 7, and profile EE') antiforms. The conductive rocks also appear to crop out west of Morton in the Bear Canyon area where they are represented by marine sandstones and siltstones of the McIntosh Formation (Fig. 8). Because of the large thickness and low resistivity of the conductive section, all of the MT soundings did not penetrate to its lower boundary, but enough did so to enable approximate modeling of the lower surface. Resistivities beneath the conductive section are poorly determined, but must be greater than 100 ohm-m. It is apparent from the MT sections of Figure 11 that the SWCC units are thicker and less laterally extensive on profile CC' than to the south on profiles AA' and BB'; this geometry is interpreted to be due to greater horizontal compression on the north end of the proposed sedimentary sequence.

A layered model for detailed MT profile EE' is shown in Figure 12. The thick conductive (3-6 ohm-m) section on the west end of the profile becomes shallower near Bear Canyon, where Eocene marine rocks of the McIntosh/Carbonado Formation crop out. The McIntosh/Carbonado Formation (Hedges, 1949; Snavely and others, 1951) is overlain by nonmarine Puget Group sedimentary units (20-80 ohm-m) and Northcraft Formation volcanic rocks (100-300 ohm-m). We interpret the section of conductive rocks (3-6 ohm-m) as contemporaneous with, and older than, the Carbonado Formation (see cross-section in Fig. 8) and equivalent to the 1-5 ohm-m section on the models of Fig. 11. The high-resistivity (>1000 ohm-m) units beneath sounding 13 may correspond to Oligocene to Miocene intrusive units that crop out 12 km west of Bear Canyon (Walsh and others, 1987), but probably is related to massive mafic units

Figure 12-Magnetotelluric 1D-model cross-section EE' (Fig. 2). Numbers in the cross-section are interpreted resistivities for the model layers and numbered, inverted triangles are MT sounding locations. Vertical exaggeration is 1:1. Location of profile shown in Fig. 2.

in the core of the uplifted Crescent basement. The relatively steep contact portrayed between the 1000 ohm-m unit and conductive (assumed McIntosh Formation) units reflects uplift of the Crescent Basement along a fault also mapped in the seismic reflection data (Figs. 8, 9).

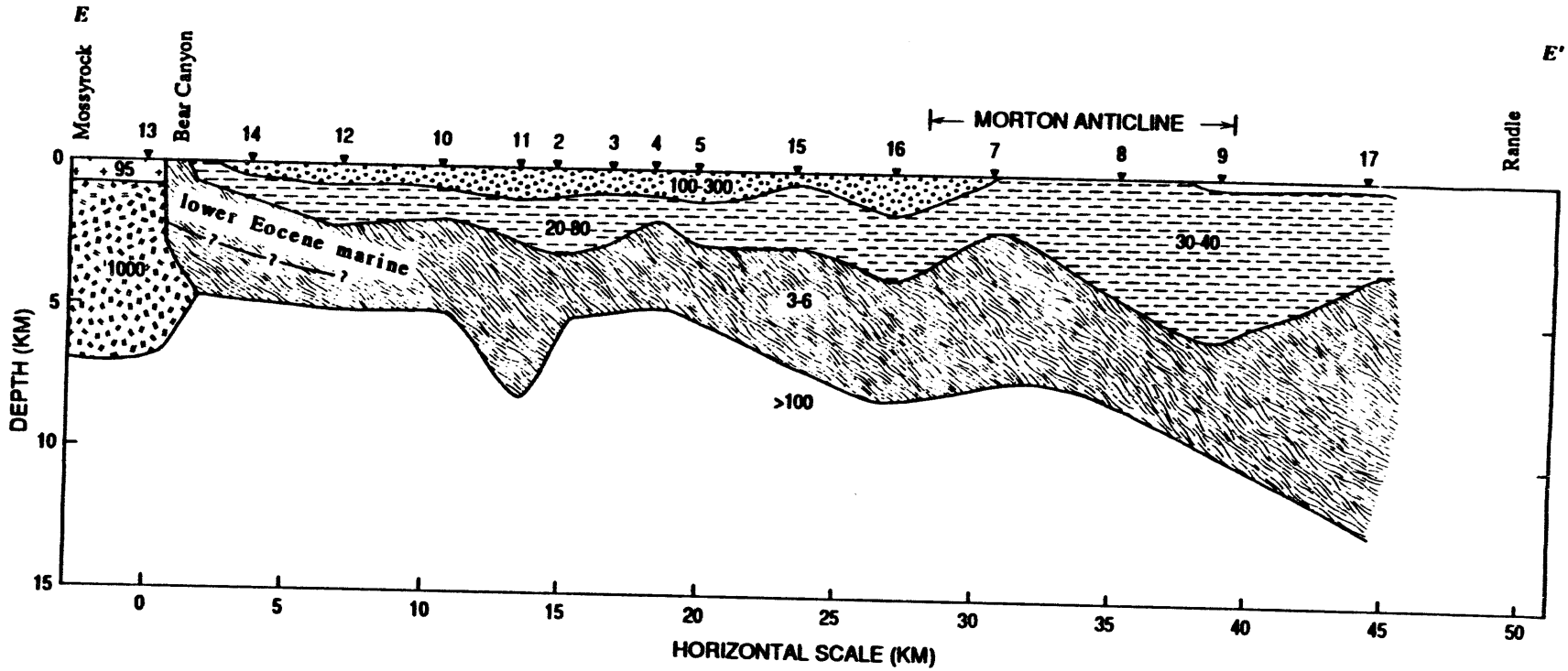
E
E'
Mossyrock
Bear Canyon
MORTON ANTICLINE
Randle
13
14
12
10
11
2
3
4
5
15
16
7
8
9
17
95
1000
lower Eocene marine
100-300
20-80
30-40
3-6
>100
DEPTH (KM)
HORIZONTAL SCALE (KM)
0
5
10
15
20
25
30
35
40
45
50

Figure 12

Gravity and Magnetic Data

Analysis of gravity and magnetic data have played a key role in understanding the nature of the SWCC and related geological units, such as Siletzia, as reported in Stanley and others (1987) and Stanley and others (1992). The mafic units of Siletzia are readily mapped with both gravity and magnetic data and Finn (1989, and in Stanley and others, 1987) has used computer models to calculate the regional boundaries of this units, as well as its thickness and physical properties. The magnetic data are especially useful because of the large magnetization contrasts provided by the Eocene and younger volcanic rocks and Crescent Formation with the sedimentary units, which are very low in magnetization. It was found by that the extension and details of the key antiforms in the region could be mapped with magnetic data, because of the thinning of volcanic rocks over their crests (Stanley and others, 1987; 1992); key faults were also evident in the magnetic data, possibly due to the effects of alteration and offsets of highly magnetic units. For these reasons, a high resolution aeromagnetic survey was acquired under DOE funding (Abrams,

Figure 13-High resolution aeromagnetic map for SWCC region from Abrams (1992).

1992). The data and some of the details regarding faults and antiformal structures are shown in Figure 13. The Skate Mtn. and Morton antiforms are clearly outlined in the

Figure 14-Geologic cross-section compiled by Phillips and others (1989) with an aeromagnetic profile obtained approximately along the seismic profile S1-S3 shown in the upper part of the figure. Bold lines are key reflection packages noted by Stanley and others (1992).

data, as are several key faults, and vents for the Northcraft Formation. Further details are better investigated with profiles from the survey data, as indicated in Figure 14, where an aeromagnetic data profile is displayed from a transect that parallels the DOE reflection lines 1,2, and 3 across the SWCC. The accompanying geological section (from Walsh, 1989) reveals that the details of the magnetic data are probably related to the thickness of the volcanics, as well as topography where these magnetic rocks were closer to the aircraft level.

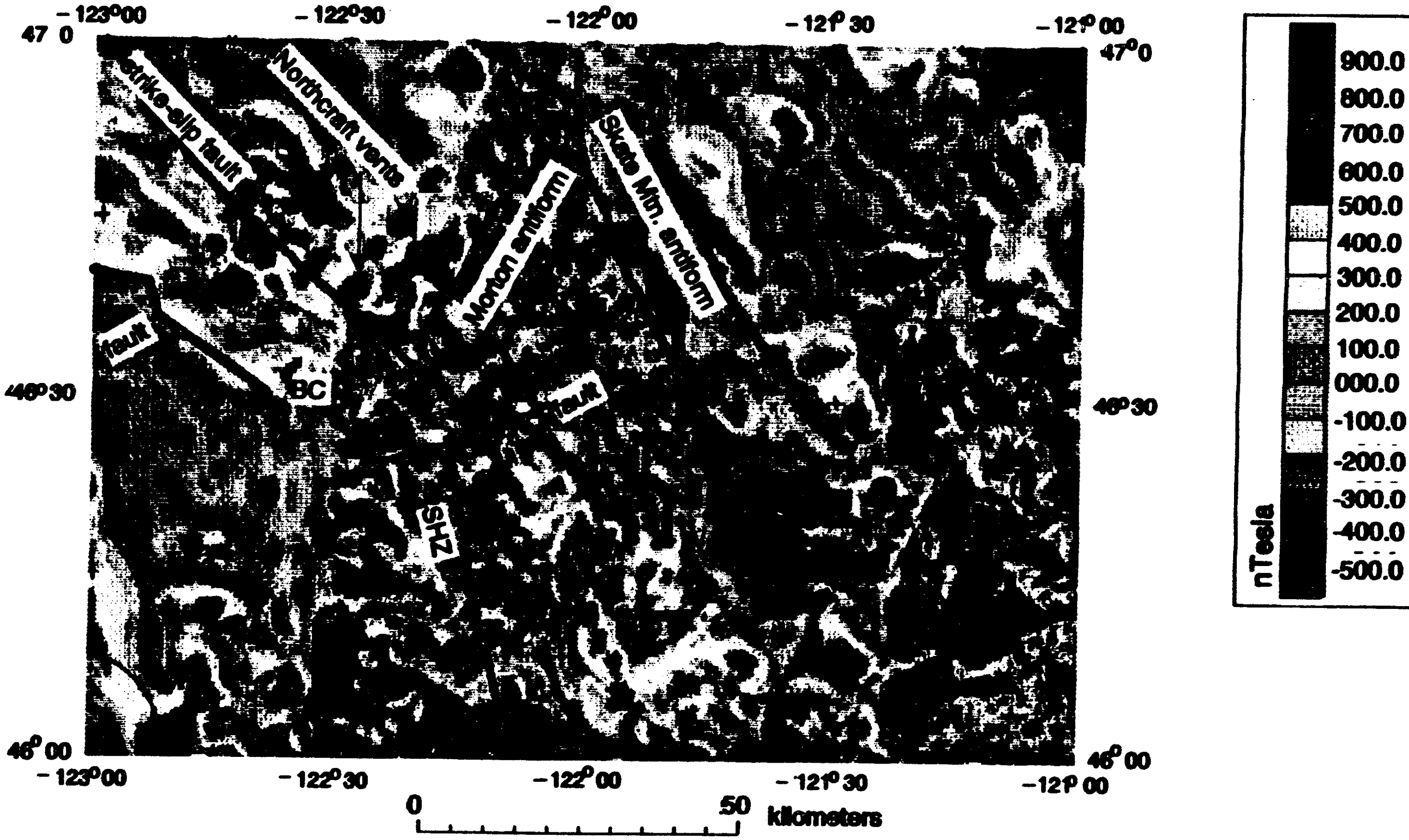

strike-slip fault
Northcraft vents
Morton antiform
Skate Mtn. antiform
fault
BC
fault
SHZ
−123°00
−122°30
−122°00
−121°30
−121°00
47°0
46°30
46°00
0
50
kilometers
900.0
800.0
700.0
600.0
500.0
400.0
300.0
200.0
100.0
000.0
-100.0
-200.0
-300.0
-400.0
-500.0
nTesla

Figure 13

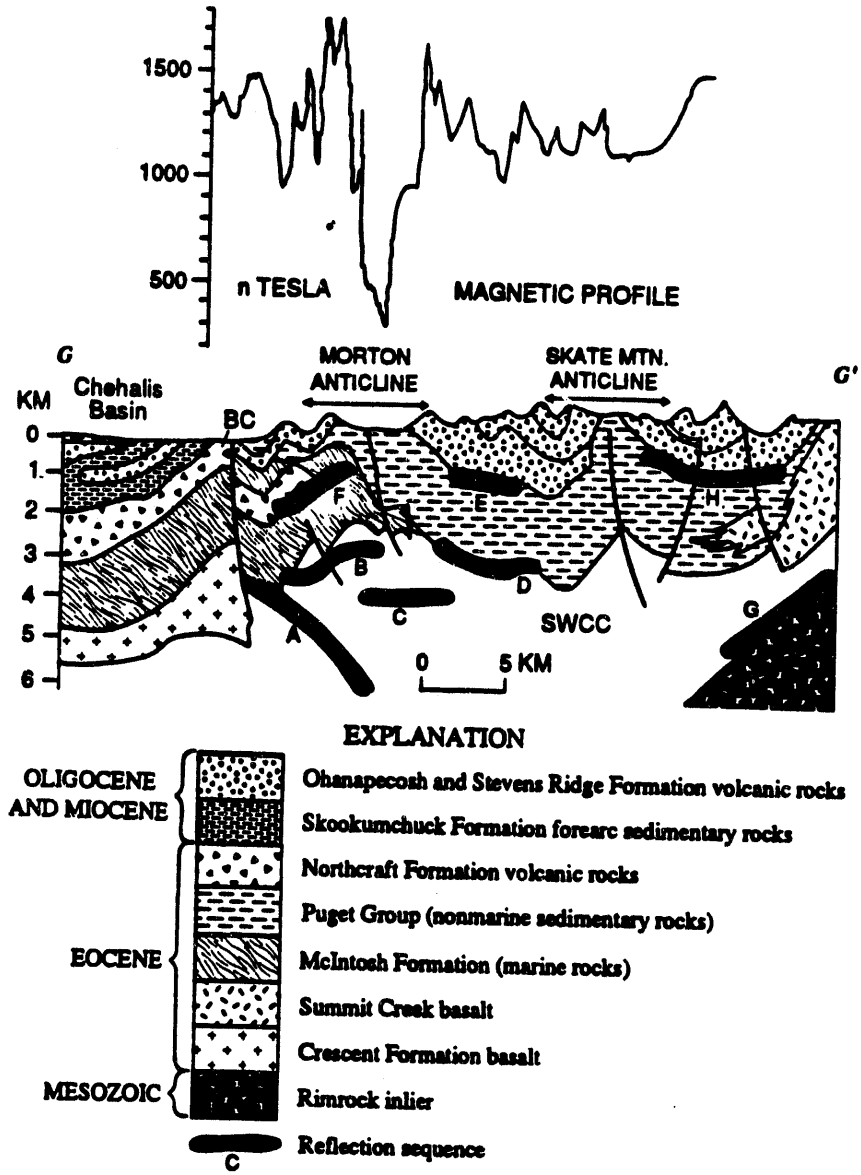

Geologic cross-section compiled by Phillips and others (1989). Added for purposes of this paper are main seismic reflection events (bold dotted lines, A-H) from figure 6. We have added Crescent Formation basement beneath the Chehalis Basin according to our interpretation and that of Ise (1985). Faults (bold solid lines) are from Phillips and others (1989). An aeromagnetic profile flown approximately along the seismic profile S1-S3 is shown in the upper part of the figure.

Figure 14

Channel Name: SJ-92-91
Description: SJ-92-91
Comment 1: good sample
Comment 2: consistent and clean
Comment 3: polish good
Comment 4:
Comment 5:
Comment 6:

	Meas1	Meas2	Ratio	Conc.
Min:	2.06			
Max:	2.40			
Mean:	2.21			
StDev:	0.08			

Pt.	X-Pos	Y-Pos	Z-Pos	Meas1	Meas2	Ratio	Conc.
1				2.18			
2				2.25			
3				2.20			
4				2.19			
5				2.19			
6				2.20			
7				2.19			
8				2.21			
9				2.17			
10				2.34			
11				2.28			
12				2.13			
13				2.12			
14				2.26			
15				2.12			
16				2.09			
17				2.19			
18				2.18			
19				2.27			
20				2.29			
21				2.29			
22				2.22			
23				2.24			
24				2.23			
25				2.21			
26				2.17			
27				2.06			
28				2.12			
29				2.20			
30				2.06			
31				2.40			
32				2.35			
33				2.15			
34				2.20			
35				2.27			

LITHOLOGY OF ROCKS IN THE SWCC

We have hypothesized (Stanley and others, 1992) that the conductive units of the SWCC are composed largely of marine sedimentary rocks based upon several observations:

(1) Interpreted resistivities of the SWCC units are about 2-5 ohm-m in most locations. These resistivity values are very typical of marine shales and shaley sandstones, as evidenced in MT soundings and well logs from Tertiary basins to the west of the SWCC region. Resistivities of nonmarine and transitional-marine sedimentary units are in the range 15-60 ohm-m in the few deep wells in the SWCC region, including the Phillips State No. 1 and Shell Thompson wells. Even some shales, such as in the marginal-marine Carbonado Formation in the bottom of the Phillips State No. 1, are not as low in resistivity as Tertiary marine units found further to the west (Cowlitz Formation, for example), as determined by wells logs and MT soundings in the Mist gas field and Chehalis basin. We assume this is due to the fact that the Carbonado Formation sampled has been flushed of marine brines in the highly disturbed environment of the Carbon River anticline and the Cowlitz Formation occurs in a stable basin environment where marine waters are still in place.

(2) Shallow depths to the conductive rocks correlates well with the location of antiforms cored with transitional marine facies of the Puget Group and marine units such as the McIntosh Formation. In addition, the conductive rocks appear to surface near Bear Canyon (Fig. 4,12) coincident with outcrops of the McIntosh Formation. There is broad evidence in recent studies for an extensive marine depositional period during and before the McIntosh Formation deposition (see discussion below on the Morton antiform).

(3) Ise (1985) used reflection data from a profile paralleling the Toutle River in the Chehalis Basin to demonstrate approximately 11,000' of additional reflective rocks beneath the bottom of a deep (10,000' TD) well near Toutle. The well had bottomed in the McIntosh Formation. Ise interpreted these reflectors to be sedimentary rocks of the McIntosh and older formations, and assumed about 5000' of this unmapped section to be the McIntosh Formation and the remainder of the sections to be older units.

ALTERNATE LITHOLOGIES FOR SWCC UNITS

Nonmarine Sediments

North and east of the SWCC region, a number of fault-bounded basins are filled with thick nonmarine sediments (Johnson, 1985; Evans and Johnson, 1989). These fault-bounded, or pull-apart (Mann and others, 1983) basins are interpreted to have been caused by oblique slip on the Straight Creek, inferred Puget (Johnson, 1984a), Leavenworth, Entiat, and Eagle Creek fault systems (Tabor and others, 1984; Johnson, 1985; Evans and Johnson, 1989). Syntectonic fill of the Swauk, Naches, Roslyn, Chuckanut, and Chumstick Formations in these Washington pull-apart basins is up to 6 km thick and consists of conglomerate, sandstone, shale, fanglomerate, and ironstone (Tabor and others, 1982). Resistivities in these nonmarine sediments are believed to be greater, in most instances, than the 2-5 ohm-m measured for the SWCC and too high to be the cause of the low resistivities in the SWCC. The Swauk, Naches, and Chumstick Formations are contemporaneous with the Puget Group, but strictly nonmarine. There is no surface evidence for marine sediments in any of these pull-apart systems, but older marine sequences related to such basins probably form part of the SWCC. However, some of the thick, nonmarine complex may have been subsequently invaded by marine fluids, especially in the near vicinity of the coastline. Such post-deposition, subsurface invasion by seawater may explain the high salinities recently (Hurst, 1991; Hurst, oral comm., 1993) found in the Chuckanut (nonmarine) Formation in the Bellingham Basin flanking Puget Sound (Fig. 2).

Geothermal Fluids

It is highly probable that low resistivities in deeper parts of the SWCC are partially due to geothermal fluids. Increased ionic mobility due to high-temperature geothermal fluids can increase the conductivity of sedimentary rocks by several hundred percent. The behavior of resistivity with temperature and salinity is well documented (Olhoeft, 1985). Resistivities of porous rocks such as those of the Swauk and Chumstick Formations can be lowered to the 1-3 ohm-m range with formation salinities of 30,000 ppm or greater; such salinities might be present in these nonmarine units if playa conditions existed during phases of basin development, deep brines were forced upward into the section, of if the sedimentary section was subsequently invaded by seawater. For the porosities of less than 10% that would be typical for sandstones at depths of greater than 5 km, a combination of temperatures of about 250°C and salinities of 10,000 ppm would be required to produce the resistivities of less than 5 ohm-m measured in the SWCC. Shale-rich parts of the Puget Group such as the Carbonado and Spiketon Formations (Buckovic, 1979) would have to be influenced less by temperature or increased salinities to be relatively conductive (as required by the SWCC) due to presence of clay minerals in the rocks.

The effect of temperature on resistivity in the SWCC region has been considered thoroughly because of the presence of three major volcanic centers: Mount Rainier, Mount St. Helens, and Mount Adams. Heat flow in the Washington Cascades has been studied by Blackwell and others (1985), who found that temperature

gradients in the region of the SWCC are about 30°C/km; thus, temperatures of 200-300°C might exist in units of the SWCC at depths of 7-9 km. On the east side of the SWCC region, near Packwood (Fig. 3), higher gradients of >50°C/km have been mapped by Barnett and Korosec (1989); thus, even higher subsurface temperatures are expected on this part of the cross-section. However, we believe that the correlation of highs on the top of the SWCC with antiforms that bring Tertiary marine units to shallower depths is an indication that the main cause of the upper part of the SWCC is lithologic in nature. The Phillips State No. 1 well is instructive to study, since it is located only about 30 km from Mount Rainier. Although the pervasive zeolitization of the lower section of the well probably indicates past geothermal activity, there is no evidence of abnormal formation temperatures in this 4.2 km hole. We believe the present thermal effect of the volcanos in the southern Washington Cascades is limited to the area very near them, as characterized by more extensive heat flow data from the Oregon Cascades volcanoes (Blackwell and Steele, 1983). The correspondence of the top surface of the SWCC to the structure of antiforms in the region argues against the concept of increased temperatures being the primary cause of low resistivities in the anomalous region, because we would expect low resistivities to become shallower to the east where subsurface temperatures are higher. However, resistivities in the deeper parts of the SWCC are very likely influenced by increased temperatures, especially in the area near Packwood and eastward where Barnett and Korosec (1989) have mapped high thermal gradients.

Stanley and others (1990) have discussed the role of similar high thermal gradients in the Oregon Cascades (where heat flow is even higher) in producing deep crustal conductors. Such conductors in Oregon are pseudo-horizontal and occur regionally at depths of 11-20 km. There is a clear association of this Oregon horizontal conductor with midcrustal seismic velocities of 6.4-6.6 km/s. This association and other factors were used to suggest the cause of the regional conductor as metamorphic fluids and partial melt. There is no way to distinguish such a thermally-related conductor from the conductor that occurs in the southern Cascades, except for the factors of morphology of its upper surface, correspondence to seismic reflectors, and relationship to tectonic features. The most recent MT profile completed was done across the south flank of Mt. Rainier (as part of a USGS Volcano Hazards project), largely within the National Park using a backpack MT system. The west end of the profile (XX', Fig. 3) started on Eocene transitional marine rocks of the Carbonado Formation in the Skate Mtn. antiform and the east end of the profile was beyond the axis of the Cascades volcanos. This profile has not been completely modeled, but indicated that the SWCC units dip almost eastward almost monotonically to depths of about 25 km, where they disappear on the east. There is no apparent shallowing near Mt. Rainier, suggesting that our assumption that the conductor is largely caused by a specific lithology and pore fluid is correct; higher geothermal gradients do not appear to affect the depth to this anomalous conductor.

Authigenic Minerals

It is possible that deeper parts of the SWCC may correspond to altered volcanic

rocks that are conductive due to development of authigenic minerals such as zeolites and smectites. We have earlier mentioned the presences of zeolites below 7200 feet in the Phillips State No. 1 well (Fig. 2). Volcanic flows with high percentages of ash generally become quite conductive when hydrothermally altered, because the high silica content and large surface-area of ash allows rapid conversion to zeolites and smectites. These authigenic minerals are highly conductive due to their ability to maintain high ion-transfer capability. Electrical geophysical studies in Newberry volcano, Oregon and Long Valley caldera, California, by Fitterman and others (1988) and Stanley and others (1976) show that tuffaceous volcanic flows can have resistivities as low as 2-8 ohm-m. These resistivities are approximately equal to those in the SWCC and although the Tertiary volcanic rocks studied electrically in the region have resistivities of about 30-500 ohm-m, this does not exclude older, more ash-rich flows at depth as a constituent of the SWCC. The development of zeolites and smectites can lower the resistivities of marine and nonmarine sedimentary rocks, as well as volcanic rocks. The extensive zeolites in the lower part of the Phillips State No. 1 lower resistivities, but not dramatically, probably because they mainly fill fractures; in ash-rich volcanic or sedimentary rocks where the ash is in depositional layers, the continuous, layered distribution of the authigenic minerals is more effective in lowering resistivities.

Pre-Tertiary Conductive Rocks

Conductive rocks older than Tertiary could be the cause of the SWCC, because unmetamorphosed marine shales and mudstones of any age are generally quite conductive (2-20 ohm-m) and graphitic metasedimentary rocks can be very conductive (1-5 ohm-m, Stanley, 1989; Stanley and others, 1990a). The only pre-Tertiary rocks mapped in the region of the SWCC are those in the Rimrock Lake inlier (Ellingson, 1972; Miller, 1989). The Rimrock Lake inlier (Figs. 2,3) consists of a Jurassic igneous complex of trondhjemitic to gabbroic rocks, some metamorphosed to amphibolite grade, and a Jurassic-Cretaceous tectonic melange of mainly arkose and mudstone. Somewhat similar rocks, generally occurring as phyllites, are found along the western margin of the North Cascades (Fig. 2). MT soundings on the melange portion of the Rimrock Lake inlier indicates high (> 200 ohm-m) resistivities at depths greater than 0.5 km, suggesting these units are thin and are probably underlain by more metamorphosed versions of the melange or by intrusive rocks. On the western flank of the North Cascades, other Mesozoic metasedimentary units have resistivities of 200-600 ohm-m, thus are probably not a cause of the SWCC.

Summary of Lithologies

In the preceding discussion regarding lithology, we outlined reasons for our preferred interpretation that conductive rocks in the SWCC correspond to Eocene, and possibly older, marine sedimentary rocks. These marine sedimentary rocks could have been deposited as part of a forearc basin/accretionary prism or in a marine pull-apart structure. Slightly less probable for the proposed lithology of the SWCC units, in our view, is that of highly altered volcanic rocks. Ranking third in probability for the SWCC

lithology is a section of nonmarine sediments beneath the lower part of the Puget Group. Of lowest probability for the SWCC lithology are Mesozoic metasedimentary units like those in the Rimrock Lake inlier or other older rocks. High temperature geothermal fluids and possibly even partial melt may play a role in reducing resistivities in the deepest part of the SWCC, but the distribution and attitude of the highly conductive rocks are such that we believe that these factors are less important than lithologic ones, at least for hydrocarbon exploration depths.

SEISMIC REFLECTION DATA

Acquisition and Processing

In order to study details of the SWCC, a deep reflection profiling program was initiated in the region. The survey was done along six profiles (Figs. 1,3 and Appendix B) by Geophysical Systems, Inc. under contract to the U.S. Department of Energy using a 1000-channel, sign-bit system (Zoback and Wentworth, 1986; Gimlin and Smith, 1980). Five vibrators with a peak force of 27,240 lbs (12382 kg) were used with a modified downsweep from 8-32 or 8-48 Hz. Vibrator point spacing ranged from 40 m to 120 m. Receiver-group spacing was 30 m on line 1 and 20 m on the remainder of the DOE seismic lines. After the initial test survey involving line 1, ray-trace models of deep structure appearing in the data was done to more effectively plan the later surveys across the SWCC. Data processing generally followed the flow chart below:

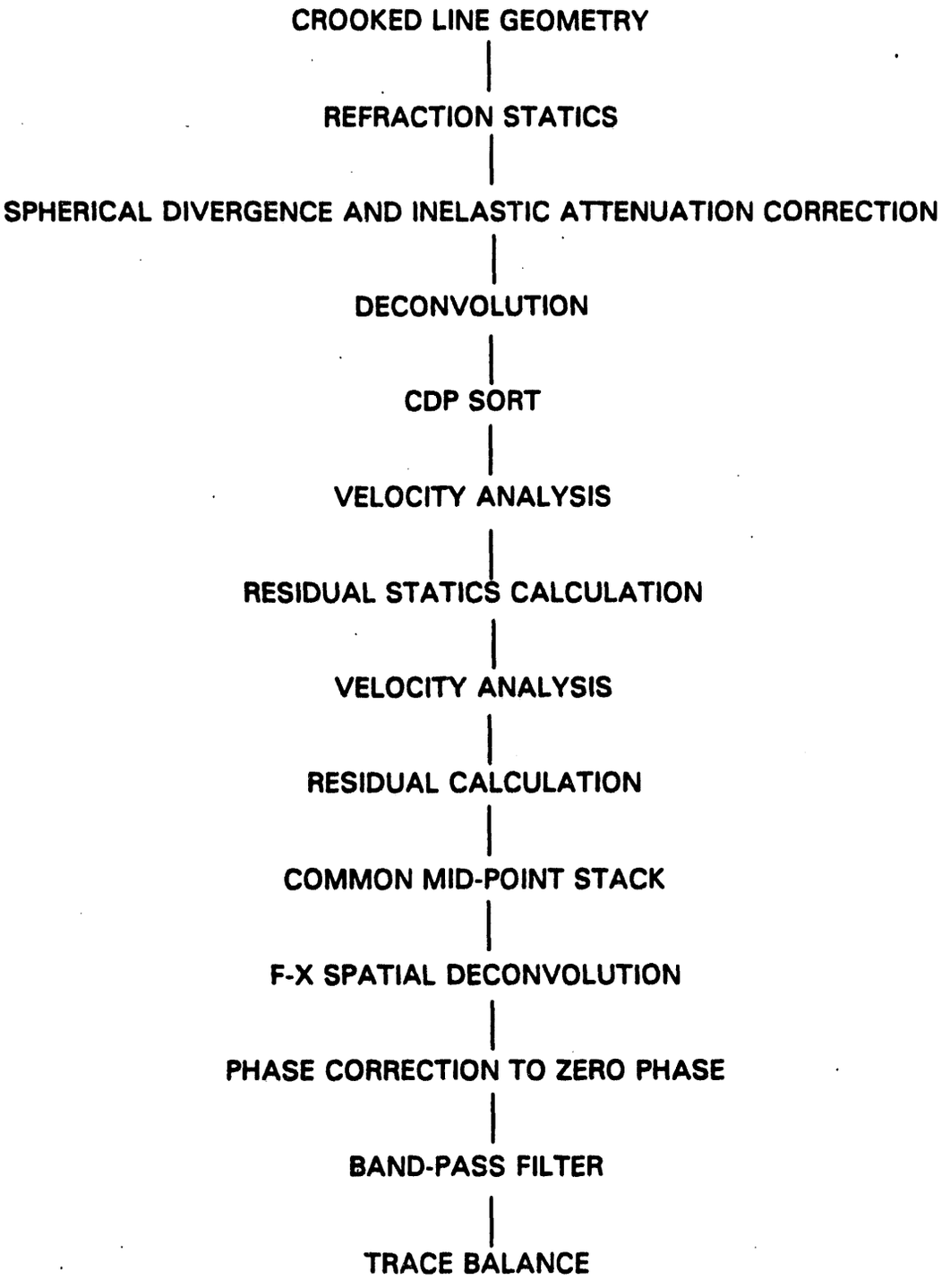

Data were stacked with a maximum of 256-fold coverage, following the steps above with two or more passes of residual statics and including horizontal

deconvolution (F-X deconvolution) for some of the data (lines 1-3). The latter technique is a predictive method to correlate events from trace to trace and produces a minimum numbers of artifacts when compared to the coherency filtering sometimes applied to poor-quality reflection data. Crooked line geometry corrections were important because of the irregular profiles, and this correction failed to clean up some of the data, notably on line 6.

In addition to the Vibroseis surveys, minor testing was done with dynamite sources; these latter tests proved promising, but the difficulties and costs involved with dynamite surveys in this region of high tourism made extensive dynamite surveying impossible. Crustal scale seismic refraction surveys have also been completed by the USGS along a north-south profile across the northern part of the SWCC, but the data were very poor over the volcanic covered area and interpretations have not been completed to date

Shotpoint and CDP (common-depth-point, Sheriff, 1984) locations for the seismic survey are contained on the CD-ROM (Zilman, 1992). The complete shotpoint data set is shown on Figure 3, with each tenth shotpoint labeled. The decade numbers on Figure 3 can be correlated with the tables in Appendix C to derive actual shotpoint numbers. The CDP path for each of the seismic profiles are quite complicated because of the non-linear nature of the profiles, thus the seismic sections actually follow a ground path that cuts across the bends in the highways used for the data acquisition and the CDP track is very wide, averaging a great deal of the subsurface. Because of the degree of geological complexity, this CDP averaging is the cause of the some of the poor data quality, and only a dense 3D survey would adequately image the complex structures. An approximate 3D survey was constructed in the region of the Morton antiform using the CDP's from lines 1, 2, 4, and 5, but because the survey had not been acquired as a 3D survey, the decimation in fold caused by selection of 3D CDP bins caused the data to be incoherent below 1 sec travel time. Thus, the constructed 3D data along the nine lines was not useable for study of structural aspects of the Morton antiform, as had been hoped. A possible approach to conducting surveys like that across the SWCC in future studies in the region or in similar areas might be the use of wide-line-profiling (WLP) as described by Michon (1993). This method uses a sequence of shotpoints offset from a linear profile to produce a modified 3D survey at a much lower cost than a normal 3D survey. The resulting data is processing in terms of calculated dip for coherent horizons. The advantage in this method is that complex sets of reflection sequences can be separated into events from unique horizons. It seems to us that the irregular access roads normally found in mountainous regions like that of the SWCC would lend themselves well to this type of modified 3D survey. We intend to investigate the possibility of applying the WLP processing methods to selected portions of the Washington DOE data.

Velocity analysis for the stacked record sections was done using automated normal moveout (NMO) and dip-move out (DMO) routines, tested by common mid-point (CMP) stacking (Sheriff, 1984; Cordier, 1985). It was found that this automatic velocity analysis was not completely satisfactory due to the geological complexity that

made the CMP stacks of poor quality in some sections. Considerable fine tuning of the automatic picks was done to try to improve the data coherency. This generally amounted to fixing the velocities over time bands and along trace spans to remove some of the variability introduced by the automatic velocity analysis. This appeared to help the data coherency in several instances, especially on lines 1 and 2 where most of this adaptive velocity picking was done.

Grau (1993) has addressed the problem of obtaining seismic velocity information from reflection data in complex regions. He defines a complex region as

Figure 15-Averaged velocity profile from several key wells west of the SWCC (solid line), with average velocity profile from stacking velocities in the Morton antiform area (dashed line), and velocity versus depth curves for Eocene shales from Gregory (1977).

one in which CMP stacking and post-stack migration make if difficult or impossible to conduct conventional processing operations. He recommends a variety of techniques to assist in complex regions, including pre-stack migration. In spite of the obvious difficulties in obtaining coherent reflection horizons and deriving good velocity models, pre-stack migration was not attempted on the Washington data because of the very large computer expenditures required for this process on 1000 channel data. Such processing might improve portion of the data, but no tests have been done to date.

The actual velocities for most of the survey are poorly known because of the lack of wells in the SWCC region. Only wells from the nearby Chehalis Basin were available for sonic log studies. Sonic logs from several of these wells are included in Appendix C. The best of these logs for velocity analysis is the relatively deep Thompson No. 1 (location in Fig. 4). This sonic log is provided in Appendix C and is shown in Figure 15 along with stacking velocity profiles from the automatic picker at four selected CDP's. The log in Figure 15 has been scaled vertically to a velocity of 12,000 feet/sec to display with the stacking velocities. The sonic log indicates velocities in the Lincoln Creek/Skookumchuck marine sandstones and shales of 8-13,000 feet/sec down to a depth of about 8000' where volcanic flows of the Northcraft Formation have higher velocities of 14,000-19,000 feet/sec. Below the Northcraft, the McIntosh Formation has velocities of about 15,000 feet/sec. The exponential increase in velocity with depth in the sedimentary rocks reflects the compaction of the sandstones and shales and increased cementation with depth. Older sedimentary rocks will also have higher velocities than younger ones, reflecting the time rate of compaction and metamorphism. Higher temperatures will also increase the metamorphism of sedimentary rocks, generally leading to higher velocities. All of these factors make it difficult to assign accurate velocities to deep sedimentary units in the study area. However Gregory (1977) has used empirical formulas to attempt to quantify the effects of fluids, depth, and age on the velocity

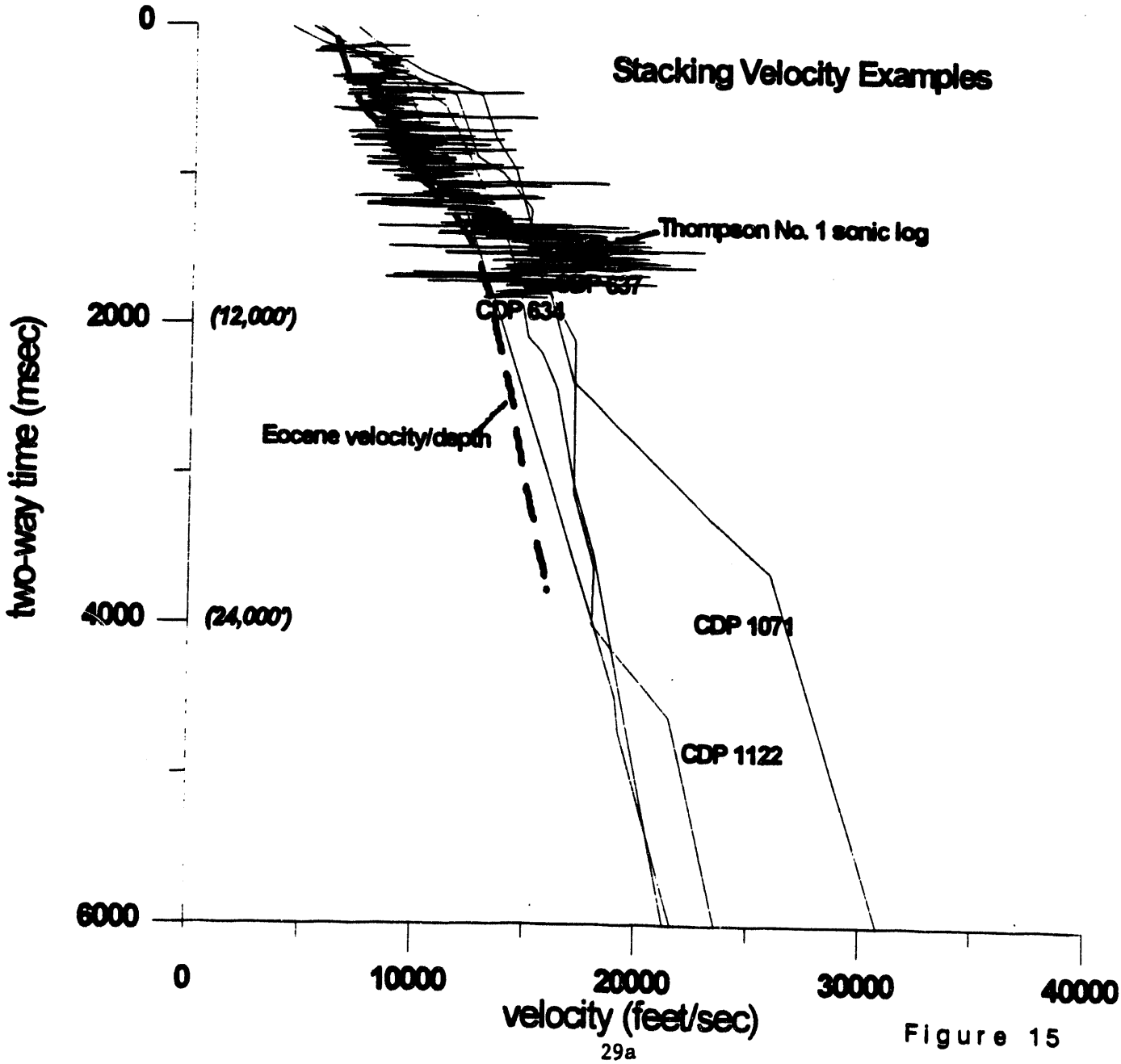
Stacking Velocity Examples
Thompson No. 1 sonic log
CDP 634
Eocene velocity/depth
CDP 1071
CDP 1122
0
2000
(12,000')
4000
(24,000')
6000
two-way time (msec)
0
10000
20000
30000
40000
velocity (feet/sec)

Figure 15

of sandstones and shales. The dashed curve in Figure 15 shows a plot of velocity/depth using the formulas of Gregory (1977) for an Eocene shale. The fit to the upper part of the Thompson well is reasonable (much of the section is Oligocene, rather than Eocene) and the deeper part suggests that some of the automatic velocity picks from the processing software are reasonable, but others are clearly out of line. For the remainder of our discussion, we will assume a velocity of 5 km/s for approximate depth conversions in the seismic sections, since our main interests are in the deeper parts of the data that correlate with the SWCC. Exact depths are not at issue in this report, but the tectonic and stratigraphic interpretation of the seismic data is the important factor.

Reflection Records Sections and Interpretations

Additional processing of the DOE reflection data was made possible with the aid of the CD-ROM developed by Nick Zilman (USGS Open File Report 92-714) which contains all of the CDP and location data. Software developed at the Colorado School of Mines Center for Wave Phenomena (Stockwell, 1993) called SU facilitate processing and display of the seismic data. This software operates under the X-windows environment on UNIX workstations and does many of the processing and display operations available with commercially available software packages. In addition, several innovative migration and 2D/3D modeling routines are available. For the seismic sections discussed in this report, we have fine-tuned the original data provided by the processing contractors in minor ways through band-pass filtering of some of the data and additional agc and trace balancing. As discussed in a later section, we have also begun 3D modeling of line 3 data to investigate sideswipe or out-plane-reflections that appear to influence the data. The data in following sections are displayed as gray-scale (256 level) amplitude plots of the processed CDP files.

A gray-scale amplitude representation of the stacked CDP record section from combined seismic lines 1 and 2 is shown in figure 16. An expanded section of a portion of the profile in the Morton anitform is shown in figure 17. The data were recorded to 15 seconds, but only the upper 6 seconds of data are shown because no coherent events were observed in the remainder of the record. The data quality is generally not adequate for interpretation at travel-times greater than 3-4 seconds. This degradation in data quality was caused by traffic noise, poorly-defined velocity functions, the presence of surface volcanics, structural complexity, and non-linear survey routes. Regardless of a lack of reflections below 3-4 seconds at increasing time, this survey represents the first reflection data suitable for intermediate-depth (down to about 8 km) structural interpretation from the Cascades. A standard exploration seismic profile across the central part of the Chehalis Basin was described by Ise (1985), but the DOE survey represents the first public domain deep-reflection data for the Washington Cascades.

We have drawn three lines on the section that represent the possible level in the reflection section of key geological horizons, (1) the base of Eocene-Miocene volcanic rocks, (2) the base of nonmarine units of the Puget Group, (3) the base of the SWCC units mapped with MT soundings. The volcanic units can be distinguished partially by

the highly variable reflectivity, with examples of very high reflectance in the upper 1 second, and by the meshing, or irregular shingling of individual reflectors. The largely nonmarine, deltaic units of the Puget Group (largely Carbonado Formation on this section) can be recognized by a variety of mildly sigmoidal, divergent reflectors characteristic of delta front/delta plain environments (Brown and Fisher, 1979, Table 1, p. 42). The units identified as related to the SWCC are probably McIntosh Formation equivalent marine units as discussed in an earlier section with the variable (low to high) reflectivity, parallel to slightly divergent stratiforms, and high continuity suggestive of distal fan delta deposits (Brown and Fisher, 1979, Table 1, p. 42).

Hunt Oil Company has applied for a permit to drill a 15,000' hydrocarbon test well in section 1 just east of the town of Morton. This location is indicated on Figure 14 and the well will sample key parts of the SWCC and packages of bright reflections indicated on the seismic section. The bright, somewhat horizontal reflection at about 1.8s travel time may be related to fluid anomalies such as overpressured brine or gas/water interfaces. However, with the inability to study the phase relationships of the seismic data with Vibroseis, we had no opportunity to evaluate this possibility. The large contrasts in reflectivity may be related to uncomformities in the assumed

Figure 16-Gray scale amplitude plot for DOE line 1 and 2 combined. The location of a proposed 15,000' drill test by Hunt Oil Co. is also indicated.

mostly marine units, but more likely is related to changes in subsidence rates and sediment supply for the distal fan delta system. Another factor in rapid lateral changes in reflectivity may be the thinning of the volcanics over the Morton antiform, which would result in better energy penetration in the region of the brightest reflections.

Detailed plots of data from seismic line 1 are shown in Figure 17 across the east flank of the Morton antiform. The layered basement reflections may be attributable to Crescent Formation basalt flows and interbedded sediments. These reflections suggest a rather monotonic dip down to travel times of about 4 seconds. The section represents unmigrated results, as most of the migration experiments for all of the seismic lines were not very satisfactory becasue of a the highly variable velocity field and poor reflection quality. Locally some good final migration sections were obtained, but for the most part, the unmigrated data proved more useful for stratigraphic interpretations. In the case of the dipping reflections on the right side of Figure 16 at 2.5-4 seconds travel time, migration pulls the most steeply dipping portion back to the left (west), but the sense of structure is the same. Also on this figure, a significant strike-slip zone is evident in the abrupt transition between two major reflective zones at 1-2 seconds on the right to three zones at similar depths on the right. This interpreted strike-slip zone probably is the continuation of the St. Helens zone (SHZ), and pcssibly connects to the fault interpreted in the magnetic data

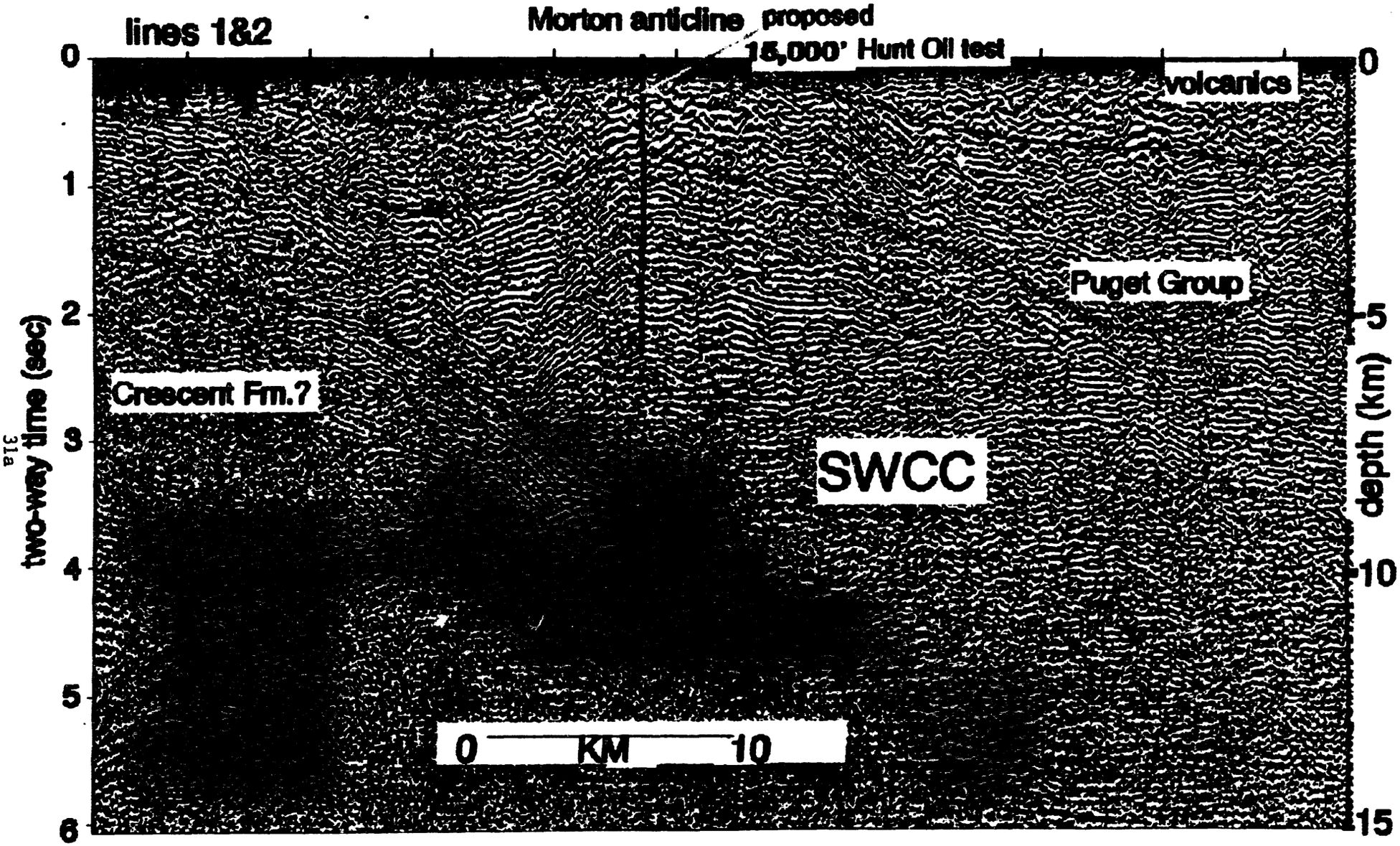
lines 1&2
Morton anticline
proposed
15,000' Hunt Oil test
volcanics
Puget Group
Crescent Fm.?
SWCC
0 KM 10
two-way time (sec)
depth (km)
0
1
2
3
4
5
6
0
5
10
15

Figure 16

of Figure 13.

Gray-scale, amplitude data from DOE seismic line 3 are shown in Figure 18. This section indicates a number of interesting features not observed in such quantity on the other five profiles. An interpreted deep volcanic basin filled with Ohanapecosh

Figure 17-Expanded plot of DOE line 1 for Morton antiform. An obvious strike-slip zone is indicated by the symbols.

Formation flows occurs on the east end of the line (just right of Packwood location) extends to travel times of 1.9 s. Velocities in the volcanic rocks are probably similar to those of the Northcraft Formation indicated on sonic logs (Appendix C) of >16,000 feet/sec. With these velocities the bottom of the volcanic pile is interpreted to be at about 15,000' (4.6 km). The thickening of the flows in the center of the basin suggests that their was syndeposition of the volcanics during downdropping of the basement. A west dipping fault can be interpreted in the volcanics just below the "oo" in the word Packwood. Part of the reason for interpreted this complete section as Ohanapecosh volcanic rocks is that the westward extention of the reflectors is discordant from a dipping section of reflectors beneath that we interpret in the next paragraph to be Eocene sedimentary rocks. However, there are minor outcrops of Eocene mudstones in the town of Packwood that would be hard to fit in with the interpretation of the reflection data. These mudstones may be landslides that came from local uplifts related to the large Oligocene/Miocene intrusions in the Packwood area (both north and southeast, Fig. 3). Outcrops of Eocene mudstones have been noted on the tops of the Tatoosh pluton just south of Mt. Rainier. In addition, geological mapping by Don Swanson, USGS (oral comm., 1993), in this region indicates a regional east-west fault that follows the Cowlitz River valley, which also shows up on the aeromagnetic data in the western Cowlitz valley (Fig. 12). These complications make it difficult to have confidence in a simple interpretation of the seismic data, but the data themselves appear relatively simple in the upper 1-2 seconds.

Below the interpreted volcanic basin, a thick monoclinally folded section of reflectors that we interpret to be associated with Eocene sedimentary rocks extends to travel times of nearly 4 seconds, where several west-dipping reflections are associated with the pre-Eocene basement. The sedimentary rocks are assumed to be nonmarine units like those that crop out in the Summit Creek area just northwest of the end of seismic profile and to Puget Group units like the Carbonado to the west (Fig. 3). Several of the deep, linear reflections on the east end of the profile were interpreted as multiples by Stanley and others (1992). There is a repetitive character to the last two events at about 4 and 5 seconds travel time, respectively; however,

Figure 18-Gray scale amplitude plot of data for DOE line 3.

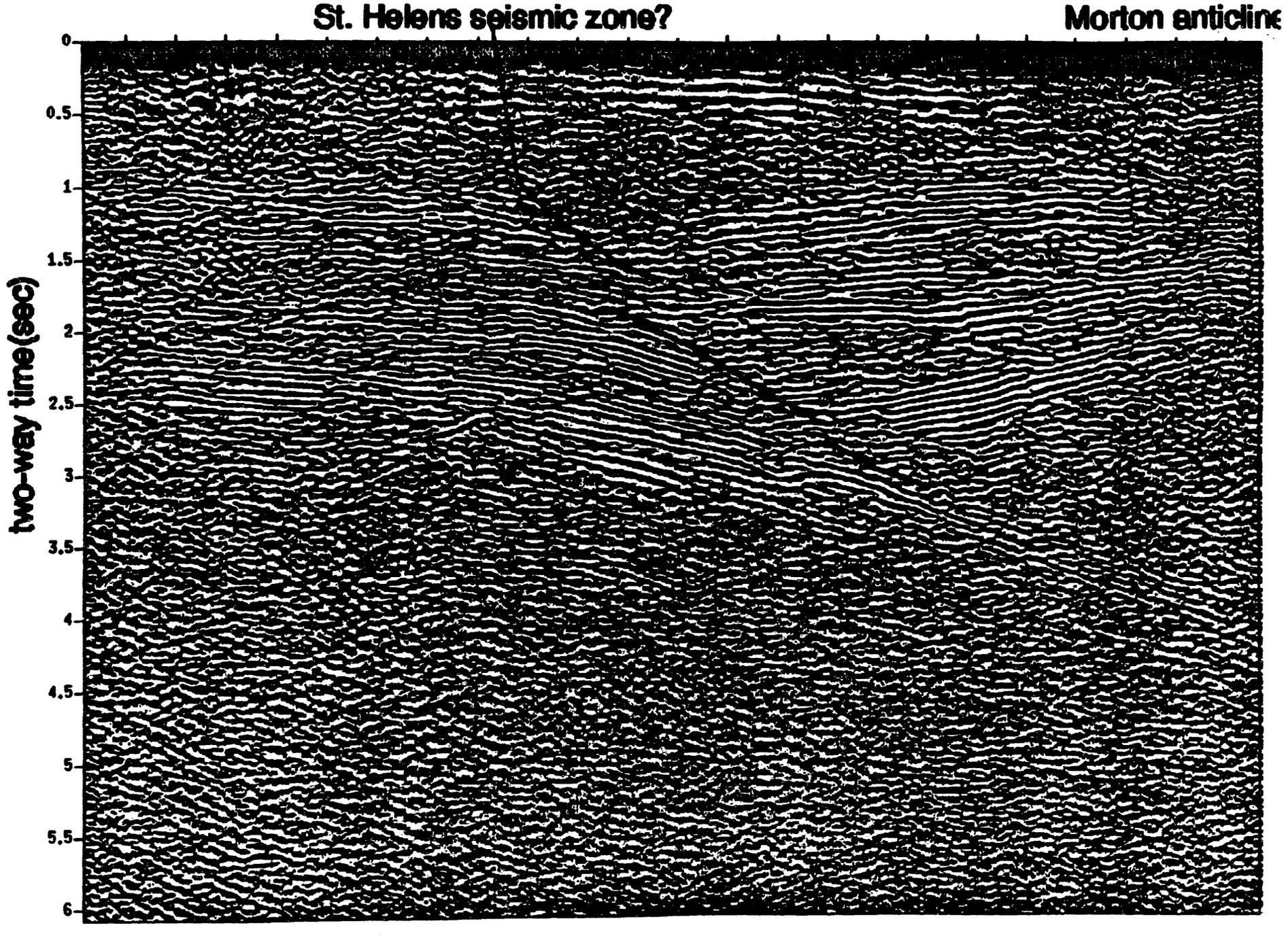
St. Helens seismic zone?
Morton anticline
0
0.5
1
1.5
2
2.5
3
3.5
4
4.5
5
5.5
6
two-way time(sec)

Figure 17

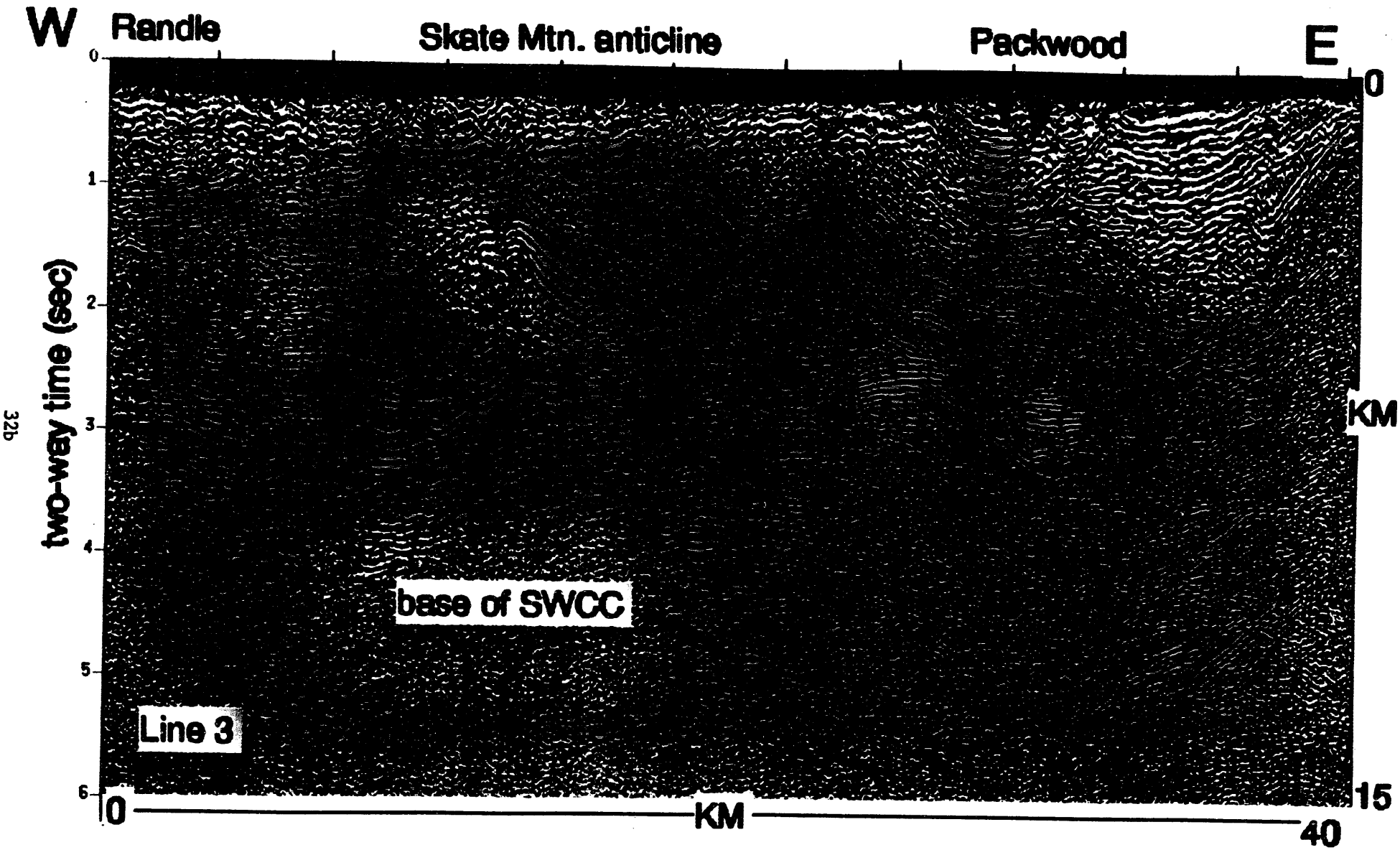
W
Randle
Skate Mtn. anticline
Packwood
E
0
1
2
3
4
5
6
two-way time (sec)
0
KM
15
base of SWCC
Line 3
0
KM
40

Figure 18

by projecting the folded reflectors to the west back toward these two events, we have now assigned the reflector at 4 seconds to pre-Tertiary basement. Details of the reflection data in this area are shown in Figure 19 from Stanley and others (1992), but we now interpret the basement as occurring at the reflection starting at the letter "I"

Figure 19-Expanded plot of the east end of DOE line 3 from Stanley and others (1992).

in "MULTIPLES" (at 3.2 seconds). With velocities chosen from the synthetic curve of Figure 14, the section from 1.9 seconds to 4 seconds would have an average velocity of about 15,000 feet/sec. The pre-Tertiary basement below the basin near Packwood is at about 10 km depth using the postulated velocities for the volcanic and sedimentary rocks.

There is an abrupt transition from the eastern folded reflectors under the Packwood area to nearly horizontal reflectors west of the Skate Mtn. anticline/antiform. From the seismic data, it is clear that the "anticline" is truly an antiform that is in actuality the upthrust flank of the synform to the east. The defining thrust is clearly imaged just below the word "Skate" on the section. Detail of the data near the thrust fault is shown in Figure 20. In a later section, we will show that this thrust has currently been reactivated as part of a strike-slip zone defined by

Figure 20-Expanded plot of DOE line 3 data for Skate Mtn. antiform.

earthquakes recorded since 1980. Hypothesized marine sedimentary rocks and high-temperature zones associated with the SWCC occupy the portion of the seismic section from 2 to 4 seconds on the west and about 3-6 seconds on the east, with a pronounced uplift in the MT model (Fig. 11) for profile AA' near the Skate Mtn. antiform. A bright, cross-cutting series of reflections just west of the word "Packwood" at 2-2.6 seconds travel time may be related to side-swipe, or out-of-plane reflections, caused by major plutons that occur north and south of the seismic profile. We are currently modeling this geometry with SU (Stockwell, 1993) to study the effect.

Krehbiel (1993a) suggested that the reflectors on the east end of DOE line 3 might be connected, past the Cascades, to Eocene sediments tested under the Columbia Plateau in deep wells there. He also stated that "Since the correlation is interrupted primarily by the Miocene-aged Cascades, this correlation seems plausible." Although the case might be made for some nonmarine units such as those at Summit Creek (Stanley and others, 1992; Vance and others, 1987) extending further to the east, it is not likely that any of the marine units do so. The nonmarine sediments

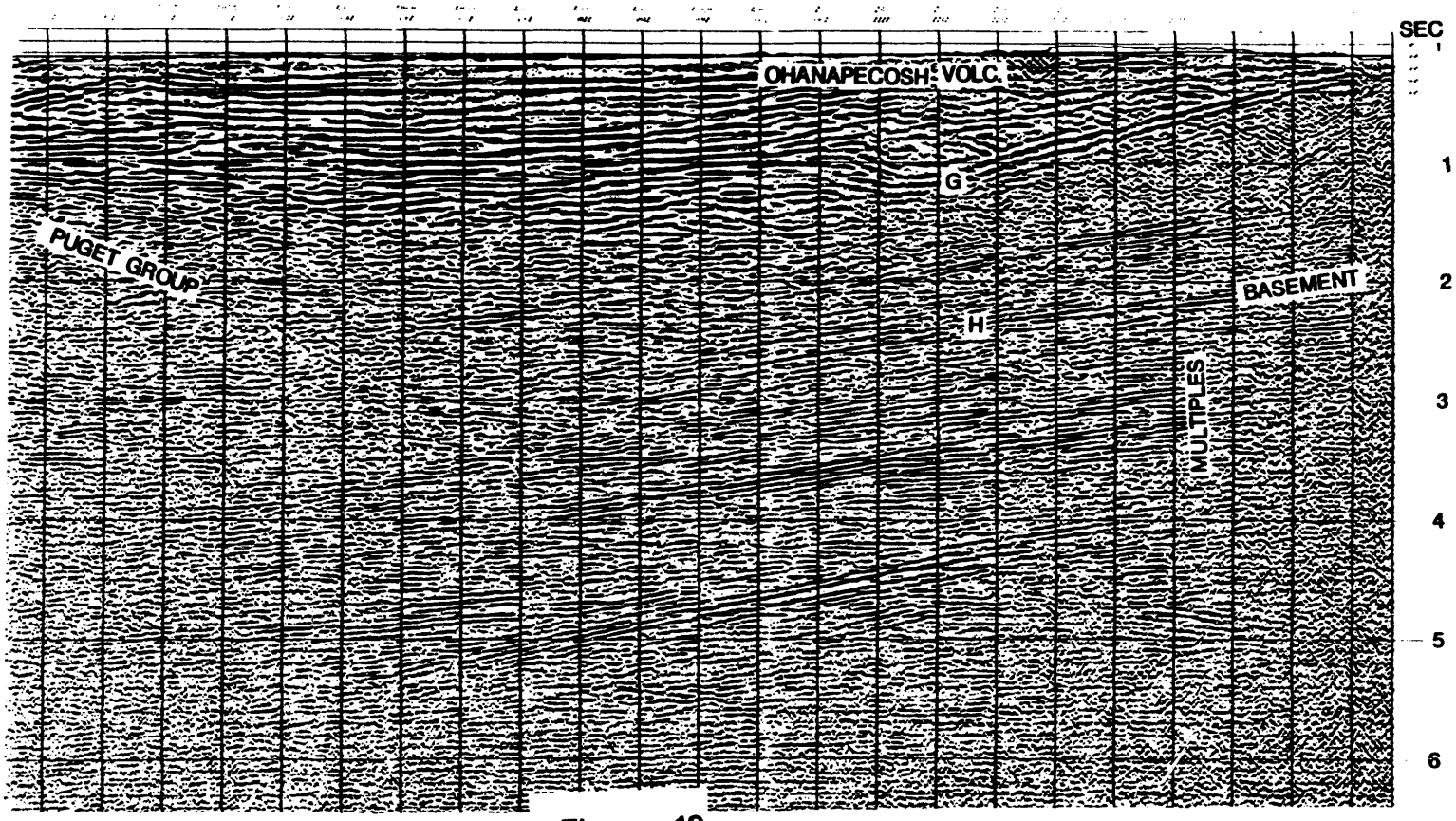
SEC
OHANAPECOSH VOLC.
G
H
PUGET GROUP
BASEMENT
MULTIPLES
1
2
3
4
5
6

Figure 19

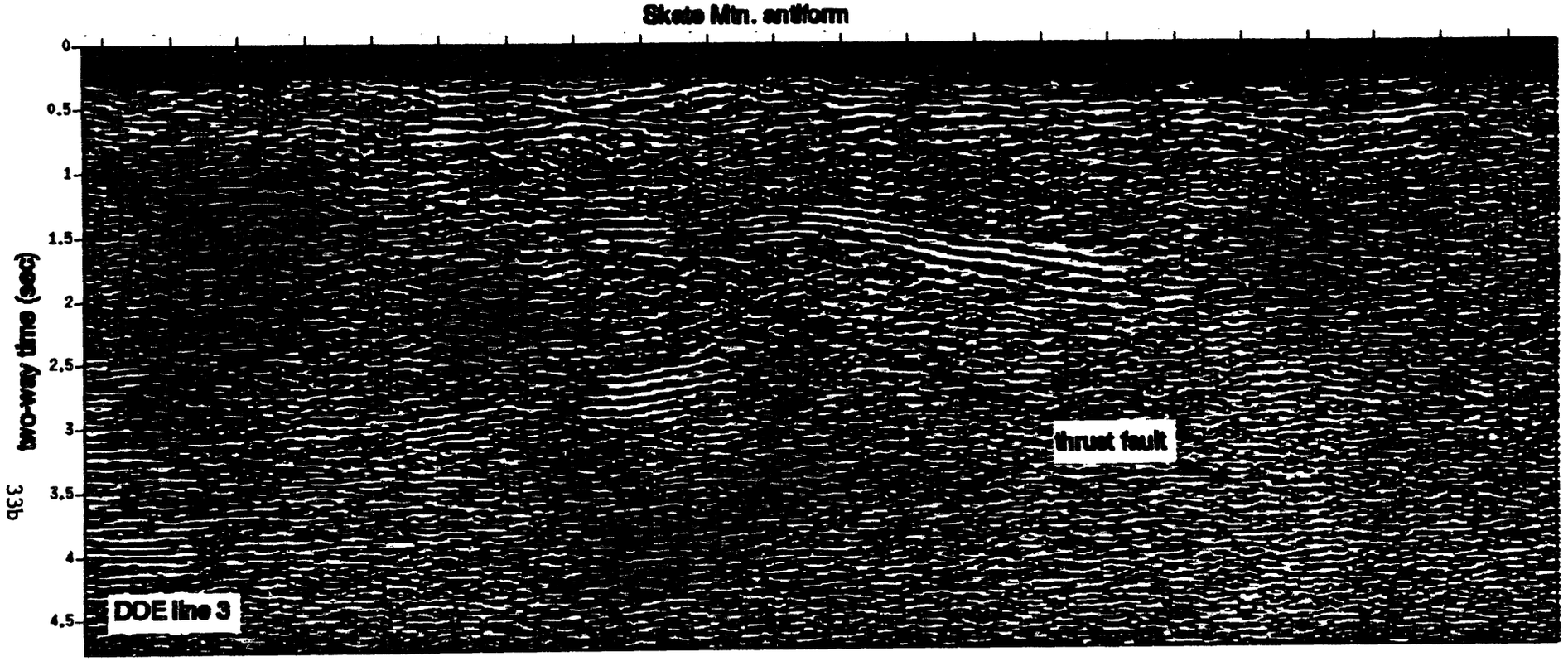
Skeie Mtn. antiform
0
0.5
1
1.5
2
2.5
3
3.5
4
4.5
two-way time (sec)
thrust fault
DOE line 3

Figure 20

beneath basalts in the Columbia Plateau may be partially correlated stratigraphically with Eocene nonmarine units in the Swauk and other basins in northwestern Washington, but there is no evidence in any of the deep wells drilled in the Plateau for similar age marine units. Additionally, the deep reflecting units that we correlate with conductive marine units in the eastern part of the SWCC dip downward to depths greater than 20 km until they disappear at the western margin of the Columbia Plateau; therefore, there it is not likely that there is any association with the Tertiary sediments in the Plateau.

Data from seismic profile 5 are shown in Figure 21. This profile (Fig. 3) crosses

Figure 21-Gray scale amplitude plot of seismic data from DOE line 5.

the Morton antiform somewhat along strike and the data are much poorer overall than on lines 1, 2, and 3. The Morton antiform upper surface is clearly imaged, as is the dipping basement sequence (see events on Figs. 16 and 17). The southwest end of line 5 actually coincides with line 1 and the appearance of the sections is the same. The Morton antiform appears to plunge to the north, as suggested by rather poor evidence in the reflection data. Data from line 6 are shown in Figure 22. These data were the poorest of the overall survey with contributing factors being use of an active

Figure 22-Gray scale amplitude plot of seismic data from DOE line 6.

logging road, very crooked profile geometry (Fig. 3), and even more complicated geological structures than occurred on the other lines. There is very little worth noting on the section for line 1 other than the rather obvious crooked geometry problem on the west end of the section (which has been highlighted). This part of the data was obtained from the shotpoints sequences 50-80 in Figure 3.

In addition to the interpretations of the seismic reflection data by Stanley and others (1992) and in this report, others have used some of the data for slightly different views of the SWCC region. The earliest of these reports is that of Boswell and others (1988). These authors interpreted stratigraphy along the west end of Lauren (then StrataSearch) seismic profile A2-3 in the Chehalis Basin (Fig. 1). The main thrust of their study was development of a seismic stratigraphy based upon the reflection data and several key well along the profile. They utilized sonic logs to compute synthetic seismograms for comparison with the profile information. Their synthetic seismograms do not provide a great deal of confidence about using synthetic seismograms for stratigraphic picks in the Chehalis Basin over long distances, and such data could not be used for stratigraphic analysis in the SWCC region because of

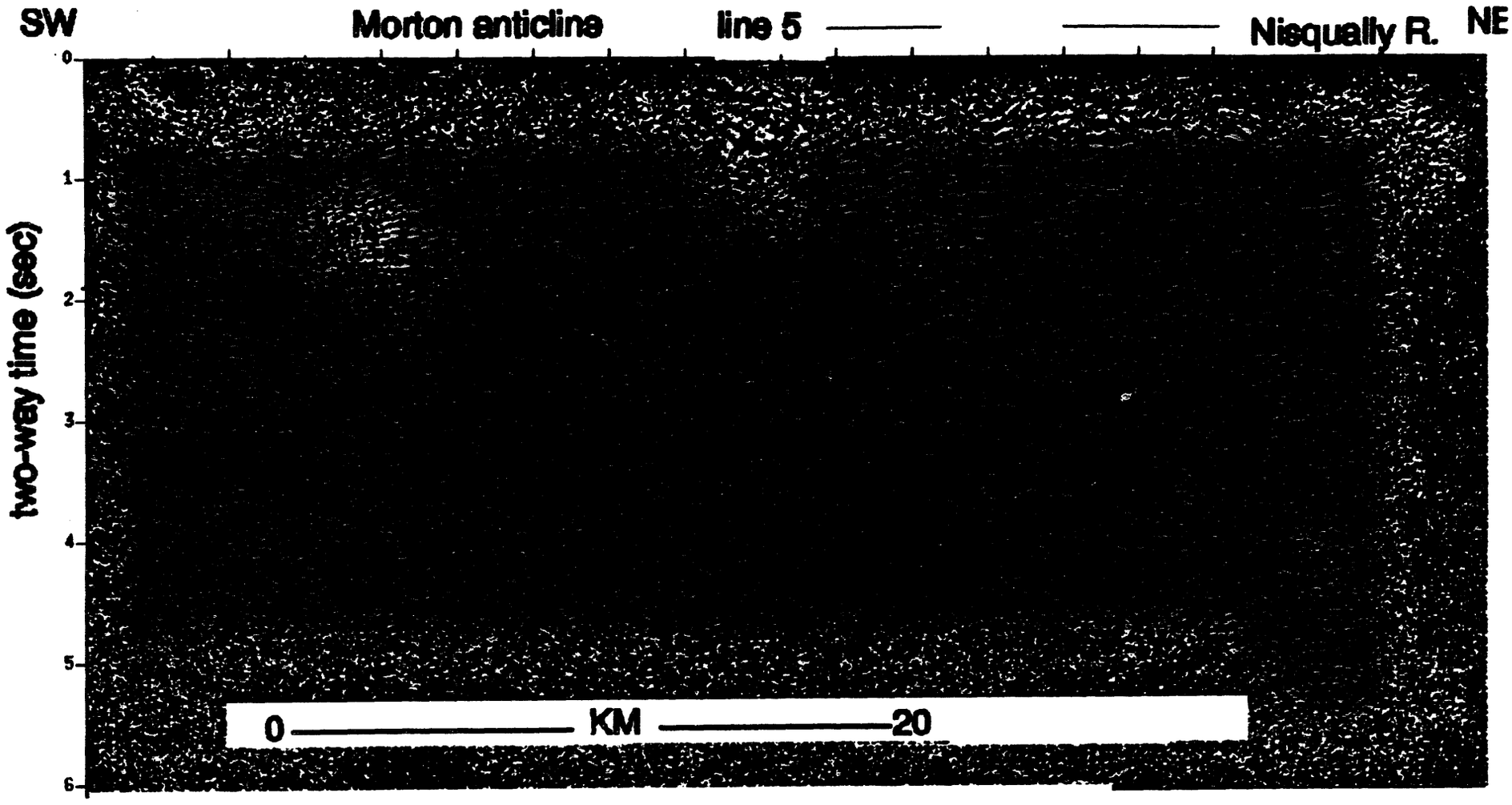
SW
Morton anticline
line 5
Nisqually R.
NE
two-way time (sec)
0
1
2
3
4
5
6
0
KM
20

Figure 21

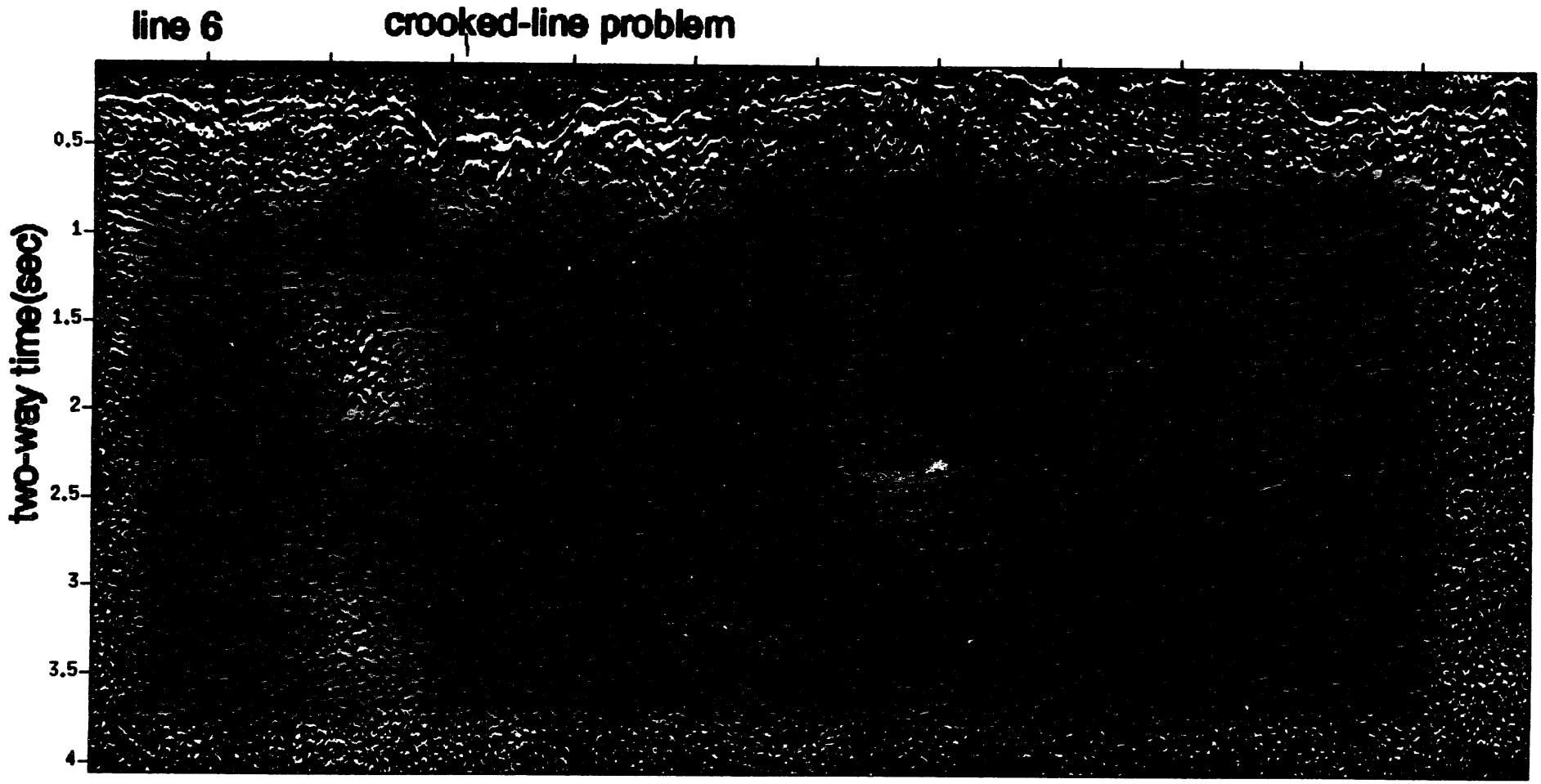

Figure 22

the lack of wells. Their main contribution involved defining depositional facies from downlap, onlap, and clinoform packages of reflectors. From these determinations they concluded that the data fit well the third-order sea-level curve of Vail and others (1987) for the Eocene-Oligocene time period, but recognize that there is disagreement by Armentrout and Suek (1987). Stratigraphic interpretation of StrataSearch data from the Chehalis Basin and DOE lines 1, 2, and 3 by Krehbeil (1993b) contained serious problems in the Chehalis Basin, as noted above. Krehbeil (1993a) interpreted the seismic data for Line 3 to indicate a large, vertical pluton in the area where we have indicated a reactivated thrust (Figs. 17,18), but the reflection horizons are continuous within the area he outlined as an intrusion, making his interpretation implausible.

SEISMICITY AND STRIKE-SLIP FAULTS

It was recognized in Stanley (1984) and Stanley and others (1987) that the structures related to the SWCC had a direct bearing on the seismicity patterns in southwestern Washington. The prominent SHZ belt of strike-slip seismicity (Fig. 23) was noted to occur on the western margin of the SWCC, along a crustal boundary discussed above between Siletzia basement and the overlying Chehalis Basin with possible pre-Tertiary basement and intervening Eocene and older marine sedimentary rocks. This boundary and the eastern boundary of the SWCC, possibly at the pre-Tertiary continental margin, appear to localize both earthquakes and the location of the three regional stratovolcanoes (Fig. 23). Further details of the seismicity can be noted in Figure 23, on which we have drawn lines where linear belts of seismicity and focal mechanism suggest strike slip faults. Besides the SHZ, another belt of linear seismicity occurs coincident with the Carbon River and Skate Mtn. antiforms west of Mt. Rainier and is known as the western Rainier seismic zone (WRSZ). Both these zones have mainly right-lateral strike-slip motion. Another, less distinct zone connects the northern part of the SHZ with the WRSZ, and contains left-lateral events. Another, minor zone of left-lateral slip occurs in the upper part of the Cowlitz River Valley and is thought to be related to the Cowlitz River fault noted by Don Swanson, USGS, discussed above. The strike-slip pattern is reminiscent of sets of anastomosing strike-slip faults in a transpressive environment typical of parts of the San Andreas fault system in southern California (Nicholsen and others, 1986). The left-lateral

Figure 23-Seismicity in the SWCC and Puget Sound region with interpreted stike slip faults and location of MT and seismic profiles across the Carbon River antiform.

motion in a predominantly dextral, oblique stress environments is explained by Nicholsen as the result of interior block distortion and rotation within a transpressive regime.

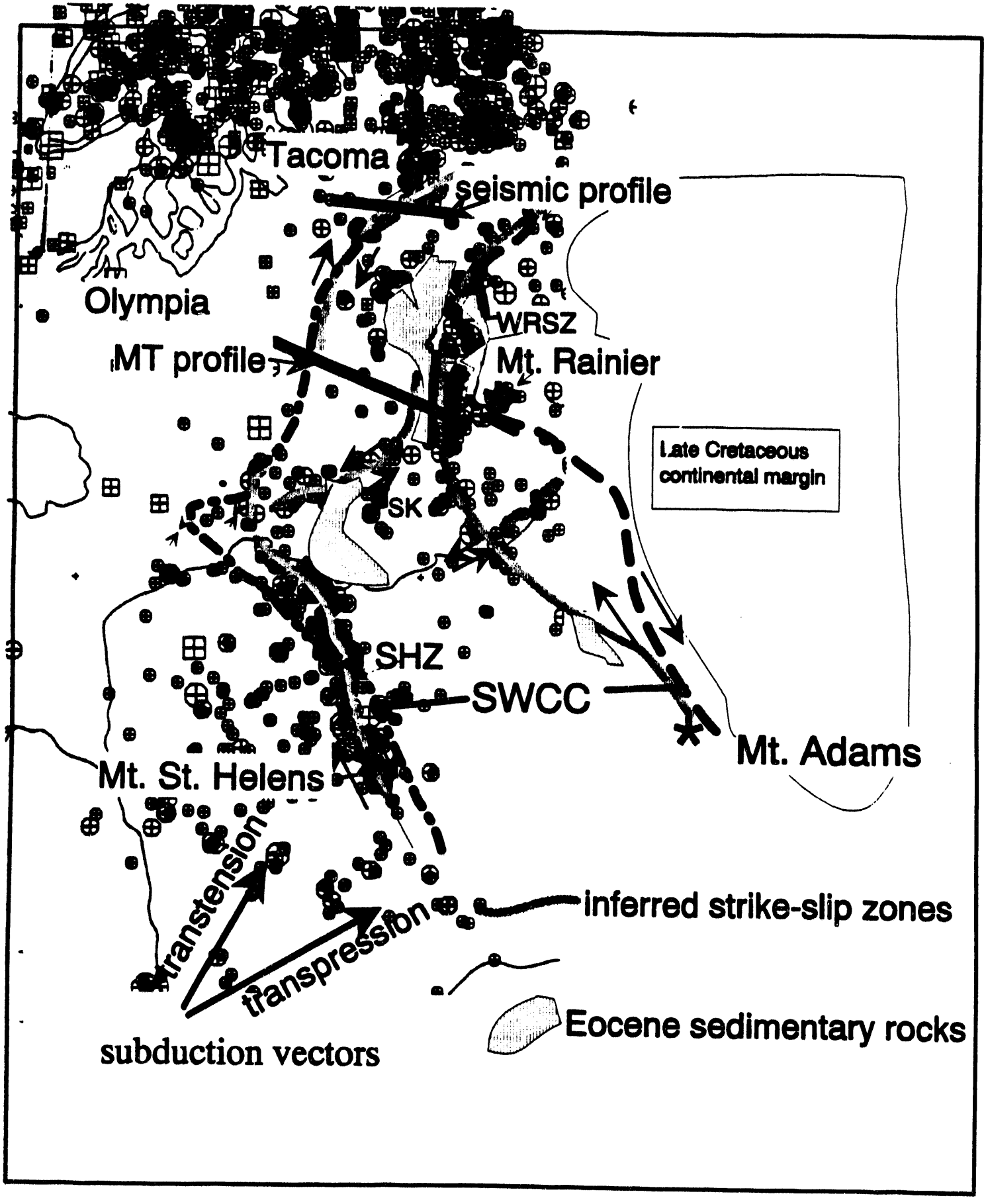
Tacoma
seismic profile
Olympia
WRSZ
MT profile
Mt. Rainier
Late Cretaceous
continental margin
SK
SHZ
SWCC
Mt. Adams
Mt. St. Helens
transtension
transpression
inferred strike-slip zones
Eocene sedimentary rocks
subduction vectors

Figure 23

As part of regional earthquake hazards studies, a detailed MT profile was completed across the WRSZ (see Fig. 23 for location). A 2D inversion of the data from

Figure 24-MT profile model across the Carbon River anticline.

this profile is shown in Figure 24, with the SWCC conductive units shown interrupted by an interpreted pluton of probable Oligocene/Miocene age. Earthquakes occur at depths of 5-15 km in the WRSZ, mostly within the SWCC and generally are probably related to reactivated internal thrusts, as we will discuss below, but a cluster of earthquakes was found to be directly related to the boundaries of the pluton.

Figure 25 shows a segment of an industry seismic line (courtesy of L. B. Industries, Denver) that crosses the trace (approximate location in Fig. 23) of the Carbon River antiform where it plunges north below Quaternary deposits (tinted part of seismic data) of the Puget Lowland. The seismic data reveal a complex zone of

Figure 25-Seismic data section from the Carbon River anticline

reverse and thrust faults, consistent with the inferred transpressional origin of the antiform (Johnson and others, 1994).

To further use seismic events to study the SWCC region, we plotted seismicity along the transect formed by seismic lines 4, 1, 2, and 3 (approximately along U.S. Highway 12). The east-west transect for the seismicity plot was 0.25 degrees wide and centered at 46.55 degrees north latitude (Fig. 3), representing data in the University of Washington catalog from 1977-1992. All events deeper than 2 km and with magnitudes greater than 1.5 were used and are plotted in Figure 26 on a simple geological cross-section constructed from the MT and seismic reflection interpretations. On the west end of the profile a deep cluster of events forms the expression of the NNW trending SHZ of Figure 23. However, in this cross-section, there appears to be a west-dipping zone of events that connects the deep cluster to the core of the Morton antiform. We interpret this zone as related to the thrusted lower surface of the Crescent Formation basement block discussed above in relation

Figure 26-Seismicity cross-section along DOE lines 1,2, and 3 with geological section background. Seismic events for a north-south span of 0.25 degrees were projected onto the east-west profile.

to Figure 8 (seismic line 4). We infer that there may be a vertical strike-slip fault that

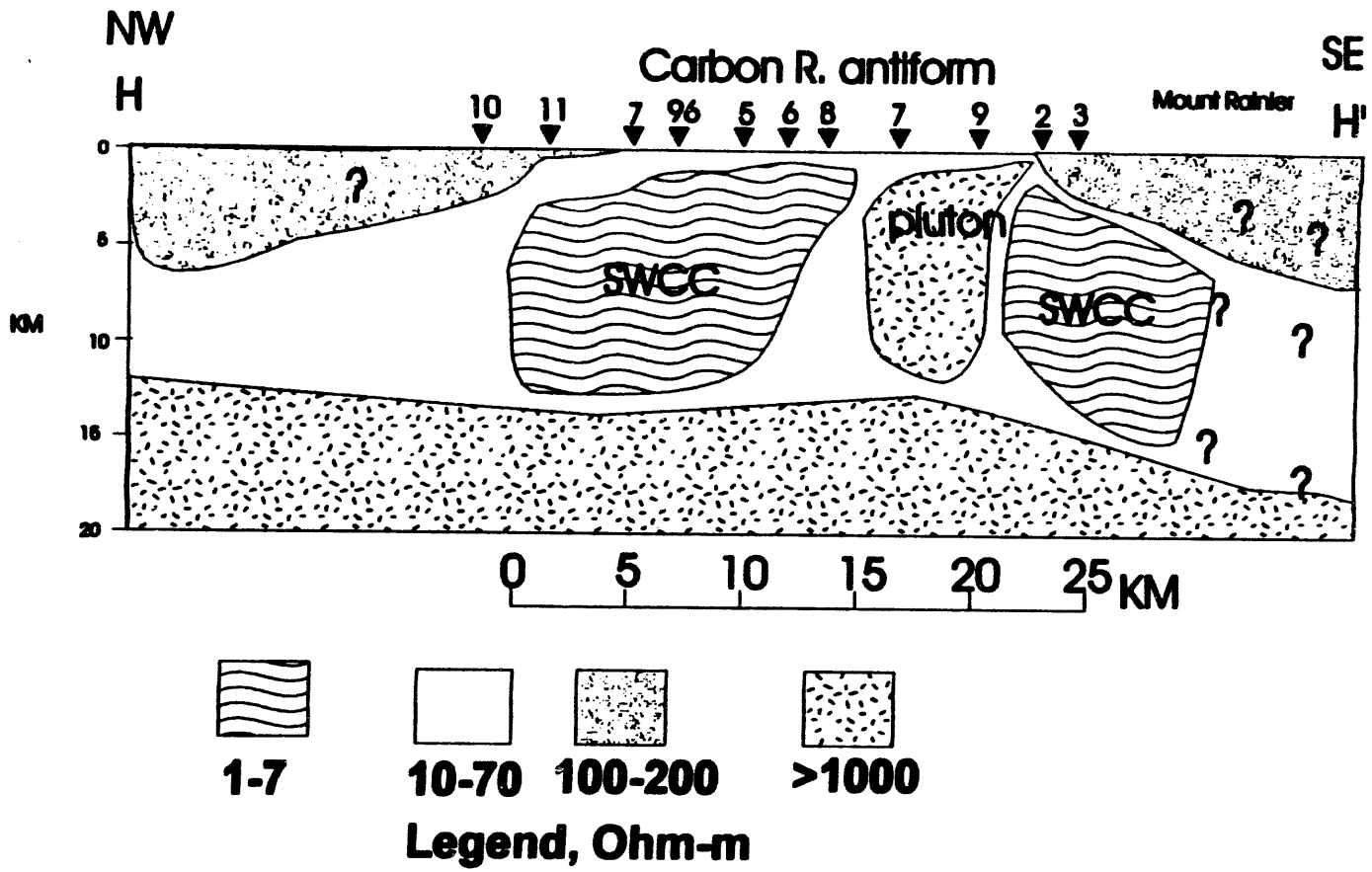
NW
H
Carbon R. antiform
SE
H'
Mount Rainier
10
11
7
96
5
6
8
7
9
2
3
0
5
10
15
20
KM
?
SWCC
pluton
SWCC
0
5
10
15
20
25 KM
1-7
10-70
100-200
>1000
Legend, Ohm-m

Figure 24

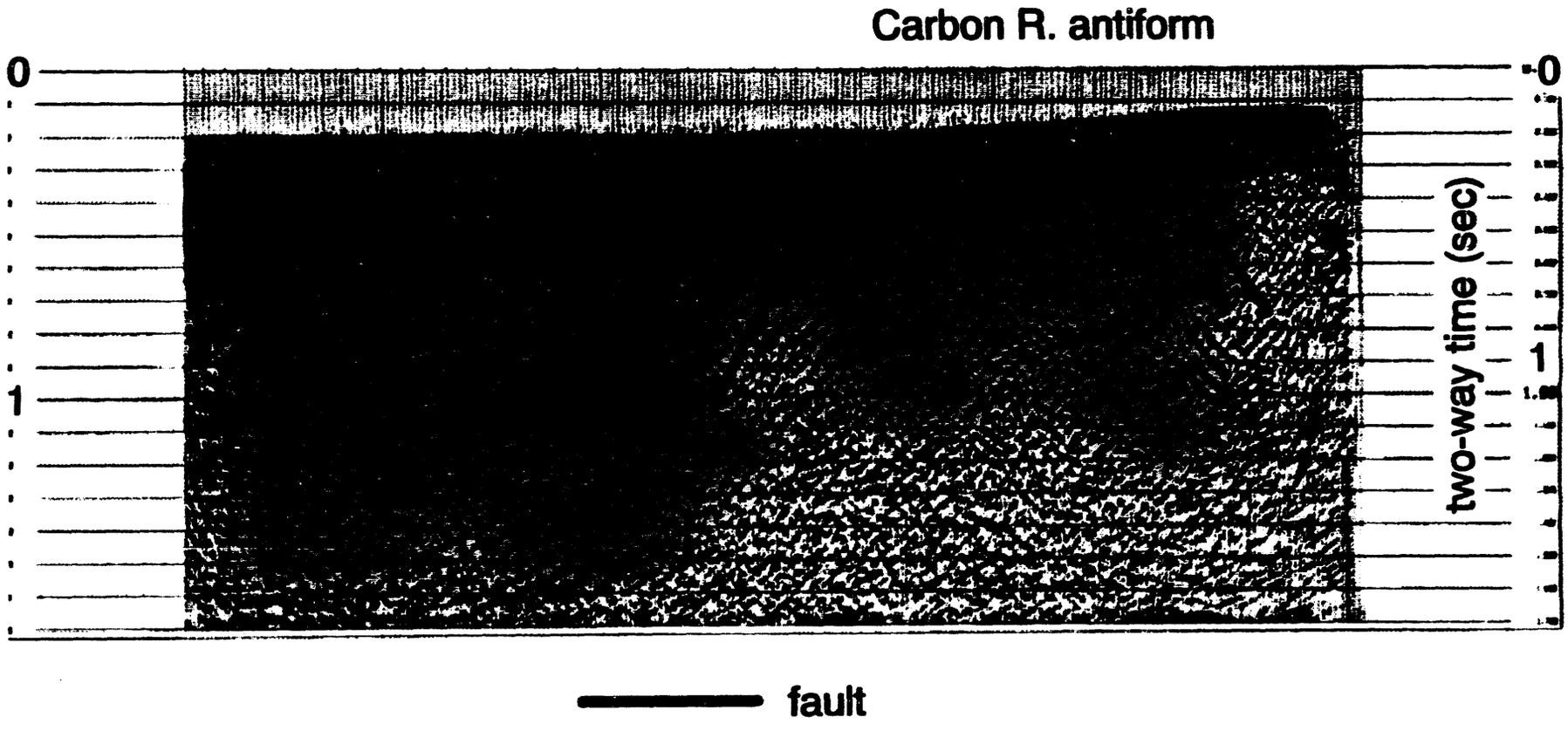

Figure 25

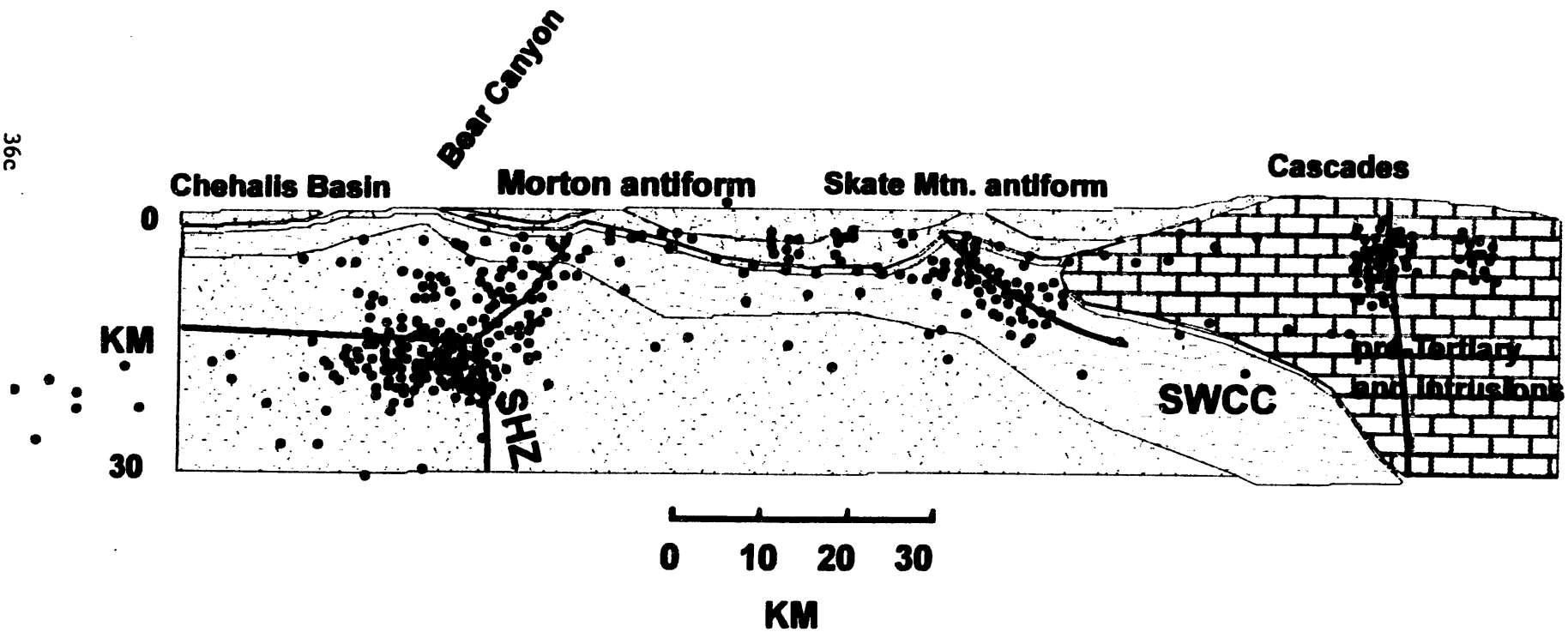
Bear Canyon
Chehalis Basin
Morton antiform
Skate Mtn. antiform
Cascades
0
KM
30
SHZ
SWCC
pre-Tertiary
and intrusions
0 10 20 30
KM

Figure 26

couples the upper-crustal part of the SHZ to the underlying plate; however, there are no details in the seismicity to confirm this and other configurations of the deep part of the SHZ are possible.

An east-dipping zone of seismicity is indicated in the core of the Skate Mtn. antiform and we interpret that this zone is related to the thrust fault interpreted on seismic line 3 (Figs. 18,19). The thrust probably formed in Late Oligocene to Miocene compression and has been reactivated under current right-lateral slip. Along the eastern margin of the Cascades a belt of seismicity occurs along a bounding strike-slip zone that is best expressed near the Goat Rocks volcano area southeast of Packwood, WA.

TECTONIC MODELS: SUBDUCTION AND/OR PULL-APART?

A summary tectonic model using the latest stratigraphic, MT, seismic reflection, seismicity, gravity, and magnetic information is shown in Figure 27. Development of the Chehalis Basin was apparently by downwarping rather than uplift of the surrounding region, as indicated by the low thermal maturity of the sedimentary rocks in the basin. The basement of the Chehalis Basin is composed of the Crescent

Figure 27-Final interpretive geological section across the Chehalis Basin and SWCC.

Formation flows and possible underlying oceanic crust, and has been uplifted through a series of normal faults to a shallow position near Bear Canyon. Significant strike-slip faults in this area make it impossible to complete accurate stratigraphic correlations from the Chehalis Basin into the Morton antiform area, but regional studies of sedimentary rocks suggest that the conductive rocks at depth in the antiform are probably like those of the McIntosh and Raging River Formations. They are overlain with thick, largely nonmarine sedimentary rocks of the Carbonado and equivalent formations. Oligocene/Miocene volcanic rocks of the Stevens Ridge Formation are in contact with Eocene volcanic of the Northcraft Formation due to the basement uplift west of Bear Canyon. Gravity and magnetic data suggest that portions of Crescent basement occur east of the Bear Canyon area. In addition, the clearly banded, continuous dipping reflections beneath the Morton antiform (Figs. 17,18) suggest a possible interlayered volcanic/sedimentary sequence or other type of layered basement rocks below the interpreted thick marine sedimentary section. Although it possible that these reflectors are associated with the Crescent Formation, other geologic units are also compatible with the reflection data. Regardless it is highly likely that at some point east of the axis of the Morton antiform, pre-Tertiary basement of allochthonous origin probably underlies the SWCC. A very thick volcanic basin developed during deposition of the Ohanapecosh volcanic flows, possibly enhanced by east-west compression that finally caused a major thrust fault in the core of the present Skate Mtn. antiform.

Most of the conductive section under the Morton antiform is probably clearly related to deposition in a pull-apart basin similar to others in Western Washington, but with probable marine deposition (see detailed discussion below on Morton antiform lithology). However, the mapped thrusting of the conductive rocks beneath the pre-Tertiary basement on the eastern margin of the SWCC indicates that the depositional model of a pull-apart basin for the overall conductive section may be overly simplistic. We suggest again, as in Stanley and others (1992) that the deeper parts of the section in the eastern half of the aromalous region may be related to an accretionary complex

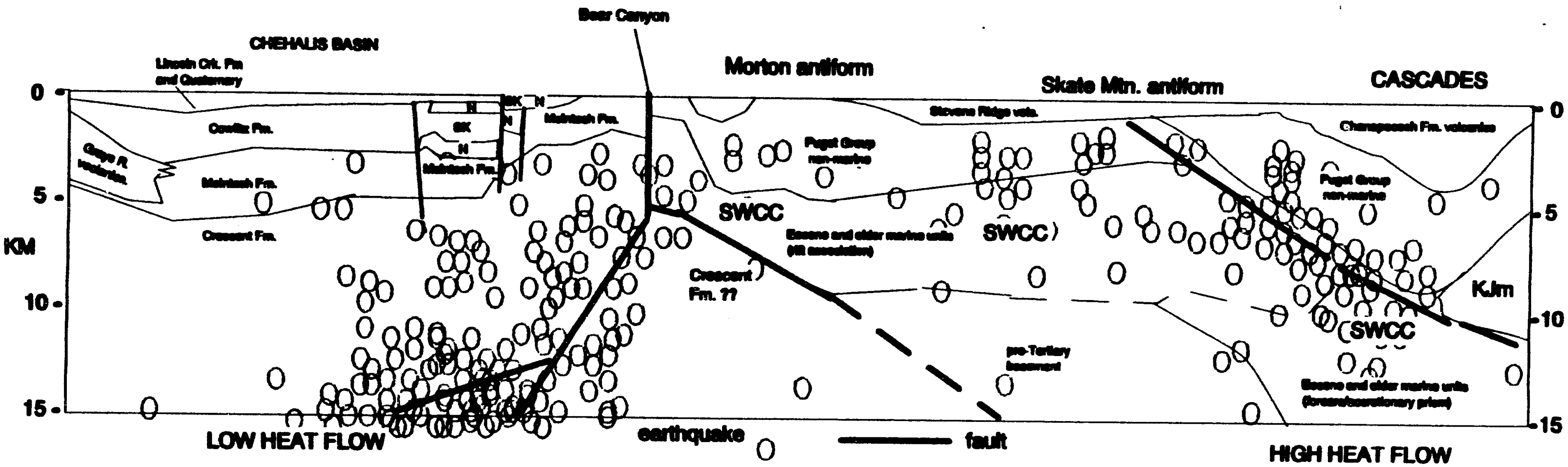

Bear Canyon
CHEHALIS BASIN
Morton antiform
Skate Mtn. antiform
CASCADES
Cowlitz Fm.
McIntosh Fm.
Crescent Fm.
Puget Group non-marine
SWCC
Crescent Fm. ??
pre-Tertiary basement
KJm
KM
0
5
10
15
LOW HEAT FLOW
earthquake
fault
HIGH HEAT FLOW

Figure 27

not exposed at the surface or in wells in this locality. Nevertheless, along the continental margin of British Columbia, including Vancouver Island, both Cretaceous forearc and post-subduction (after suturing) sediments, as well as marine and nonmarine rift sediments are found in the Queen Charlotte and Georgia basins (Yorath, 1987). The Cretaceous marine sedimentary units are part of a subduction-related and post-suture sedimentary sequence that extends from central California to Alaska, and probably also occurred in western Washington.

Up to 5 km of a Neogene rift assemblage, both marine and nonmarine, occurs in the Queen Charlotte Basin on top of unknown thicknesses of upper Cretaceous, post-suture marine and nonmarine sedimentary rocks (Yorath, 1987). The basin basement is formed by lower Cretaceous subduction units that have been thrust over Wrangellia (an accreted terrane that extends from Vancouver Island to southcentral Alaska; Jones and others, 1977). In the southern Georgia Basin, along the east side of Vancouver Island, about 3 km of upper Cretaceous to Paleocene, Nanaimo Group marine and nonmarine sedimentary rocks are overlain by 3 km of nonmarine Eocene Chuckanut sedimentary units (P. D. Hurst, oral comm., 1993). Eisbacher (1985) interprets the Nanaimo Basin (southern part of Georgia Basin) as part of a forearc system dominated by strike-slip, and that coeval, distal trench deposits were removed by dextral slip or subducted beneath the continental margin. We envision that the mix of trench and marine/nonmarine pull-apart sedimentary units found in the Queen Charlotte and Georgia Basins may also occur in the SWCC, with the largest volume being marine.

We suggest that the SWCC first developed as portrayed in Figure 28 during oblique subduction of the Kula plate beneath North America as part of a typical accretionary prism and forearc basin. By Paleocene, the dextral-slip component of

Figure 28-Paleotectonic development of the SWCC region from Stanley and others (1992).

oblique subduction probably led to a pull-apart environment for the forearc region. The formation of pull-apart structures in the forearc region led to thick marine, rift sediments being deposited upon late Cretaceous-Paleocene accretionary sediments. This transtensional environment may have interacted in a complex manner with a local, small spreading center to cause a thick build-up of oceanic basalts and seamounts (Siletzia), forming a new forearc basement. Allochthonous terrane slices of pre-Tertiary rocks may also have been transported northward into contact with the rift/accretionary assemblage; remaining forearc sediments of late Cretaceous age migrated northward along with other margin components to the present Vancouver Island region. Local volcanic centers erupted the Eocene Tukwila and Northcraft Formations. An accretionary prism/forearc basin system formed outboard of the Siletzia complex; thereafter, thick volcanic flows of the Ohanapecosh Formation

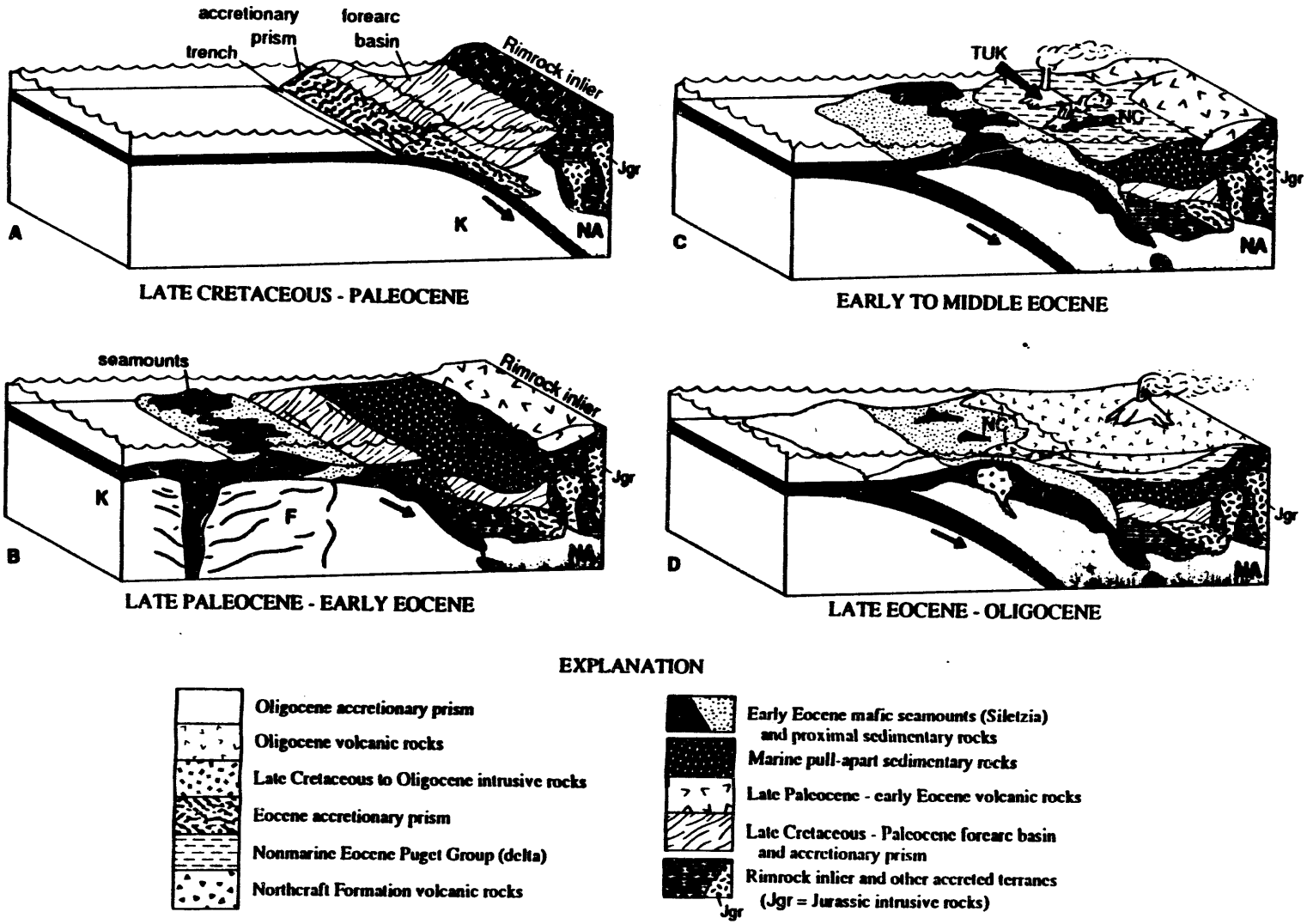

-Our interpretation of tectonic development of western Washington from late Cretaceous to Oligocene adapted from Armentrout and Suek (1985), Ise (1985), Snavely (1987), Eisbacher (1987), and Johnson (1987). See text for explanation.

Figure 28

signaled the establishment of the Cascades volcanic arc associated with the new subduction zone.

This concludes our discussion on the regional tectonics of the SWCC region, and we turn in the next section to a detailed analysis of the most obvious hydrocarbon exploration target in the area, the Morton antiform.

MORTON ANTIFORM STRATIGRAPHY AND SEDIMENTOLOGY

Five stratigraphic sections through portions of the upper part of the Carbonado Formation were measured in the Morton antiform (locations in Figs. 4,29 and Appendix A) ranging in thickness from approximately 110 m to 500 m. Figure 28 is used as an index only, since our geological mapping (Fig. 4) has revised some of the contacts represented on the original map of Walsh and other (1987). A 33-m-thick section was also measured from outcrops at Bear Canyon. Appendix A includes 1) maps showing exact locations of the measured sections; 2) plots of the measured sections; and 3) raw vitrinite reflectance data collected for samples from within the sections. Rocks in these sections consist of interbedded intervals of mainly nonmarine rocks and mainly shallow to marginal marine rocks. Volcaniclastic and volcanic rocks form significant parts of two sections. Rocks are referred to as the Carbonado Formation (Fig. 5), following the stratigraphic usage of Willis (1898) and Gard (1968) for rocks of similar age and facies exposed along strike to the north in the Carbon

Figure 29-Details of the Morton antiform region geology and location of measured stratigraphic sections. Section paths are shown on detailed topographic maps in Appendix A.

River antiform.

Lithology and sedimentology

Lithology and sedimentology of strata exposed in the Morton antiform and cored in the AMOCO 83-5 borehole are briefly discussed below and will be described in detail in future publications. These strata consist of mainly of siliciclastic and less common volcaniclastic rocks deposited in nonmarine to shallow- or marginal-marine environments.

Nonmarine deposits

Nonmarine intervals within the section dominate, comprising about 67 percent of the measured sections. Strata are of inferred fluvial channel and overbank origin. Fluvial channel deposits consist of trough crossbedded, low-angle to horizontal bedded, ripple-laminated, and structureless, very light gray to very pale orange, fine- to coarse-grained sandstone and rare conglomerate. Fluvial sandstone bodies are typically 5 to 20 m thick; the 70-m sandstone body of inferred fluvial origin at the top of the South Fork of the Tilton River section is an anomaly. Sandstone bodies of inferred fluvial origin generally have sharp erosive bases. Upper contacts of sandstone bodies with overlying fine-grained strata are both graded and sharp. Sandstone bodies contain abundant internal low-angle scour surfaces indicating vertical aggradation was an important process in sandstone body development. Conversely, no structures suggestive of lateral accretion (e.g., thick sets of low angle crossbeds) were

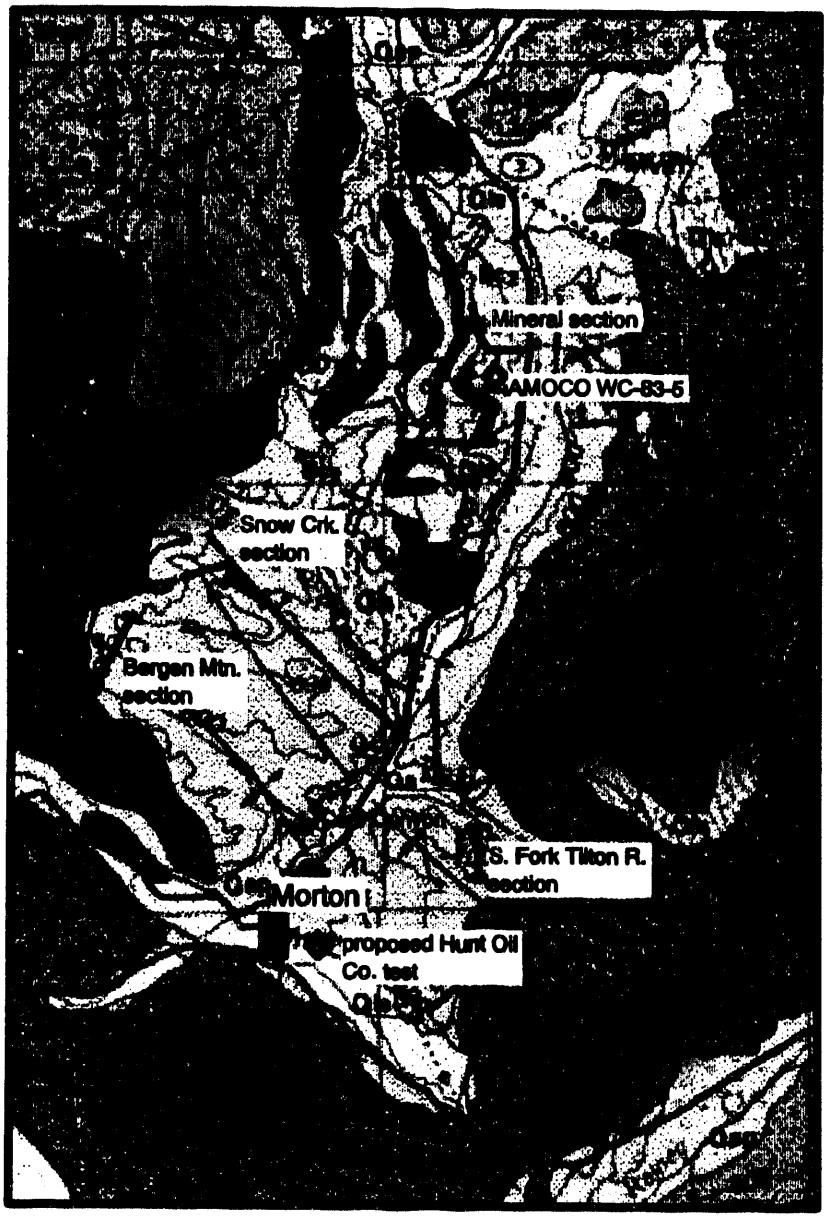

0 10

KM

Figure 29

recognized. These structures may never have formed or, alternatively, the quality and scale of outcrop might preclude their recognition. Sandstone bodies could generally not be traced laterally because of limited outcrop and gentle to steep structural dips. However, one fluvial sandstone body in the Mineral section (Appendix) that could be traced laterally thinned dramatically from 14 m to just 5 m in just 100 m, suggesting

Figure 30-Paleocurrent data for measured sections in the Morton antiform.

a ribbon geometry. Paleocurrent data (Fig. 30) indicate sediment transport was to the west (X = 280°, n = 113).

Three lines of evidence suggest that at least some of these fluvial sandstone bodies formed as distributary channels on a delta plain: (1) The alternating marine-nonmarine character of the stratigraphic sections; (2) evidence for significant vertical aggradation within sandstone bodies; and (3) the apparent ribbon geometry of at least some sandstone bodies. Both (2) and (3) suggest channels occupied the relatively straight courses typical of distributary channels.

Strata interpreted as nonmarine overbank deposits (includes levee, floodplain, shallow lake, floodplain channel, crevasse splay, and peat swamp environments) consist of mudstone to fine-grained sandstone, and less common carbonaceous shale and coal. Parallel and (or) ripple lamination are common, however in many cases primary sedimentary structure has been partly or wholly destroyed by burrows, root traces, and pedogenesis. Fossil plant material (wood and leaf fragments) is common in these beds. Within thick fine-grained intervals, (1) uncommon lenticular beds of ripple-laminated, horizontal bedded, and trough crossbedded very fine to fine grained sandstone (generally less than 1 m thick) are inferred floodplain channel deposits; and (2) sheet-like beds of ripple-laminated and horizontal bedded very fine grained to fine grained sandstone (generally less than 50 cm thick) are inferred crevasse splay deposits. Beds of carbonaceous shale and coal (representing peat swamp deposition) range in thickness from a few cm to about 3 m.

Marginal- to shallow-marine deposits

Strata of inferred marginal to shallow marine origin comprise about 33% of the measured stratigraphic sections. These rocks typically consist of parallel-, ripple-, or wavy-laminated very fine to coarse-grained sandstone, and less common parallel- to ripple-laminated mudstone with thin (< 1 cm) sandstone laminations. Both current- and wave-ripple lamination were recognized, and many ripple sets include thin mudstone drapes. Primary stratification has been partly to completely destroyed in most beds by bioturbation. Burrow diameters range in scale from a few millimeters to several centimeters. The most common burrow forms are *Skolithos, Ophiomorpha, Scoyenia, Asterosoma,* and *Teichichnus*. Both shell fragments (pelecypod and gastropod) and plant fragments are common. Concentrated shell lags are rare and

Morton antiform paleocurrent data

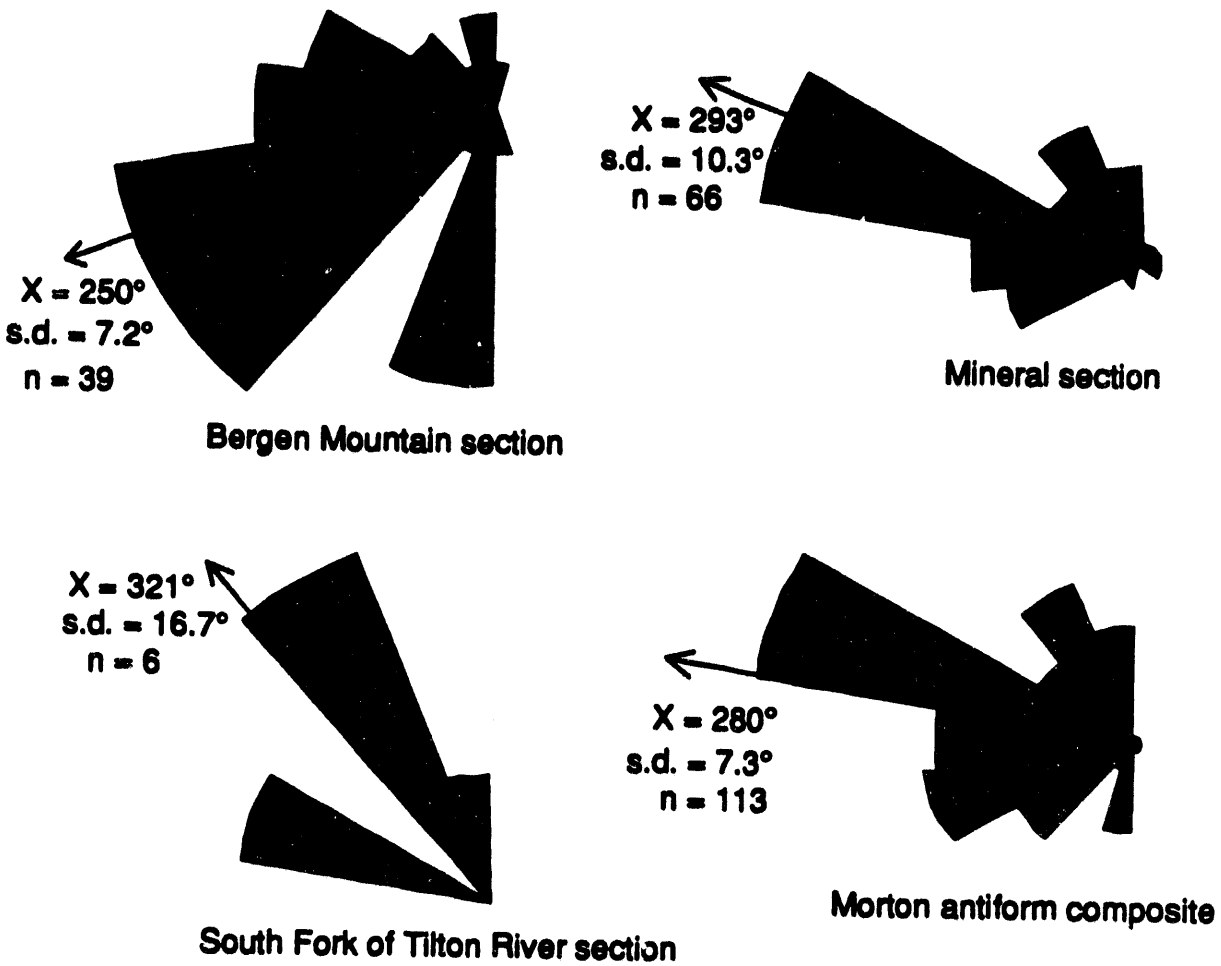

Figure 30

typically thin (< 15 cm). Oval concretions occur in both mudstone and sandstone. Bioturbated sandstone beds range in color from yellowish gray to greenish gray to light bluish gray and are commonly mottled. This range of colors is distinctly different from the typical very light gray to very pale orange color of sandstone in fluvial sandstone bodies. Mudstone beds are typically medium gray to grayish black. Primary stratification, bioturbation, and fossil content indicate these sandstone and mudstone facies are marine in origin. Their alternating occurrence in sections that include thick fluvial/distributary channel sandstone bodies suggests they formed in a delta front to prodelta setting. The abundance of plant fragments suggests that these facies were not significantly reworked by waves or tides.

Volcaniclastic and pyroclastic deposits

Volcaniclastic rocks are common in the Mineral and AMOCO WC-83-5 measured sections (Appendix). Volcaniclastic strata include tuffaceous sandstone, tuff, tuffaceous conglomerate, and tuffaceous breccia-conglomerate. Volcanic sandstone is typically olive gray to olive black, in strong contrast to the much lighter color of fluvial sandstone bodies. Beds are as thick as 8 m, generally massive, can not be traced laterally, and are commonly poorly exposed (and) or heavily weathered. Grains are fine-grained to granular, typically subrounded, and moderately sorted. Many beds have erosive lower contacts. Crude horizontal stratification and(or) grading is reflected by grain size variations in a few beds. Relatively thin (< 30 cm) lenses of volcanic conglomerate are present in several volcanic sandstone beds. These conglomerate beds typically have moderately sorted, subrounded clasts, and are both clast- and matrix-supported. The texture and structure of most beds of volcaniclastic sandstone suggest they formed by redeposition of primary volcanic deposits in fluvial environments. It is possible that a few poorly exposed beds formed as pyroclastic flows.

Lithic to vitric tuff (fine tuff to lapillistone) beds are as thick as about 100 cm and range in color from white to greenish gray. Lighter colored beds are commonly more vitric rich, have sheet-like geometry with sharp, parallel, upper and lower contacts, suggesting origin as fallout. Darker beds are more lithic rich, commonly lenticular, and mainly formed as pyroclastic flows.

Two beds (290 to 320 cm thick) of volcanic breccia conglomerate are present in the Mineral section (Appendix). These beds include a mix of angular to rounded volcanic clasts (as large as 25 cm) dispersed in a fine to coarse ash matrix. The presence of a thin baked zone below one of these beds suggests origin as a pyroclastic flow.

Depositional model

Carbonado Formation strata exposed in the Morton antiform and in the AMOCO WC-83-5 borehole include facies suggesting deposition in mixed nonmarine and marginal- to shallow-marine environments. The presence of thick fluvial sandstone bodies indicates these environments occupied a delta-plain to prodelta setting. Paleocurrent data indicate that drainage was to the west. The presence of

volcaniclastic and pyroclastic strata indicate that nearby active volcanoes contributed sediment to the delta. This general model is consistent with that proposed by Buckovic (1978) for a larger area in southwest Washington. Within this type of deltaic setting, the major nonvolcanic controls on siliciclastic facies deposition are sediment supply, eustasy, and subsidence. Nonmarine deposition occurred when the combination of these factors led to a relative lowering of base level; shallow- to marginal-marine deposition occurred during relative rises of base level. At a smaller scale, autochtohnous processes (e.g., abandonment of delta lobes) can also affect marine-nonmarine patterns of deltaic deposition.

Correlation of Morton antiform sections

Reconstruction of the stratigraphy of the Carbonado Formation in the Morton antiform area is problematic for several reasons: (1) The area is densely vegetated. As a result, outcrops are sparse and mainly restricted to cuts on recently built logging roads and to exposures in stream channels; (2) The area has not been geologically mapped in detail. Existing published maps (Fisher, 1957; Schasse, 1987) are of a reconnaissance nature. (3) The Morton antiform is structurally complex, characterized by many faults and small-scale folds (e.g., Fisher, 1957; Schasse, 1987). Offsets on faults can be significant; for example, geologic relationships indicate that a fault in the alluvium-filled valley between Morton and Mineral valley (the valley of the Tilton River and Roundup Creek) has a minimum displacement of about 800 m. Some of these structures may have been syndepositional (e.g., Johnson, 1985, Johnson and others, 1994), creating local differential subsidence and (or) uplift. (4) Marker beds within stratigraphic sequences have not been recognized, and there was no doubt complex interfingering of nonmarine, shallow- to marginal-marine, and volcanic depositional facies. There may have been more than one active volcanic center contributing volcanic detritus to the Carbonado Formation in the Morton area. (5) The location of the contact between the Carbonado and Northcraft Formation is not straightforward. For example, the contact in the area of the Mineral measured section (Appendix A) used in this report is significantly lower in the section than that mapped by Schasse (1987).

Figure 31 highlights the problem of stratigraphic correlation and the lack of marker beds. The figure shows schematic stratigraphic columns for the Mineral,

Figure 31-Stratigraphic correlation section with fixed Northcraft level.

Bergen Mountain, and South Fork of the Tilton River measured sections (Appendix). All three sections are overlain by sections of mainly volcanic rocks and therefore are inferred to represent the top of the Carbonado Formation in the Morton antiform. Alignment of the sections on this contact, however, shows that the general stratigraphy for each column defined by the alternating marine and nonmarine intervals

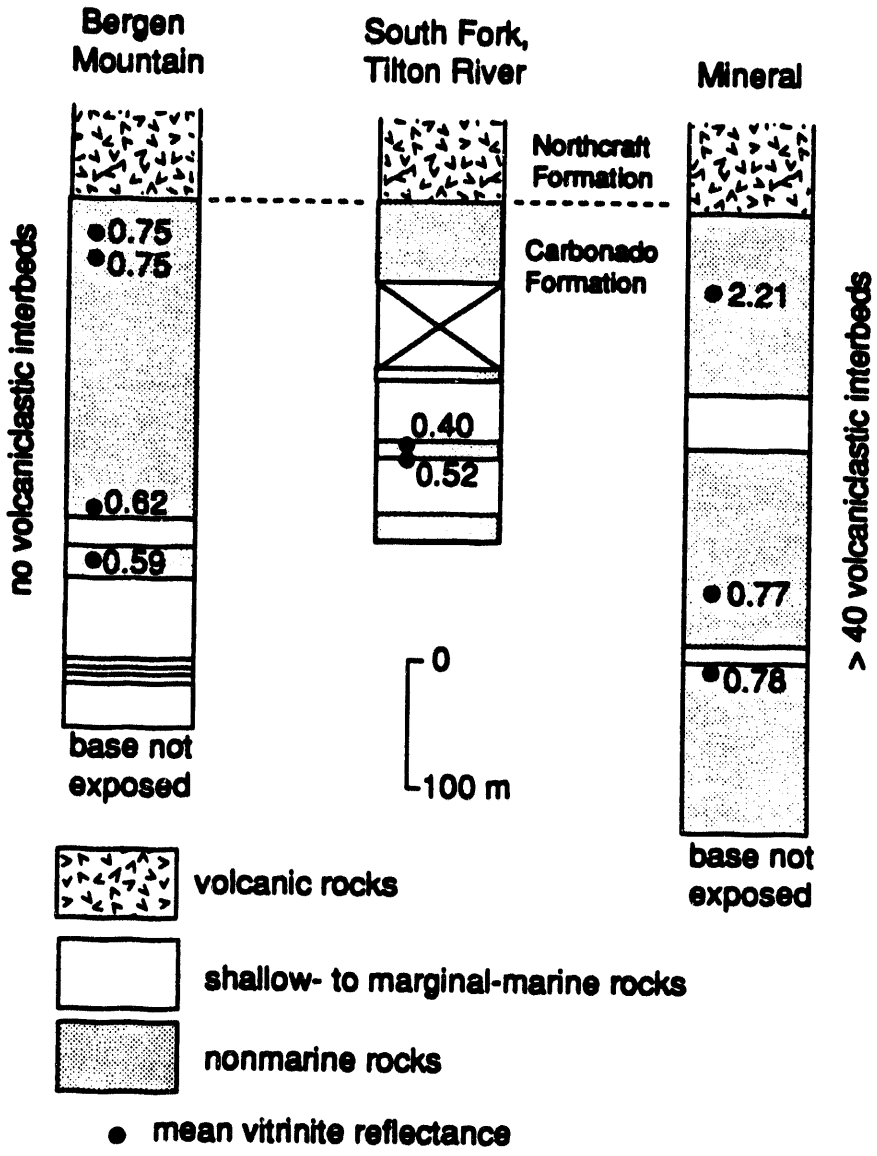
Bergen Mountain
South Fork, Tilton River
Mineral
Northcraft Formation
Carbonado Formation
no volcaniclastic interbeds
> 40 volcaniclastic interbeds
0.75
0.75
0.62
0.59
0.40
0.52
2.21
0.77
0.78
0
100 m
base not exposed
base not exposed
volcanic rocks
shallow- to marginal-marine rocks
nonmarine rocks
mean vitrinite reflectance

Figure 31

cannot be matched from one column to the next. For an area as small as the Morton antiform, one would expect that the thicker marine intervals (indicative of significant transgressions) should be correlative. Moreover, the Mineral section includes more than 40 interbeds of volcaniclastic rocks (including many units of inferred airfall origin) while no volcaniclastics were recognized in the Bergen Mountain and South Fork of the Tilton River sections. These problems illustrate the stratigraphic complexity of the Carbonado Formation, and indicate that stratigraphic correlation in even a small

Figure 32-Stratigraphic correlation section with variable Northcraft level.

structurally complex area can be difficult with a limited data base.

Figure 31 provides a more realistic correlation of the five measured stratigraphic sections, the present best guess based on rationale outlined below. The Mineral surface section and the AMOCO WC-83-5 borehole section are approximately 1 km apart. The local area between the two sites is structurally complex (Schasse, 1987), so simple projection of structural attitudes from one site to the other does not demonstrate absolute stratigraphic position. The Mineral section forms the top of the local Carbonado section and therefore must at least partly overlie the AMOCO WC-83-5 borehole section. A distinctive, thick, purplish-gray volcaniclastic unit occurs at the base of the Mineral section and was not recognized in the borehole core. Therefore, there is no duplication between the two sections; the amount of missing rock between the two sections cannot be determined based on outcrop data.

Farther south, the Bergen Mountain and Snow Creek sections are about 4 km apart, but separated by faults [illegible]lds (Schasse, 1987). The Bergen Mountain section is overlain by volcanic [illegible]f the Northcraft Formation and is therefore at least locally at the top of the Carbonado section. Map patterns (Schasse, 1987) indicate the Snow Creek section must lie well below the Bergen Mountain section, but there is insufficient data to calculate its absolute stratigraphic position.

Although both the Mineral and Bergen Mountain sections (about 12 km apart) are overlain by the volcanic Northcraft Formation, direct correlation of the two sections seems highly unlikely because (as discussed above) of the significant difference in the number of volcanic interbeds (Fig. 30 and Appendix A) and the lack of correlation between marine and nonmarine intervals in the two sections. Mapping by Hagen (1987) indicates that the main intrusive center for the Northcraft Formation was centered in the southwestern portion of T. 14 N., R. 3 E. (secs. 28, 29, 30, 31, 32, 33), approximately 11 km from the Bergen Mountain section and 19 km from the Mineral section (Fig. 3). Therefore, the effects of Northcraft volcanism should have been recorded earlier in the Bergen Mountain section than the Mineral section. We infer that these effects resulted in deposition of thick Northcraft flows in the Bergen Mountain area (with only minor significant siliciclastic deposition) synchronous with continued deltaic deposition (with increasing volcanic input) to the north in the Mineral

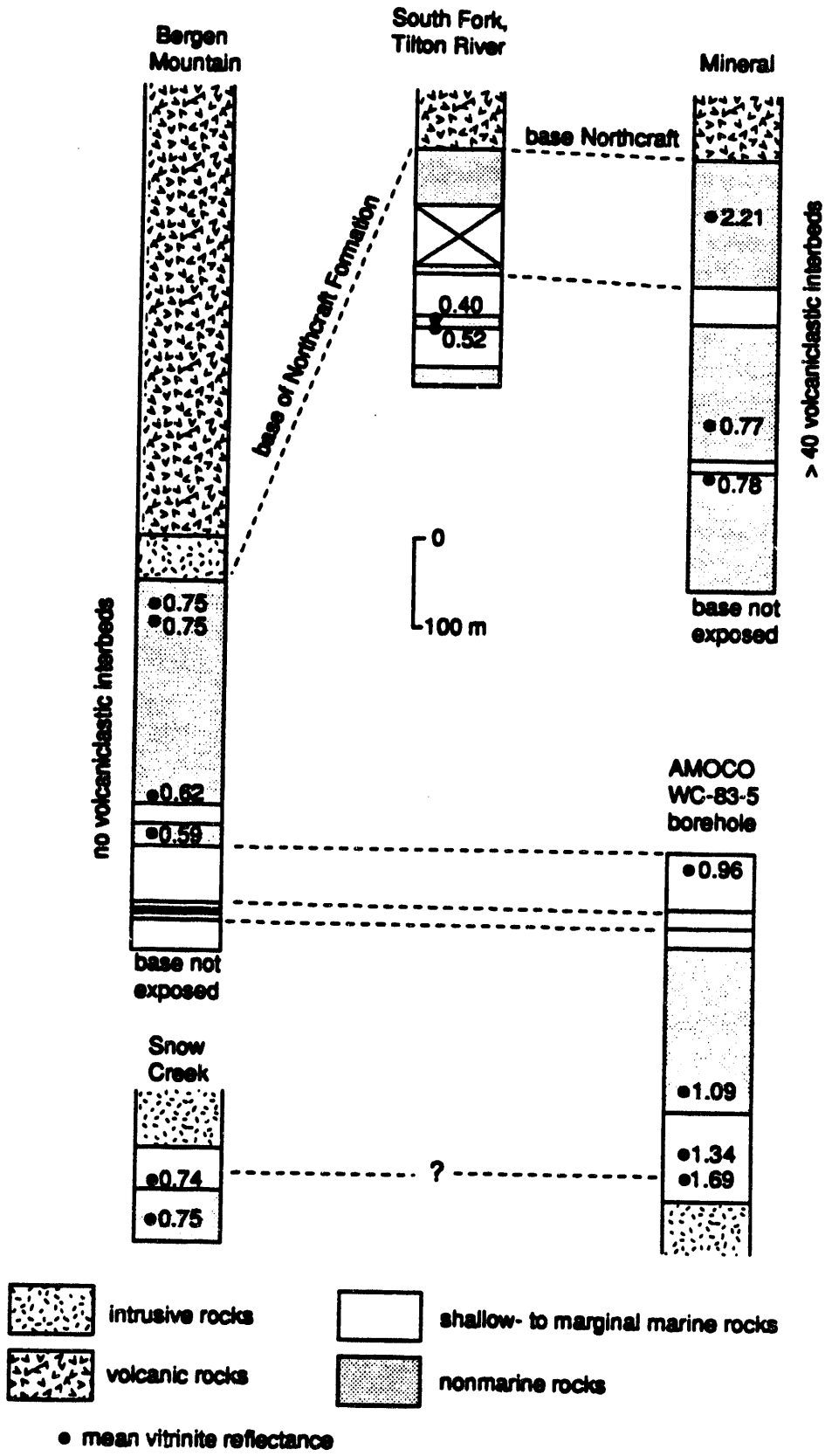
Bergen Mountain
South Fork, Tilton River
Mineral
base Northcraft
base of Northcraft Formation
•2.21
0.40
0.52
•0.77
•0.78
> 40 volcaniclastic interbeds
0
100 m
base not exposed
no volcaniclastic interbeds
•0.75
•0.75
•0.62
•0.59
AMOCO WC-83-5 borehole
•0.96
base not exposed
Snow Creek
•1.09
•1.34
•1.69
•0.74
•0.75
?
intrusive rocks
volcanic rocks
shallow- to marginal marine rocks
nonmarine rocks
• mean vitrinite reflectance

Figure 32

area. This relationship is shown in Figure 32.

Correlation of the lower part of the Bergen Mountain section with the upper part of the AMOCO WC-83-5 borehole (Fig. 31) is based on a similar sequence of marine-nonmarine-marine depositional intervals in the two sections. If this speculative correlation is correct, there is approximately 310 m of unmeasured strata between the Mineral section and the AMOCO WC-83-5 borehole section. Given these matches, the highest stratigraphic position that the Snow Creek measured section could occupy (Figure 34) is equivalent to the base of the AMOCO WC-83-5 borehole section. It could occur significantly lower in the stratigraphic sequence.

The South Fork of the Tilton River section is located 11 km from the Bergen Mountain section, 13 km from the Mineral section, and about 22 km from the Northcraft volcanic center of Hagen (1987; Fig. 2). Using the logic applied above regarding proximity to the Northcraft volcanic center, one might infer that the Carbonado-Northcraft contact in the South Fork of the Tilton River section should be higher than in the Bergen Mountain section. Placement of this contact at the same position as in the Mineral section is supported by a similar position of the highest nonmarine-marine facies boundary. This placement is also consistent with relatively low vitrinite reflectance values from the South Fork of the Tilton River section, indicating relatively less heating from burial and intrusions (despite a more eastern location closer to the axis of the Cascade Mountains) than in the Bergen Mountain section. Two factors argue against the high stratigraphic position of the South Fork of the Tilton River section: (1) The marine interval in the Mineral section is thinner than in the dominantly marine part (includes both marine intervals) of the South Fork of the Tilton River section. This contrast could reflect a major facies change, with a marine embayment lying south (South Fork Tilton River area) of a west-flowing delta lobe to the north (Mineral area). (2) The South Fork of the Tilton River section apparently lacks volcaniclastic interbeds. However, in that most of the well-exposed strata in this section have a marine origin (the upper nonmarine interval is very poorly exposed) and were subjected to significant sediment mixing by currents and bioturbation, this would not be unexpected.

Given these tentative correlations, there is a minimum of about 1200 m of stratigraphic section of the Carbonado Formation exposed at the surface or in the relatively shallow subsurface in the Morton antiform.

WHAT ROCKS UNDERLIE THE MORTON ANTIFORM?

The discussion above indicates there is a minimum of about 1200 m of the Carbonado Formation exposed at the surface or in the relatively shallow subsurface in the Morton antiform. Three DOE seismic reflection lines (1-2, 4, 5) cross the Morton antiform and reveal about 2.5 to 3 seconds of coherent reflectors beneath the Morton antiform. At typical expected velocities for these rocks (see earlier section on seismic velocity analysis) these reflectors probably represent about 4-5 kilometers of stratigraphic section. Structural complexity in the region makes analysis of seismic facies (e.g., Sangree and Widmier, 1977) difficult. Reflectors in the upper 2 seconds below the Morton antiform are continuous to discontinuous, have moderate to high amplitudes, and tabular to wedge-shaped external forms (Figure 17). These characteristics typify delta-plain-to-shelf depositional environments in which there is significant interbedding of different lithologies (i.e., mudstones and sandstones), a setting similar to that inferred above for the rocks at the surface and shallow subsurface in the Morton antiform. Seismic, surface outcrop, and borehole data thus indicate there is at least 4 km of Eocene deltaic strata in the Morton antiform.

The quality of seismic data below 2 seconds in the Morton antiform does not permit seismic facies analysis, nor does it allow accurate placement of the contact of the sedimentary sequence and its basement. Based on magnetotelluric data, Stanley and others (1992) showed a 3-4 km thick upper unit (30-40 ohm-m) in the Morton antiform (see MT model in Fig. 12) that is here interpreted as the deltaic sequence described above. Below this interval, Stanley and others (1992) recognized a thick (3-5 km) highly conductive (1-5 ohm-m) unit (Figs. 11 and 12) which they suggest is comprised of marine sedimentary rocks and corresponding to the SWCC. Regional geology and stratigraphy provide clues as to the nature of this lower unit in the Morton antiform area.

In the Tiger Mountain area about 100 km north of the Morton antiform, fluvial-deltaic rocks of the late middle Eocene Tiger Mountain Formation, similar in age and lithology to the Carbonado Formation in the Morton antiform, overlie early middle Eocene rocks of the Raging River Formation (Vine, 1969; Johnson, 1992; Fig. 5). The Raging River Formation consists of a diverse assemblage of rocks including fluvial conglomerates and relatively deep marine (upper to middle bathyal; water depths of 500-2,000 m) mudstones. The Raging River Formation has a minimum thickness of about 1,000 m; its base is not exposed.

Snavely and others (1951, 1958) described the stratigraphy of the McIntosh Lake area, about 40-45 km west-northwest of the Morton antiform. In this area, the McIntosh Formation (~ 1,000 m thick, base not exposed) coarsens upward from dominantly marine mudstone in the lower part of the unit to fluvial-distributary channel deposits (i.e., the Tenino Sandstone) at the top of the unit. When compared with the benthonic foraminifera biofacies lists of Ingle (1980), foraminifera recovered from the McIntosh marine mudstones suggest upper bathyal deposition (water depths of 150 to 500 m) for the marine mudstones. The McIntosh Formation is overlain by volcanic rocks of the Northcraft Formation and deltaic rocks of the Skookumchuck

Formation.

Relationships in both the Tiger Mountain and McIntosh Lake area support both a regional and local (for the Morton area) paleogeographic model in which Eocene deltaic facies prograded to the west and southwest over fine-grained marine rocks. This transition occurred earlier in the Tiger Mountain area than in the McIntosh Lake area because of its more northeastern location (Figs. 5). Fine-grained marine rocks of the Raging River and McIntosh Formations are analogs for the deeply buried conductive rocks in the Morton antiform.

Could the entire SWCC in the Morton area and elsewhere be composed of these Eocene marine mudstones? If so, a complete section of Eocene strata at Morton would be at least 8 km thick. Correlative Eocene basins (for example, Swauk Basin, Chuckanut Basin, Puget Basin) in the Washington Cascades have transtenional origins and are characterized by thick sedimentary fills (commonly more than 5 km) and rapid sediment accumulation rates (Johnson, 1985). These basins do not form major conductive anomalies, however they contain mainly nonmarine rocks and they have been uplifted and eroded. Given a more outboard paleogeographic position and a different Neogene tectonic history (burial below the Cascades), they would be characterized by similar conductive anomalies. Regional relationships are thus consistent with origin of the Morton portion of the SWCC as a deeply buried Eocene marine mudstone unit in a transtensional basin. However, as discussed earlier, the deep units that appear to be thrust well eastward beneath pre-Tertiary rocks could be associated with a pre-Eocene subduction complex.

THE MORTON ANTIFORM HYDROCARBON PLAY

Prospective hydrocarbon plays should include good (organic-rich and thermally-mature) source rocks, reservoir rocks, and a viable trap and seal. In the following section we discuss these aspects of the Morton antiform area.

Source rocks

In the Morton area, the most likely source rocks are the Eocene marine mudstones that form at least the upper part of the SWCC. As discussed above, these strata were probably deposited at bathyal water depths in a prodeltaic setting. Strata of the Raging River Formation to the north and the McIntosh Formation to the west provide surface exposures of these facies (Fig. 5). There are very limited organic geochemical data from the Raging River Formation (Johnson, 1992), and no available data from the McIntosh.

For the Raging River Formation (Johnson, 1992), rock-eval pyrolysis shows that unit 3 bathyal mudstone from the AMOCO WC-83-14 core are now overmature with respect to hydrocarbon generation (T_{max} = 533°- 542° for three samples) and thus cannot be reliably evaluated as petroleum source rocks (Peters, 1986). Vitrinite reflectance values in five samples from this core range from 1.96 ± 0.33 (depth of 498 m) to 1.65 ± 0.08 (depth of 69 m) and similarly indicate overmaturity. Despite these indicators of high thermal maturity, there is still as much as 0.8-0.9 percent total organic carbon in fine-grained marine rocks of the Raging River Formation. This remnant organic content is an indication that the rocks were once more organic rich and capable of generating hydrocarbons. The common occurrence of terrestrial organic matter in the organic-rich mudstones is consistent with their inferred prodeltaic setting, and suggests they would be gas-prone source rocks.

Coals and carbonaceous shales in the deltaic upper sedimentary unit of the Morton antiform might also be viable gas-prone source rocks. These mainly nonmarine organic-rich rocks do not represent a large volume of strata in the measured sections (Appendix B).

The thermal maturity of organic-rich rocks in the Morton antiform is both laterally and vertically variable and appears to be related to heat sources from burial, local intrusions, and possibly heating from overlying volcanic flows. Vitrinite reflectance values from the measured sections (Fig. 8; Appendix A) illustrate this complex thermal regime. In samples from the AMOCO WC-83-5 borehole, there is a rapid decrease in mean vitrinite reflectance (R_m) above the intrusion that occurs at the base of the borehole, from 1.69 percent at about 30 m above the intrusion to 1.09 percent about 130 m above the intrusion. The steep thermal gradient associated with this intrusion was also noted by Esposito (1993) based on clay-mineral reactions. R_m in a sample from near the top of the 400 m core (0.96 percent) indicates a much lower paleo-geothermal gradient that was probably mainly controlled by burial. This burial-related gradient appears to continue upward and include the two samples in the overlying Mineral section (R_m = 0.77 and 0.78 percent). However, the highest sample in that section yielded a R_m of 2.21 percent. The only viable explanation for

this anomalously high value is proximity to a nearby, concealed intrusion.

Farther south, the lowest four samples in the Bergen Mountain-Snow Creek area (Fig. 34) suggest a shallow paleo-geothermal gradient that was mainly controlled by burial (values of 0.74 to 0.62 percent). There does not appear to be a significantly elevated paleo-geothermal gradient associated with the thick intrusion (> 130 m) that caps the short Snow Creek section. In contrast, the 45-m-thick intrusion that caps the Bergen Mountain section has resulted in a notable inversion of Rm, with higher values at 25 and 50 m below the top of the section (0.74 and 0.75 percent) than at about 250 and 300 m below the top of the section (0.62 and 0.59 percent). These Rm measurements indicate that the thermal effects of different intrusions in the Morton area varies significantly, based on a combination of intrusion depth, thickness, and composition.

The lowest R_m values in the Morton antiform are from the South Fork of the Tilton River section (0.40 and 0.52 percent). These samples lie closest to the axis of the Cascade Range and therefore should have been subjected to the highest regional thermal gradients (Walsh and Lingley, 1991). Their relatively low values indicate that they were either not buried as deeply or that they have been consistently isolated from centers of intrusive activity, such as that associated with the volcanic Northcraft Formation (Hagen, 1987).

Although thermal maturity varies significantly in rocks at or near the surface in the Morton antiform, most rocks are near the lower part of or well within the hydrocarbon-generating window (Tissot and Welte, 1978). Based on limited data, thermal maturity in the Morton antiform locale appears to increase westward, possibly controlled by proximity to the intrusive center for the Northcraft Formation. Depending on their depth of burial and proximity to intrusions, source rocks in the Morton antiform subsurface might yield either wet or dry gas. Maximum burial and gas generation/migration probably occurred in the late Oligocene or early Miocene (Walsh and Lingley, 1991). Possible deeper source rocks may exist to the east in the lower parts of the SWCC that are inferred to include subduction complex units. For these hypothesized units a higher heat flow and deeper burial mean that the units would have been sourcing hydrocarbons during and prior to the late Oligocene and Miocene, but likely at highest rates prior to formation of the Morton antiform. For the latter reasons, it may be unlikely that any hydrocarbons sourced from these deeper, eastern sedimentary rocks were retained within the Morton antiform.

Reservoir rocks

Beds of fine- to coarse-grained sandstone of fluvial-distributary channel origin (see above) comprise the best reservoir rocks in the strata exposed at the surface or in the shallow subsurface. These channel bodies are typically 5-20 m thick, but can be as thick as 70 m. Given their inferred deltaic setting, they probably have ribbon geometry, elongate east to west. Shallow-marine sandstone beds within the described section are typically heavily bioturbated and less viable source rocks. There could be bathyal turbidite sandstones in deeper subsurface (the SWCC) below the Morton antiform, but this hypothesis can only be tested by drilling.

No quantitative porosity and permeability data have been collected from the

fluvial-distributary channel sandstone bodies in the described sections. In four of the five measured sections, these bodies are typically well cemented. In the South Fork of the Tilton River section, however, sandstone bodies are notably friable and porous.

Preliminary petrographic analysis of just 4 samples from fluvial-distributary sandstone bodies in the AMOCO WC-83-5 borehole reveals arkosic compositions (mean QFL of 38, 39, 23) consistent with compositions of Eocene fluvial and deltaic sandstones elsewhere in western Washington (Buckovic, 1978; Frizzell, 1978; Johnson, 1985). Lithic fragments are primarily volcanic and sedimentary in origin. These samples have minimal porosity (< 5 percent) and significant calcite cement and clay pseudomatrix. Pseudomatrix was mainly produced by alteration of lithic fragments and detrital mafic minerals.

Given the available data, it is difficult to predict porosity and permeability in the subsurface. Sands of similar composition interbedded with rocks of low thermal maturity (0.5 percent > R_m) are gas reservoirs at the Mist Field in northwestern Oregon (Armentrout and Suek, 1985) and gas-storage reservoirs in the nearby Chehalis Basin (Fig. 4). One would expect greater breakdown of detrital grains and increased circulation of cementing diagenetic fluids with higher thermal maturities and proximity to intrusions, factors that appear to characterize most of the Morton antiform. It may be that secondary porosity is needed to produce viable reservoirs in the subsurface of the Morton antiform.

Trap and seal

The Morton antiform is not a simple anticline. Rather, it is a structurally high area where middle Eocene sedimentary rocks have been brought to the surface through a complex network of folds and faults (Schasse, 1987). Several relatively small-scale structural traps might be present along crests of small anticlines or in small fault blocks as at the Mist gas field in northwest Oregon (Armentrout and Suek, 1985). The maximum closure based upon the seismic data interpretation (Fig. 31) is about 2000', but actual traps are likely thinner than this. Stratigraphic traps or combined structural-stratigraphic traps might be present where fluvial-distributary channel sandstones pinchout against interbedded fine-grained rocks.

Prior to Miocene and younger uplift and erosion, volcanic rocks of the Northcraft and Ohanapecosh Formations covered the Morton antiform area and would have provided a highly effective seal. After removal of this regional seal, local seals might have been provided by impermeable mudstone and volcaniclastic strata, and by intrusions. The abundant faults in the Morton antiform would have a negative impact on preserving the integrity of both traps and seals.

SUMMARY AND CONCLUSIONS

Extensive geophysical studies have outlined a anomalous part of the Earth's crust in the southern Washington Cascades region. Seismic reflection surveys were designed from MT, gravity, and magnetic models. The seismic data were obtained where there were no previous results, and although the data were of marginal quality much was learned about the application of seismic methods in volcanic areas. Future studies in such areas should involve more testing of dynamite source methods, wide-line-profiling, wide-angle shooting, and other innovative techniques designed to obtain deep images of the earth in complex geological settings. Standard industry exploration methods will not achieve the type of information required in frontier areas such as that of the SWCC region.

The effectiveness of the MT method was well demonstrated and models computed for this complex geological region were found to essentially agree with key details of an extensive deep seismic reflection survey. In areas where no wells were available it would have been impossible to sort out any lithological information from the seismic data alone, but with a combination of MT, gravity, magnetic, seismicity, and seismic reflection data, a detailed tectonic/stratigraphic model has been developed. This model draws heavily upon geological and geophysical information from the Chehalis Basin and other nearby basins, but remains to be tested with drilling. A proposed 15,000' drill hole to be completed by Hunt Oil Co. in 1994 should answer key questions about the Morton antiform in detail and provide ground truth for our proposed broader models of the region. Maximum benefit from this well could be obtained by intensive analysis of core and cuttings as well as geochemical sampling while drilling of both gases and bore fluids. Hunt Oil has suggested that it will provide core and cuttings to the USGS for future studies. In addition, the USGS can be available for continuous gas sampling during the drilling and completion of the hole.

A detailed stratigraphic and play analysis of the Morton antiform area was completed for this report, using new data acquired under the USGS Evolution of Sedimentary Basins program. This particular play analysis represents the end member in a program of frontier research using reconnaissance geophysics to identify areas where deeply sourced methane may be trapped in shallow structures. It seems likely that there are viable gas-prone source rocks beneath the Morton antiform and possible deeper units may occur to the east in lateral parts of the SWCC. The presence of reservoir-quality sandstones in the deeper (> 1,000 m?) subsurface of the Morton antiform is probably dependent on isolation from intrusions and(or) development of secondary porosity. The abundant small-scale deformation in the Morton antiform has probably had a strong negative effect on hydrocarbon trapping and sealing mechanisms.

ACKNOWLEDGMENTS

The authors wish to thank a number of individuals who contributed to our understanding of the SWCC region and more directly to materials used in this report. Bill Lingley and Tim Walsh, Washington Department of Natural Resources, provided a great deal of essential information on well locations, well reports, and general geological information. Carol Finn, USGS, has worked for several years on analyzing gravity and magnetic data for the region and provided most of the models for these data sets referenced in this and earlier reports on the region. Gerda Abrams, USGS, reduced and processed the aeromagnetic survey funded by DOE. Gary Latham and Keith Westhusing planned much of the seismic survey and bird-dogged the field acquisition. Rick Steinik and others at Golden Geophysical played a key role in allowing high-quality processing of DOE seismic lines 1,2, and 3. John Contino, Geotrace Technologies was responsible for processing seismic lines 4,5, and 6. Tom Ise, Consulting Geologist, aided our initial understanding of the Chehalis Basin with his 1985 publication and personal discussions. We are grateful to L. B. Industries for providing seismic reflection data in the Carbon River antiform. Tom Mroz, DOE, provided digitized sonic logs from key wells. Nick Zilman, USGS, produced the very useful seismic data CD-ROM and associated users software. Lastly and most importantly, W. J. Gwilliam Deep Gas Project manager, made this research possible with his unflagging enthusiasm for the potential of finding large volumes of unknown gas source rocks in the western U.S. Cordillera.

REFERENCES

Abrams, Gerda, 1992, Aeromagnetic survey of the Morton, Washington are: U.S. Geological Survey Open-File Rept. 92-251.

Acuna, M. H., Searce, C. S., Seek, J. B. and Scheifele, J., 1973, The MAGSAT vector magnetometer-a precision fluxgate magnetometer for the measurement of the geomagnetic field: Technical Memorandum No. 79656, NASA Goddard Space Flight Center, Greenbelt, Maryland, 18 pp.

Anstey, Nigel A., 1977, Seismic interpretation: the physical aspects: International Human Resources Development Corporation, Boston, MA, 625 p.

Armentrout, J.M., and Suek, D.H., 1985, Hydrocarbon exploration in western Oregon and Washington: American Association of Petroleum Geologists Bulletin, v. 69, p. 627-643.

Babcock, R.S., Burmester, R.F., Engebretson, E.C., and Warnock, A., 1992, A rifted origin for the Crescent basalts and related rocks in the northern Coast Range volcanic province, Washington and British Columbia: Journal of Geophysical Research, p. 6,799-6,821.

Barnett, D. B. and M. A. Korosec, 1989, Results of the 1988 geothermal gradient test drilling project for the State of Washington: Washington Division of Geology and Earth Resources, Open-File Report 89-2, 54 p.

Belt, E. S., 1968, Post-Acadian rifts and related facies, eastern Canada: in Zen, E-An, White, W. S., Hadley, J. B., and Thompson, J. B., eds., Studies in Appalachian geology, Northern and Maritime, New York, Interscience, p. 95-113.

Blackwell, D. D., J. L. Steele, and S. A. Kelley, 1985, Heat flow and geothermal studies in the State of Washington: U.S. Department of Energy Report ID/12307-1, 77pp.

Blackwell, D. D., and J. L. Steele, 1983, A summary of heat flow studies in the Cascade Range: Transactions of the Geothermal Resources Council, v. 7, p. 233-236.

Boswell, R., Wilson, T.W., and Donaldson, A.C., 1988, Evaluation of a seismic line across the Puget downwarp, southwestern Washington: DOE Final Report, 24 p.

Braislin, D. B., D. D. Hastings, and P. D. Snavely, Jr., 1971, Petroleum potential of western Oregon and Washington and adjacent continental margin: in Future Petroleum Provinces of the United States-Their Geology and Potential: American Association of Petroleum Geologists Memoir 15, v. 1, 229-238.

Brown, L. F., Jr., and W. L. Fisher, 1979, Principles of seismic stratigraphic interpretion; Interpretaion of depositional systems and lithofacies from seismic data: Seismic stratigraphic interpretation and petroleum exploration: AAPG Continuing Education Course Notes Series #16, University of Texas at Austin, 56 p.

Brown and Ruth Laboratories, Inc., 1982, Pacific Northwest Regional petroleum geochemistry of the onshore and offshore sediments of Washington and Oregon-Pan American Petroleum Company OCS-P-0141, offshore Jefferson

County, Washington:
Buckovic, W.A., 1978, The Eocene deltaic systm of west-central Washington, in Armentrout, J.M., Cole, M.R., and TerBest, H. Jr., Cenozoic Paleogeography of the western United States: Society of Economic Palentologists and Mienralogists, Pacific Section, p. 147-164.
Cady, W. M., 1975, Tectonic setting of the Tertiary volcanic rocks of the Olympic Peninsula, Washington: U.S. Geological Survey Journal of Research, v. 3, p. 573-582.
Carey, S. W., 1958, A tectonic approach to continental drift: in Carey, S. W., ed., Continental drift: A symposium, University of Tasmania, p. 177-355.
Clarke, J., Gamble, T.D., Goubau, W.M., Koch, R.H. and Miracky, R.F., 1983, Remote-reference magnetotellurics: equipment and procedures, Geophys. Prospecting, 31, 149-170.
Clowes, R.M., Brandon, M.T., Green, A.G., Yorath, C.J., Sutherland Brown, A., Kanasewich, E.R., and Spencer, C., 1987, LITHOPROBE - Southern Vancouver Island: Cenozoic subduction complex imaged by deep seismic reflections: Canadian Journal of Earth Sciences, v. 24, p. 31-51.
Cordier, J. -P., 1985, Velocities in Reflection Seismology: Reidel, Dorcrecht, 201 pp.
Davis, G. D., J. W. H. Monger, and B. C. Burchfiel, 1978, Mesozoic construction of the Cordilleran "Collage", central British Columbia to central California: in Mesozoic Paleogeography of the Western United States: Pacific Section, Society of Economic Paleontologists and Mineralogists, Pacific Coast Paleogeography Symposium 2, Los Angeles, p. 33-70.
Dietz, Lynn D., and W. L. Ellsworth, 1990, The October 17, 1898 Loma Prieta, California, earthquake and its aftershocks: geometry of the sequence from high-resolution locations: Geophysical Research Letters, v. 17, no. 8, p. 1353-1359.
Dobrin, M. B., and Savit, C. H., 1988, Introduction to Geophysical Prospecting: Fourth Edition, McGraw-Hill, New York, 867p.
Eisbacher, G. H., 1985, Pericollisional strike-slip faults and synorogenic basins, Canadian Cordillera: in Biddle, K. T., and Nicholas Cristie-Blick, eds., Strike-slip Deformation, Basin Formation, and Sedimentation, Society of Economic Paleontologists and Mineralogists Special Publication 37, p. 265-282.
Ellingson, J. A., 1972, The rocks and structure of the White Pass area, Washington: Northwest Science, v. 46, p. 9-24.
Ellingson, J. A., 1972, The rocks and structure of the White Pass area, Washington: Northwest Science, v. 46, p. 9-24.
Esposito, K.J., 1993, Thermal effects of thin igneous intrusions on the illitization reaction in a Tertiary basin, southwestern Washington state [M.S. thesis]: Golden, Colorado School of Mines, 142 p.
Evans, J. E., 1988, Depositional environments, basin evolution, and tectonic significance of the Eocene Chumstick Formation, Cascade Range, Washington: unpublished Ph.D. thesis, University of Washington, Seattle, 325 p.
Evans, J. E., and S. Y. Johnson, 1989, Paleogene strike-slip basins of central Washington: Swauk and Chumstick Formations: in N. L. Joseph and others,

eds., Geologic Guidebook for Washington and Adjacent Areas, Washington Division of Geology and Earth Resources Information Circular 86.

Finn, C. A., 1989, Structure of the convergent Washington margin: in Proceedings of the Workshop XLIV Geological, Geophysical, and Tectonic Setting of the Cascade Range, U.S. Geological Survey Open-File Rept. 89-178, p. 291-317.

Fisher, R.V., 1957, Stratigraphy of the Puget Group and Keechulus group in the Elbe-Packwood area of southwestern Washington [Ph.D. thesis]: Seattle, University of Washington, 157 p., 10 plates.

Fitterman, D. V., W. D. Stanley, and R. J. Bisdorf, 1988, Electrical structure of Newberry volcano: Journal Geophysical Research, 93, p. 10120-10131.

Frizzell, V.A., Jr., 1978, Petrology of Paleogene nonmarine sandstones in Washington, in Armentrout, J.M., Cole, M.R., and TerBest, H. Jr., Cenozoic Paleogeography of the western United States: Society of Economic Palentologists and Mienralogists, Pacific Section, p. 113-118.

Galloway, W. E., 1974, Deposition and diagenetic alteration of sandstone in northeast Pacific arc-related basins: implications for graywacke genesis: Geological Society of America Bulletin, 85, 379-390.

Gamble, T.D., Goubau, W.M. and Clarke, John, 1979, Magnetotellurics with a remote reference, Geophysics, 44, 53-68.

Gard, L.M., 1968, Bedrock geology of the Lake Tapps Quadrangle, Pierce County, Washington: U.S. Geological Survey Professional Paper 388-B, p. B1-B33.

Gimlin, D. R. and J. W. Smith, 1980, A comparison of seismic trace summing techniques: Geophysics, v. 45, p. 1017-1041.

Globerman, B. R., and M. E. Beck, Jr., 1979, Cenozoic tectonic rotations in the western cordillera: new evidence from the Washington Coast Range: EOS, Transactions of the American Geophysical Union, 60, 816.

Grau, G., 1993, Seismic velocities in complex media: Journal of Applied Geophysics, 29, 271-284.

Gregory, A. R., 1977, Aspects of rock physics from laboratory and log data that are important to seismic intepretation: in Seismic Stratigraphy -Applications to Hydrocarbon Exploration, p. 15-46, ed. C. E. Payton, AAPG, Tulsa, Memoir 26.

Gwilliam, W. J., 1990, Deep Gas Technology Status Report: Morgantown Energy Technology Center Report 90/0271, U.S. Department of Energy.

Hagan, R.A., 1987, The geology and petrology of the Northcraft Formation, Lewis County, Washington [M.S. thesis]: Eugene, University of Oregon, 252 p.

Hurst, P. D., 1991, Petroleum geology of the Bellingham Basin, Washington and evaluation of the AHEL and Partners Birch Bay No. 1 well: Washington Geology, 19, 16-18.

Hedges, Joseph W., 1949, A geology of the Bear Canyon area: M.S. Thesis, College of Puget Sound.

Henriksen, D.A., 1956, Eocene stratigraphy of the lower Cowlitz River-eastern Willapa Hills area, southwestern Washington: Washington Division of Mines and Geology Bulletin 43, 122 p.

Hilde, T. W.C., 1983, Sediment subduction versus accretion around the Pacific: in

Tectonophysics, Convergence and Subduction, T.W.C. Hilde and S. Uyeda, eds.
Ingle, J.C., Jr., Cenozoic paleobathymetry and depositonal hisotry of selected sequences within the southern California continental borderland: Cushman Foundation Special Publication 19, p. 163-195.
Ise, F. T., 1985, Washington and Oregon-are there other rocks to explore: Oil and Gas Journal, August 12, p. 112-115.
Johnson, S.Y., 1984, Evidence for a margin-truncating transcurrent fault (pre-Late Eocene) in western Washington; Geology, v. 12, p. 538-541.
Johnson, S.Y., 1985, Eocene strike-slip faulting and nonmarine basin formation in Washington, in Biddle, K.T., and Christie-Blick, Nicholas (eds.), Strike-slip deformation, basin formation, and sedimentation: Society of Economic Paleontologists and Mineralogists, Special Publication 37, p. 283-302.
Johnson, S.Y., 1992, Stratigraphy and sedimentology of the Raging River Formation (early? and middle Eocene), King County, Washington: U.S. Geological Survey Open-File report 92-581, 38 p.
Johnson, S.Y., and Yount, J.C., Toward a better udnerstanding of the Paleogene paleogeography of the Puget Lowland, western Washington. Geological Society of America Abstracts with Programs, v. 24, p. 36.
Johnson, S.Y., 1993, Analysis of Cenozoic subsidence at three sites in the Seattle basin area, Washington: U.S. Geological Survey Open-File Report 93-332, 17 p.
Johnson, S.Y., Potter, C.J., and Armentrout, J.M., 1994 (in press), Origin and evolution of the Seattle basin and Seattle fault: Geology, v. 24, p.
Kleinhous, L. C., E. A. Balcells-Baldwin, and Jones, R. E., 1984, A paleogeographic reinterpretation of some middle Cretaceous units, north-central Oregon: Evidence for a submarine turbidite system: in Nilsen, T. H., ed., Geology of the Upper Cretaceous Hornbrook Formation, Oregon and California: Society of Economic Paleontologists and Mineralogists, Pacific Section, Field Trip Guidebook 42, p. 239-257.
Krehbiel, S., 1993a, Seismic, maturity data point to S.W. Washington potential: Oil and Gas Journal, 91, no. 12, p. 107-111.
Krehbiel, S., 1993b, Depth estimates of seismic reflection data in SW Washington: The Leading Edge, p. 1076-1081.
Kvenvolden, K. A. and P. D. Snavely, Jr., 1987, Hydrocarbon generation at the convergent margin of coastal Washington and Oregon: in Procedings of the Unconventioanl Gas Recovery Contractors Review Meetin, ed. C. A. Komar, U.S. Department of Energy, Morgantown Energy Technology Center Report 87/6080, p. 137-148.
Lee, C. D., F. D. Vine, and R. G. Ross, 1983, Electrical conductivity models for the continental crust based upon laboratory measurements on high grade metamorphic rocks: Geophysical Journal of the Royal Astronomical Society, v. 72, p. 353-371.
Magill, J., A. Cox, and R. Duncan, 1981, Tillamook volcanic series: further evidence for tectonic rotation of the Oregon Coast Range: Journal of Geophysical

AIIM

Association for Information and Image Management

1100 Wayne Avenue, Suite 1100
Silver Spring, Maryland 20910
301/587-8202

Centimeter

1 2 3 4 5 6 7 8 9 10 11 12 13 14 15 mm

1 2 3 4 5

Inches

1.0 1.1 1.25 1.4 1.6 1.8 2.0 2.2 2.5 2.8 3.2 3.6 4.0 4.5 5.0 5.6 6.3

2 of 2

Research, 86, 2953-2970.
McKee, E. H., D. A. Swanson, and T. L. Wright, 1977, Duration and volume of Columbia River Basalt volcanism, Washington, Oregon, and Idaho: (abs) Geological Society of America Abs. with Programs, 9, 463-464.
Michon, D., 1993, Reconnaissance profiles with WLP in complex geological regions: Journal of Applied Geophysics, 29, 285-300.
Miller, R.B., 1989, The Mesozoic Rimrock Lake inlier, southern Washington Cascades - implications for the basement to the Columbia embayment: Geological Society of America Bulletin, v. 101, p. 1289-1305.
Miller, R.B., Mattinson, J.M., Funk, S.A.G., Hopson, C.A., and Treat, C.L., 1993, Tectonic evolution of Mesozoic rocks in the southern and central Washington Cascades, in Dunn, E.G., and McDougall, K., eds., Mesozoic paleogeography of the western United States - II: Pacific Section SEPM, Book 71, p. 81-98.
Misch, Peter, 1977, Dextral displacements at some major strike faults in the North Cascades: (abs), Geological Society of Canada. Programs with Abstracts, p. 37.
Mitchum, R. M., Jr., P. R. Vail, and J. B. Sangree, 1977, Stratigraphic interpretation of reflection patterns in depositional sequences: in Seismic Stratigraphy - Applications to Hydrocarbon Exploration, p. 117-134, ed. C. E. Payton, AAPG, Tulsa, Memoir 26.
Muller, J. E., 1977, Evolution of the Pacific margin, Vancouver Island, and adjacent regions: Canadian Journal of Earth Sciences, v. 14, no. 9, p. 2062-2085.Geological Survey of Canada, Paper 69-25, 77 p.
Mullineaux, D. R., 1970, Geology of the Renton, Auburn, and Black Diamond quadrangles, King County, Washington: U.S. Geological Survey Professional Paper no. 672, 92 p.
Nicholsen, Craig, L. Seeber, P. Williams, and L. R. Sykes, 1986, Seismicity and fault kinematics through the eastern Transverse Ranges, California: block rotation, strike-slip faulting and low-angle thrusts: Journal of Geophysical Research, 91, B5, 4891-4908.
Northwest Oil Report, 1983, Shell confirms Saddle Mountain Flaring: v. 25, no. 19, Portland, Oregon.
Olhoeft, G. R., 1985, Low-frequency electrical properties: Geophysics, 50, no. 12, 2492-2503.
Olmstead, D. L., 1989, Hydrocarbon exploration and occurrences in Oregon: Oregon Department of Geology and Mineral Industries, Oil and Gas Investigation No. 15, Portland, 78 p.
Peters, K.E., 1986, Guidelines for evaluating petroleum source rock using programmed pyrolysis: American Association of Petroleum Geologists Bulletin, v. 70, p. 318-329.
Phillips, W. M. and T. J. Walsh, 1989, Eocene transition from oceanic to arc volcanism, southwest Washington: in Proceedings of Workshop XLIV, Geological, Geophysical, and Tectonic Setting of the Cascade Range, U.S. Geological Survey Open-File Report No. 89-178 p. 199-256.
Price, R. A., J. W. H. Monger, and J. A. Roddick, 1985, Cordilleran cross-section;

Calgary to Vancouver: Trip No. 3 in Field Guides to Geology and Mineral Deposits in the Southern Canadian Cordillera, Geological Survey of America, Cordilleran Section Meeting, Vancouver, B.C., Edited by Dirk Tempelman-Kluit.

Rau, W.W., and Armentrout, J.M., 1983, Grays Harbor basin, in Armentrout, J.M., Hull, D.A., Beaulieu, J.D., and Rau, W.W., eds., Correlation of Cenozoic stratigraphic units of western Oregon and Washington: Oregon Department of Geology and Mineral Industries Oil and Gas Inestigation 7, p. 56-59.

Rau, W.W., Armentrout, J.M., and Easterbrook, D.J., 1983, Centralia Chehalis area, in Armentrout, J.M., Hull, D.A., Beaulieu, J.D., and Rau, W.W., eds., Correlation of Cenozoic stratigraphic units of western Oregon and Washington: Oregon Department of Geology and Mineral Industries Oil and Gas Inestigation 7, p. 60-63.

Sangree, J.B., and Widmier, J.M., 1977, Seismic interpretation of depositional facies, in Payton, C.E., ed., Seismic stratigraphy - applications to hydrocarbon exploration: American Association of Petroleum Geologists Bulletin, Memoir 26, p. 165-184

Schasse, H.W., 1987, Geologic map of the Centralia Quadrangle, Washington: Washington Divsion of Geology and Earth Sciences Open-File Report 87-11, 27 p. text, scale, 1:100,000.

Sheriff, R. E., 1984, Encyclopedic Dictionary of Exploration Geophysics: Soc. Explor. Geophys., Tulsa, 2nd ed., 323 pp.

Simpson, R. W., and A .V. Cox, 1977, Paleomagnetic evidence for tectonic rotation of the Oregon Coast Range: Geology, 5, 585-589.

Snavely, P.D., Jr., 1987, Tertiary geologic framework, neotectonics, and petroleum potential of the Oregon-Washington continental margin, in Scholl, E.W., Grantz, A., and Vedder, J.G., eds., Geology and resource potential of the continental margin of western North America and adjacent ocean basins, Beaufort Sea to Baja California: Circum-Pacific Council for Energy and Mineral Resources, Earth Science Series, v. 6, p. 305-335.

Snavely, P. D., Jr., N. S. MacLeod, and H. C. Wagner, 1968, Tholeitic and alkalic basalts of the Eocene Siletz River Volcanics, Oregon Coast Range: American Journal of Science, v. 266, p. 454-481.

Snavely, P.D., Jr., Brown, R.D., Jr., Roberts, A.E., and Rau, W.W., 1958, Geology and coal resources of the Centralia-Chehalis district, Washington: U.S. Geological Survey Bulletin 1053, 159 p.

Snavely, P.D., Jr., Rau, W.W., Hoover, L. Jr., and Roberts, A.E., 1951, McIntosh Formation, Centralia-Chehalis coal district, Washington: American Association of Petroleum Geologists Bulletin, v. 35, p. 1052-1061.

Stanley, W. D., D. B. Jackson, and A. A. R. Zohdy, 1976, Deep electrical investigations in the Long Valley geothermal area, California: Journal of Geophysical Research, 81, p. 810-820.

Stanley, W. D. and Tinkler, R. D., 1983, A practical, low-noise coil system for magnetotellurics: U.S. Geological Survey Open-File Report 83-85, 18 pp.

Stanley, W.D., Finn, C., and Plesha, J.L., 1987, Tectonics and conductivity structures in the southern Washington Cascades: Journal of Geophysical Research, v. 81, p. 810-820.

Stanley, W. D., G. S. Fuis, and W. D. Mooney, 1989, Details of crustal structure in the Cascade Range and surrounding regions from seismic and magnetotelluric data: in Proceedings of Workshop XLIV, Geological, Geophysical, and Tectonic Setting of the Cascade Range, U.S. Geological Survey Open-File Report. 89-178.

Stanley, W.D., Gwilliam, W.J., Latham, F., and Westhusing, K., 1992, The southern Washington Cascade conductor -- A previously unrecognized thick sedimentary sequence? American Association of Petroleum Geologists Bulletin, v. 76, p. 1569-1585.

Stanley, W. D., V. F. Labson, W. J. Nokleberg, Bela Csejtey, Jr., and M. A. Fisher, 1990, The Denali fault system and Alaska Range of Alaska: evidence for underplated Mesozoic flysch from magnetotelluric surveys: Geological Society of America Bulletin, 102, 160-173.

Sternberg, B. K., J. C. Washburne, and L. Pellerin, 1988, Correction for the static shift in magnetotellurics using transient electromagnetic soundings: Geophysics, v. 53, p. 1459-1468.

Stockwell, John, 1993, Complete listing of CWP Public Domain Program Self-Documentation: Center for Wave Phenomena, Colorado School of Mines, Golden, Colorado.

Tabor, R. W., R. B. Waitt, V. A. Frizzell, D. A. Swanson, G. R. Byerly, R. D. Bentley, 1982, Geologic map of the Wenatchee 1:100,000 quadrangle, Washington: U.S. Geological Survey,
Miscellaneous Investigation Series Map I-1311, 26 p., 1 plate.

Tabor, R. W., V. A. Frizzell, Jr., J. A. Vance, and C. W. Naeser, 1984, Ages and stratigraphy of lower and middle Tertiary sedimentary and volcanic rocks of the central Cascades, Washington: application to the tectonic history of the Straight Creek fault: Geological Society of America Bulletin, 95, no. 1, 26-44.

Tissot, B.P., and Welte, D.H., 1978, Petroleum formation and occurrence: New york, Springer-Verlag, 538 p.

Vail, P. R., R. M. Mitchum, Jr., R. G. Todd, J. M. Widmier, S. Thompson, III, J. B. Sangree, J. N. Bubb, and W. G. Hatfield, 1977, Seismic stratigraphy and global changes in seal level: in Seismic Stratigraphy-Applications to Hydrocarbon Exploration, p. 49-205, ed. C. E. Payton, AAPG, Tulsa, Memoir 26.

Vine, J.D., 1969, Geology and coal resources of the Cumberland, Hobart, and Maple Valley quadrangles, King County, Washington: U.S. Geological Survey Professional Paper 624, 67 p.

Vozoff, Keeva, The magnetotelluric method in the exploration of sedimentary basins, Geophysics, 37, 98-141, 1972.

Walsh, T.J., Korosec, M.A., Phillips, W.M., Logan, R.L., and Schasse, H.W., 1987, Geologic Map of Washington - southwest quadrant: Washington Division of Geology and Earth Resources, Geologic Map GM-34, 28 p., scale 1:250,000.

Walsh, T.J., and Lingley, W.S. Jr., 1991, Coal maturation and the natural gas potential of western and central Washington: Washington Division of Geology and Earth Resources Open-File Report 91-2, 26 p.

Walsh, T. J. and W. M. Phillips, 1983, Rank of Eocene coals in western and central

Washington State: a reflection of Cascade plutonism: Washington Dept. of Natural Resources, Open-File Report 83-16.

Weaver, C.S., and Smith, S.W., 1983, Regional tectonic and earthquake hazard implications of a crustal fault zone in southwestern Washington: Journal of Geophysical Research, v. 88, p. 10,371-10,383.

Wells, R.E., 1981, Geologic map of the eastern Willapa Hills - Cowlitz, Lewis, Pacific, and Wahkiakum Counties, Washington: U.S. Geological Survey Open-File Report 81-674, scale, 1:62,500.

Wells, R.E., and Rau, W.W., 1983, South flank Willapa Hills, in Armentrout, J.M., Hull, D.A., Beaulieu, J.D., and Rau, W.W., eds., Correlation of Cenozoic stratigraphic units of western Oregon and Washington: Oregon Department of Geology and Mineral Industries Oil and Gas Inestigation 7, p. 51-55.

Wells, R.E., Engebretson, D.C., Snavely, P.D., Jr., and Coe, R.S., 1984, Cenozoic plate motions and the volcano-tectonic evolution of western Oregon and Washington: Tectonics, v. 3, p. 274-294.

Wells, R. E., Engebretson, D. C., Snavely, P. D., Jr., and R. S. Coe, 1984, Cenozoic plate motions and the volcano-tectonic evolution of western Oregon and Washington: Tectonics, 3, 275-294.

Willis, Bailey, 1898, Some coal fields of Puget Sound, in U.S. Geological Survey, 18th Annual Report, part 3-C, p. 393-436.

Wolfe, J. A., 1978, A paleobotanical interpretation of Tertiary climates in the northern hemisphere: American Scientist, v. 66, p. 694-703.

Yorath, C. J., 1987, Petroleum geology of the Canadian Pacific continental margin: in Geology and Resource Potential of the Continental Margin of Western North America and Adjacent Ocean Basins-Beaufort Sea to Baja California, eds., D. W. Scholl, Arthur Grantz, and J. G. Vedder, Circum-Pacific Council for Energy and Mineral Resources Earth Science Series, v. 6, p. 283-304.

Zilman, F. N., 1993, U. S. Department of Energy Morgantown Energy Technology Center Deep Seismic Reflection Studies in the Pacific Northwest U.S.: U.S. Geological Survey Open File Rept. 92-714.

Zoback, M. D. and C. M. Wentworth, 1986, Crustal studies in central California using and 800-channel reflection recording system: in eds. Brazangi, Muawia and Brown, Larry, Reflection Seismology: A Global Perspective, 183-196.

Appendix A

Detailed Stratigraphic Data for Surface Sections and Wells

The following sections contains detailed stratigraphic information from measured sectins at locations indicated in Figures 4 and 29. An explanation for the patterns on the section is shown in Figure A1.

Figure A1-Explanation for pattern symbols on measured sections in following illustrations.

AMOCO WC-83-5 stratigraphic section

Figure A2-Index map with locations of AMOCO WC-83-5 well and "Mineral" measured section.

The AMOCO WC-83-5 borehole site (Fig. A2) is located in SW 1/4. sec. 29, T. 14 N., R. 5 E. (Mineral 7.5' U.S.G.S. topographic quadrangle). The measured section (Fig. A3) is based on description of nearly continuous core, collected in the borehole from a depth of 156.1 m to the total depth of 608.7 m (1,996.5 ft). The lowest 25.2 m (82.6 ft) of core consists of medium-grained intrusive rock and the mean

Figure A3-Core section description for AMOCO WC-83-5 well.

structural dip in cored strata is about 20° thus the section thickness (~401 m) is smaller than the total length of the core. The core included three intervals (~47 percent of the core) interpreted as shallow- to marginal-marine deposits, and two intervals (~53 percent of the core) interpreted as nonmarine deposits. Vitrinite reflectance was analyzed for four samples.

Explanation for measured sections


breccia-conglomerate


conglomerate

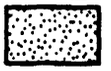
massive arkosic sandstone, siltstone

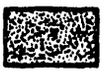
massive volcano-lithic sandstone, siltstone


crossbedded sandstone


horizontal to low-angle bedded sandstone


sandstone with mudstone partings


mudstone with sandstone partings

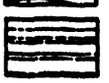
laminated siltstone, mudstone


carbonaceous shale


coal

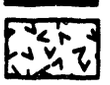
volcanic tuff or flow


igneous intrusion


ripple mark


convolute stratification


burrow, bioturbation


shell or shell fragment

plant fragment


root trace or cast


paleocurrent indicator


fault

scour surface

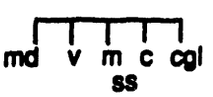

grain size

md - mudstone

v - very fine grained sandstone

m - medium-grained sandstone

c - coarse-grained sandstone

cgl - conglomerate

nm - mainly nonmarine depositional environment

msm - mainly marginal or shallow marine depositional environment

Figure A1

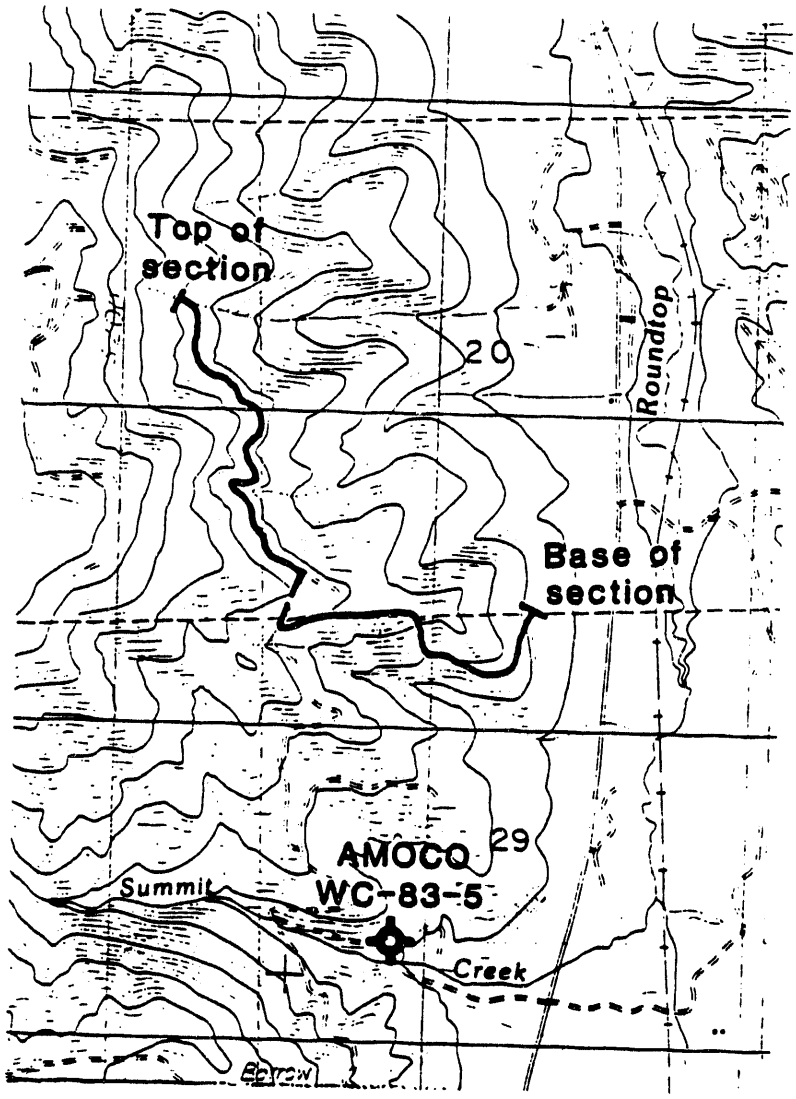
Top of section
20
Roundtop
Base of section
29
AMOCO
WC-83-5
Summit
Creek
Borrow

Figure A2

AMOCO WC-83-5: 500 - 1,000 feet

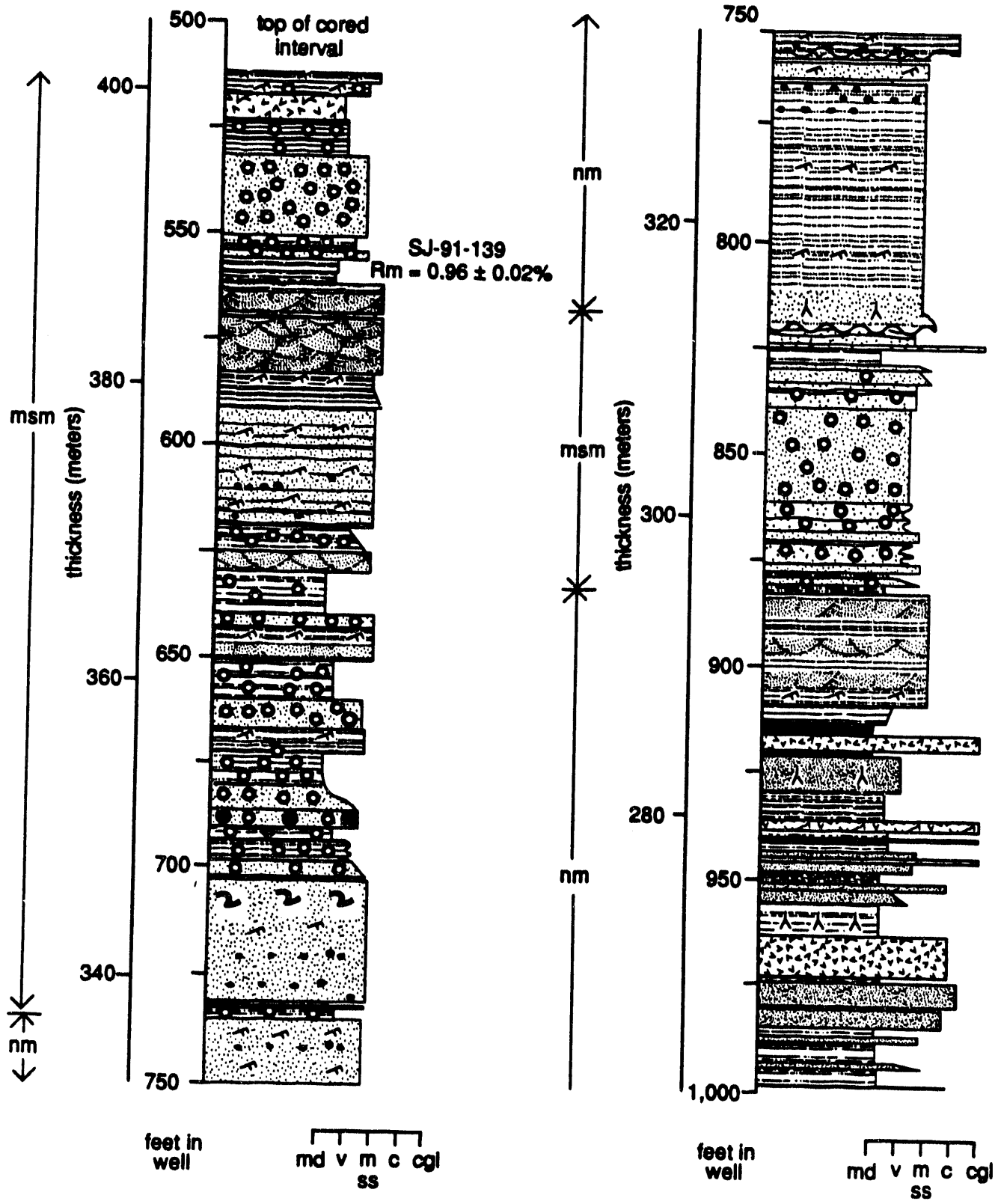

Figure A3

AMOCO WC-83-5: 1,000 - 1,500 feet

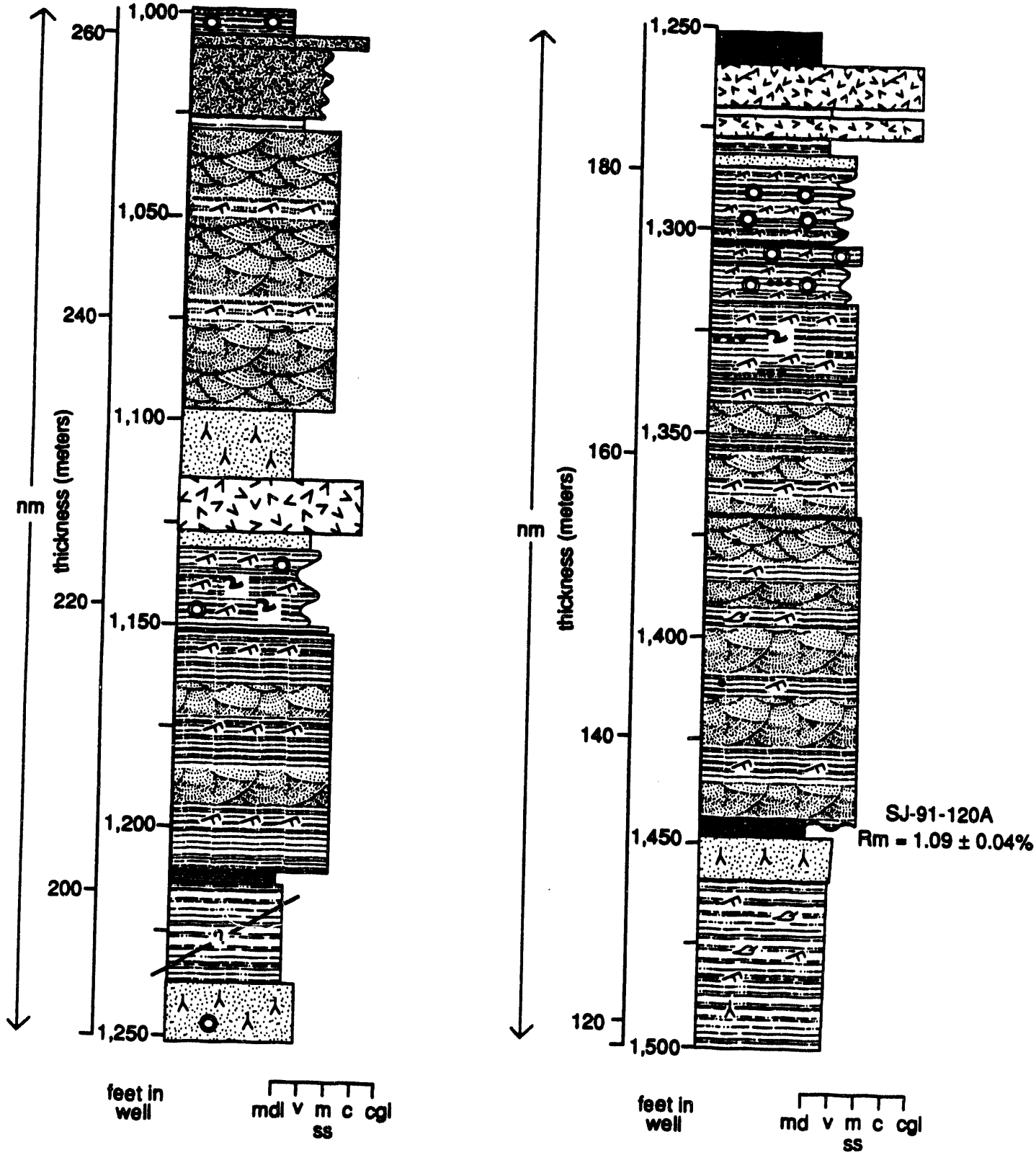

AMOCO WC-83-5: 1,500-2,000 feet

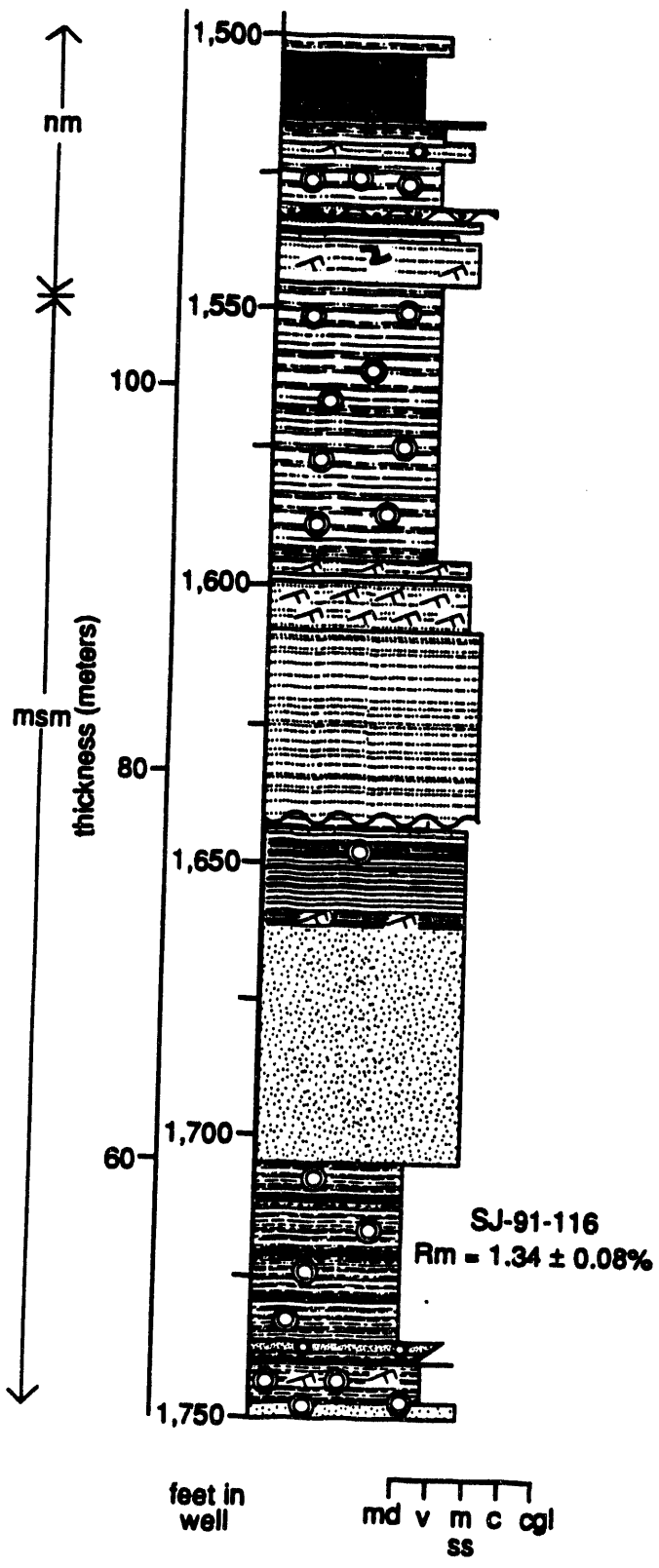

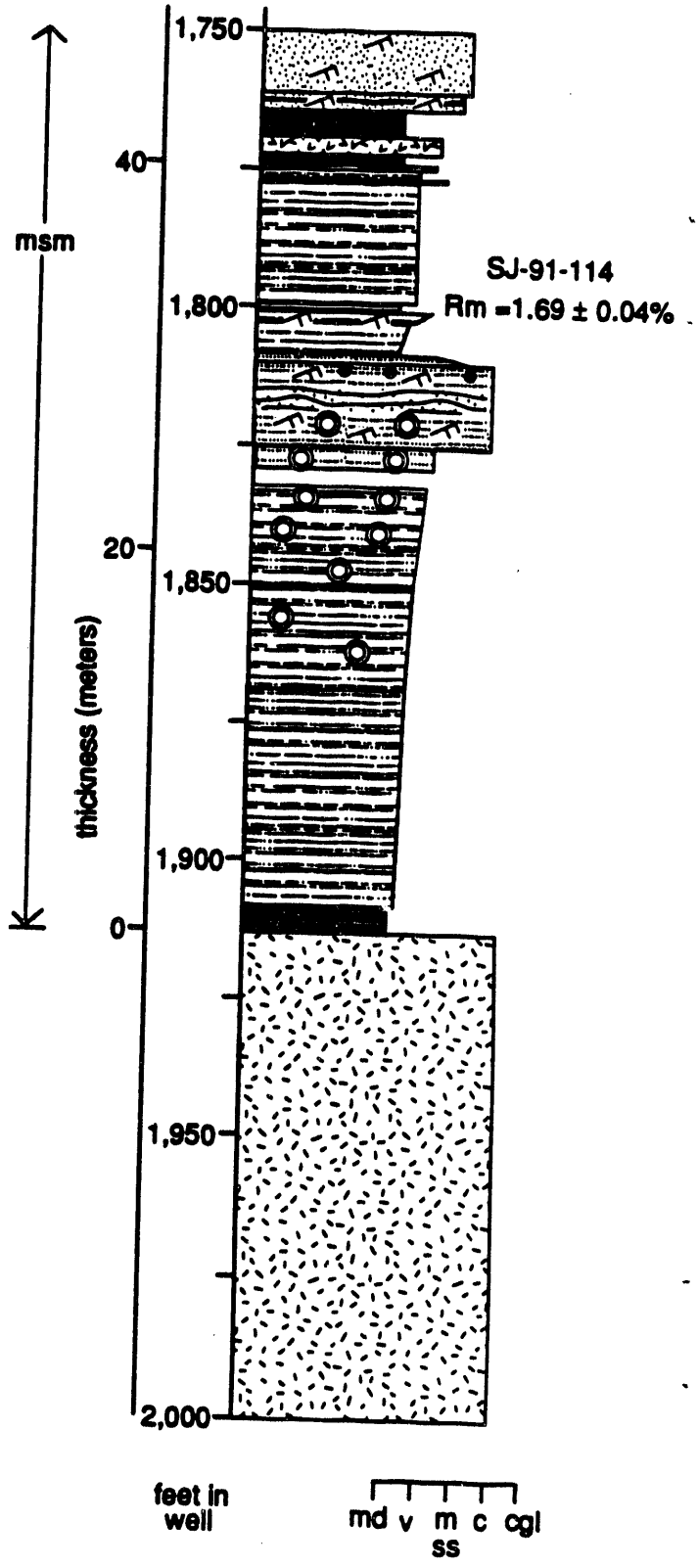

Table A1- Vitrinite Reflectance data for AMOCO WC-83-5 well.

File Name: SJ-91114
Channel Name: SJ-91-114
Description: core, coal, good sample
Comment 1:
Comment 2:
Comment 3:
Comment 4:
Comment 5:
Comment 6:

	Meas1	Meas2	Ratio	Conc.
Min:	1.60			
Max:	1.80			
Mean:	1.69			
StDev:	0.04			

Pt.	X-Pos	Y-Pos	Z-Pos	Meas1	Meas2	Ratio	Conc.
1				1.76			
2				1.64			
3				1.72			
4				1.72			
5				1.75			
6				1.66			
7				1.68			
8				1.66			
9				1.69			
10				1.63			
11				1.66			
12				1.69			
13				1.74			
14				1.66			
15				1.60			
16				1.68			
17				1.68			
18				1.65			
19				1.63			
20				1.70			
21				1.75			
22				1.75			
23				1.65			
24				1.65			
25				1.68			
26				1.70			
27				1.66			
28				1.69			
29				1.78			
30				1.71			
31				1.66			
32				1.64			
33				1.66			
34				1.70			
35				1.68			
36				1.69			
37				1.70			
38				1.80			
39				1.73			
40				1.66			

File Name: SJ-91116
Channel Name: SJ-91-116
Description: core, coaly, fair sample
Comment 1:
Comment 2:
Comment 3:
Comment 4:
Comment 5:
Comment 6:

	Meas1	Meas2	Ratio	Conc.
Min:	1.22			
Max:	1.48			
Mean:	1.34			
StDev:	0.08			

Pt.	X-Pos	Y-Pos	Z-Pos	Meas1	Meas2	Ratio	Conc.
1				1.44			
2				1.33			
3				1.29			
4				1.31			
5				1.43			
6				1.26			
7				1.33			
8				1.28			
9				1.41			
10				1.41			
11				1.37			
12				1.31			
13				1.38			
14				1.38			
15				1.28			
16				1.28			
17				1.39			
18				1.48			
19				1.38			
20				1.37			
21				1.31			
22				1.22			
23				1.47			
24				1.36			
25				1.26			
26				1.23			
27				1.23			
28				1.25			
29				1.42			
30				1.27			

File Name: SJ91120A
Channel Name: SJ-91-91-120A
Description: core, coal, good sample
Comment 1:
Comment 2:
Comment 3:
Comment 4:
Comment 5:
Comment 6:

	Meas1	Meas2	Ratio	Conc.
Min:	0.92			
Max:	1.17			
Mean:	1.09			
StDev:	0.04			

Pt.	X-Pos	Y-Pos	Z-Pos	Meas1	Meas2	Ratio	Conc.
1				1.04			
2				1.09			
3				1.09			
4				0.92			
5				0.97			
6				1.05			
7				1.03			
8				1.13			
9				1.03			
10				1.03			
11				1.06			
12				1.11			
13				1.07			
14				1.08			
15				1.08			
16				1.14			
17				1.14			
18				1.08			
19				1.08			
20				1.15			
21				1.14			
22				1.11			
23				1.12			
24				1.14			
25				1.16			
26				1.14			
27				1.08			
28				1.10			
29				1.11			
30				1.17			
31				1.09			
32				1.09			
33				1.10			
34				1.13			
35				1.09			
36				1.09			
37				1.09			
38				1.09			
39				1.09			
40				1.11			
41				1.09			
42				1.07			
43				1.10			
44				1.10			
45				1.10			
46				1.15			
47				1.07			
48				1.08			
49				1.11			
50				1.09			

File Name: SJ91-139
Channel Name: SJ-91-139
Description: core, coal, good sample
Comment 1:
Comment 2:
Comment 3:
Comment 4:
Comment 5:
Comment 6:

	Meas1	Meas2	Ratio	Conc.
Min:	0.90			
Max:	1.00			
Mean:	0.96			
StDev:	0.02			

Pt.	X-Pos	Y-Pos	Z-Pos	Meas1	Meas2	Ratio	Conc.
1							
2				0.97			
3				0.98			
4				0.97			
5				0.95			
6				0.98			
7				0.96			
8				0.97			
9				0.97			
10				0.98			
11				0.94			
12				0.94			
13				1.00			
14				0.96			
15				0.98			
16				0.94			
17				0.99			
18				0.95			
19				0.97			
20				0.96			
21				0.95			
22				0.98			
23				0.96			
24				0.92			
25				0.96			
26				0.93			
27				0.92			
28				0.98			
29				0.96			
30				0.98			
31				0.96			
32				0.96			
33				0.98			
34				0.96			
35				0.94			
36				0.93			
37				0.94			
38				0.98			
39				0.98			
40				0.99			
41				0.98			
42				0.99			
43				0.94			
44				0.99			
45				0.98			
46				0.90			
47				0.92			
48				0.99			
49				0.97			
50				0.93			
				0.99			

Mineral stratigraphic section

The Mineral stratigraphic section (location on Fig. A4) of the Carbonado Formation was measured in NE 1/4, NW 1/4, sec. 29; SW 1/4 sec. 20; and SE 1/4, NE 1/4, sec. 19, T. 14 N., R. 5 E. (Mineral 7.5' U.S.G.S. topographic quadrangle), on the western

Figure A4-Location of "Mineral" stratigraphic section.

slopes of the valley between the towns of Morton and Mineral. The base of this section (Fig. A5) is located approximately 1,000 m north-northeast of the AMOCO WC-83-5 borehole. The section is approximately 494 m thick (Fig. A4). The lower 80 m of the section is exposed in cuts on logging roads low on the valley flank. This lowest part of the section was pieced together from several discontinuous outcrops

Figure A5-Measured section along "Mineral" profile, location in Fig. A4).

of variable quality with relatively similar structural dips. These outcrops are cut by several faults, however, which might have disrupted primary stratigraphic order. The portion of the measured section between 80 m and 131 m is mostly covered and corresponds to recently logged terrain above the lower road. The upper part of the section (130 to 494 m) was measured in nearly continuous, excellent exposures along a north-trending log road higher on the valley flank.

At the top of the Mineral measured section, sedimentary rocks with an increasingly large component of volcanic and volcaniclastic rocks are overlain by massive volcanic rocks. Schasse (1987) included these volcanic rocks as one of several volcanic interbeds within the Puget Group (Carbonado Formation), well below the contact with the volcanic Northcraft Formation. Based on reconnaissance surveys, my observation is that the rocks above the top of the Mineral measured section and below the mapped contact with the Northcraft Formation are predominantly volcanic in origin. Hence, I would place the contact between the Carbonado Formation and the Northcraft Formation at the top of the Mineral section.

Nonmarine deposition is interpreted for three thick intervals comprising about 91 percent of the measured section; shallow- to marginal-marine deposition is inferred for two thin intervals comprising about 9 percent of the section. Vitrinite reflectance was analyzed for three samples.

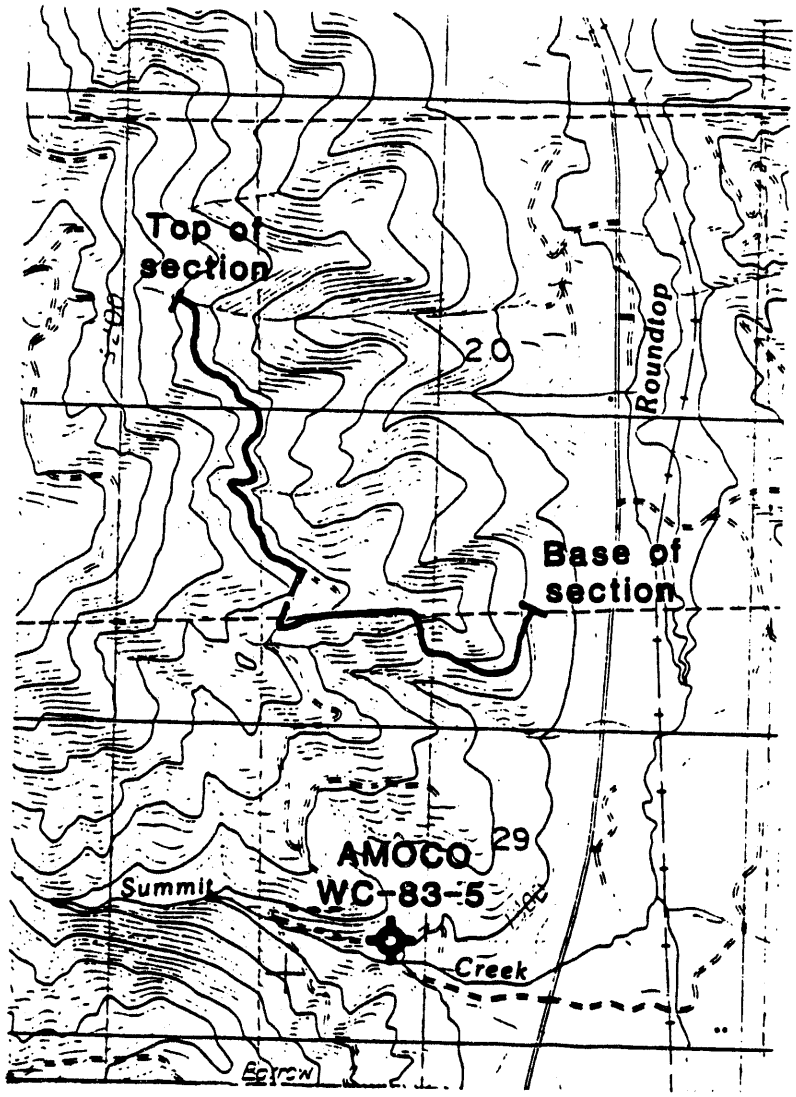
Top of section
20
Roundtop
Base of section
29
AMOCO
WC-83-5
Summit
Creek

Figure A4

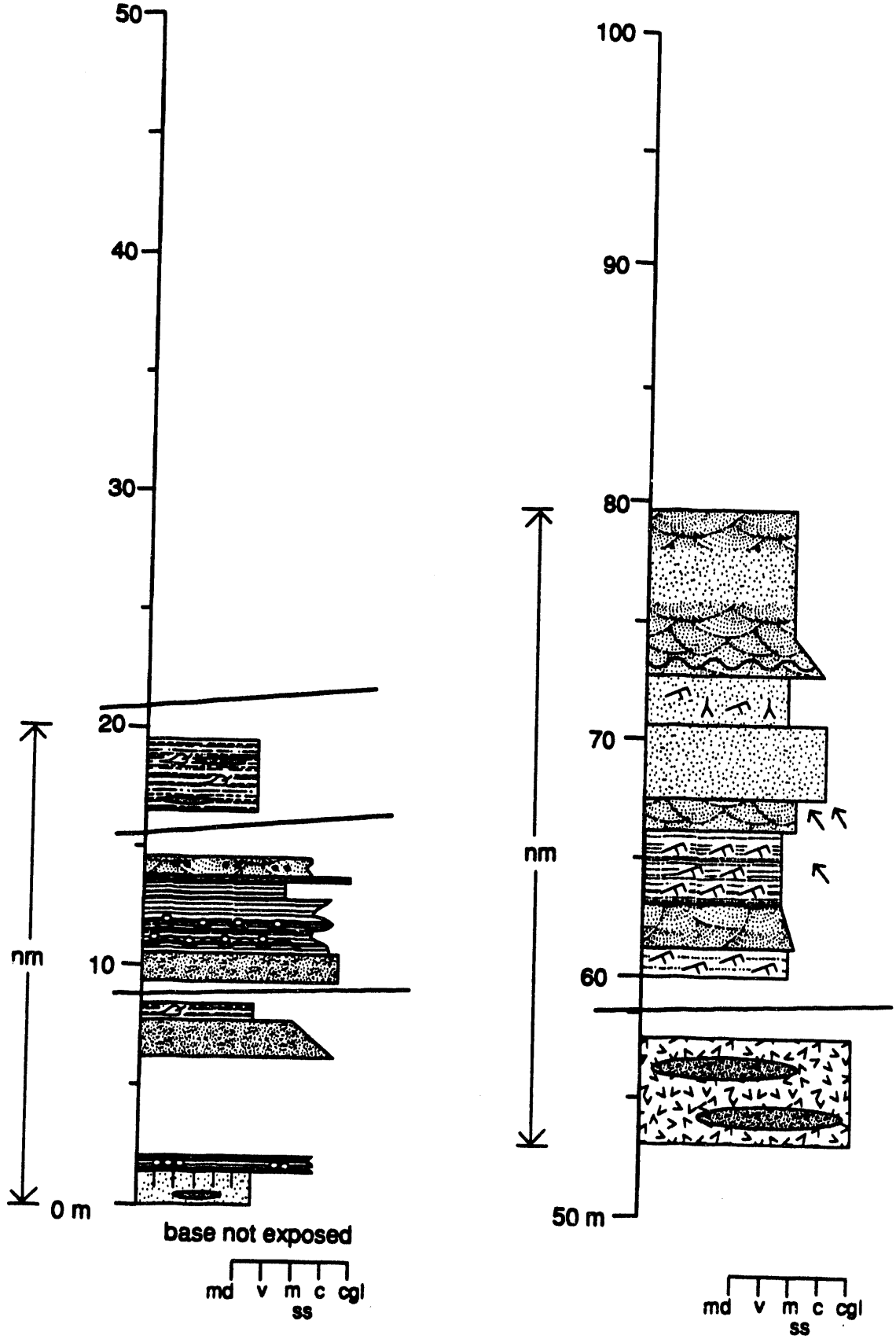
50
40
30
20
10
nm
0 m
base not exposed
md v m c cgl
ss
100
90
80
70
60
nm
50 m
md v m c cgl
ss

Figure A5

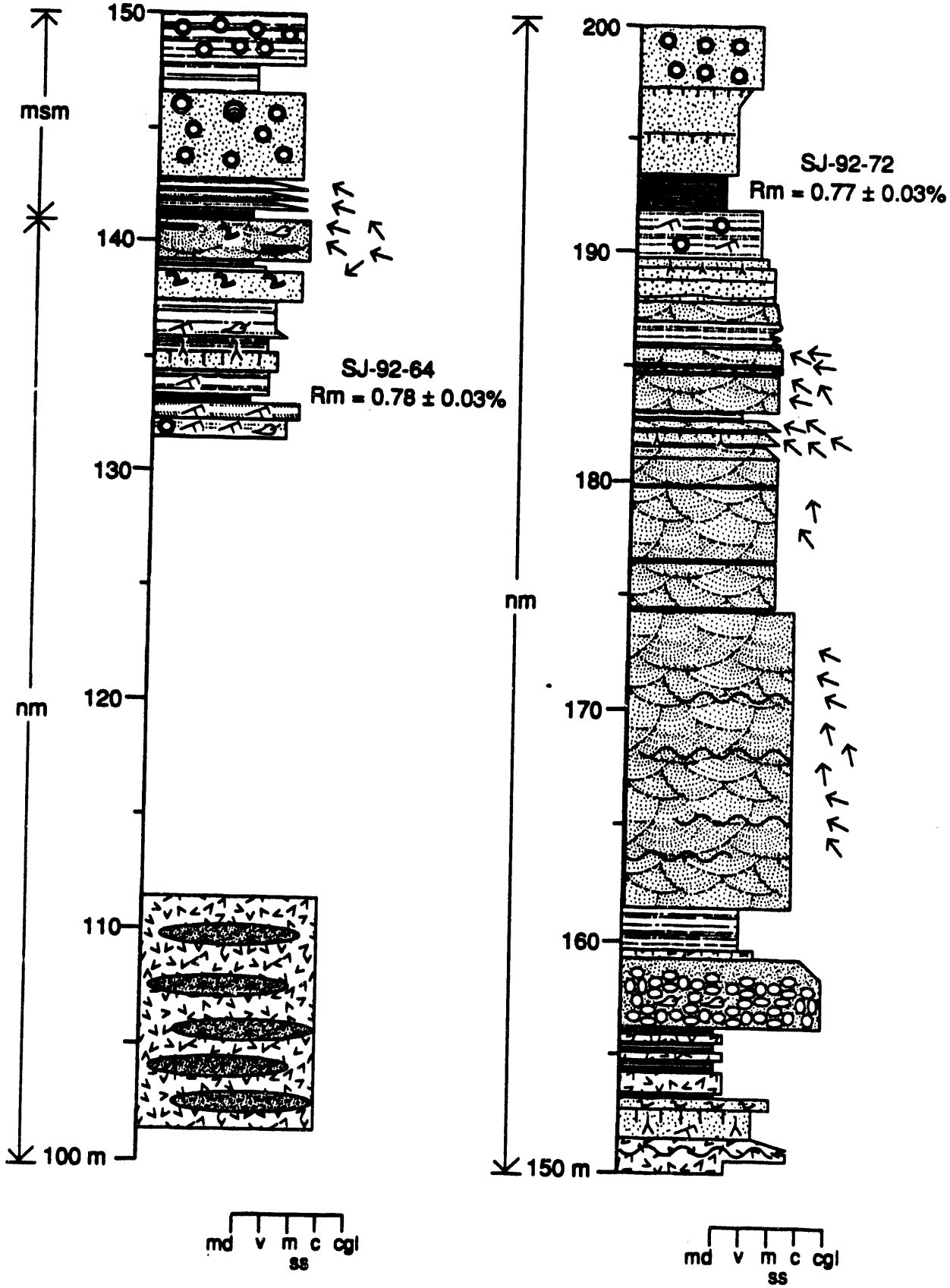
150
msm
140
SJ-92-64
Rm = 0.78 ± 0.03%
130
nm
120
110
100 m
md v m c cgl
ss
200
SJ-92-72
Rm = 0.77 ± 0.03%
190
180
nm
170
160
150 m
md v m c cgl
ss

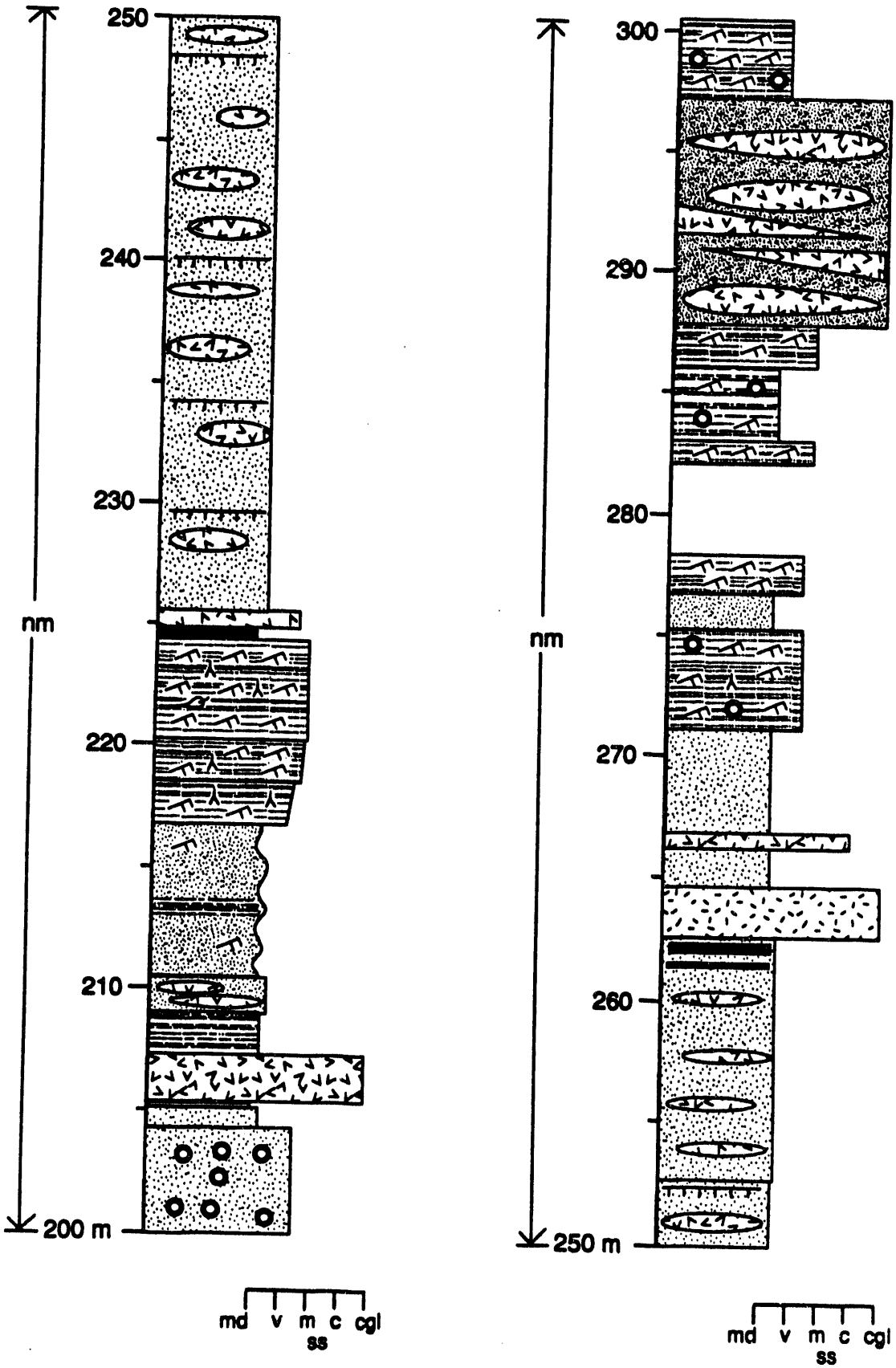
250
240
230
220
210
200 m
nm
md v m c cgl
ss
300
290
280
270
260
250 m
nm
md v m c cgl
ss

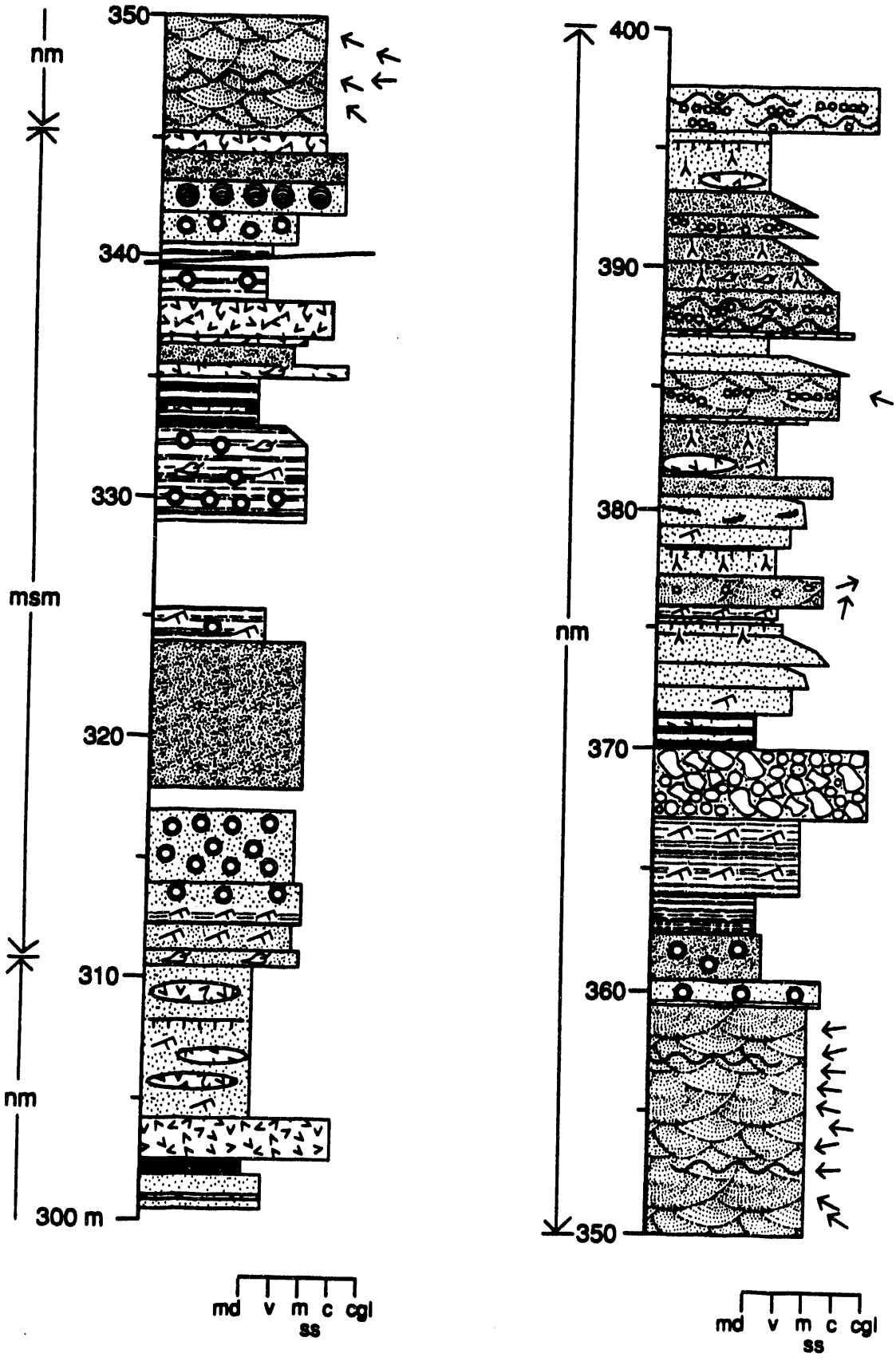
350
340
330
320
310
300 m
nm
msm
nm
md v m c cgl
ss
400
390
380
370
360
350
nm
md v m c cgl
ss

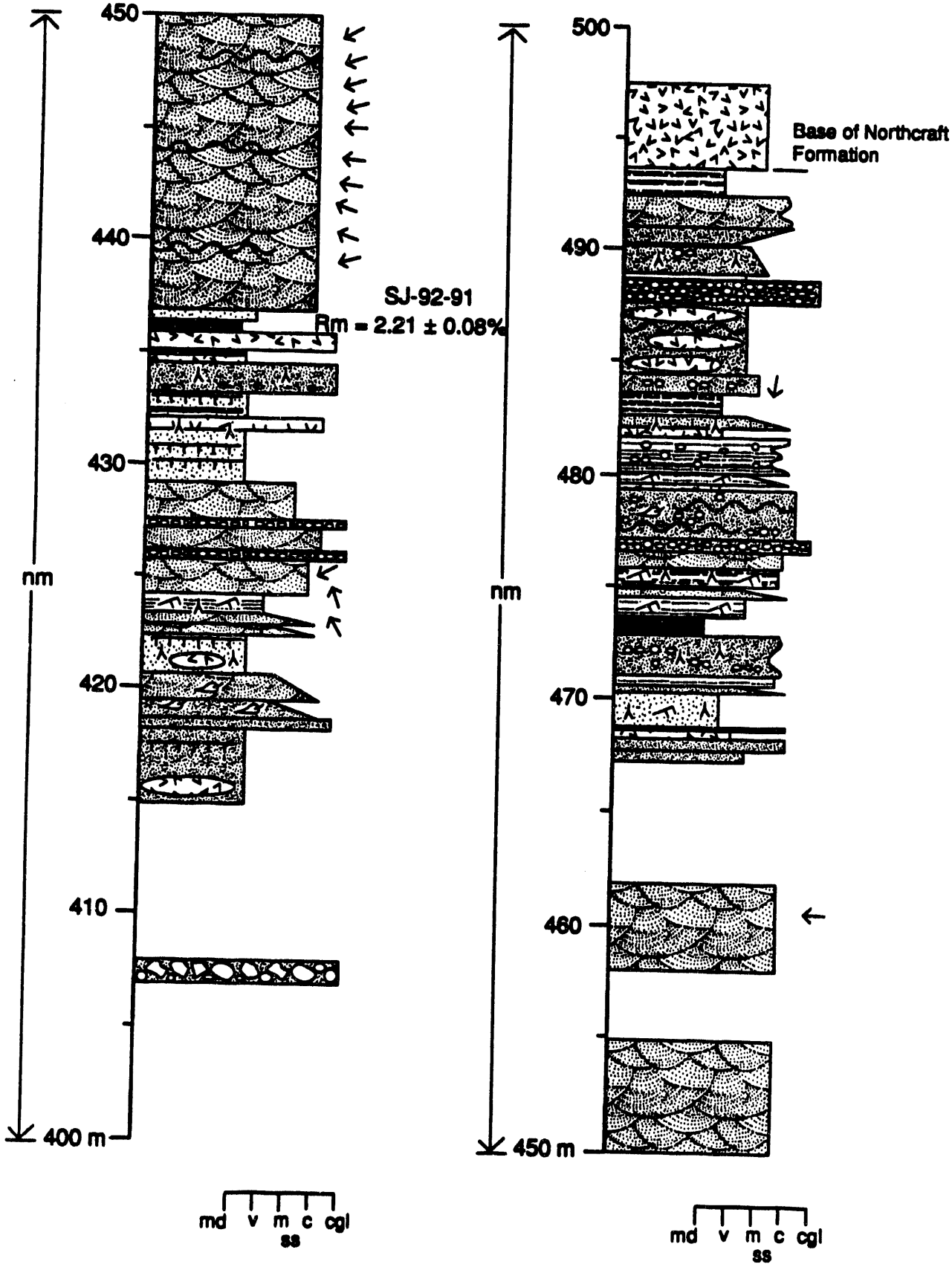
450
440
430
420
410
400 m
nm
SJ-92-91
Rm = 2.21 ± 0.08%
md v m c cgl
ss
500
490
480
470
460
450 m
nm
Base of Northcraft Formation
md v m c cgl
ss

Table A2-Vitrinite reflectance data for Mineral stratigraphic section.

File Name: SJ92-64
Channel Name: SJ-92-64
Description: SJ-92-64
  Comment 1: good sample
  Comment 2: consistent and clean
  Comment 3: polish good
  Comment 4:
  Comment 5:
  Comment 6:

	Meas1	Meas2	Ratio	Conc.
Min:	0.72			
Max:	0.82			
Mean:	0.78			
StDev:	0.03			

Pt.	X-Pos	Y-Pos	Z-Pos	Meas1	Meas2	Ratio	Conc.
1				0.76			
2				0.74			
3				0.79			
4				0.80			
5				0.72			
6				0.74			
7				0.73			
8				0.78			
9				0.77			
10				0.73			
11				0.75			
12				0.75			
13				0.79			
14				0.74			
15				0.79			
16				0.78			
17				0.80			
18				0.79			
19				0.80			
20				0.79			
21				0.79			
22				0.78			
23				0.82			
24				0.78			
25				0.80			
26				0.79			
27				0.78			
28				0.80			
29				0.82			
30				0.76			
31				0.81			
32				0.81			
33				0.79			
34				0.81			
35				0.79			

Channel Name: SJ-92-91
Description: SJ-92-91
Comment 1: good sample
Comment 2: consistent and clean
Comment 3: polish good
Comment 4:
Comment 5:
Comment 6:

	Meas1	Meas2	Ratio	Conc.
Min:	2.06			
Max:	2.40			
Mean:	2.21			
StDev:	0.08			

Pt.	X-Pos	Y-Pos	Z-Pos	Meas1	Meas2	Ratio	Conc.
1				2.18			
2				2.25			
3				2.20			
4				2.19			
5				2.19			
6				2.20			
7				2.19			
8				2.21			
9				2.17			
10				2.34			
11				2.28			
12				2.13			
13				2.12			
14				2.26			
15				2.12			
16				2.09			
17				2.19			
18				2.18			
19				2.27			
20				2.29			
21				2.29			
22				2.22			
23				2.24			
24				2.23			
25				2.21			
26				2.17			
27				2.06			
28				2.12			
29				2.20			
30				2.06			
31				2.40			
32				2.35			
33				2.15			
34				2.20			
35				2.27			

File Name: SJ-9[illegible]-72
Channel Name: SJ-[illegible]-72
Description: SJ-9[illegible]-[illegible]
Comment 1: good sample
Comment 2: clean, consistent vitrinite
Comment 3:
Comment 4:
Comment 5:
Comment 6:

	Meas1	Meas2	Ratio	Conc.
Min:	0.73			
Max:	0.83			
Mean:	0.77			
StDev:	0.03			

Pt.	X-Pos	Y-Pos	Z-Pos	Meas1	Meas2	Ratio	Conc.
1				0.75			
2				0.74			
3				0.76			
4				0.75			
5				0.73			
6				0.74			
7				0.74			
8				0.79			
9				0.79			
10				0.78			
11				0.80			
12				0.80			
13				0.78			
14				0.77			
15				0.78			
16				0.76			
17				0.76			
18				0.74			
19				0.73			
20				0.76			
21				0.79			
22				0.80			
23				0.83			
24				0.82			
25				0.78			
26				0.74			
27				0.73			
28				0.78			
29				0.76			
30				0.78			

Bergen Mountain stratigraphic section

The Bergen Mountain stratigraphic section (Fig. A6) of the Carbonado Formation was measured in SW 1/4, sec. 9; SE 1/4, sec. 8; and NE 1/4, sec. 17, T. 13 N., R.

Figure A6-Location of Bergen Mountain stratigraphic section.

4 E. (Morton 7.5' U.S.G.S. topographic quadrangle). The section is 424 m thick and was measured in cuts on a logging road about 700 to 1,700 m northeast of Bergen Mountain. The measured section includes significant cover (about 23 percent) but only a few small faults were recognized and it is inferred to be stratigraphically intact. The base of the section corresponds to the first good outcrops along the road. At the top of the section (Fig. A7), the highest Carbonado strata are cut by a medium-grained, andesitic dike or sill. Based on bedding-plane attitudes in underlying and

Figure A7-Measured section at Bergen Mountain location.

overlying rocks, this intrusive body is about 46 m thick. Rocks exposed above the intrusion include volcanic flows, tuffs, and associated intrusions assigned to the Northcraft Formation.

The lower 168 m of the section consists of three (7 to 24 m thick) intervals of inferred nonmarine origin and four intervals (5 to 63 m thick) of inferred shallow- to marginal-marine origin. The upper 256 m of the section has an inferred nonmarine origin. Overall, the section is inferred to include about 70 percent nonmarine strata and 30 percent shallow to marginal marine strata. Vitrinite reflectance was analyzed for four samples.

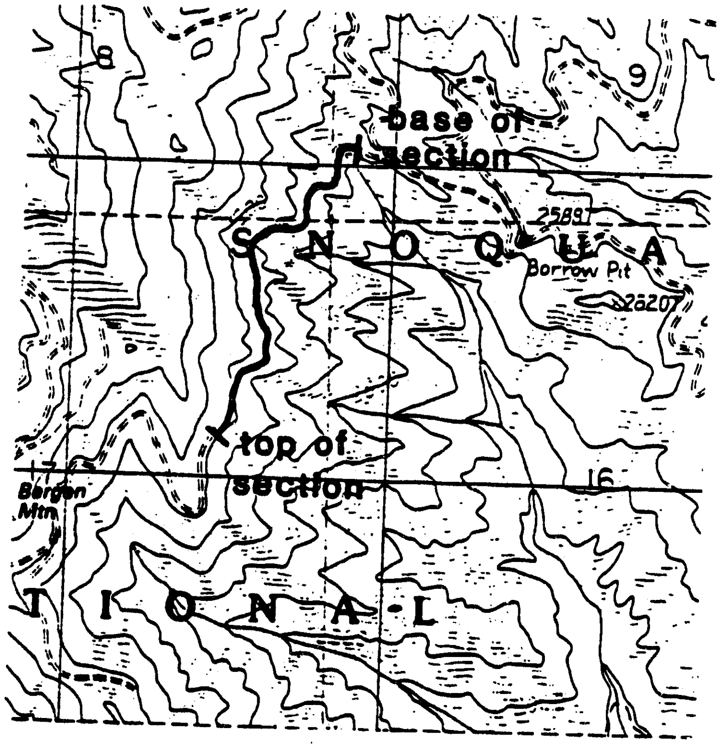
8
9
base of
section
2589
S N O Q U A
Borrow Pit
2620
top of
section
16
Bergen
Mtn
T I O N A L

Figure A6

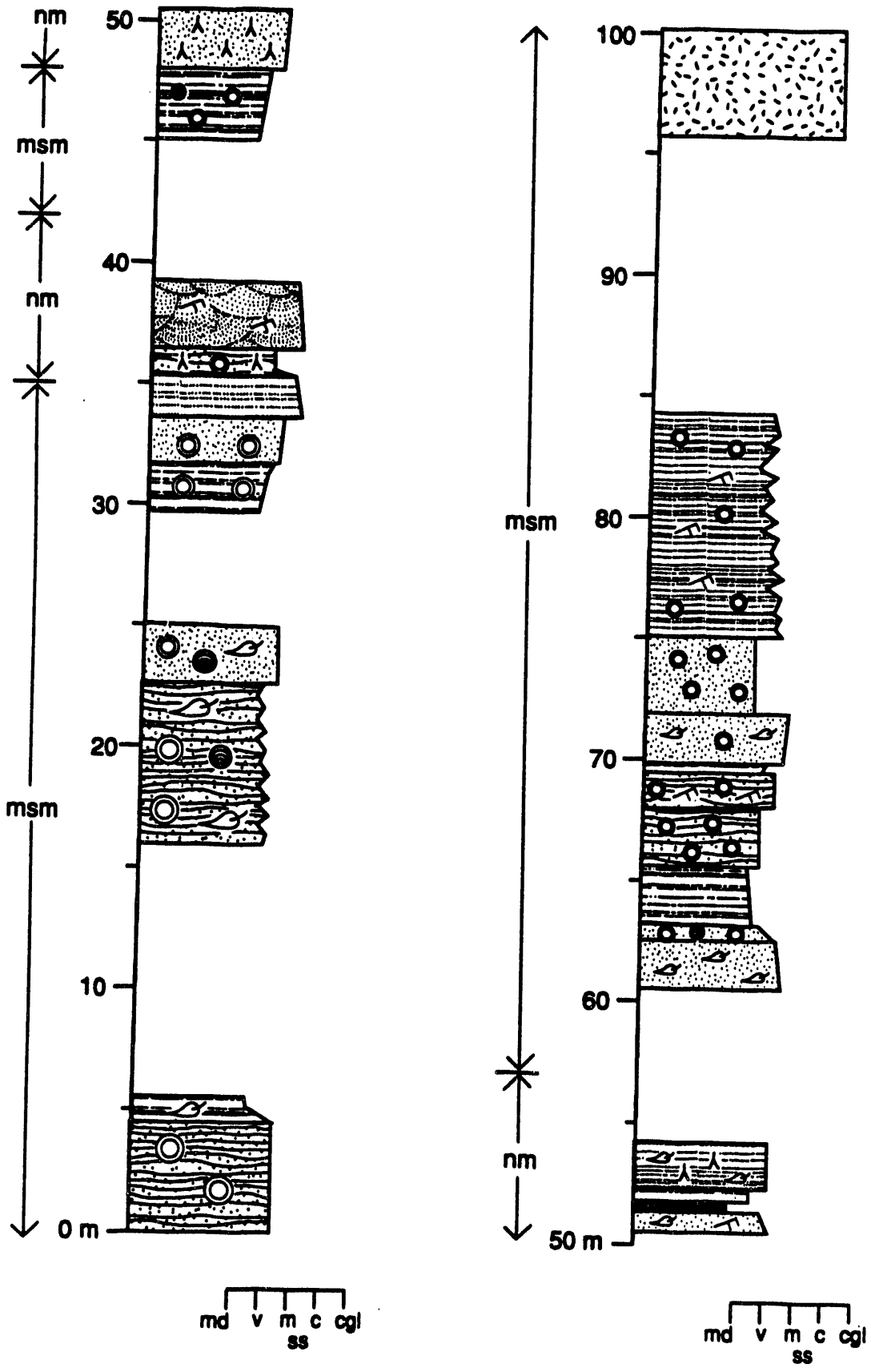
nm
msm
nm
msm
50
40
30
20
10
0 m
md v m c cgl
ss
100
90
msm
80
70
60
nm
50 m
md v m c cgl
ss

Figure A7

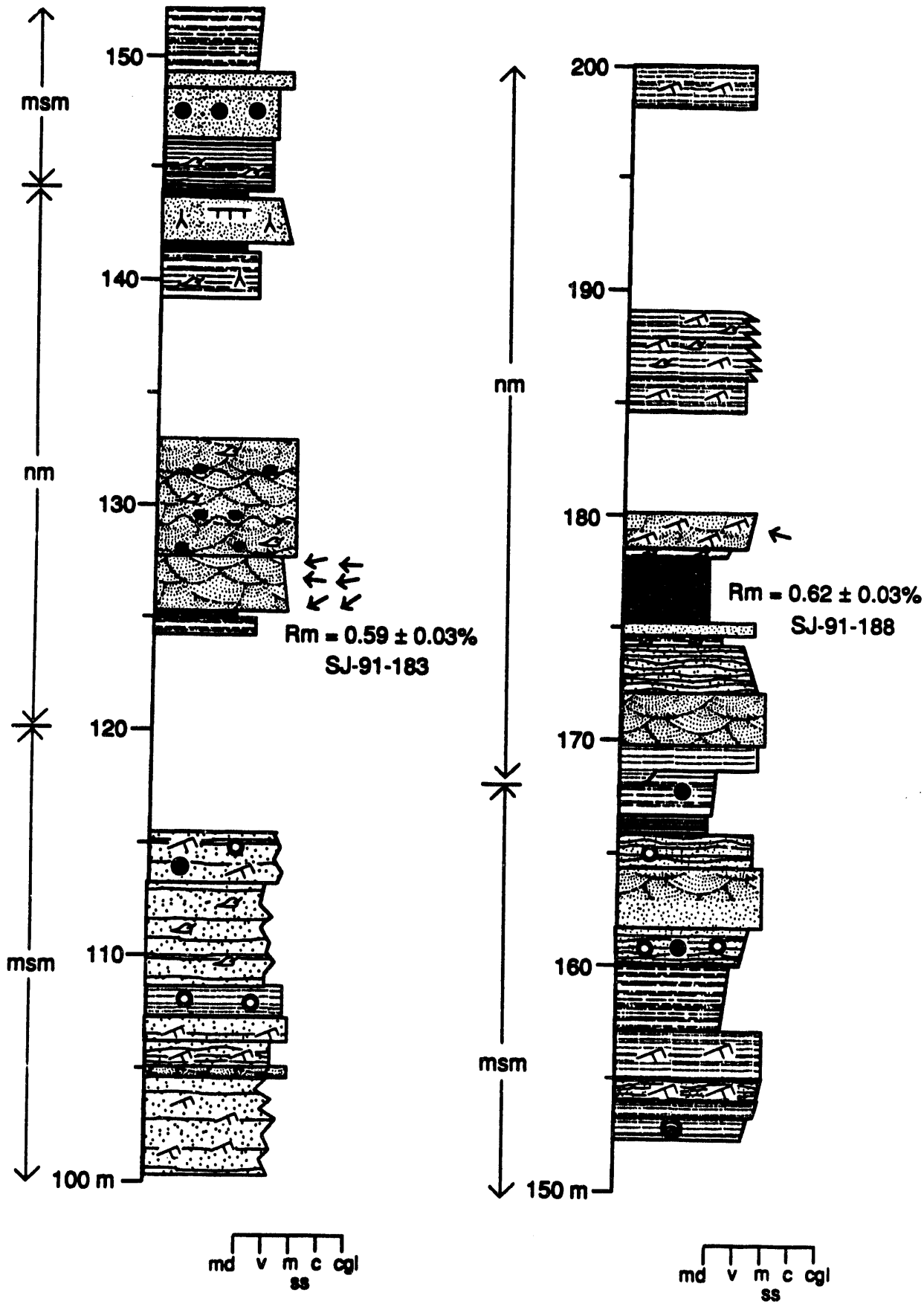
150
140
130
120
110
100 m
msm
nm
msm
Rm = 0.59 ± 0.03%
SJ-91-183
md v m c cgl
ss
200
190
180
170
160
150 m
nm
msm
Rm = 0.62 ± 0.03%
SJ-91-188
md v m c cgl
ss

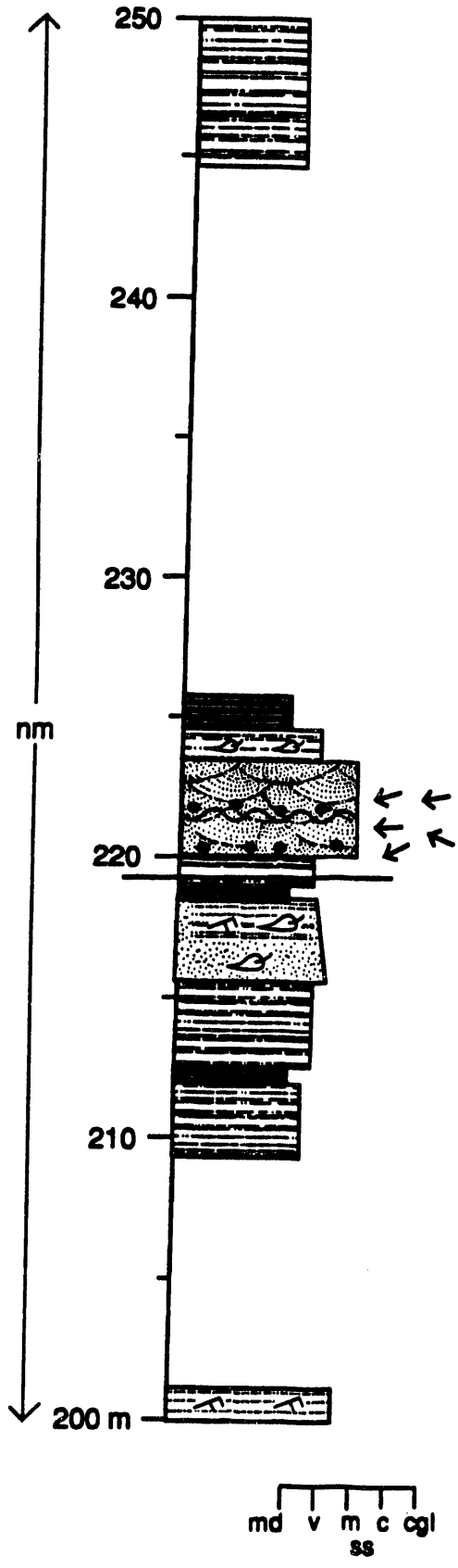
250
240
230
220
210
200 m
nm
md v m c cgl
ss

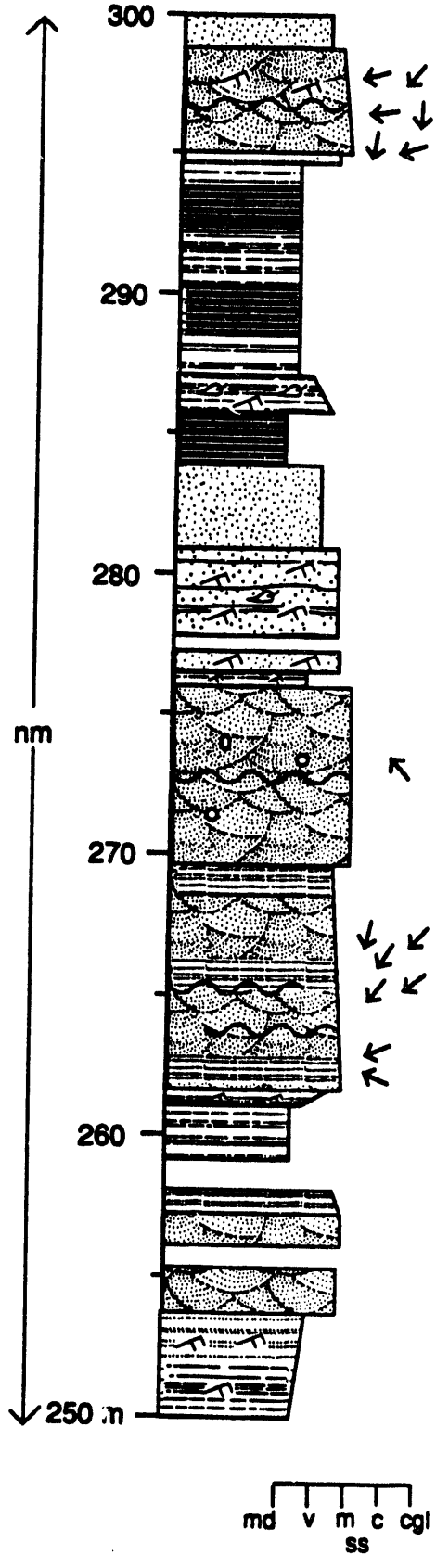
300
290
280
270
260
250 m
nm
md v m c cgl
ss

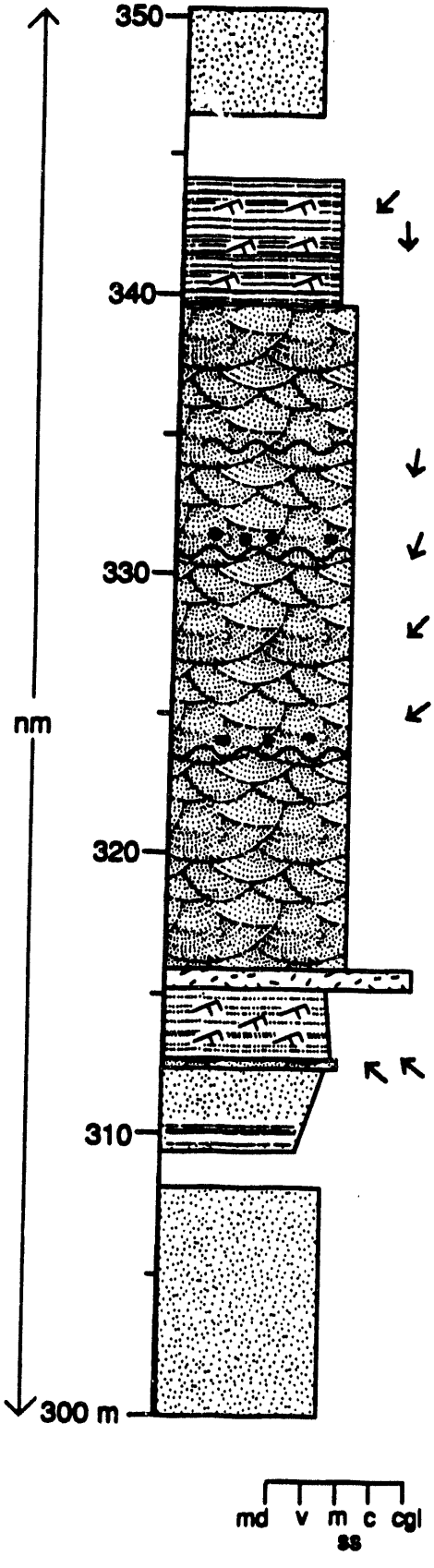
350
340
330
320
310
300 m
nm
md v m c cgl
ss

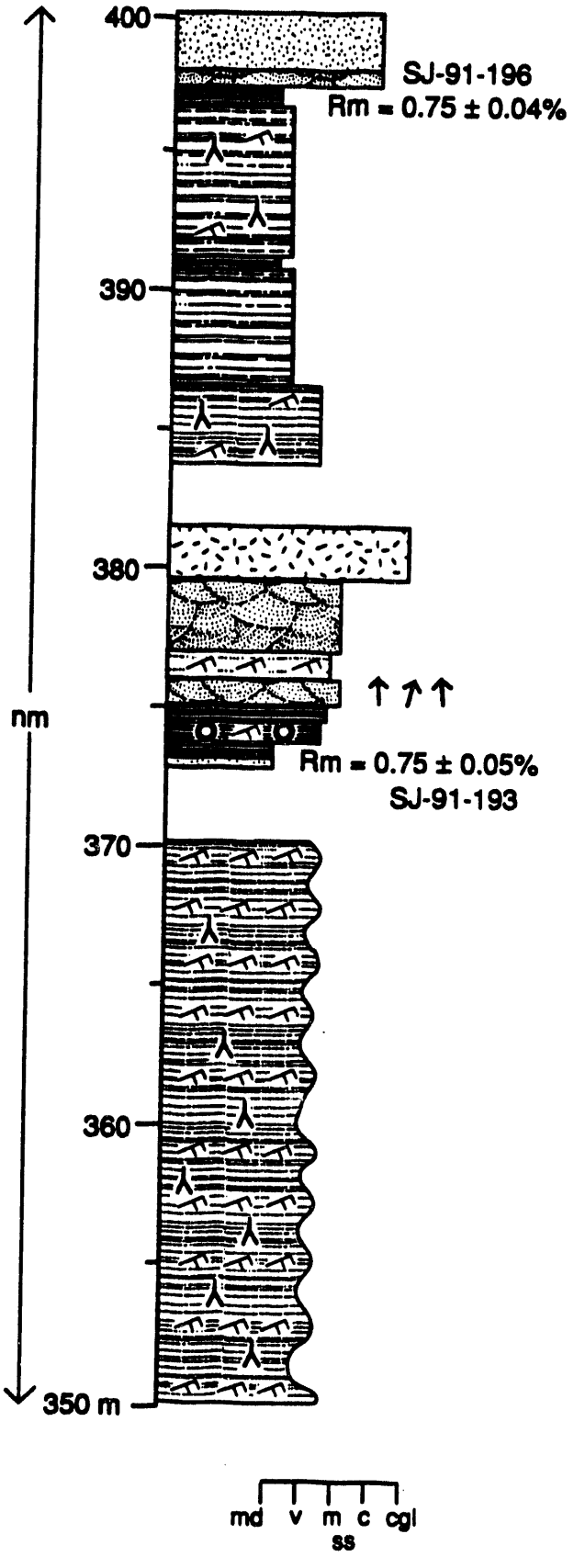
400
390
380
370
360
350 m
nm
SJ-91-196
Rm = 0.75 ± 0.04%
Rm = 0.75 ± 0.05%
SJ-91-193
md v m c cgl
ss

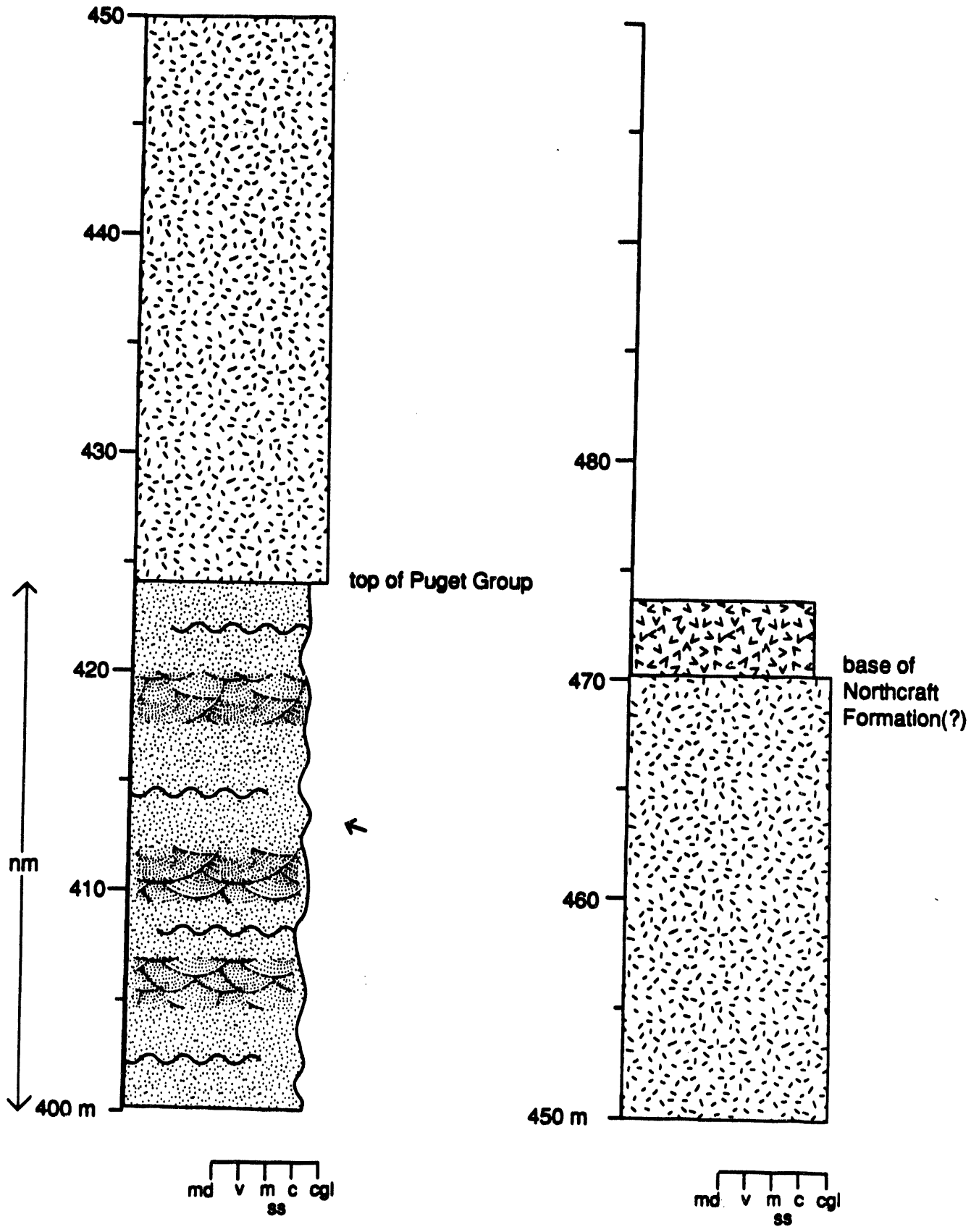
450
440
430
420
410
400 m
nm
top of Puget Group
md v m c cgl
ss
480
470
460
450 m
base of
Northcraft
Formation(?)
md v m c cgl
ss

Table A3-Vitrinite reflectance data for Bergen Mountain section.

File Name: SJ91-183
Channel Name: SJ-91-183
Description: outcrop, coal, good sample
Comment 1:
Comment 2:
Comment 3:
Comment 4:
Comment 5:
Comment 6:

	Meas1	Meas2	Ratio	Conc.
Min:	0.53			
Max:	0.67			
Mean:	0.59			
StDev:	0.03			

Pt.	X-Pos	Y-Pos	Z-Pos	Meas1	Meas2	Ratio	Conc.
1				0.57			
2				0.57			
3				0.55			
4				0.56			
5				0.56			
6				0.55			
7				0.60			
8				0.58			
9				0.64			
10				0.61			
11				0.61			
12				0.59			
13				0.57			
14				0.55			
15				0.57			
16				0.57			
17				0.59			
18				0.61			
19				0.57			
20				0.64			
21				0.61			
22				0.60			
23				0.63			
24				0.61			
25				0.57			
26				0.58			
27				0.57			
28				0.58			
29				0.58			
30				0.61			
31				0.53			
32				0.59			
33				0.61			
34				0.62			
35				0.61			
36				0.62			
37				0.54			
38				0.65			
39				0.60			
40				0.66			
41				0.63			
42				0.60			
43				0.62			
44				0.58			
45				0.67			
46				0.57			
47				0.60			
48				0.62			
49				0.59			
50				0.55			

File Name: SJ-91188
Channel Name: SJ-91-188
Description: outcrop, coal good sample
Comment 1:
Comment 2:
Comment 3:
Comment 4:
Comment 5:
Comment 6:

	Meas1	Meas2	Ratio	Conc.
Min:	0.52			
Max:	0.67			
Mean:	0.62			
StDev:	0.03			

Pt.	X-Pos	Y-Pos	Z-Pos	Meas1	Meas2	Ratio	Conc.
1				0.61			
2				0.63			
3				0.58			
4				0.65			
5				0.64			
6				0.52			
7				0.61			
8				0.62			
9				0.64			
10				0.58			
11				0.63			
12				0.63			
13				0.56			
14				0.57			
15				0.56			
16				0.63			
17				0.63			
18				0.64			
19				0.64			
20				0.64			
21				0.67			
22				0.58			
23				0.61			
24				0.63			
25				0.62			
26				0.64			
27				0.60			
28				0.64			
29				0.64			
30				0.64			
31				0.66			
32				0.61			
33				0.61			
34				0.62			
35				0.63			
36				0.60			
37				0.65			
38				0.61			
39				0.60			
40				0.59			

File Name: SJ-91193
Channel Name: SJ-91-193
Description: outcrop, coal good sample
Comment 1:
Comment 2:
Comment 3:
Comment 4:
Comment 5:
Comment 6:

	Meas1	Meas2	Ratio	Conc.
Min:	0.67			
Max:	0.83			
Mean:	0.75			
StDev:	0.05			

Pt.	X-Pos	Y-Pos	Z-Pos	Meas1	Meas2	Ratio	Conc.
1				0.78			
2				0.77			
3				0.74			
4				0.69			
5				0.72			
6				0.71			
7				0.73			
8				0.77			
9				0.74			
10				0.72			
11				0.78			
12				0.80			
13				0.81			
14				0.67			
15				0.83			
16				0.82			
17				0.74			
18				0.75			
19				0.78			
20				0.76			
21				0.76			
22				0.80			
23				0.70			
24				0.69			
25				0.75			
26				0.75			
27				0.83			
28				0.81			
29				0.79			
30				0.76			
31				0.67			
32				0.76			
33				0.67			
34				0.67			
35				0.69			
36				0.72			
37				0.69			
38				0.79			
39				0.72			
40				0.74			

File Name: SJ-91196
Channel Name: SJ-91-196
Description: outcrop, coal good sample
Comment 1:
Comment 2:
Comment 3:
Comment 4:
Comment 5:
Comment 6:

	Meas1	Meas2	Ratio	Conc.
Min:	0.62			
Max:	0.84			
Mean:	0.74			
StDev:	0.04			

Pt.	X-Pos	Y-Pos	Z-Pos	Meas1	Meas2	Ratio	Conc.
1				0.76			
2				0.76			
3				0.76			
4				0.72			
5				0.81			
6				0.72			
7				0.75			
8				0.84			
9				0.75			
10				0.83			
11				0.75			
12				0.72			
13				0.72			
14				0.70			
15				0.67			
16				0.69			
17				0.62			
18				0.70			
19				0.72			
20				0.71			
21				0.73			
22				0.71			
23				0.77			
24				0.72			
25				0.74			
26				0.73			
27				0.75			
28				0.76			
29				0.70			
30				0.80			
31				0.78			
32				0.70			
33				0.69			
34				0.65			
35				0.73			
36				0.75			
37				0.72			
38				0.70			
39				0.74			
40				0.81			
41				0.77			
42				0.76			
43				0.70			
44				0.78			
45				0.77			

Snow Creek stratigraphic section

The Snow Creek stratigraphic section (Fig. A8) of the Carbonado Formation was measured in W 1/2, sec. 11 and NE 1/4, sec. 10, T. 13 N., R. 4 E. (The Rockies 7.5'

Figure A8-Location of Snow Creek stratigraphic section.

U.S.G.S. topographic quadrangle). The section is nearly continuous, about 108 m thick, and was measured in the bed of Snow Creek late in the summer during low discharge. The base of the section corresponds to the lowest good creek-bed exposures in this area. The section (Fig. A9) is overlain by a thick (> 130 m)

Figure A9-Measured Snow Creek section lithology.

porphyritic intrusion. Strata of inferred nonmarine origin occur between 0-63 m and 73-79 m in the section. Strata of inferred shallow- to marginal-marine origin occur between 63-73 m and 79-108 m in the section. Vitrinite reflectance was analyzed for two samples.

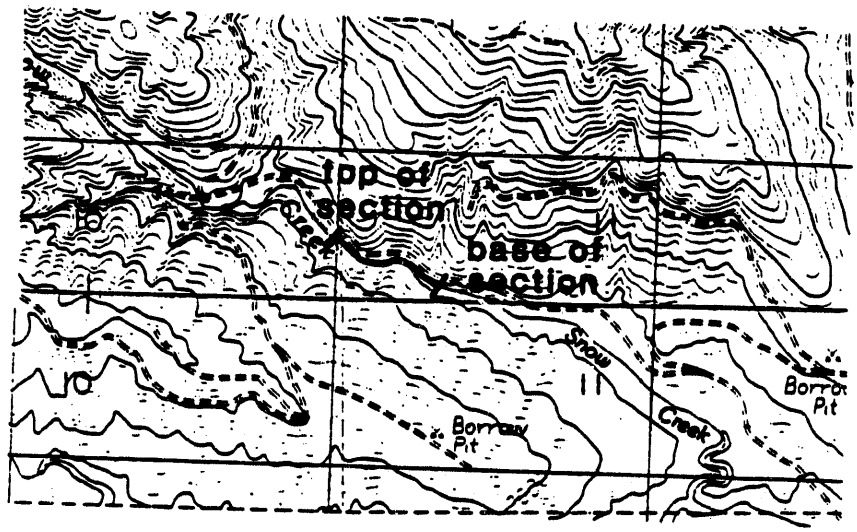
top of section
base of section
Borrow Pit
Snow
Creek
Borrow Pit

Figure A8

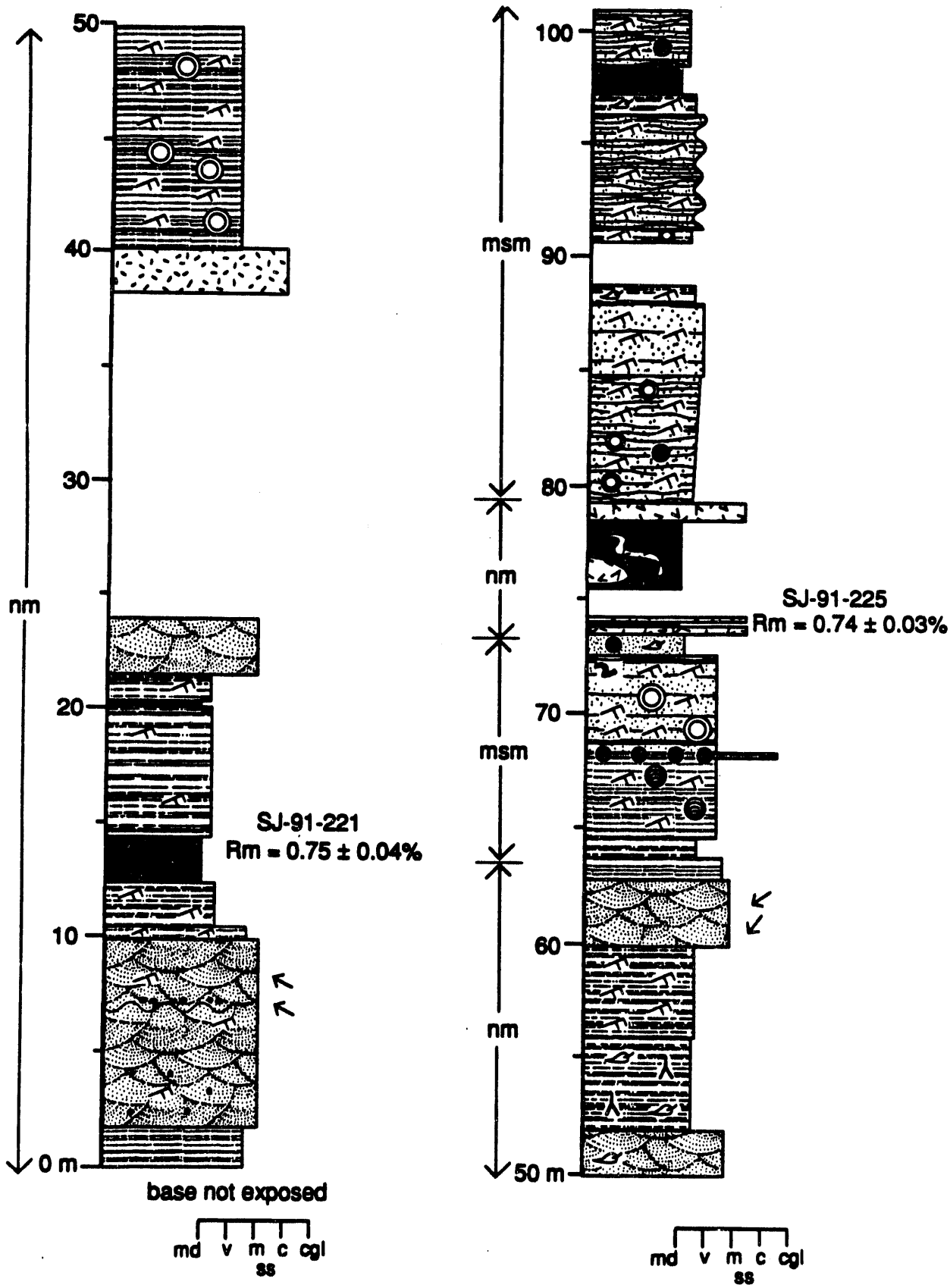
50
40
30
20
10
0 m
nm
SJ-91-221
Rm = 0.75 ± 0.04%
base not exposed
md v m c cgl
ss
100
90
80
70
60
50 m
msm
nm
msm
nm
SJ-91-225
Rm = 0.74 ± 0.03%
md v m c cgl
ss

Figure A9

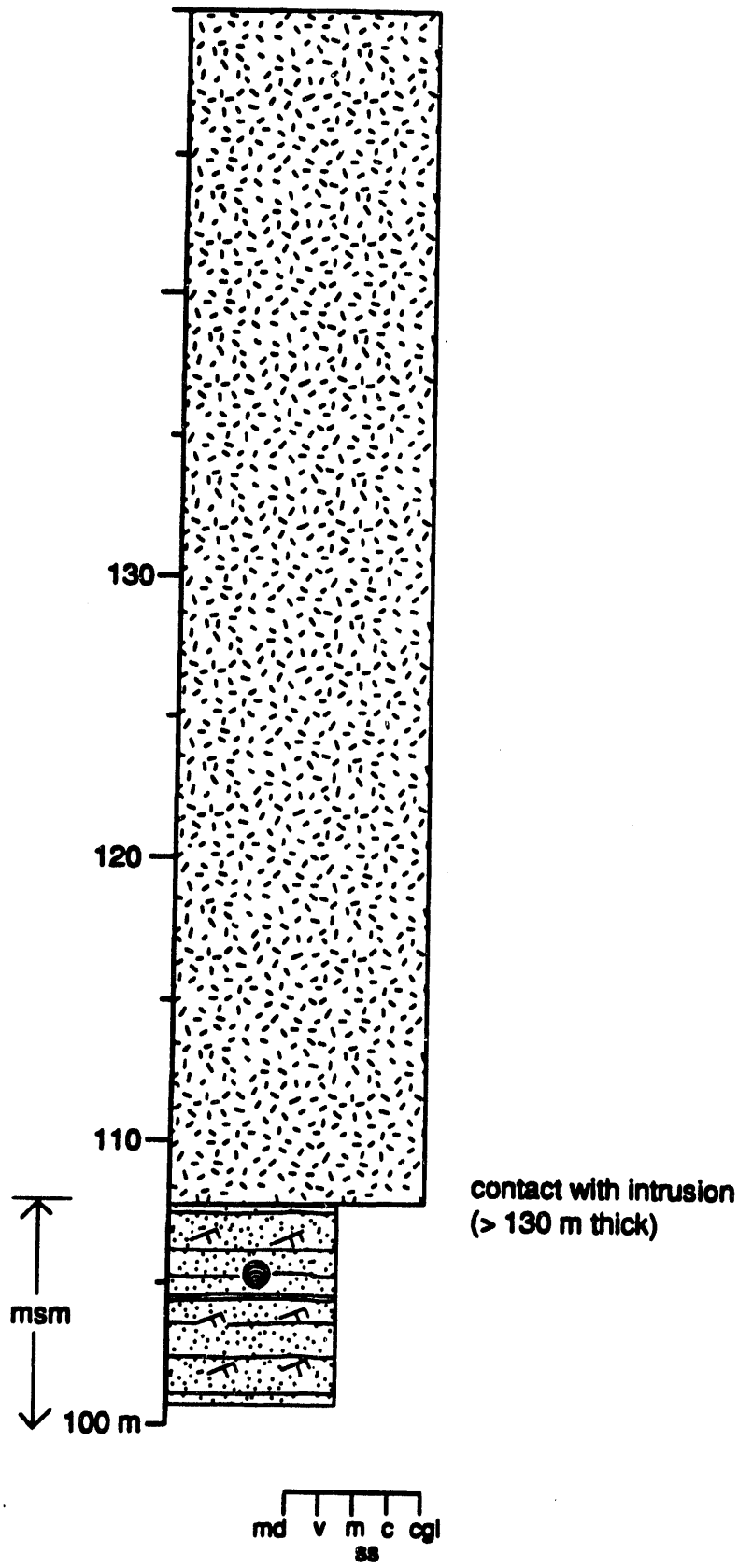
130
120
110
msm
100 m
contact with intrusion
(> 130 m thick)
md
v
m
c
cgl
ss

Table A4-Vitrinite reflectance data for Snow Creek section.

File Name: SJ91-221
Channel Name: SJ-91-221
Description: outcrop, coal, good sample
Comment 1:
Comment 2:
Comment 3:
Comment 4:
Comment 5:
Comment 6:

	Meas1	Meas2	Ratio	Conc.
Min:	0.65			
Max:	0.84			
Mean:	0.75			
StDev:	0.04			

Pt.	X-Pos	Y-Pos	Z-Pos	Meas1	Meas2	Ratio	Conc.
1				0.79			
2				0.76			
3				0.75			
4				0.76			
5				0.77			
6				0.69			
7				0.73			
8				0.80			
9				0.81			
10				0.72			
11				0.79			
12				0.77			
13				0.80			
14				0.79			
15				0.79			
16				0.70			
17				0.68			
18				0.70			
19				0.80			
20				0.75			
21				0.70			
22				0.70			
23				0.69			
24				0.78			
25				0.76			
26				0.76			
27				0.68			
28				0.79			
29				0.76			
30				0.76			
31				0.76			
32				0.71			
33				0.73			
34				0.75			
35				0.76			
36				0.70			
37				0.76			
38				0.77			
39				0.71			
40				0.72			
41				0.65			
42				0.71			
43				0.84			
44				0.83			
45				0.78			
46				0.70			
47				0.71			
48				0.70			
49				0.68			
50				0.73			

File Name: SJ91-225
Channel Name: SJ-91-225
Description: outcrop, coal, good sample
Comment 1:
Comment 2:
Comment 3:
Comment 4:
Comment 5:
Comment 6:

	Meas1	Meas2	Ratio	Conc.
Min:	0.66			
Max:	0.80			
Mean:	0.74			
StDev:	0.03			

Pt.	X-Pos	Y-Pos	Z-Pos	Meas1	Meas2	Ratio	Conc.
1				0.80			
2				0.75			
3				0.75			
4				0.78			
5				0.74			
6				0.72			
7				0.68			
8				0.68			
9				0.77			
10				0.79			
11				0.79			
12				0.66			
13				0.68			
14				0.75			
15				0.69			
16				0.76			
17				0.72			
18				0.75			
19				0.72			
20				0.69			
21				0.75			
22				0.79			
23				0.75			
24				0.77			
25				0.76			
26				0.75			
27				0.68			
28				0.74			
29				0.79			
30				0.75			
31				0.76			
32				0.77			
33				0.76			
34				0.76			
35				0.74			
36				0.70			
37				0.76			
38				0.75			
39				0.73			
40				0.73			
41				0.71			
42				0.73			
43				0.73			
44				0.69			
45				0.73			
46				0.70			
47				0.73			
48				0.78			
49				0.69			
50				0.75			

South Fork of Tilton River stratigraphic section

The Coal Creek stratigraphic section (Fig. A10) of the Carbonado Formation was measured in NW 1/4, sec. 32, T. 13 N., R. 5 E. (Glenoma 7.5' U.S.G.S. topographic quadrangle). The section is approximately 272 m thick. The lower 134 m of the

Figure A10-Location of South Fork Tilton River (Coal Creek) stratigraphic section.

section were measured in well-exposed cuts along logging roads on the south flank of the valley of the South Fork of the Tilton River; the base of the section corresponds to the lowest exposures on this road network. Strata (Fig. A11) of inferred nonmarine origin occur between 0-20 m, 62-78, and 126-134 m in this lower interval. Strata of inferred shallow- to marginal-marine origin occur between 20-68 m and 78-126 m in

Figure A11-South Fork Tilton River measured section data.

this lower interval. The section is covered from approximately 134 to 204 m. The upper 70 m are poorly exposed in the steep flanks of a small drainage. This upper interval consists entirely of sandstone and has an inferred nonmarine origin. This section is overlain by poorly exposed, fine-grained volcanic rocks considered here as part of the Northcraft Formation. This contact is lower on the valley flank than mapped by Schasse (1987). Two samples were analyzed for vitrinite reflectance.

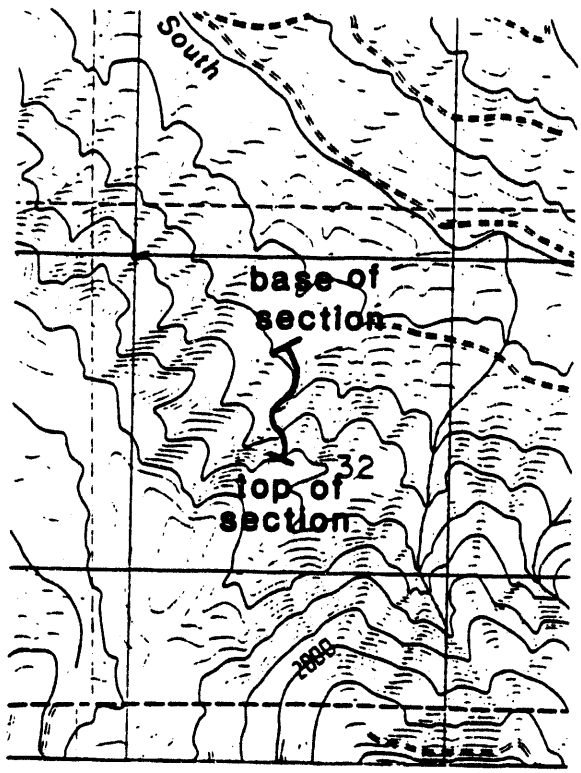

Figure A10

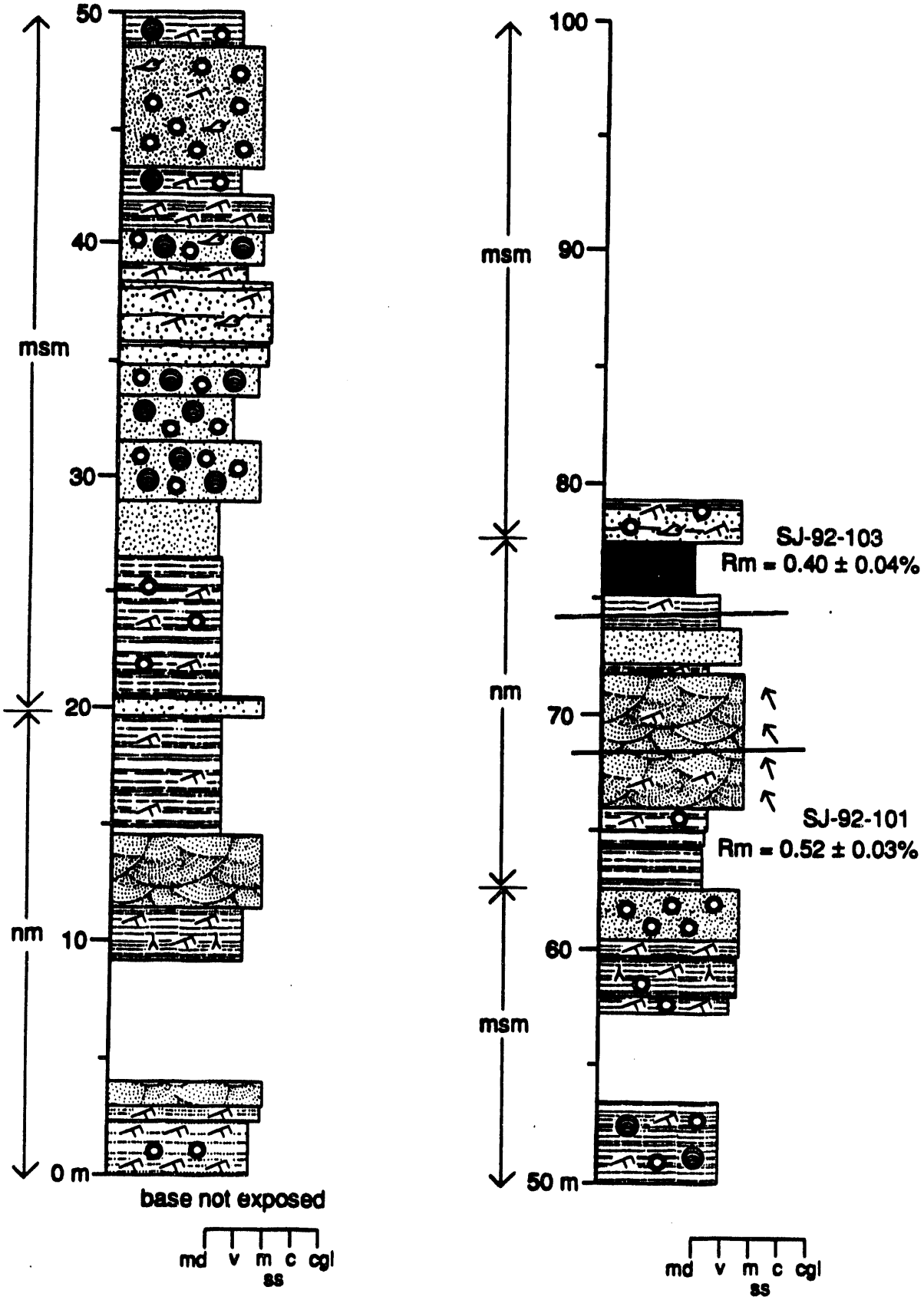
50
40
30
20
10
0 m
msm
nm
base not exposed
md v m c cgl
ss
100
90
80
70
60
50 m
msm
nm
msm
SJ-92-103
Rm = 0.40 ± 0.04%
SJ-92-101
Rm = 0.52 ± 0.03%
md v m c cgl
ss

Figure A11

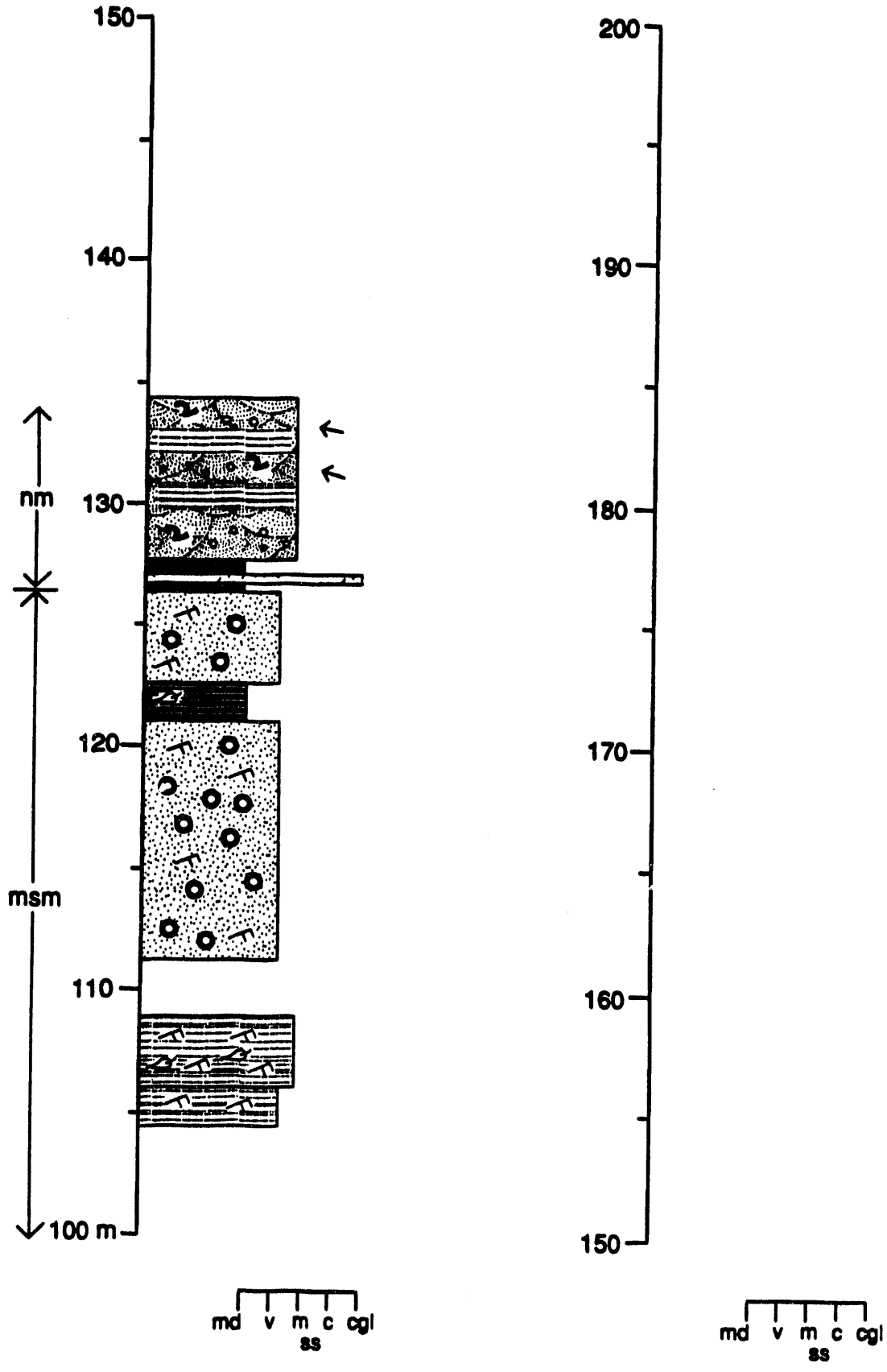
150
140
130
120
110
100 m
200
190
180
170
160
150
nm
msm
md v m c cgl
ss
md v m c cgl
ss

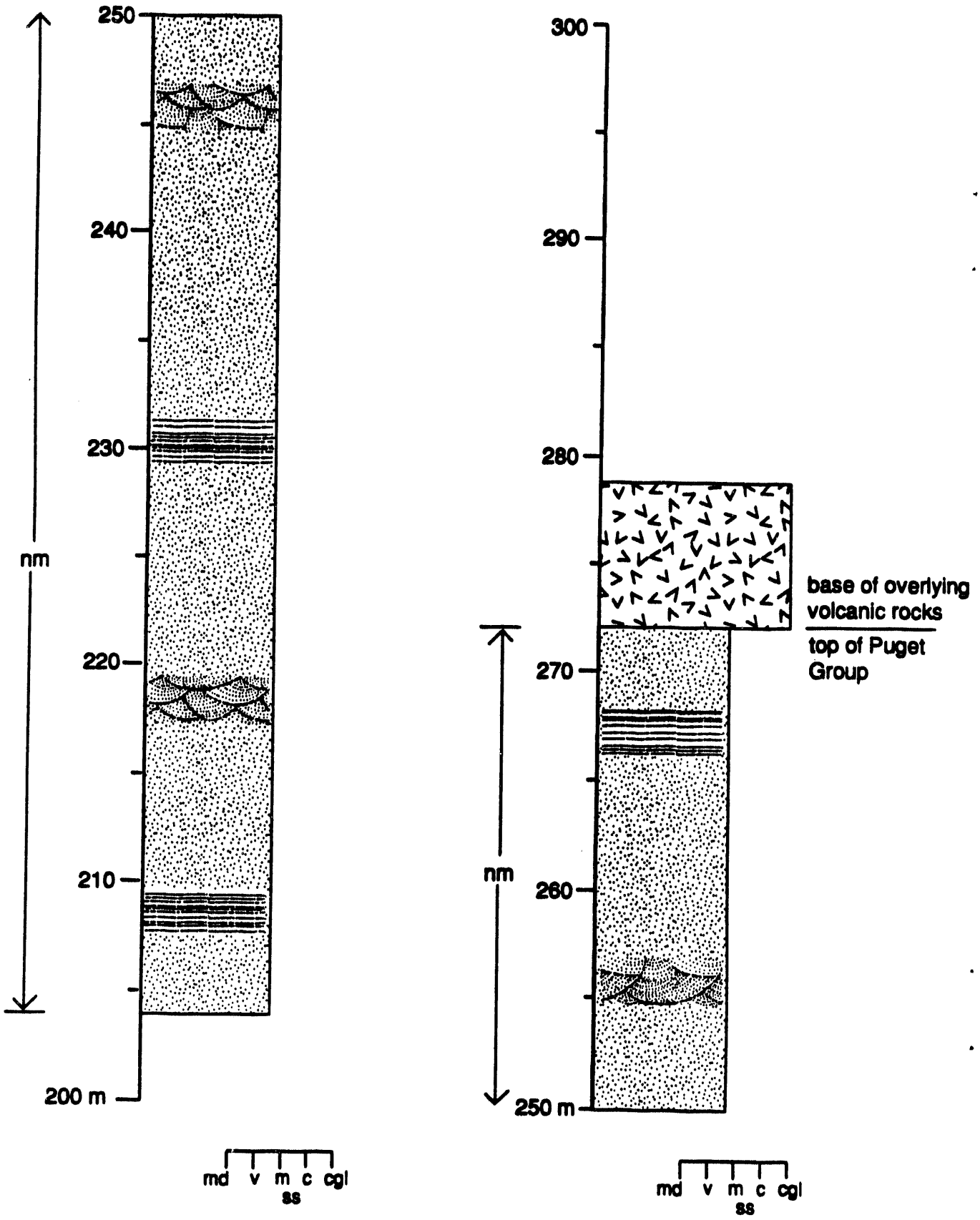
250
240
230
220
210
200 m
nm
md v m c cgl
ss
300
290
280
270
260
250 m
nm
base of overlying volcanic rocks
top of Puget Group
md v m c cgl
ss

Table A5-Vitrinite reflectance data for South Fork Tilton River samples.

File Name: SJ92-101
Channel Name: SJ-92-101
Description: SJ-92-101
Comment 1: good sample
Comment 2: consistent and clean
Comment 3: polish good
Comment 4:
Comment 5:
Comment 6:

	Meas1	Meas2	Ratio	Conc.
Min:	0.47			
Max:	0.58			
Mean:	0.52			
StDev:	0.03			

Pt.	X-Pos	Y-Pos	Z-Pos	Meas1	Meas2	Ratio	Conc.
1				0.56			
2				0.56			
3				0.51			
4				0.49			
5				0.49			
6				0.55			
7				0.51			
8				0.47			
9				0.55			
10				0.53			
11				0.54			
12				0.52			
13				0.48			
14				0.49			
15				0.57			
16				0.56			
17				0.58			
18				0.49			
19				0.52			
20				0.51			
21				0.51			
22				0.56			
23				0.53			
24				0.55			
25				0.50			
26				0.53			
27				0.51			
28				0.47			
29				0.53			
30				0.50			
31				0.50			
32				0.49			
33				0.48			
34				0.49			
35				0.47			

File Name: SJ92-103
Channel Name: SJ-92-103
Description: SJ-92-103
Comment 1: good sample
Comment 2: consistent and clean
Comment 3: polish fair
Comment 4:
Comment 5:
Comment 6:

	Meas1	Meas2	Ratio	Conc.
Min:	0.33			
Max:	0.49			
Mean:	0.40			
StDev:	0.04			

Pt.	X-Pos	Y-Pos	Z-Pos	Meas1	Meas2	Ratio	Conc.
1				0.37			
2				0.39			
3				0.41			
4				0.40			
5				0.42			
6				0.39			
7				0.40			
8				0.39			
9				0.40			
10				0.38			
11				0.33			
12				0.41			
13				0.43			
14				0.46			
15				0.46			
16				0.41			
17				0.44			
18				0.39			
19				0.44			
20				0.39			
21				0.36			
22				0.40			
23				0.40			
24				0.39			
25				0.49			
26				0.48			
27				0.33			
28				0.37			
29				0.37			
30				0.43			
31				0.40			
32				0.40			
33				0.38			
34				0.40			
35				0.40			

Bear Canyon stratigraphic section

The Bear Canyon stratigraphic section (Fig. A12) of the Carbonado Formation was measured in SE 1/4, sec. 18, T. 13 N., R. 3 E. (Mossyrock 7.5' U.S.G.S.

Figure A12- Bear Canyon measured section location.

topographic quadrangle). The section is about 33 m thick. Exposures are on the east flank of Bear Canyon, beginning with a Highway 508 roadcut and ending with exposures on steep valley walls north of the Highway. Neither top or base of the section are exposed. The lower 11 m of the section (Fig. A13) are of inferred shallow- to marginal-marine origin. The upper 22 m of the section are of inferred nonmarine origin. No vitrinite reflectance data is available for this section as of this

Figure A13-Measured section at Bear Canyon.

date.

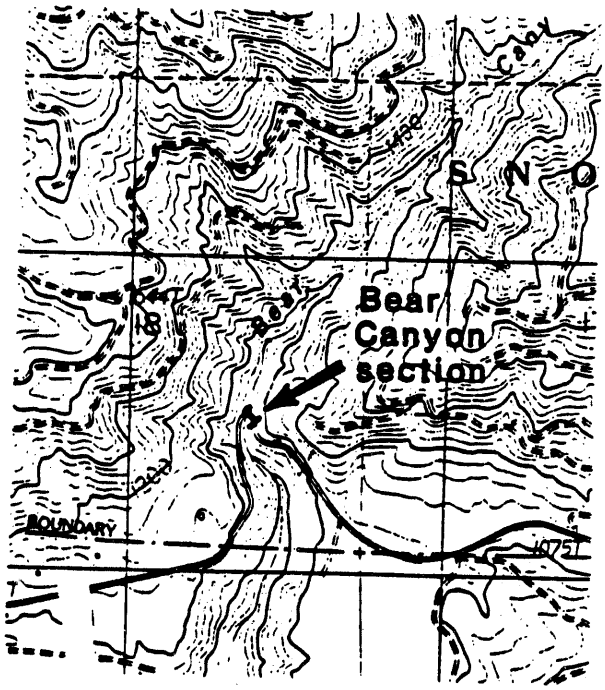

Figure A12

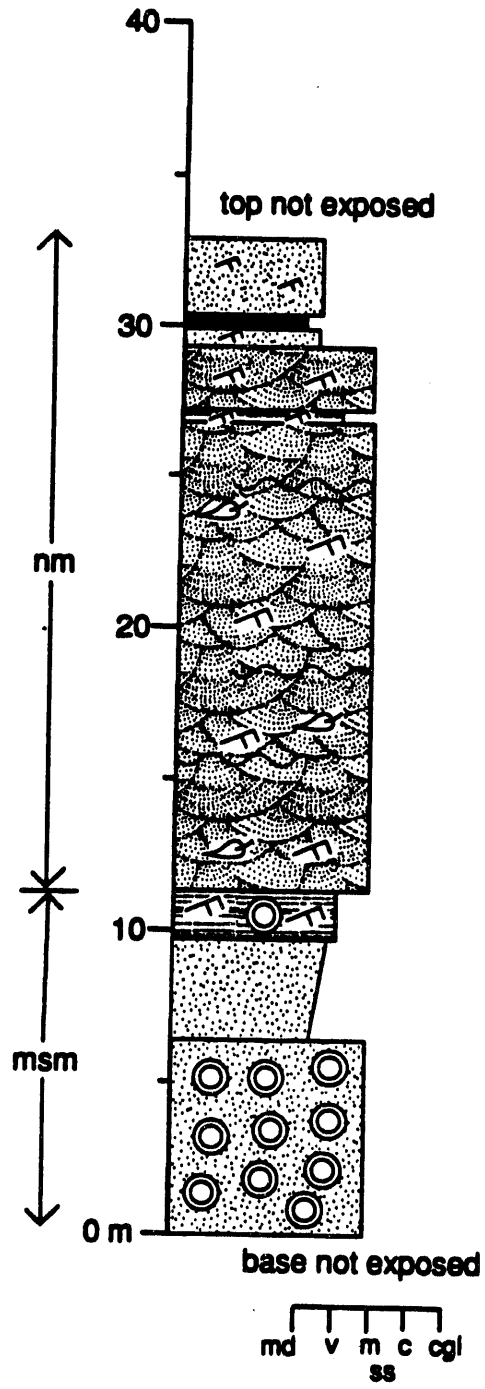
40
top not exposed
30
nm
20
10
msm
0 m
base not exposed
md
v
m
c
cgl
ss

Figure A13

Appendix B

Velocity Information

The sonic logs on the following pages are from selected wells in the Chehalis Basin used to assess the velocities of the sedimentary and volcanic rocks. These were compared to stacking velocities and empirical velocity estimates for sedimentary rocks as shown in Figure 15.

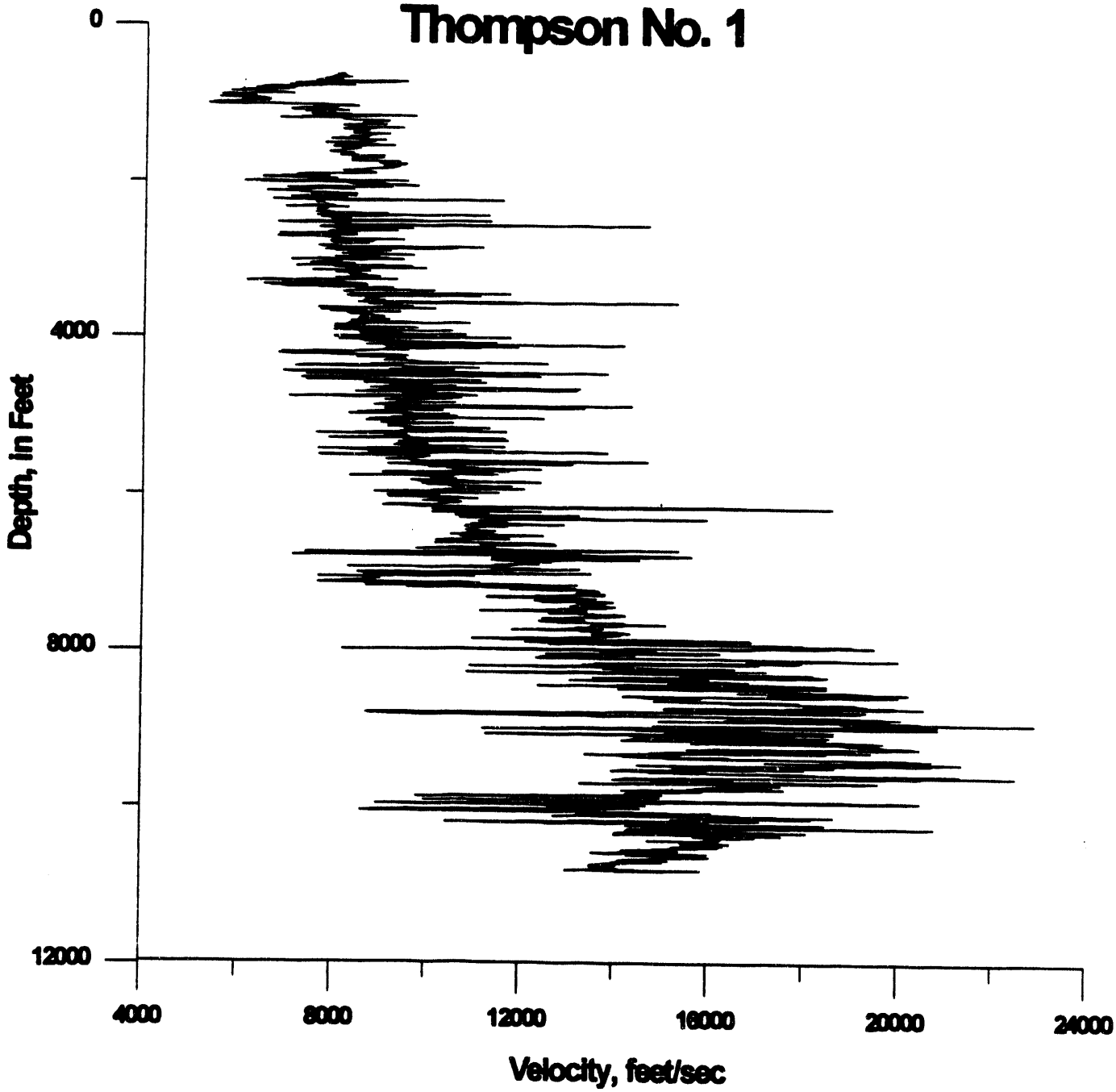
Thompson No. 1
0
4000
8000
12000
Depth, in Feet
4000
8000
12000
16000
20000
24000
Velocity, feet/sec

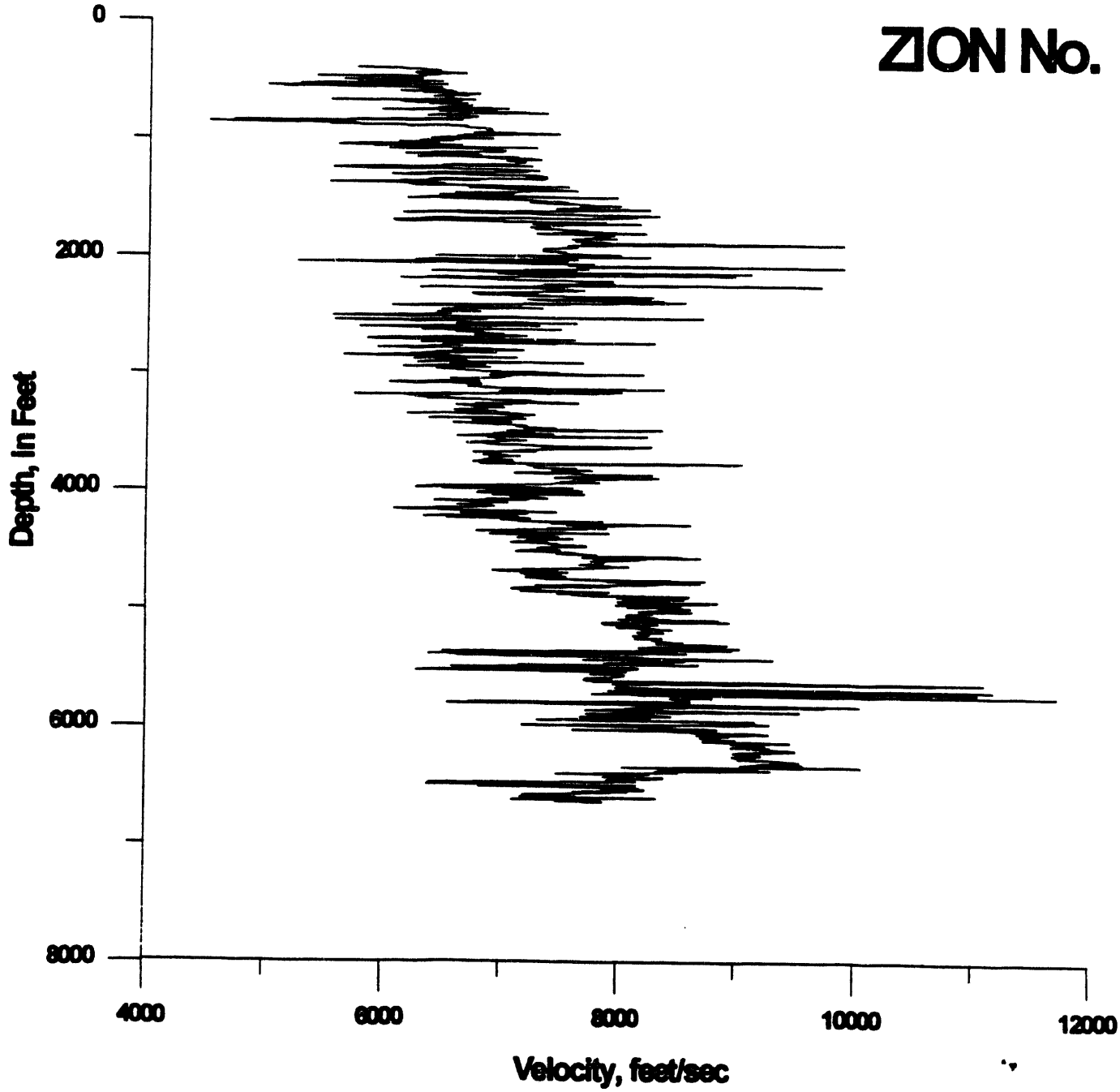
ZION No. 1
0
2000
4000
6000
8000
Depth, In Feet
4000
6000
8000
10000
12000
Velocity, feet/sec

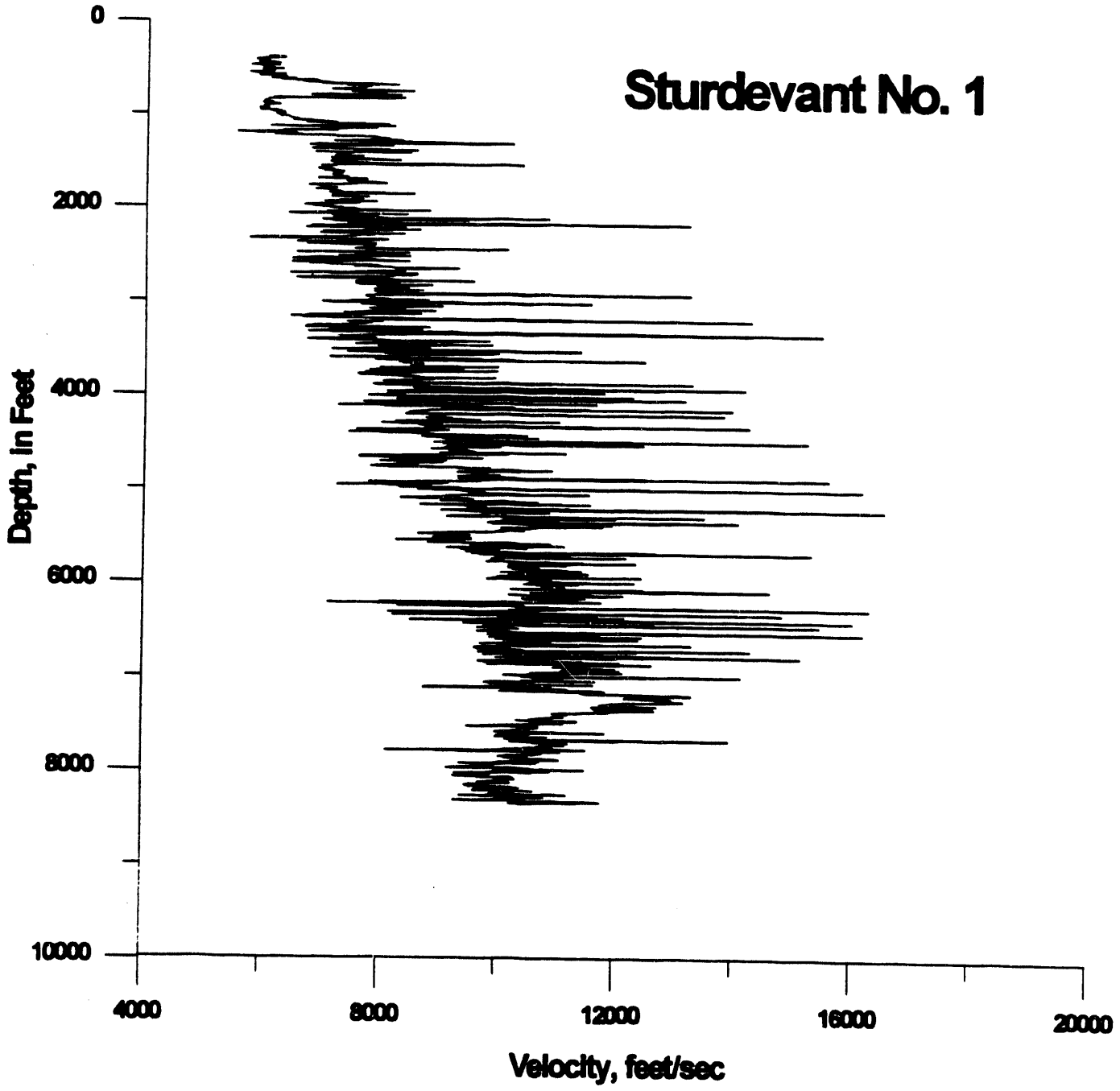
Sturdevant No. 1
0
2000
4000
6000
8000
10000
Depth, In Feet
4000
8000
12000
16000
20000
Velocity, feet/sec

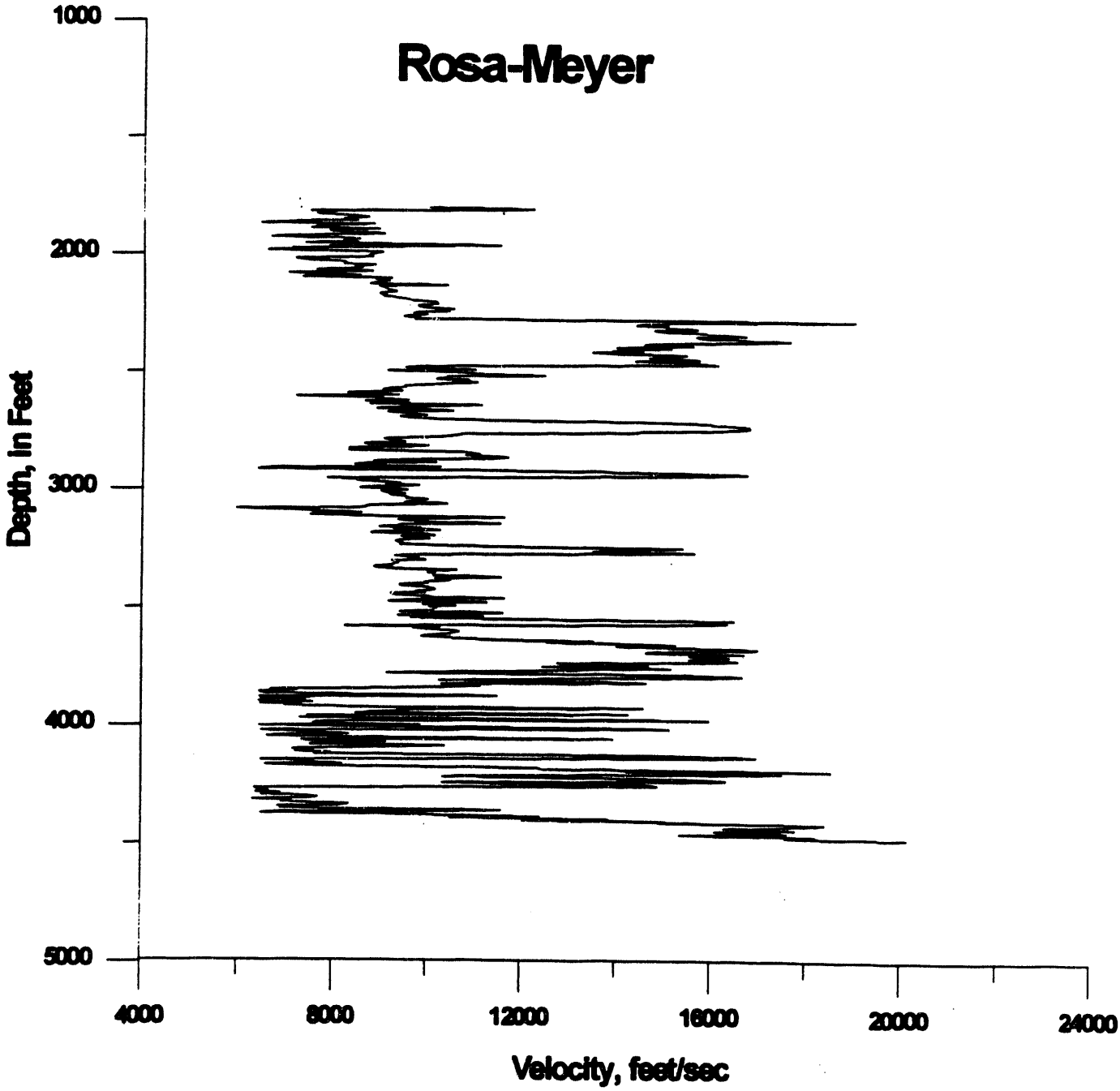
Rosa-Meyer
1000
2000
3000
4000
5000
Depth, In Feet
4000
8000
12000
16000
20000
24000
Velocity, feet/sec

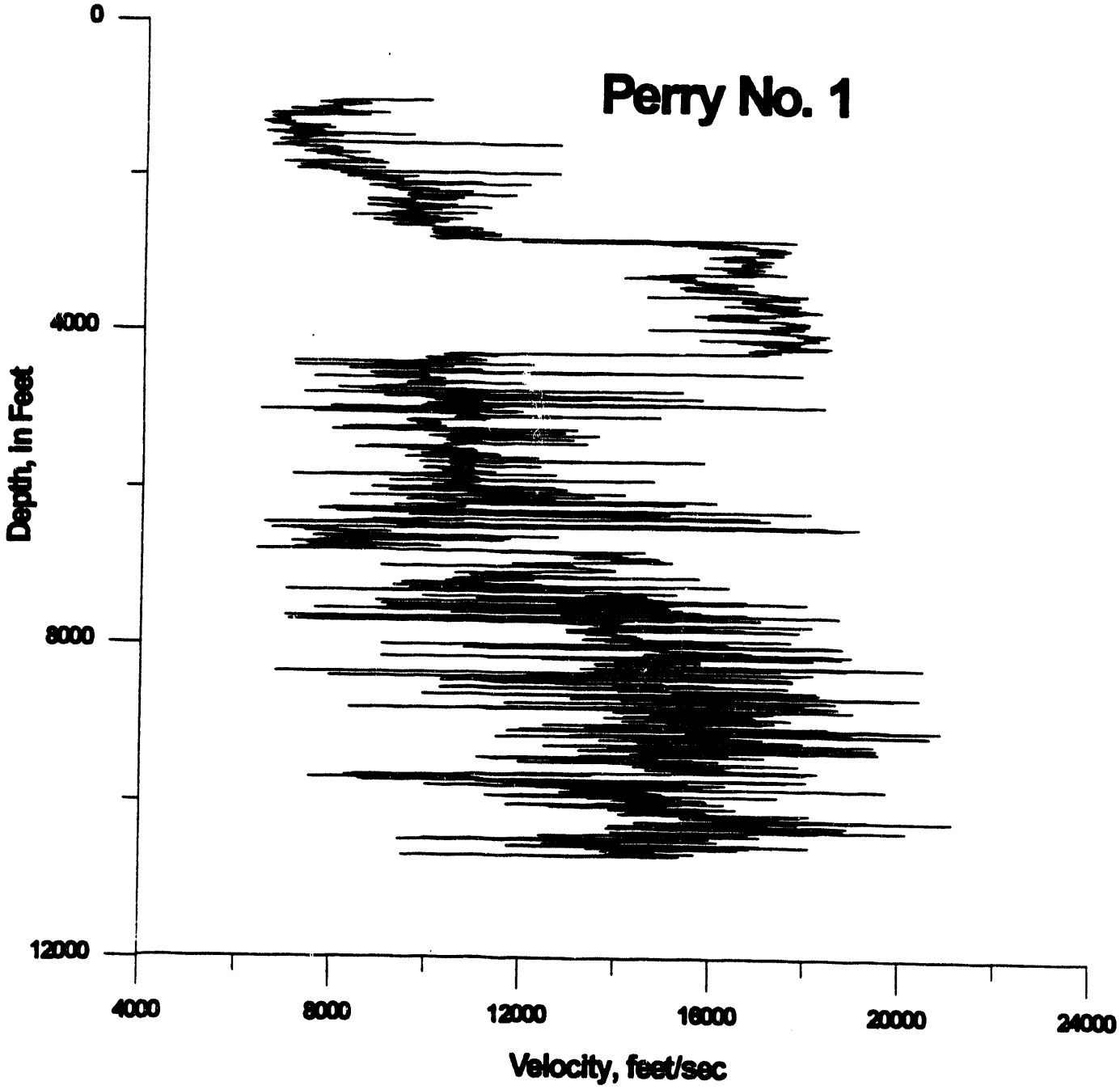
Perry No. 1
0
4000
8000
12000
Depth, In Feet
4000
8000
12000
16000
20000
24000
Velocity, feet/sec

Shotpoint Locations

Shotpoint location table for the DOE seismic lines follow. Exact shotpoint locations can be keyed to the geologic map of Figure 2 by counting off by tens. Line 4 shotpoints run from east to west, line 5 from south to north, and the remainder run from east to west.

<line id>	< spt >	< UTM x >	< UTM y >	<longitude>	<latitude>
LINE-1&2	101	538210.625000	5153621.500000	-122.501701	46.537041
LINE-1&2	110	538478.625000	5153611.000000	-122.498207	46.536930
LINE-1&2	120	538781.125000	5153600.500000	-122.494263	46.536819
LINE-1&2	130	539054.187500	5153627.000000	-122.490700	46.537041
LINE-1&2	140	539352.187500	5153679.000000	-122.486809	46.537491
LINE-1&2	150	539645.375000	5153761.500000	-122.482979	46.538219
LINE-1&2	160	539938.625000	5153828.000000	-122.479149	46.538799
LINE-1&2	170	540236.625000	5153890.500000	-122.475258	46.539341
LINE-1&2	180	540514.375000	5153998.500000	-122.471626	46.540298
LINE-1&2	190	540781.312500	5154153.500000	-122.468132	46.541679
LINE-1&2	200	541033.375000	5154324.500000	-122.464828	46.543201
LINE-1&2	210	541296.187500	5154475.000000	-122.461388	46.544540
LINE-1&2	220	541562.812500	5154582.500000	-122.457901	46.545490
LINE-1&2	230	541861.312500	5154644.500000	-122.454002	46.546028
LINE-1&2	240	542159.500000	5154665.500000	-122.450111	46.546200
LINE-1&2	250	542458.000000	5154645.500000	-122.446220	46.546001
LINE-1&2	260	542756.375000	5154630.000000	-122.442329	46.545841
LINE-1&2	270	543053.875000	5154588.500000	-122.438454	46.545448
LINE-1&2	280	543347.125000	5154485.000000	-122.434639	46.544498
LINE-1&2	290	543588.812500	5154314.500000	-122.431503	46.542950
LINE-1&2	300	543825.875000	5154123.000000	-122.428429	46.541210
LINE-1&2	310	544093.125000	5153983.500000	-122.424957	46.539940
LINE-1&2	320	544385.500000	5153921.500000	-122.421150	46.539360
LINE-1&2	330	544689.500000	5153875.000000	-122.417191	46.538921
LINE-1&2	340	544992.500000	5153874.500000	-122.413239	46.538898
LINE-1&2	350	545295.687500	5153937.000000	-122.409279	46.539440
LINE-1&2	360	545584.125000	5153942.500000	-122.405518	46.539471
LINE-1&2	370	545845.625000	5153782.000000	-122.402122	46.538010
LINE-1&2	380	546092.812500	5153601.000000	-122.398918	46.536362
LINE-1&2	390	546360.625000	5153466.000000	-122.395439	46.535130
LINE-1&2	400	546643.125000	5153399.500000	-122.391762	46.534512
LINE-1&2	410	546946.312500	5153389.500000	-122.387810	46.534401
LINE-1&2	420	547249.875000	5153399.500000	-122.383850	46.534470
LINE-1&2	430	547507.312500	5153549.500000	-122.380478	46.535801
LINE-1&2	440	547763.500000	5153699.000000	-122.377121	46.537128
LINE-1&2	450	547989.500000	5153905.500000	-122.374153	46.538971
LINE-1&2	460	548226.687500	5154097.500000	-122.371040	46.540680
LINE-1&2	470	548468.500000	5154289.500000	-122.367867	46.542389
LINE-1&2	480	548735.375000	5154418.000000	-122.364372	46.543530
LINE-1&2	490	549038.500000	5154413.000000	-122.360420	46.543461
LINE-1&2	500	549327.312500	5154366.000000	-122.356659	46.543018
LINE-1&2	510	549624.625000	5154351.000000	-122.352783	46.542858
LINE-1&2	520	549871.687500	5154536.500000	-122.349541	46.544510
LINE-1&2	530	550124.125000	5154713.000000	-122.346230	46.546082

LINE-1&2	540	550386.312500	5154836.000000	-122.342796	46.547169
LINE-1&2	550	550683.875000	5154857.500000	-122.338913	46.547340
LINE-1&2	560	550982.312500	5154785.500000	-122.335030	46.546669
LINE-1&2	570	551270.312500	5154691.500000	-122.331284	46.545799
LINE-1&2	580	551568.375000	5154645.000000	-122.327400	46.545361
LINE-1&2	590	551856.187500	5154713.500000	-122.323639	46.545952
LINE-1&2	600	552124.125000	5154852.000000	-122.320129	46.547180
LINE-1&2	610	552381.375000	5155002.000000	-122.316757	46.548512
LINE-1&2	620	552642.625000	5155163.000000	-122.313332	46.549938
LINE-1&2	630	552905.125000	5155312.500000	-122.309891	46.551262
LINE-1&2	640	553157.625000	5155467.500000	-122.306580	46.552639
LINE-1&2	650	553419.500000	5155622.000000	-122.303146	46.554008
LINE-1&2	660	553593.312500	5155815.000000	-122.300858	46.555729
LINE-1&2	670	553891.687500	5155865.500000	-122.296959	46.556160
LINE-1&2	680	554194.687500	5155855.000000	-122.293007	46.556042
LINE-1&2	690	554487.000000	5155804.000000	-122.289200	46.555561
LINE-1&2	700	554785.375000	5155734.500000	-122.285316	46.554909
LINE-1&2	710	555062.875000	5155704.000000	-122.281700	46.554611
LINE-1&2	720	555339.812500	5155673.000000	-122.278091	46.554310
LINE-1&2	730	555628.375000	5155582.500000	-122.274338	46.553471
LINE-1&2	740	555910.875000	5155461.500000	-122.270668	46.552361
LINE-1&2	750	556136.125000	5155274.500000	-122.267754	46.550659
LINE-1&2	760	556363.187500	5155067.500000	-122.264816	46.548779
LINE-1&2	770	556547.375000	5154825.000000	-122.262444	46.546581
LINE-1&2	780	556728.000000	5154588.000000	-122.260117	46.544430
LINE-1&2	790	556994.312500	5154451.500000	-122.256660	46.543179
LINE-1&2	800	557251.500000	5154290.500000	-122.253326	46.541710
LINE-1&2	810	557441.625000	5154052.500000	-122.250877	46.539551
LINE-1&2	820	557631.687500	5153811.000000	-122.248428	46.537361
LINE-1&2	830	557796.687500	5153563.000000	-122.246307	46.535118
LINE-1&2	840	558037.687500	5153386.500000	-122.243187	46.533508
LINE-1&2	850	558284.625000	5153209.000000	-122.239990	46.531891
LINE-1&2	860	558495.500000	5152997.500000	-122.237267	46.529968
LINE-1&2	870	558732.000000	5152811.500000	-122.234207	46.528271
LINE-1&2	880	558988.375000	5152674.500000	-122.230881	46.527020
LINE-1&2	890	559234.687500	5152508.500000	-122.227692	46.525501
LINE-1&2	900	559440.500000	5152291.500000	-122.225037	46.523529
LINE-1&2	910	559707.375000	5152165.000000	-122.221573	46.522369
LINE-1&2	920	559953.687500	5151998.500000	-122.218384	46.520851
LINE-1&2	930	560118.312500	5151745.500000	-122.216270	46.518559
LINE-1&2	940	560293.312500	5151508.500000	-122.214020	46.516411
LINE-1&2	950	560478.375000	5151266.000000	-122.211639	46.514210
LINE-1&2	960	560709.687500	5151079.000000	-122.208649	46.512508
LINE-1&2	970	560997.187500	5151008.500000	-122.204910	46.511848
LINE-1&2	980	561300.125000	5150927.500000	-122.200974	46.511089
LINE-1&2	990	561567.812500	5150797.000000	-122.197502	46.509892

LINE-1&2	1000	561845.125000	5150756.000000	-122.193893	46.509499
LINE-1&2	1010	562132.812500	5150847.000000	-122.190132	46.510288
LINE-1&2	1020	562441.000000	5150867.000000	-122.186111	46.510441
LINE-1&2	1030	562729.187500	5150857.500000	-122.182358	46.510330
LINE-1&2	1040	562995.875000	5150988.000000	-122.178864	46.511478
LINE-1&2	1050	563227.500000	5151181.000000	-122.175819	46.513191
LINE-1&2	1060	563484.375000	5151346.500000	-122.172447	46.514660
LINE-1&2	1070	563751.187500	5151473.000000	-122.168953	46.515770
LINE-1&2	1080	564018.500000	5151604.500000	-122.165451	46.516930
LINE-1&2	1090	564285.687500	5151736.000000	-122.161949	46.518089
LINE-1&2	1100	564547.312500	5151857.000000	-122.158524	46.519150
LINE-1&2	1110	564825.625000	5151988.500000	-122.154877	46.520309
LINE-1&2	1120	565061.312500	5152164.500000	-122.151779	46.521870
LINE-1&2	1130	565298.125000	5152357.000000	-122.148666	46.523579
LINE-1&2	1140	565523.687500	5152544.500000	-122.145699	46.525242
LINE-1&2	1150	565785.875000	5152700.000000	-122.142258	46.526619
LINE-1&2	1160	566048.187500	5152852.500000	-122.138817	46.527962
LINE-1&2	1170	566309.812500	5153008.000000	-122.135384	46.529339
LINE-1&2	1180	566566.875000	5153150.000000	-122.132011	46.530590
LINE-1&2	1190	566833.812500	5153306.500000	-122.128510	46.531971
LINE-1&2	1200	567086.125000	5153457.000000	-122.125198	46.533298
LINE-1&2	1210	567342.500000	5153604.000000	-122.121834	46.534599
LINE-1&2	1220	567610.625000	5153755.000000	-122.118317	46.535931
LINE-1&2	1230	567867.000000	5153897.000000	-122.114952	46.537182
LINE-1&2	1240	568134.187500	5154017.500000	-122.111450	46.538239
LINE-1&2	1250	568421.687500	5154104.500000	-122.107689	46.538990
LINE-1&2	1260	568714.625000	5154179.500000	-122.103859	46.539639
LINE-1&2	1270	568997.375000	5154261.000000	-122.100159	46.540340
LINE-1&2	1280	569285.375000	5154350.500000	-122.096390	46.541119
LINE-1&2	1290	569542.187500	5154503.000000	-122.093018	46.542461
LINE-1&2	1300	569798.500000	5154659.000000	-122.089653	46.543839
LINE-1&2	1310	570025.000000	5154846.000000	-122.086670	46.545502
LINE-1&2	1320	570280.687500	5154996.000000	-122.083313	46.546822
LINE-1&2	1330	570537.500000	5155146.500000	-122.079941	46.548149
LINE-1&2	1340	570814.625000	5155260.500000	-122.076309	46.549149
LINE-1&2	1350	571117.375000	5155285.500000	-122.072357	46.549339
LINE-1&2	1360	571409.625000	5155211.500000	-122.068558	46.548641
LINE-1&2	1370	571696.375000	5155145.500000	-122.064827	46.548019
LINE-1&2	1380	571993.875000	5155071.500000	-122.060959	46.547321
LINE-1&2	1390	572280.875000	5154991.500000	-122.057228	46.546570
LINE-1&2	1400	572557.875000	5154916.000000	-122.053627	46.545860
LINE-1&2	1410	572854.875000	5154836.000000	-122.049767	46.545109
LINE-1&2	1420	573131.625000	5154742.000000	-122.046173	46.544231
LINE-1&2	1430	573398.875000	5154606.000000	-122.042709	46.542980
LINE-1&2	1440	573675.375000	5154477.000000	-122.039124	46.541790
LINE-1&2	1450	573973.125000	5154437.500000	-122.035248	46.541401

LINE-1&2	1460	574265.000000	5154396.500000	-122.031448	46.541000
LINE-1&2	1470	574567.375000	5154357.000000	-122.027512	46.540611
LINE-1&2	1480	574854.187500	5154297.000000	-122.023781	46.540039
LINE-1&2	1490	575141.625000	5154241.500000	-122.020042	46.539509
LINE-1&2	1500	575433.625000	5154192.000000	-122.016243	46.539028
LINE-1&2	1510	575731.687500	5154172.000000	-122.012360	46.538818
LINE-1&2	1520	576018.875000	5154082.500000	-122.008629	46.537979
LINE-1&2	1530	576311.000000	5154027.500000	-122.004829	46.537449
LINE-1&2	1540	576607.500000	5154082.500000	-122.000954	46.537910
LINE-1&2	1550	576874.500000	5154207.000000	-121.997452	46.539001
LINE-1&2	1560	577162.125000	5154277.000000	-121.993690	46.539600
LINE-1&2	1570	577443.375000	5154331.500000	-121.990013	46.540058
LINE-1&2	1580	577756.187500	5154352.500000	-121.985931	46.540211
LINE-1&2	1590	578043.875000	5154272.000000	-121.982193	46.539452
LINE-1&2	1600	578320.625000	5154187.500000	-121.978600	46.538658
LINE-1&2	1604	578439.125000	5154167.000000	-121.977058	46.538460

<line id>	< spt >	< UTM x >	< UTM y >	<longitude>	<latitude>
LINE-3	3001	573200.000000	5154793.500000	-122.045273	46.544689
LINE-3	3031	573731.687500	5154465.500000	-122.038391	46.541679
LINE-3	3039	573877.875000	5154427.500000	-122.036491	46.541321
LINE-3	3060	574311.312500	5154338.000000	-122.030853	46.540470
LINE-3	3081	574738.375000	5154244.500000	-122.025299	46.539581
LINE-3	3100	575097.875000	5154181.500000	-122.020622	46.538971
LINE-3	3120	575471.000000	5154099.000000	-122.015770	46.538189
LINE-3	3145	575965.187500	5154029.500000	-122.009338	46.537510
LINE-3	3161	576300.812500	5153909.500000	-122.004982	46.536388
LINE-3	3167	576386.500000	5153890.500000	-122.003868	46.536209
LINE-3	3174	576539.312500	5153883.500000	-122.001877	46.536129
LINE-3	3182	576685.125000	5153915.500000	-121.999969	46.536400
LINE-3	3214	577307.375000	5154124.500000	-121.991821	46.538212
LINE-3	3240	577832.312500	5154168.000000	-121.984970	46.538540
LINE-3	3251	578027.812500	5154118.500000	-121.982430	46.538071
LINE-3	3267	578345.375000	5153985.500000	-121.978310	46.536839
LINE-3	3298	578949.687500	5153776.500000	-121.970467	46.534889
LINE-3	3305	579065.000000	5153777.500000	-121.968964	46.534882
LINE-3	3320	579358.000000	5153694.500000	-121.965157	46.534100
LINE-3	3340	579748.812500	5153701.500000	-121.960060	46.534119
LINE-3	3358	580126.875000	5153701.000000	-121.955132	46.534069
LINE-3	3390	580761.812500	5153657.500000	-121.946861	46.533600
LINE-3	3420	581359.625000	5153587.500000	-121.939079	46.532902
LINE-3	3453	581994.500000	5153543.500000	-121.930809	46.532429
LINE-3	3490	582700.687500	5153940.500000	-121.921532	46.535912
LINE-3	3509	583066.500000	5153934.000000	-121.916763	46.535809
LINE-3	3520	583299.500000	5153927.500000	-121.913727	46.535721
LINE-3	3540	583689.875000	5153922.000000	-121.908638	46.535622
LINE-3	3560	584104.687500	5153921.500000	-121.903229	46.535568
LINE-3	3580	584513.312500	5153910.000000	-121.897903	46.535412
LINE-3	3599	584879.812500	5153897.000000	-121.893127	46.535252
LINE-3	3618	585215.687500	5153897.500000	-121.888748	46.535210
LINE-3	3640	585715.500000	5153896.500000	-121.882233	46.535141
LINE-3	3670	586326.375000	5153897.500000	-121.874268	46.535069
LINE-3	3679	586546.312500	5153904.000000	-121.871399	46.535099
LINE-3	3690	586717.125000	5153909.500000	-121.869171	46.535130
LINE-3	3720	587321.312500	5153885.000000	-121.861298	46.534828
LINE-3	3758	588090.187500	5153890.500000	-121.851273	46.534779
LINE-3	3795	588841.625000	5153885.000000	-121.841476	46.534630
LINE-3	3824	589408.500000	5153860.000000	-121.834091	46.534328
LINE-3	3832	589597.812500	5153878.500000	-121.831619	46.534470
LINE-3	3838	589714.000000	5153896.500000	-121.830101	46.534618
LINE-3	3850	589952.375000	5153922.500000	-121.826988	46.534821
LINE-3	3870	590361.125000	5153984.000000	-121.821648	46.535320
LINE-3	3890	590770.125000	5154021.500000	-121.816307	46.535599

LINE-3	3913	591227.187500	5154058.000000	-121.810341	46.535870
LINE-3	3917	591300.500000	5154084.000000	-121.809380	46.536091
LINE-3	3930	591563.375000	5154114.500000	-121.805946	46.536331
LINE-3	3951	591978.187500	5154158.500000	-121.800529	46.536671
LINE-3	3971	592381.187500	5154095.500000	-121.795288	46.536049
LINE-3	3982	592594.875000	5154047.000000	-121.792511	46.535580
LINE-3	4016	593272.687500	5153923.000000	-121.783699	46.534370
LINE-3	4025	593461.500000	5153897.500000	-121.781242	46.534119
LINE-3	4044	593846.125000	5153928.500000	-121.776222	46.534340
LINE-3	4054	594034.687500	5153884.500000	-121.773773	46.533920
LINE-3	4076	594402.187500	5154298.000000	-121.768898	46.537590
LINE-3	4080	594499.000000	5154316.000000	-121.767632	46.537739
LINE-3	4109	595034.187500	5154518.000000	-121.760612	46.539478
LINE-3	4120	595235.000000	5154626.500000	-121.757973	46.540428
LINE-3	4130	595398.375000	5154761.500000	-121.755814	46.541618
LINE-3	4148	595684.875000	5154999.500000	-121.752029	46.543720
LINE-3	4155	595782.125000	5155103.500000	-121.750740	46.544640
LINE-3	4170	596001.125000	5155317.000000	-121.747841	46.546532
LINE-3	4193	596299.125000	5155671.000000	-121.743881	46.549671
LINE-3	4205	596505.375000	5155829.500000	-121.741158	46.551071
LINE-3	4236	596955.625000	5156213.500000	-121.735207	46.554459
LINE-3	4250	597198.312500	5156396.000000	-121.732002	46.556068
LINE-3	4267	597465.875000	5156635.500000	-121.728462	46.558182
LINE-3	4297	597928.500000	5157007.000000	-121.722351	46.561459
LINE-3	4315	598195.687500	5157226.000000	-121.718819	46.563389
LINE-3	4331	598445.125000	5157428.000000	-121.715523	46.565170
LINE-3	4360	598907.125000	5157788.000000	-121.709419	46.568340
LINE-3	4383	599277.687500	5158087.500000	-121.704521	46.570980
LINE-3	4394	599454.625000	5158209.000000	-121.702187	46.572048
LINE-3	4424	599964.875000	5158612.000000	-121.695442	46.575600
LINE-3	4445	600263.187500	5158856.000000	-121.691498	46.577751
LINE-3	4457	600408.625000	5159044.000000	-121.689560	46.579418
LINE-3	4464	600493.500000	5159179.000000	-121.688423	46.580620
LINE-3	4475	600548.812500	5159367.500000	-121.687660	46.582310
LINE-3	4481	600554.687500	5159509.000000	-121.687553	46.583580
LINE-3	4500	600518.125000	5159880.500000	-121.687950	46.586929
LINE-3	4524	600506.125000	5160356.000000	-121.688004	46.591209
LINE-3	4530	600542.625000	5160479.000000	-121.687500	46.592312
LINE-3	4546	600688.375000	5160784.000000	-121.685532	46.595032
LINE-3	4554	600798.625000	5160905.500000	-121.684067	46.596111
LINE-3	4580	601114.000000	5161302.000000	-121.679863	46.599628
LINE-3	4606	601430.625000	5161735.500000	-121.675636	46.603481
LINE-3	4620	601588.000000	5162003.500000	-121.673523	46.605869
LINE-3	4632	601735.000000	5162125.000000	-121.671577	46.606941
LINE-3	4660	601935.625000	5162668.500000	-121.668839	46.611801
LINE-3	4692	602184.187500	5163273.000000	-121.665459	46.617199

LINE-3	4710	602300.000000	5163614.000000	-121.663872	46.620251
LINE-3	4713	602336.125000	5163688.000000	-121.663383	46.620911
LINE-3	4728	602488.812500	5163919.500000	-121.661339	46.622971
LINE-3	4743	602652.625000	5164182.500000	-121.659142	46.625309
LINE-3	4770	603072.187500	5164517.500000	-121.653587	46.628262
LINE-3	4794	603461.625000	5164809.500000	-121.648438	46.630829
LINE-3	4821	603868.187500	5165145.500000	-121.643051	46.633789
LINE-3	4826	603965.687500	5165218.500000	-121.641762	46.634430
LINE-3	4850	604299.812500	5165554.500000	-121.637321	46.637402
LINE-3	4870	604500.875000	5165920.000000	-121.634613	46.640659
LINE-3	4877	604616.375000	5166030.000000	-121.633080	46.641628
LINE-3	4900	604956.687500	5166341.500000	-121.628563	46.644379
LINE-3	4920	605515.375000	5166057.000000	-121.621330	46.641731
LINE-3	4940	605740.687500	5166266.500000	-121.618340	46.643581
LINE-3	4954	605953.812500	5166533.500000	-121.615494	46.645950
LINE-3	4962	605911.000000	5166975.000000	-121.615952	46.649929
LINE-3	4965	605986.500000	5167000.000000	-121.614960	46.650139
LINE-3	4980	606245.687500	5167140.000000	-121.611542	46.651360
LINE-3	4994	606478.687500	5167304.500000	-121.608459	46.652802
LINE-3	5016	606757.000000	5167682.500000	-121.604736	46.656158
LINE-3	5028	606819.625000	5167903.000000	-121.603867	46.658131
LINE-3	5030	606819.187500	5167958.500000	-121.603859	46.658630
LINE-3	5051	606883.000000	5168378.500000	-121.602928	46.662399
LINE-3	5079	607254.625000	5168824.500000	-121.597969	46.666351
LINE-3	5097	607387.312500	5169141.000000	-121.596161	46.669182
LINE-3	5113	607627.187500	5169373.000000	-121.592972	46.671230
LINE-3	5133	608005.500000	5169502.000000	-121.587997	46.672329
LINE-3	5154	608321.000000	5169782.500000	-121.583809	46.674801
LINE-3	5168	608598.687500	5169916.500000	-121.580147	46.675961
LINE-3	5177	608718.125000	5170063.000000	-121.578552	46.677261
LINE-3	5189	608787.875000	5170301.000000	-121.577583	46.679390
LINE-3	5195	608825.875000	5170429.500000	-121.577057	46.680538
LINE-3	5209	608901.812500	5170716.500000	-121.575996	46.683109
LINE-3	5218	608907.687500	5170874.500000	-121.575882	46.684528
LINE-3	5219	608908.187500	5170911.500000	-121.575867	46.684860
LINE-3	5232	608661.812500	5171112.500000	-121.579041	46.686710

<line id>	< spt >	< UTM x >	< UTM y >	<longitude>	<latitude>
LINE-4	7135	509432.000000	5158762.000000	-122.876892	46.584320
LINE-4	7276	510199.500000	5158425.000000	-122.866882	46.581280
LINE-4	7250	510699.093750	5158202.000000	-122.860367	46.579262
LINE-4	7220	511265.406250	5157960.500000	-122.852982	46.577080
LINE-4	7208	511527.406250	5157922.000000	-122.849564	46.576729
LINE-4	7200	511661.812500	5157921.500000	-122.847809	46.576721
LINE-4	7180	512064.093750	5157903.000000	-122.842560	46.576550
LINE-4	7165	512392.687500	5157896.000000	-122.838272	46.576481
LINE-4	7114	513404.093750	5157870.500000	-122.825073	46.576229
LINE-4	7067	514355.187500	5157648.000000	-122.812668	46.574211
LINE-4	7042	514806.187500	5157781.500000	-122.806778	46.575401
LINE-4	7020	515268.687500	5157781.500000	-122.800743	46.575390
LINE-4	6985	515987.812500	5157769.000000	-122.791359	46.575260
LINE-4	6967	516353.187500	5157768.500000	-122.786591	46.575249
LINE-4	6954	516585.000000	5157870.500000	-122.783562	46.576160
LINE-4	6949	516676.093750	5157896.000000	-122.782372	46.576389
LINE-4	6931	516974.906250	5157679.000000	-122.778481	46.574429
LINE-4	6899	517645.093750	5157622.000000	-122.769737	46.573898
LINE-4	6883	517974.593750	5157882.000000	-122.765427	46.576229
LINE-4	6864	518357.312500	5157772.000000	-122.760437	46.575230
LINE-4	6838	518892.593750	5157833.000000	-122.753448	46.575760
LINE-4	6820	519239.187500	5157694.000000	-122.748932	46.574501
LINE-4	6806	519549.812500	5157632.500000	-122.744881	46.573940
LINE-4	6797	519720.093750	5157602.500000	-122.742661	46.573662
LINE-4	6786	519895.812500	5157505.000000	-122.740372	46.572781
LINE-4	6763	520389.000000	5157572.500000	-122.733932	46.573372
LINE-4	6742	520736.000000	5157663.500000	-122.729401	46.574181
LINE-4	6729	520991.312500	5157870.500000	-122.726059	46.576038
LINE-4	6718	521173.906250	5158003.500000	-122.723671	46.577229
LINE-4	6704	521459.687500	5158004.500000	-122.719940	46.577229
LINE-4	6670	522116.187500	5158004.000000	-122.711372	46.577202
LINE-4	6648	522591.000000	5158004.500000	-122.705177	46.577190
LINE-4	6646	522645.906250	5158004.500000	-122.704460	46.577190
LINE-4	6605	523448.687500	5158120.000000	-122.693977	46.578201
LINE-4	6583	523886.312500	5158198.500000	-122.688263	46.578892
LINE-4	6563	524276.406250	5158290.000000	-122.683167	46.579700
LINE-4	6540	524671.375000	5158479.500000	-122.678001	46.581390
LINE-4	6508	525273.312500	5158814.000000	-122.670128	46.584381
LINE-4	6460	525943.000000	5159539.000000	-122.661346	46.590881
LINE-4	6429	526361.875000	5159977.500000	-122.655853	46.594810
LINE-4	6414	526538.875000	5160257.500000	-122.653526	46.597321
LINE-4	6400	526672.312500	5160487.500000	-122.651772	46.599388
LINE-4	6369	527037.625000	5160999.500000	-122.646973	46.603981
LINE-4	6331	527670.625000	5161346.500000	-122.638687	46.607079
LINE-4	6329	527718.312500	5161384.000000	-122.638062	46.607410

LINE-4	6320	527858.625000	5161505.500000	-122.636223	46.608501
LINE-4	6305	528046.875000	5161718.500000	-122.633751	46.610409
LINE-4	6284	528357.375000	5162036.000000	-122.629677	46.613251
LINE-4	6266	528698.375000	5162084.000000	-122.625221	46.613670
LINE-4	6250	529008.625000	5162078.000000	-122.621170	46.613602
LINE-4	6230	529415.812500	5162077.500000	-122.615852	46.613579
LINE-4	6200	530110.687500	5162154.000000	-122.606773	46.614239
LINE-4	6173	530652.875000	5162141.500000	-122.599693	46.614101
LINE-4	6167	530762.687500	5162142.000000	-122.598259	46.614101
LINE-4	6143	531257.000000	5162243.500000	-122.591797	46.614990
LINE-4	6129	531549.312500	5162211.500000	-122.587982	46.614689
LINE-4	6111	531884.500000	5162129.000000	-122.583611	46.613930
LINE-4	6090	532250.687500	5161924.000000	-122.578842	46.612068
LINE-4	6067	532665.187500	5161669.500000	-122.573448	46.609760
LINE-4	6056	532847.875000	5161592.500000	-122.571068	46.609058
LINE-4	6009	533780.375000	5161599.000000	-122.558891	46.609070
LINE-4	5984	534274.687500	5161388.500000	-122.552452	46.607151
LINE-4	5954	534865.687500	5161337.500000	-122.544739	46.606659
LINE-4	5939	535140.125000	5161287.000000	-122.541161	46.606190
LINE-4	5931	535335.375000	5161261.500000	-122.538612	46.605949
LINE-4	5922	535493.500000	5161203.500000	-122.536552	46.605419
LINE-4	5890	536152.625000	5161197.500000	-122.527946	46.605331
LINE-4	5852	536896.000000	5161184.000000	-122.518242	46.605171
LINE-4	5810	537743.187500	5161184.500000	-122.507179	46.605129
LINE-4	5771	538542.125000	5161165.500000	-122.496750	46.604912
LINE-4	5766	538633.312500	5161166.000000	-122.495560	46.604912
LINE-4	5754	538871.687500	5161165.000000	-122.492447	46.604889
LINE-4	5741	539102.812500	5161038.000000	-122.489441	46.603729
LINE-4	5724	539419.875000	5160891.000000	-122.485313	46.602390
LINE-4	5714	539578.000000	5160833.000000	-122.483253	46.601860
LINE-4	5695	539949.812500	5160903.500000	-122.478394	46.602470
LINE-4	5676	540273.625000	5160981.000000	-122.474159	46.603149
LINE-4	5670	540383.375000	5161158.500000	-122.472710	46.604740
LINE-4	5665	540365.125000	5161274.000000	-122.472939	46.605782
LINE-4	5654	540487.125000	5161376.000000	-122.471336	46.606689
LINE-4	5639	540664.000000	5161140.500000	-122.469048	46.604561
LINE-4	5629	540810.312500	5161019.000000	-122.467148	46.603458
LINE-4	5620	540980.500000	5161005.500000	-122.464928	46.603329
LINE-4	5616	541053.875000	5161032.000000	-122.463966	46.603561
LINE-4	5607	541260.812500	5161114.500000	-122.461258	46.604290
LINE-4	5600	541382.500000	5161088.500000	-122.459671	46.604050
LINE-4	5586	541644.875000	5161006.000000	-122.456253	46.603291
LINE-4	5582	541706.125000	5161032.000000	-122.455452	46.603519
LINE-4	5565	542041.187500	5161076.500000	-122.451073	46.603901
LINE-4	5556	542286.625000	5161413.000000	-122.447838	46.606911
LINE-4	5537	542639.000000	5161238.500000	-122.443253	46.605320

LINE-4	5528	542760.500000	5161162.500000	-122.441673	46.604630
LINE-4	5517	542955.312500	5161051.000000	-122.439140	46.603611
LINE-4	5493	543199.187500	5160613.500000	-122.435997	46.599659
LINE-4	5488	543271.875000	5160489.500000	-122.435059	46.598541
LINE-4	5479	543338.875000	5160364.500000	-122.434196	46.597408
LINE-4	5456	543746.187500	5160120.500000	-122.428902	46.595188
LINE-4	5454	543770.375000	5160089.500000	-122.428589	46.594910
LINE-4	5438	543928.375000	5159827.500000	-122.426552	46.592541
LINE-4	5427	544098.687500	5159634.500000	-122.424347	46.590790
LINE-4	5404	544415.000000	5159304.500000	-122.420250	46.587799
LINE-4	5378	544689.125000	5158830.000000	-122.416718	46.583511
LINE-4	5352	544937.687500	5158424.000000	-122.413513	46.579842
LINE-4	5325	545485.687500	5158230.000000	-122.406380	46.578060
LINE-4	5310	545771.875000	5158193.000000	-122.402649	46.577709
LINE-4	5300	545972.375000	5158199.500000	-122.400032	46.577751
LINE-4	5294	546124.187500	5158218.500000	-122.398048	46.577911
LINE-4	5240	547194.812500	5158350.000000	-122.384064	46.579021
LINE-4	5214	547699.500000	5158411.500000	-122.377472	46.579540
LINE-4	5195	548095.500000	5158456.000000	-122.372299	46.579910
LINE-4	5180	548405.500000	5158505.000000	-122.368248	46.580330
LINE-4	5165	548691.375000	5158579.500000	-122.364510	46.580978
LINE-4	5136	549257.187500	5158798.500000	-122.357101	46.582909
LINE-4	5121	549525.000000	5158867.500000	-122.353600	46.583511
LINE-4	5112	549688.875000	5158978.500000	-122.351448	46.584499
LINE-4	5088	550145.812500	5159148.000000	-122.345467	46.585991
LINE-4	5076	550395.125000	5159191.500000	-122.342209	46.586361
LINE-4	5067	550577.687500	5159166.000000	-122.339828	46.586121
LINE-4	5056	550717.375000	5159023.000000	-122.338020	46.584820
LINE-4	5054	550747.625000	5158980.000000	-122.337631	46.584431
LINE-4	5020	551221.875000	5158468.000000	-122.331497	46.579788
LINE-4	4993	551593.125000	5158055.500000	-122.326698	46.576050
LINE-4	4980	551818.125000	5157937.500000	-122.323776	46.574970
LINE-4	4976	551903.187500	5157900.500000	-122.322670	46.574631
LINE-4	4965	552091.500000	5157831.000000	-122.320221	46.573990
LINE-4	4951	552322.625000	5157675.500000	-122.317223	46.572571
LINE-4	4933	552639.625000	5157457.000000	-122.313110	46.570580
LINE-4	4909	552949.312500	5157082.500000	-122.309113	46.567188
LINE-4	4902	553101.812500	5157033.000000	-122.307129	46.566730
LINE-4	4888	553491.125000	5156852.000000	-122.302071	46.565071
LINE-4	4860	553880.125000	5156833.000000	-122.296997	46.564869
LINE-4	4845	554178.125000	5156796.000000	-122.293114	46.564510
LINE-4	4840	554269.312500	5156733.000000	-122.291931	46.563938
LINE-4	4832	554495.687500	5156986.500000	-122.288948	46.566200
LINE-4	4823	554654.187500	5156913.500000	-122.286888	46.565529
LINE-4	4815	554751.625000	5156821.000000	-122.285629	46.564690
LINE-4	4806	554866.875000	5156674.000000	-122.284142	46.563358

LINE-4	4803	554891.375000	5156625.500000	-122.283829	46.562920
LINE-4	4800	554940.687500	5156600.500000	-122.283188	46.562691
LINE-4	4792	555044.187500	5156661.500000	-122.281830	46.563229
LINE-4	4782	555269.375000	5156594.500000	-122.278900	46.562611
LINE-4	4772	555409.312500	5156649.500000	-122.277069	46.563091
LINE-4	4769	555482.875000	5156650.000000	-122.276108	46.563091
LINE-4	4757	555683.812500	5156557.500000	-122.273499	46.562241
LINE-4	4749	555763.312500	5156435.000000	-122.272476	46.561131
LINE-4	4744	555836.375000	5156374.500000	-122.271530	46.560581
LINE-4	4733	555939.687500	5156331.000000	-122.270187	46.560181
LINE-4	4720	556286.812500	5156177.000000	-122.265678	46.558769
LINE-4	4710	556451.187500	5156104.500000	-122.263542	46.558102
LINE-4	4687	556847.625000	5155871.500000	-122.258400	46.555969
LINE-4	4669	557139.312500	5155637.500000	-122.254623	46.553841
LINE-4	4654	557432.187500	5155594.500000	-122.250809	46.553429
LINE-4	4638	557742.687500	5155484.500000	-122.246773	46.552410
LINE-4	4623	557993.000000	5155300.000000	-122.243530	46.550732
LINE-4	4610	558139.687500	5155129.000000	-122.241638	46.549179
LINE-4	4580	558656.812500	5154767.500000	-122.234940	46.545879
LINE-4	4565	558815.500000	5154515.500000	-122.232903	46.543598
LINE-4	4557	558895.125000	5154393.000000	-122.231880	46.542488
LINE-4	4528	559217.812500	5153871.500000	-122.227737	46.537769
LINE-4	4518	559321.187500	5153712.500000	-122.226410	46.536331
LINE-4	4500	559674.875000	5153620.500000	-122.221809	46.535469
LINE-4	4485	559869.375000	5153418.000000	-122.219299	46.533630
LINE-4	4480	559918.312500	5153331.500000	-122.218674	46.532848
LINE-4	4460	560186.687500	5152994.500000	-122.215218	46.529789
LINE-4	4451	560205.187500	5152841.500000	-122.214996	46.528412
LINE-4	4441	560150.187500	5152657.500000	-122.215736	46.526760
LINE-4	4433	560168.125000	5152504.000000	-122.215523	46.525379
LINE-4	4423	560321.000000	5152376.000000	-122.213547	46.524212
LINE-4	4418	560314.000000	5152252.500000	-122.213654	46.523102
LINE-4	4400	560332.312500	5151891.500000	-122.213463	46.519852
LINE-4	4389	560289.875000	5151682.000000	-122.214043	46.517971
LINE-4	4386	560277.687500	5151615.000000	-122.214211	46.517368
LINE-4	4380	560339.187500	5151548.000000	-122.213417	46.516762
LINE-4	4370	560466.812500	5151369.000000	-122.211777	46.515141
LINE-4	4364	560533.312500	5151272.000000	-122.210922	46.514259
LINE-4	4355	560674.500000	5151149.000000	-122.209099	46.513142
LINE-4	4350	560765.812500	5151088.000000	-122.207916	46.512581
LINE-4	4340	560954.312500	5151033.000000	-122.205467	46.512070
LINE-4	4330	561167.812500	5150989.500000	-122.202690	46.511662
LINE-4	4302	561661.125000	5150768.500000	-122.196289	46.509628
LINE-4	4297	561758.375000	5150756.500000	-122.195023	46.509510
LINE-4	4292	561856.187500	5150756.500000	-122.193748	46.509499
LINE-4	4280	562087.812500	5150836.500000	-122.190720	46.510201

LINE-4	4276	562148.875000	5150873.000000	-122.189919	46.510521
LINE-4	4267	562356.000000	5150879.500000	-122.187218	46.510559
LINE-4	4265	562367.500000	5150848.500000	-122.187073	46.510281
LINE-4	4263	562380.125000	5150817.000000	-122.186913	46.509998
LINE-4	4258	562441.125000	5150744.500000	-122.186127	46.509338
LINE-4	4251	562557.125000	5150799.000000	-122.184608	46.509819
LINE-4	4245	562672.125000	5150769.500000	-122.183113	46.509541
LINE-4	4233	562800.312500	5150541.500000	-122.181473	46.507481
LINE-4	4212	562897.875000	5150168.000000	-122.180252	46.504108
LINE-4	4210	562934.687500	5150118.500000	-122.179779	46.503658
LINE-4	4180	563099.000000	5149518.000000	-122.177719	46.498241
LINE-4	4164	563166.375000	5149236.500000	-122.176880	46.495701
LINE-4	4146	563026.000000	5148880.500000	-122.178757	46.492512
LINE-4	4130	562824.812500	5148635.000000	-122.181412	46.490318
LINE-4	4116	562696.875000	5148377.000000	-122.183113	46.488010
LINE-4	4111	562721.187500	5148285.000000	-122.182808	46.487179
LINE-4	4104	562837.187500	5148168.000000	-122.181313	46.486118
LINE-4	4095	563001.687500	5148119.000000	-122.179176	46.485661
LINE-4	4084	563154.500000	5147959.500000	-122.177208	46.484211
LINE-4	4077	563288.375000	5147923.000000	-122.175468	46.483871
LINE-4	4069	563428.000000	5147850.000000	-122.173660	46.483200
LINE-4	4050	563805.875000	5147837.500000	-122.168739	46.483051
LINE-4	4045	563915.625000	5147813.000000	-122.167313	46.482819
LINE-4	4037	564000.375000	5147715.000000	-122.166222	46.481930
LINE-4	4033	564037.500000	5147640.500000	-122.165749	46.481258
LINE-4	4027	564080.500000	5147512.500000	-122.165207	46.480099
LINE-4	4018	564202.000000	5147371.500000	-122.163643	46.478821
LINE-4	4012	564256.875000	5147279.000000	-122.162941	46.477982
LINE-4	4001	564244.625000	5147052.000000	-122.163132	46.475941

<line id>	< spt >	< UTM x >	< UTM y >	<longitude>	<latitude>
LINE-5	-1	544885.500000	5153789.500000	-122.414642	46.538139
LINE-5	961	544924.687500	5153784.000000	-122.414131	46.538090
LINE-5	992	545540.625000	5153884.500000	-122.406090	46.538952
LINE-5	1001	545724.000000	5153847.000000	-122.403702	46.538601
LINE-5	1011	545891.687500	5153731.500000	-122.401527	46.537552
LINE-5	1025	546150.312500	5153579.000000	-122.398170	46.536160
LINE-5	1046	546592.875000	5153389.000000	-122.392418	46.534420
LINE-5	1085	547395.812500	5153362.000000	-122.381950	46.534119
LINE-5	1089	547492.187500	5153388.500000	-122.380692	46.534351
LINE-5	1108	547858.125000	5153575.500000	-122.375900	46.536011
LINE-5	1110	547915.187500	5153612.500000	-122.375153	46.536339
LINE-5	1161	548768.812500	5154264.000000	-122.363953	46.542141
LINE-5	1171	548948.187500	5154364.500000	-122.361603	46.543030
LINE-5	1176	549057.875000	5154396.000000	-122.360168	46.543308
LINE-5	1185	549226.125000	5154438.000000	-122.357971	46.543671
LINE-5	1220	549985.000000	5154344.000000	-122.348083	46.542770
LINE-5	1228	550145.812500	5154425.500000	-122.345978	46.543491
LINE-5	1250	550521.375000	5154702.000000	-122.341049	46.545952
LINE-5	1253	550566.187500	5154733.500000	-122.340462	46.546230
LINE-5	1255	550604.625000	5154758.000000	-122.339958	46.546452
LINE-5	1260	550687.875000	5154802.000000	-122.338867	46.546841
LINE-5	1279	551102.375000	5154895.500000	-122.333450	46.547649
LINE-5	1313	551810.875000	5154748.000000	-122.324226	46.546268
LINE-5	1330	552163.375000	5154709.000000	-122.319633	46.545891
LINE-5	1334	552248.687500	5154724.500000	-122.318520	46.546021
LINE-5	1348	552558.500000	5154814.500000	-122.314468	46.546810
LINE-5	1380	553160.375000	5155152.500000	-122.306580	46.549801
LINE-5	1415	553698.187500	5155457.000000	-122.299530	46.552502
LINE-5	1436	554204.687500	5155719.500000	-122.292892	46.554821
LINE-5	1456	554613.375000	5155800.500000	-122.287552	46.555519
LINE-5	1464	554834.187500	5155836.000000	-122.284668	46.555820
LINE-5	1473	554983.187500	5155852.000000	-122.282722	46.555950
LINE-5	1495	555428.875000	5155787.000000	-122.276917	46.555328
LINE-5	1513	554840.125000	5155700.500000	-122.284607	46.554600
LINE-5	1520	554969.187500	5155715.500000	-122.282921	46.554722
LINE-5	1529	554980.625000	5155745.000000	-122.282768	46.554989
LINE-5	-3	555393.625000	5155740.000000	-122.277382	46.554909
LINE-5	1578	556107.687500	5155748.000000	-122.268066	46.554920
LINE-5	-1	556105.312500	5155813.500000	-122.268089	46.555511
LINE-5	-1	556590.687500	5155952.500000	-122.261742	46.556721
LINE-5	1606	554970.375000	5156295.500000	-122.282837	46.559940
LINE-5	1614	554960.500000	5156413.000000	-122.282951	46.561001
LINE-5	1618	555006.000000	5156492.500000	-122.282349	46.561710
LINE-5	1629	555199.125000	5156545.000000	-122.279823	46.562168
LINE-5	1638	555362.875000	5156608.500000	-122.277679	46.562729

LINE-5	1642	555427.000000	5156634.000000	-122.276840	46.562950
LINE-5	1647	555482.000000	5156564.500000	-122.276131	46.562321
LINE-5	1658	555677.625000	5156535.000000	-122.273582	46.562038
LINE-5	1690	555991.812500	5157089.500000	-122.269417	46.567001
LINE-5	1727	556346.312500	5157702.500000	-122.264717	46.572491
LINE-5	1730	556391.500000	5157739.500000	-122.264122	46.572819
LINE-5	1734	556455.500000	5157771.500000	-122.263283	46.573101
LINE-5	1738	556544.375000	5157767.500000	-122.262123	46.573059
LINE-5	1749	556739.375000	5157744.000000	-122.259583	46.572830
LINE-5	1756	556880.312500	5157806.500000	-122.257736	46.573380
LINE-5	1770	556966.812500	5158058.500000	-122.256577	46.575642
LINE-5	1773	557001.625000	5158088.500000	-122.256119	46.575909
LINE-5	1775	557030.500000	5158119.000000	-122.255737	46.576180
LINE-5	1790	557316.000000	5158223.000000	-122.251999	46.577091
LINE-5	1801	557464.625000	5158398.500000	-122.250038	46.578659
LINE-5	1814	557516.625000	5158648.000000	-122.249329	46.580898
LINE-5	1852	557904.375000	5159304.000000	-122.244186	46.586769
LINE-5	1869	558073.000000	5159581.000000	-122.241951	46.589249
LINE-5	1896	558307.375000	5160061.500000	-122.238831	46.593552
LINE-5	1930	558668.000000	5160664.000000	-122.234047	46.598942
LINE-5	1932	558690.625000	5160688.500000	-122.233749	46.599159
LINE-5	1946	558759.187500	5160962.500000	-122.232819	46.601620
LINE-5	1978	558824.500000	5161580.000000	-122.231888	46.607170
LINE-5	2008	558971.687500	5162182.500000	-122.229889	46.612579
LINE-5	2038	559108.687500	5162755.500000	-122.228027	46.617722
LINE-5	2053	559089.000000	5163031.500000	-122.228249	46.620209
LINE-5	2058	559133.000000	5163134.500000	-122.227661	46.621132
LINE-5	2064	559201.812500	5163207.500000	-122.226753	46.621780
LINE-5	2067	559259.875000	5163238.000000	-122.225990	46.622051
LINE-5	2082	559514.000000	5163423.000000	-122.222649	46.623692
LINE-5	2092	559695.687500	5163470.000000	-122.220268	46.624100
LINE-5	2098	559806.375000	5163509.000000	-122.218819	46.624439
LINE-5	2110	560015.375000	5163639.000000	-122.216072	46.625591
LINE-5	2122	560067.375000	5163865.000000	-122.215363	46.627621
LINE-5	2136	560232.125000	5164106.500000	-122.213181	46.629780
LINE-5	2144	560358.312500	5164216.500000	-122.211517	46.630760
LINE-5	2151	560407.812500	5164348.000000	-122.210854	46.631939
LINE-5	2172	560447.687500	5164800.000000	-122.210274	46.636002
LINE-5	2175	560458.312500	5164847.500000	-122.210129	46.636429
LINE-5	2200	559966.000000	5165309.500000	-122.216499	46.640629
LINE-5	2216	560080.812500	5165628.500000	-122.214958	46.643490
LINE-5	2224	560146.500000	5165779.500000	-122.214081	46.644840
LINE-5	2248	560517.000000	5166156.500000	-122.209190	46.648201
LINE-5	2250	560544.000000	5166198.500000	-122.208832	46.648579
LINE-5	2277	560758.375000	5166712.000000	-122.205963	46.653179
LINE-5	2297	560800.875000	5167128.500000	-122.205353	46.656921

LINE-5	2325	560797.687500	5167680.500000	-122.205322	46.661888
LINE-5	2331	560810.687500	5167829.500000	-122.205132	46.663231
LINE-5	2336	560814.687500	5167895.000000	-122.205070	46.663818
LINE-5	2360	560942.375000	5168375.500000	-122.203339	46.668129
LINE-5	2389	561094.312500	5168939.500000	-122.201279	46.673191
LINE-5	2394	561095.625000	5169040.500000	-122.201248	46.674099
LINE-5	2413	561131.875000	5169428.000000	-122.200722	46.677582
LINE-5	2435	561150.875000	5169855.500000	-122.200417	46.681431
LINE-5	2466	561137.812500	5170461.000000	-122.200508	46.686878
LINE-5	2495	561095.000000	5171054.000000	-122.200989	46.692219
LINE-5	2510	561010.312500	5171346.500000	-122.202057	46.694859
LINE-5	2525	560846.000000	5171619.500000	-122.204170	46.697330
LINE-5	2545	560764.125000	5171984.000000	-122.205193	46.700619
LINE-5	2562	560802.625000	5172337.000000	-122.204643	46.703789
LINE-5	2563	560799.000000	5172402.500000	-122.204681	46.704380
LINE-5	2585	560679.687500	5172783.500000	-122.206192	46.707821
LINE-5	2598	560487.812500	5173014.000000	-122.208672	46.709911
LINE-5	2605	560356.187500	5173104.000000	-122.210381	46.710732
LINE-5	2622	559983.000000	5173273.500000	-122.215240	46.712292
LINE-5	2628	559895.875000	5173359.000000	-122.216370	46.713070
LINE-5	2633	559832.125000	5173434.000000	-122.217194	46.713749
LINE-5	2654	559579.375000	5173810.500000	-122.220451	46.717159
LINE-5	2680	559262.875000	5174262.000000	-122.224533	46.721249
LINE-5	2710	558869.000000	5174769.000000	-122.229622	46.725849
LINE-5	2715	558840.625000	5174876.000000	-122.229980	46.726810
LINE-5	2721	558856.500000	5174982.500000	-122.229759	46.727772
LINE-5	2728	558938.687500	5175099.000000	-122.228668	46.728809
LINE-5	2732	559024.375000	5175155.000000	-122.227539	46.729309
LINE-5	2758	559581.000000	5175414.000000	-122.220222	46.731590
LINE-5	2790	560031.500000	5175954.000000	-122.214256	46.736408
LINE-5	2815	560377.625000	5176377.000000	-122.209671	46.740181
LINE-5	2829	560564.875000	5176592.000000	-122.207191	46.742100
LINE-5	2841	560737.625000	5176806.000000	-122.204903	46.744011
LINE-5	2864	560936.187500	5177218.000000	-122.202248	46.747700
LINE-5	2879	561014.812500	5177517.000000	-122.201180	46.750381
LINE-5	2893	561080.125000	5177799.500000	-122.200287	46.752918
LINE-5	2920	561220.000000	5178309.000000	-122.198387	46.757488
LINE-5	2954	561358.875000	5178979.500000	-122.196480	46.763512
LINE-5	2959	561373.375000	5179098.500000	-122.196274	46.764580
LINE-5	2960	561411.187500	5179100.000000	-122.195778	46.764591
LINE-5	2961	561921.875000	5179244.000000	-122.189072	46.765839

<line id>	< spt >	< UTM x >	< UTM y >	<longitude>	<latitude>
LINE-6	1	526493.625000	5187058.500000	-122.652573	46.838509
LINE-6	2	526740.625000	5186605.000000	-122.649361	46.834419
LINE-6	3	527153.125000	5185460.500000	-122.644020	46.824100
LINE-6	4	527274.125000	5185334.000000	-122.642441	46.822960
LINE-6	5	527349.500000	5185265.500000	-122.641457	46.822338
LINE-6	6	527701.500000	5185166.000000	-122.636848	46.821430
LINE-6	7	527778.875000	5185164.500000	-122.635834	46.821411
LINE-6	1001	527982.000000	5185158.500000	-122.633171	46.821350
LINE-6	1006	528238.625000	5185171.000000	-122.629807	46.821449
LINE-6	1018	528465.000000	5185182.000000	-122.626839	46.821541
LINE-6	1030	528738.375000	5185096.500000	-122.623260	46.820759
LINE-6	1045	529458.125000	5185132.000000	-122.613823	46.821049
LINE-6	1080	529609.625000	5185089.500000	-122.611839	46.820660
LINE-6	1088	529874.000000	5185175.500000	-122.608368	46.821419
LINE-6	1102	530220.500000	5185258.500000	-122.603821	46.822151
LINE-6	1119	530329.375000	5185347.500000	-122.602386	46.822948
LINE-6	1127	530438.500000	5185408.500000	-122.600952	46.823490
LINE-6	1134	530579.687500	5185449.000000	-122.599098	46.823849
LINE-6	1141	530740.375000	5185451.000000	-122.596992	46.823860
LINE-6	1149	530925.375000	5185461.000000	-122.594566	46.823940
LINE-6	1158	531154.875000	5185411.000000	-122.591560	46.823479
LINE-6	1169	531474.687500	5185250.500000	-122.587379	46.822021
LINE-6	1188	531924.187500	5185217.500000	-122.581490	46.821701
LINE-6	1210	532343.312500	5185404.000000	-122.575981	46.823360
LINE-6	1233	532419.375000	5185430.000000	-122.574982	46.823589
LINE-6	1236	532714.187500	5185483.500000	-122.571114	46.824059
LINE-6	1253	532785.125000	5185498.500000	-122.570183	46.824188
LINE-6	1256	533398.312500	5185323.000000	-122.562157	46.822578
LINE-6	1288	533509.875000	5185251.500000	-122.560699	46.821930
LINE-6	1295	533691.125000	5185004.500000	-122.558342	46.819698
LINE-6	1310	533888.375000	5184699.000000	-122.555779	46.816940
LINE-6	1330	534098.000000	5184575.500000	-122.553040	46.815819
LINE-6	1343	534587.625000	5184161.500000	-122.546654	46.812069
LINE-6	1375	534709.500000	5184124.000000	-122.545059	46.811722
LINE-6	1382	535255.187500	5184168.000000	-122.537903	46.812092
LINE-6	1410	535535.125000	5184087.500000	-122.534241	46.811352
LINE-6	1424	535868.000000	5184110.500000	-122.529877	46.811539
LINE-6	1442	536235.687500	5184039.000000	-122.525063	46.810879
LINE-6	1459	536298.187500	5184010.000000	-122.524246	46.810612
LINE-6	1462	536675.625000	5183978.500000	-122.519302	46.810310
LINE-6	1482	536771.687500	5183861.500000	-122.518051	46.809250
LINE-6	1491	536907.312500	5183784.500000	-122.516281	46.808552
LINE-6	1498	537003.500000	5183667.500000	-122.515030	46.807491
LINE-6	1507	537360.875000	5183474.000000	-122.510361	46.805729
LINE-6	1527	537533.875000	5183377.500000	-122.508102	46.804852

LINE-6	1537	537888.812500	5183224.000000	-122.503464	46.803452
LINE-6	1557	538283.687500	5183009.500000	-122.498306	46.801498
LINE-6	1589	538461.375000	5182994.000000	-122.495979	46.801350
LINE-6	1606	538800.375000	5182971.000000	-122.491539	46.801121
LINE-6	1625	539142.625000	5182816.000000	-122.487068	46.799709
LINE-6	1632	539290.187500	5182866.500000	-122.485130	46.800152
LINE-6	1644	539374.687500	5183112.500000	-122.484001	46.802361
LINE-6	1662	539362.500000	5183469.000000	-122.484131	46.805569
LINE-6	1669	539336.625000	5183594.500000	-122.484459	46.806702
LINE-6	1678	539417.125000	5183750.500000	-122.483391	46.808102
LINE-6	1691	539597.500000	5183938.500000	-122.481010	46.809780
LINE-6	1704	539834.375000	5184032.500000	-122.477898	46.810612
LINE-6	1718	540056.687500	5184209.500000	-122.474968	46.812191
LINE-6	1735	540395.187500	5184257.000000	-122.470528	46.812599
LINE-6	1742	540519.125000	5184271.500000	-122.468903	46.812721
LINE-6	1768	541004.125000	5184416.500000	-122.462532	46.813999
LINE-6	1787	541301.875000	5184702.500000	-122.458603	46.816551
LINE-6	1800	541328.187500	5184946.500000	-122.458237	46.818748
LINE-6	1814	541370.500000	5185221.500000	-122.457657	46.821220
LINE-6	1820	541416.187500	5185354.000000	-122.457047	46.822411
LINE-6	1835	541619.500000	5185571.000000	-122.454361	46.824348
LINE-6	1848	541722.812500	5185787.500000	-122.452988	46.826290
LINE-6	1851	541763.187500	5185824.000000	-122.452454	46.826618
LINE-6	1873	542176.312500	5186010.500000	-122.447021	46.828270
LINE-6	1889	542450.375000	5186003.500000	-122.443428	46.828190
LINE-6	1900	542693.312500	5186050.000000	-122.440239	46.828590
LINE-6	1905	542769.875000	5186087.000000	-122.439232	46.828918
LINE-6	1920	542980.687500	5186305.500000	-122.436447	46.830872
LINE-6	1920	543333.000000	5186520.000000	-122.431808	46.832779
LINE-6	1958	543639.875000	5186639.000000	-122.427773	46.833832
LINE-6	1970	543885.375000	5186565.000000	-122.424561	46.833149
LINE-6	1984	544140.000000	5186600.500000	-122.421219	46.833450
LINE-6	1996	544401.000000	5186634.500000	-122.417793	46.833740
LINE-6	2020	544882.000000	5186668.500000	-122.411484	46.834011
LINE-6	2040	545286.125000	5186704.500000	-122.406181	46.834309
LINE-6	2065	545778.687500	5186743.000000	-122.399719	46.834621
LINE-6	2073	545939.500000	5186716.000000	-122.397614	46.834370
LINE-6	2100	546464.312500	5186649.000000	-122.390739	46.833729
LINE-6	2120	546852.187500	5186590.000000	-122.385658	46.833172
LINE-6	2133	547125.875000	5186565.500000	-122.382072	46.832932
LINE-6	2155	547552.375000	5186650.000000	-122.376472	46.833660
LINE-6	2182	548085.687500	5186755.500000	-122.369469	46.834572
LINE-6	2184	548157.125000	5186768.000000	-122.368530	46.834679
LINE-6	2200	548453.375000	5186827.000000	-122.364639	46.835190
LINE-6	2240	549253.500000	5186967.000000	-122.354134	46.836391
LINE-6	2255	549520.375000	5186984.000000	-122.350632	46.836521

LINE-6	2265	549704.812500	5186987.500000	-122.348213	46.836540
LINE-6	2279	550003.875000	5186921.000000	-122.344299	46.835918
LINE-6	2283	550075.000000	5186903.500000	-122.343369	46.835758
LINE-6	2292	550225.000000	5186847.000000	-122.341408	46.835239
LINE-6	2298	550339.000000	5186785.000000	-122.339920	46.834671
LINE-6	2302	550327.000000	5186766.000000	-122.340080	46.834499
LINE-6	2305	550398.625000	5186755.500000	-122.339142	46.834400
LINE-6	2315	550507.000000	5186673.000000	-122.337730	46.833649
LINE-6	2321	550616.125000	5186640.500000	-122.336304	46.833351
LINE-6	2330	550780.625000	5186582.000000	-122.334152	46.832809
LINE-6	2352	551179.187500	5186382.000000	-122.328949	46.830978
LINE-6	2359	551307.687500	5186326.500000	-122.327271	46.830471
LINE-6	2366	551424.125000	5186254.000000	-122.325752	46.829811
LINE-6	2368	551455.125000	5186237.500000	-122.325348	46.829659
LINE-6	2386	551817.375000	5186196.500000	-122.320602	46.829262
LINE-6	2387	551836.187500	5186179.500000	-122.320358	46.829109
LINE-6	2394	551822.625000	5186066.500000	-122.320549	46.828091
LINE-6	2396	551864.500000	5186073.500000	-122.320000	46.828152
LINE-6	2398	551893.312500	5186098.000000	-122.319618	46.828369
LINE-6	2401	551947.375000	5186106.500000	-122.318909	46.828442
LINE-6	2406	552055.812500	5186086.000000	-122.317490	46.828251
LINE-6	2407	552080.187500	5186087.500000	-122.317169	46.828259
LINE-6	2412	552137.375000	5186007.000000	-122.316429	46.827530
LINE-6	2420	552279.187500	5185898.000000	-122.314583	46.826542
LINE-6	2425	552346.875000	5185871.000000	-122.313698	46.826290
LINE-6	2432	552490.625000	5185882.500000	-122.311813	46.826382
LINE-6	2434	552527.375000	5185860.000000	-122.311333	46.826180
LINE-6	2439	552596.000000	5185803.000000	-122.310440	46.825661
LINE-6	2441	552621.500000	5185755.500000	-122.310112	46.825230
LINE-6	2445	552712.375000	5185742.000000	-122.308922	46.825100
LINE-6	2454	552881.312500	5185724.000000	-122.306709	46.824928
LINE-6	2456	552905.125000	5185731.000000	-122.306396	46.824989
LINE-6	2460	553032.187500	5185699.000000	-122.304733	46.824692
LINE-6	2470	553168.125000	5185603.500000	-122.302963	46.823818
LINE-6	2476	553190.625000	5185491.500000	-122.302681	46.822811
LINE-6	2487	553186.687500	5185277.000000	-122.302757	46.820881
LINE-6	2500	553202.375000	5185016.000000	-122.302582	46.818531
LINE-6	2510	553216.000000	5184802.500000	-122.302429	46.816608
LINE-6	2529	553295.500000	5184436.500000	-122.301430	46.813309
LINE-6	2540	553333.312500	5184241.500000	-122.300957	46.811550
LINE-6	2548	553291.000000	5184091.000000	-122.301529	46.810200
LINE-6	2551	553268.687500	5184043.000000	-122.301826	46.809769
LINE-6	2553	553281.812500	5184007.500000	-122.301659	46.809448
LINE-6	2554	553311.375000	5184014.500000	-122.301270	46.809509
LINE-6	2559	553380.187500	5183946.500000	-122.300377	46.808891
LINE-6	2564	553490.125000	5183890.500000	-122.298943	46.808380

LINE-6	2571	553592.625000	5183888.000000	-122.297600	46.808350
LINE-6	2575	553678.500000	5183855.500000	-122.296478	46.808048
LINE-6	2584	553763.187500	5183686.000000	-122.295387	46.806519
LINE-6	2596	553982.187500	5183617.500000	-122.292526	46.805882
LINE-6	2619	554171.687500	5183196.500000	-122.290092	46.802078
LINE-6	2630	554373.375000	5183103.000000	-122.287460	46.801220
LINE-6	2659	554922.625000	5183211.500000	-122.280251	46.802151
LINE-6	2680	555352.187500	5183156.500000	-122.274628	46.801620
LINE-6	2692	555542.625000	5183038.000000	-122.272148	46.800541
LINE-6	2724	555864.625000	5182466.000000	-122.267998	46.795368
LINE-6	2750	556285.875000	5182131.500000	-122.262520	46.792320
LINE-6	2775	556645.812500	5181822.500000	-122.257843	46.789509
LINE-6	2797	556987.312500	5181544.500000	-122.253403	46.786980
LINE-6	2819	557390.812500	5181374.000000	-122.248138	46.785412
LINE-6	2840	557797.187500	5181264.500000	-122.242828	46.784389
LINE-6	2860	558174.625000	5181147.000000	-122.237900	46.783298
LINE-6	2885	558667.687500	5180993.000000	-122.231461	46.781872
LINE-6	2895	558852.375000	5180868.000000	-122.229057	46.780731
LINE-6	2924	559333.875000	5180535.000000	-122.222794	46.777691
LINE-6	2951	559783.375000	5180260.500000	-122.216942	46.775181
LINE-6	2972	560122.375000	5180029.500000	-122.212532	46.773071
LINE-6	2990	560482.000000	5179905.000000	-122.207840	46.771919
LINE-6	3002	560701.187500	5179829.500000	-122.204979	46.771221
LINE-6	3033	561314.500000	5179668.000000	-122.196968	46.769711
LINE-6	3040	561436.875000	5179607.000000	-122.195374	46.769150
LINE-6	3043	561480.500000	5179566.500000	-122.194809	46.768780
LINE-6	9999	561692.6875[illegible]	[illegible]79210.500000	-122.192078	46.765560
LINE-6	3066	561706.812[illegible]	[illegible]9139.500000	-122.191902	46.764919
LINE-6	3071	561811.6875[illegible]	[illegible]9085.000000	-122.190536	46.764420
LINE-6	3092	562233.375000	5179213.000000	-122.184998	46.765530
LINE-6	3097	562323.000000	5179217.000000	-122.183823	46.765560
LINE-6	3120	562772.687500	5179114.000000	-122.177948	46.764591
LINE-6	3150	563203.625000	5179533.000000	-122.172249	46.768318
LINE-6	3175	563770.875000	5179384.500000	-122.164841	46.766930
LINE-6	3200	564285.625000	5179252.500000	-122.158119	46.765690
LINE-6	3220	564680.312500	5179115.500000	-122.152969	46.764420
LINE-6	3240	565070.000000	5178968.500000	-122.147888	46.763062
LINE-6	3265	565542.875000	5178771.000000	-122.141724	46.761238
LINE-6	3285	565944.125000	5178635.000000	-122.136490	46.759972
LINE-6	3315	566525.875000	5178405.500000	-122.128906	46.757851
LINE-6	3350	567212.375000	5178244.000000	-122.119942	46.756329
LINE-6	3392	568049.125000	5178052.500000	-122.109016	46.754520
LINE-6	3425	568700.312500	5178282.000000	-122.100456	46.756519
LINE-6	3454	569256.187500	5178492.000000	-122.093147	46.758350
LINE-6	3470	569595.000000	5178521.000000	-122.088707	46.758579
LINE-6	3500	570183.187500	5178553.500000	-122.081001	46.758808

LINE-6	3525	570676.875000	5178589.500000	-122.074532	46.759079
LINE-6	3550	571170.812500	5178609.000000	-122.068062	46.759201
LINE-6	-1	571391.125000	5178608.000000	-122.065178	46.759171

Appendix C

MT AND SEISMIC-REFLECTION DATA AND PHYSICAL PROPERTIES

Physical Properties

The ability to interpret lithology from the MT and seismic data sets is dependent upon our understanding of the electrical and acoustic properties of rocks under the temperatures and pressures encountered in the Cascade Range and surrounding region. The following, short discussion of rock properties is included to provide a background for statements concerning lithological correlations of various MT and seismic models in this paper.

Electrical resistivity vary over an extremely large dynamic range, with common rock resistivities typically ranging from 1 to 10,000 ohm-m. Rock-forming minerals are normally very resistive at surface pressures and temperatures, with the exception of metallic minerals and graphitic carbon, which are very low in resistivity. For most rocks, resistivity is controlled by ionic conduction through fluids in pore spaces or intergranular coatings, rather than electronic conduction through the mineral matrix. This ionic-controlled resistivity is a function of salinity of the pore fluids, temperature, and pressure, and is important for sedimentary and other rocks with connected porosities of greater than a few tenths of a percent. Ionic mobility increases and resistivity decreases as temperature is increased, but the effect on resistivity reaches a maximum at temperatures around 200-250°C for depths of a few km.

As porous rocks are buried to depths greater than a few km, porosities are decreased due to lithostatic loading until the rocks normally become highly resistive. In shales, ionic conduction also occurs in trapped water in clays and zeolites; as a result, the resistivity of shales will be low (1-20 ohm-m) and varies less than other sedimentary rocks as porosity decreases. As shales are metamorphosed, both porosity and layered clays are destroyed, but low resistivities can be maintained due to formation of carbonaceous or iron mineral films along fissile planes in the metashales. Intrusive rocks have very low porosity and thus are normally very resistive, typically in the range of 500-20,000 ohm-m. Fracture porosity and intense alteration of intrusive rocks can lower their resistivity well below this range. Unaltered volcanic rocks have very high resistivities when pore waters are very fresh; however, as volcanic rocks increase in age, development of authigenic minerals (clays and zeolites) dramatically decreases their resistivity. Typical values for tuffaceous-rich (non-welded tuff and ash alters very fast) flows and volcaniclastic rocks of Tertiary age in the Oregon Cascades are less than 20 ohm-m. Metamorphism of crustal rocks beyond zeolite facies generally increases resistivities, except for metamorphosed shales in which carbonaceous and/or metallic-mineral coatings may develop. Another exception to high resistivities in metamorphic rocks occurs upon dehydration of greenschist or amphibolite facies minerals in the rocks, as demonstrated by Lee and others (1983); their laboratory measurements on high-grade metamorphic rocks at temperatures up to 300°C and pressures of 0.4GPa indicated lowered resistivities that they attributed to high-pore-pressure fluids from mineral dehydration. As temperature and pressure increases, partial melting may occur, leading to a decrease in resistivity of the rocks by up to two orders of magnitude if there is sufficient interconnection

between intergranular melt films.

Accuracies in the MT models are influenced largely by data quality, selection of strike direction, frequency-independent shifts of curves due to near-surface complexities (similar to weathering problems in seismic reflection surveys; Sternberg and others, 1989) and oversimplified model geometry.

Seismic compressional-wave velocities in crustal rocks vary over a much narrower range than do resistivities, typically ranging from 2-7.4 km/s. Velocities for Tertiary sedimentary rocks are typically 3-5 km/s. Compressional velocities for Cascades volcanic rocks range from 4-6 km/s, controlled by porosity, weathering, and proportion of mafic minerals. The velocity of intrusive rocks is influenced by the proportion of mafic to quartz minerals in the rocks, with felsic rocks such as granite having velocities of about 5-6 km/s and intermediate to mafic intrusive rocks ranging higher than 6.3 km/s. Approximate velocities for the formations of interest to our study determined from sonic logs, stacking velocities, and analogy with similar geologic units. The recording of reflections from geologic formations is dependent upon sufficient acoustic contrast and favorable geometry of the reflecting surfaces (Anstey, 1977).

The seismic reflection data outlines two key pieces of structural information: (1) folding corresponding to mapped anticlines and synclines and (2) basal dipping reflectors on the west and east ends of a long profile through the study area. Migration of the reflection data has only been done for the western part of this long profile because poor data quality for much of the profile did not warrant migration of the whole data set. Interpretation of unmigrated data will not affect general structural analyses for the anticlinal structures, but use of unmigrated data for the dipping reflectors on the west and east ends of the profile had to be handled cautiously. Because no wells were available along the reflection profiles, velocity information from wells in the nearby Chehalis basin, in combination with stacking velocities and empiral curves were used to aid processing and interpretation of the data. Approximate depth conversions used in the subsequent discussions and figures assume average velocities of 5 km/s .

Appendix D

Details of The Magnetotelluric Method

MT data consist of measurements of the orthogonal components of time-varying, surface magnetic fields and their associated electric fields. These fields occur naturally as a result of electromagnetic induction in the Earth from magnetic variations originating in the ionosphere and atmosphere. In our surveys, horizontal electric fields were sensed using an L-shaped, 3-electrode array with dipole lengths of 37.5 m. The orthogonal, horizontal magnetic fields in the direction of the electric-field measurement array were sensed using permalloy-cored induction coils (Stanley and Tinkler, 1983). The vertical magnetic field was measured only at selected sounding sites when a ring-core fluxgate magnetometer (Acuna, 1973) was deployed for magnetic field sampling instead of the induction coils. Time-series recordings of the electrical and magnetic field data were acquired using a computer-controlled data-acquisition system, with the computer and other electronics powered by marine storage batteries. The acquisition system used an analog signal-conditioning system for pre-whitening of the input spectrum and post-amplification, combined with a 12-bit analog-to-digital convertor. Data were recorded to disk for pass-bands at the three frequency ranges of 2-300 Hz, 0.05-3 Hz, and 0.002-0.2 Hz. The measurements spanned a period of about 2-3 hours and included 3 to 6 recordings of the higher frequency bands and 1-4 recordings of the lowest frequency band. At selected sounding sites, the ring-core fluxgate magnetometer was used instead of the induction coils for magnetic field measurement to obtain vertical magnetic field data and to extend the MT data to frequencies of .0002 Hz (one decade lower than that obtainable with the three standard bands above). An automated, battery-powered, data-acquisition system designed by V. F. Labson, U.S.G.S. (pers. comm., 1989) was used with the ring-core magnetometer system and associated electric field sensors (identical to that used for the three standard bands). The automated system was deployed for at least 9 hours to record the lower frequency data .

The time-series data were converted to complex cross-spectra using FFT (Fast-Fourier-transform) techniques. Least-squares, cross-spectral analysis (Bendat and Piersol, 1971) were used to solve for a tensor transfer function relating the observed electric fields to the magnetic fields, under the assumption that the Earth consists of a two-input, two-output linear system with the magnetic fields as input and the electric field as outputs:

$$Z_{ij} = E_i + H_j$$

Where Z_{ij} is the impedance tensor, E_i are the two horizontal electric fields, and H_j the two horizontal magnetic fields.

When the vertical magnetic field was measured, the vertical field transfer function (or "tipper") was solved for, with the assumption that the vertical field is the output of a two -input, one-output system (with the vertical field as the output):

$$H_z = AH_x + BH_y$$

Where H_x and H_y are the horizontal magnetic fields, H_z is the vertical magnetic field, and A and B are the transfer function elements.

The impedance tensor, Z_{ij}, is treated as amplitude and phase quantitites. The amplitude of the tensor is converted to "apparent resistivities" using the relationship between the resistivity of a homogeneous earth to the tensor impedance relationship

$$\rho_a = \frac{1}{\omega\mu_0}\left[\frac{E_i}{H_j}\right]^2$$

between surface electric and magnetic fields:
Where E_i and H_j are the orthogonal electric and magnetic field pairs, ω is the radian frequency, and μ_0 is the magnetic permeability (assumed to be the same as free space at MT frequencies).

The phase of the impedance tensor is given by the arctangent of the amplitude of the real part of the tensor to the imaginary part:

$$\Phi = \arctan\frac{Z_R}{Z_I}$$

The measured resistivity and phase values are plotted versus frequency for computer modeling. Both the resistivity and phase data are normally used in the modeling, although it can be demonstrated that they are not independent through the Hilbert transform (Bendat and Piersol, 1971). Prior to conversion to resistivity and phase, the tensor is normally rotated into principal directions that usually correspond to the direction of maximum and minimum resistivity. For a two-dimensional (2-D) earth the MT fields can be decoupled into transverse electric (TE) and transverse magnetic (TM) modes; two-dimensional modeling is generally done to fit both modes. When the geology satisfies the 2-D assumption, the MT data for the TE mode is assumed to represent the situation when the electric field is along the geologic strike and the TM mode for the electric field across strike. A measure of the correctness of the 2D assumption for MT data is provided by the skew of the impedance tensor, defined as the ratio of the magnitude of the diagonal elements over the off-diagonal elements (Vozoff, 1972). If the geology is truly 2D, then the skew will be zero. Remote or local reference sensors can be used to help reduce bias in the impedance determinations due to instrument or environmental noise [Gamble and others, 1979; Clark and others, 1983]. Although reference techniques were not used in our survey,

we did sort cross-power files to select optimal signal-to-noise data sets.

Man-made electrical noise, such as powerlines and irrigation pumps can have a negative effect on MT data quality. In the survey area, there are numerous small powerlines that did not affect data quality as long as the soundings were done about 0.4 km distance from them. Large sprinkler systems driving by electric irrigation pumps were more of a problem and were not approached closer than 1 mile for soundings. Local lightning, wind and rainstorms can also degrade data quality, but these can be generally avoided by planning surveys to miss the most active thunderstorm periods. The MT signals that originate in the ionisphere and from equatorial lightning belts vary in spectral densities (amplitudes) from several factors. The lower frequency ionispheric signals (.0001 to 1 Hz) are related to sunspot activity and the last three years have been ones of high sunspot activity and good signal levels, but even in low sunspot activity, the MT signals are adequate for year-round MT surveys. Higher frequency MT signals (1 Hz to 10,000 Hz) generated largely from equatorial lightning storms that propagates in the earth-ionispheric waveguide have minimums in amplitude in the northern hemisphere winter; this amplitude minimum does cause problems with some wintertime MT surveys using the higher frequency ranges. An excellent introduction to the MT method and references for a more advanced understanding are contained in Dobrin and Savit (1988).

DATE
FILMED
6/14/94
END